THE UNIVERSITY OF ALBERTA

AN INTERACTIVE SPECTRAL LIBRARY FOR INDUCTIVELY COUPLED PLASMA ATOMIC EMISSION SPECTROMETRY

by

SHI LIU

©

A thesis submitted to the Faculty of Graduate Studies and Research in partial fulfillment of the requirement for the degree of Doctor of Philosophy.

DEPARTMENT OF CHEMISTRY

EDMONTON ALBERTA

FALL 2001

National Library of Canada
Acquisitions and Bibliographic Services
395 Wellington Street
Ottawa ON K1A 0N4
Canada

Bibliothèque nationale du Canada
Acquisitions et services bibliographiques
395, rue Wellington
Ottawa ON K1A 0N4
Canada

Your file Votre référence

Our file Notre référence

The author has granted a non-exclusive licence allowing the National Library of Canada to reproduce, loan, distribute or sell copies of this thesis in microform, paper or electronic formats.

L'auteur a accordé une licence non exclusive permettant à la Bibliothèque nationale du Canada de reproduire, prêter, distribuer ou vendre des copies de cette thèse sous la forme de microfiche/film, de reproduction sur papier ou sur format électronique.

The author retains ownership of the copyright in this thesis. Neither the thesis nor substantial extracts from it may be printed or otherwise reproduced without the author's permission.

L'auteur conserve la propriété du droit d'auteur qui protège cette thèse. Ni la thèse ni des extraits substantiels de celle-ci ne doivent être imprimés ou autrement reproduits sans son autorisation.

0-612-69840-8

Canada

THE UNIVERSITY OF ALBERTA
LIBRARY RELEASE FORM

NAME OF AUTHOR: Shi Liu

TITLE OF THESIS: An Interactive Spectral Library for Inductively Coupled Plasma Atomic Emission Spectrometry

DEGREE: Doctor of Philosophy

YEAR THIS DEGREE GRANTED: 2001

Permission is hereby granted to the University of Alberta Library to reproduce single copies of this thesis and to lend or sell such copies for private, scholarly research purposes only.

The author reserves all other publication and other rights in association with the copyright in the thesis, and except as hereinbefore provided, neither the thesis nor substantial portion thereof may be printed or otherwise reproduced in any material form whatever without the author's prior written permission.

Shi Liu

Shi Liu
University of Alberta
Department of Chemistry
Edmonton, Alberta
T6G 2G2

Date: Sept 28, 2001

THE UNIVERSITY OF ALBERTA

FACULTY OF GRADUATE STUDIES AND RESEARCH

The undersigned certify that they have read, and recommended to the Faculty of Graduate Studies and Research, for acceptance, a thesis entitled AN INTERACTIVE SPECTRAL LIBRARY FOR INDUCTIVELY COUPLED PLASMA ATOMIC EMISSION SPECTROMETRY submitted by SHI LIU in partial fulfillment of the requirement for the degree of DOCTOR OF PHILOSOPHY.

Dr. Gary Horlick (Supervisor)

Dr. John-Bruce Green

Dr. Mark R. Freeman

Dr. Mariusz Klobukowski

Dr. Mark T. McDermott (Chairperson)

Dr. Ramon M. Barnes (External Examiner)

Date: Oct 1, 2001

To my family.

ABSTRACT

An ICP-AES Spectral Library for 71 elements has been built with spectra acquired using high purity standards with a UV-Visible Fourier transform spectrometer. This Spectral Library is one of the only spectroscopic data sets that provide complete coverage (i.e. full spectra) for the elements with spectral lines exclusively from ICP-AES. It also provides spectral line intensities for the ICP discharge, which is important for interference considerations. This Spectral Library has superior wavelength accuracy that is inherent to FTS. The overall average wavelength error of the Spectral Library was no greater than 1.05 pm when compared with literature data. As this Spectral Library is stored and distributed in an interactive format, it should bring revolutionary change to the way spectral data can be used.

As such, it is expected that the Spectral Library will find wide range of applications in both industrial and academic environments. Some applications, including scanning spectrum simulation with spectra addition, spectral line identification with spectra subtraction, and assessment of spectral interferences for commercial ICP-AES spectrometers, are introduced as examples. In addition to the MAC based SpectroPlot Program, instructions are provided for two Microsoft Windows based commercial software packages which allow access to the Spectral Library with IBM-PC compatible computers.

Some other related work, including analysis of solution mixtures on the ICP-FTS; direct analysis of solid form Standard Reference Materials with a powder pump coupled to the ICP-FTS; and the calibration with solid standards using the powder pump for the ICP-FTS are also presented in this thesis.

ACKNOWLEDGEMENTS

I would like to express my sincere appreciation to my supervisor, Dr. Gary Horlick, for all he has taught me and shared with me. His guidance, understanding, patience, and friendship have been invaluable. This work could not have been done without his great enthusiasm and generous support.

Special thanks to Drs. Mark McDermott, John-Bruce Green, Mariusz Klobukowski, Mark Freeman, and Ramon Barnes for their precious advice and valuable time.

I would like to thank everyone in the department who have helped and encouraged me. Special thanks to Youbin Shao, for his friendship and help in everything, including many useful discussions on instrumentation and spectroscopy; to Albert Chilton and the electronic shop, for their help in electronics of the FTS instrument; and to Lin Ferguson, for printing and preparing the thesis for editing.

My thanks also extend to the Department of Chemistry, University of Alberta; and to Dr. Samantha Tan and ChemTrace Corp.

Finally I wish to thank my lovely wife, Yali Shu, and son, Shuyang Liu, whose patience and encouragement have always been with me along this long journey pursuing my degree. It is their love and support that made the difference.

TABLE OF CONTENTS

CHAPTER 1. INTRODUCTION 1

1.1. THESIS OBJECTIVE. 1

1.2. ICP-AES AND ITS APPLICATION 3

1.2.1. Role of ICP-AES in Elemental Analysis. 3

1.2.2. A Brief Review of Analysis with ICP-AES. 4

1.2.3. ICP-AES Remains Competitive. 5

1.3. ICP-AES INSTRUMENTATION 7

1.3.1. Overview 7

1.3.2. Simultaneous Spectrometer. 8

1.3.3. Scanning Spectrometer. 11

1.3.4. Fourier Transform Spectrometer. 13

1.4. THE NEED FOR ICP-AES SPECTRAL REFERENCE DATA 15

1.5. ICP-FTS: SOLUTIONS FOR THE SPECTRAL LIBRARY 21

1.5.1. Digital Fourier Transform 21

1.5.2. Building the Spectral Library with ICP-FTS. 30

REFERENCE 32

CHAPTER 2. ICP-FTS AND OPERATIONS 43

2.1. THE UV - VISIBLE FTS INSTRUMENT. 43

2.1.1. Optical System. 43

2.1.2. Drive Motion Control System. 45

2.1.3. Data Acquisition System. 46

2.2. OPERATION OF THE INSTRUMENTS 48

2.2.1. Operation of the ICP. 48

2.2.2. Operation of the FTS 50

2.2.3. FTS operation parameters. 54

2.3. SOLUTIONS. 55

REFERENCE 58

CHAPTER 3. THE ICP-AES SPECTRAL LIBRARY 59

3.1. INTRODUCTION TO THE SPECTRAL LIBRARY 59

3.2. WAVELENGTH CALIBRATION 62

3.2.1. Calibration of the Spectra 65

3.2.2. Major Spectral Lines of the Elements 65

3.3. SPECTRAL LINE WAVELENGTH ACCURACY 68

3.3.1. Overview 68

3.3.2. A Close Look at Wavelength Accuracy. 73

3.3.3. Line Hyperfine Structure and Wavelength Accuracy 79

3.3.4. Wavelength Bias in FTS Measurement 86

3.3.5. Calibration with Average Laser Wavelength 101

3.4. SPECTRAL LINE SHAPE AND RESOLUTION 110

3.5. CONTROL OF SPECTRAL QUALITY. 115

3.5.1. Alias Lines. 115

3.5.2. Ar lines 118

3.5.3. Lines from Other Sources 123

REFERENCE 126

CHAPTER 4. SOME APPLICATIONS FOR THE SPECTRAL LIBRARY 127

4.1. INTERACTIVE ICP-AES SPECTRAL DATA 128

4.2. REMOVAL OF ARGON LINES WITH SPECTRA SUBTRACTION 135

4.3. SCANNING SPECTRUM SIMULATION AND SPECTRAL LINE IDENTIFICATION 144

4.3.1. The Objective of the Simulation 144

4.3.2. Spectrum Simulation and Resolution Control 145

4.3.3. Identification of Spectral Lines 150

4.4. ASSESSMENT OF SPECTRAL INTERFERENCE. 157

4.4.1. Simulation of Optima Spectral Windows 157

4.4.2. Interference on Rare Earth Elements 164

REFERENCE 169

CHAPTER 5. THE SPECTRAL LIBRARY FOR MICROSOFT WINDOWS PLATFORM 170

5.1. DEVELOPING SPECTRAL LIBRARY FOR WINDOWS PLATFORM. 170
5.1.1. The Need 170
5.1.2. Design Guidelines for the User Interface 171
5.1.3. Some Comments on the Interface Development 173
5.2. SPECTRAL LIBRARY BASED ON ORIGIN. 175
5.2.1. The Spectral Library Interface 175
5.2.2. Viewing the Spectra 177
5.2.3. Viewing Spectra in Detail 179
5.2.4. Fast Fourier Transform in Origin. 185
5.2.5. Wavelength Calibration in Origin. 187
5.3. SPECTRAL LIBRARY BASED ON WAVEMETRICS' IGOR PRO 190
5.3.1. Strength and Weakness of Igor Pro 190
5.3.2. Viewing Spectra or Interferograms with Igor Pro 191
5.3.3. Fourier Transform and Wavelength Calibration 196
5.3.4. Advanced FFT Operation 199
REFERENCE 201

CHAPTER 6. MEASUREMENT OF MIXTURES WITH ICP-AES-FTS 203

6.1. QUALITATIVE MEASUREMENT OF AQUEOUS MIXTURES 203
6.1.1. NIST Water Standard 203
6.1.2. Qualitative Measurement of Multi-element Solutions 204
6.2. POWDER PUMP SAMPLING ICP-FTS MEASUREMENT 217
6.3. QUALITATIVE MEASUREMENT FOR SOLID STANDARD REFERENCE MATERIALS. 230
6.4. CALIBRATION OF ICP-FTS WITH SOLID SAMPLES. 241
REFERENCE 244

CHAPTER 7. SUMMARY AND FUTURE DIRECTIONS. 245

7.1. SUMMARY OF CURRENT RESEARCH WORK. 245

7.2. FUTURE DIRECTIONS FOR THE SPECTRAL LIBRARY. 249

7.2.1. Improvements to the spectra. 249

7.2.2. Improve the accessibility to the data. 251

7.2.3. Not the end. 252

APPENDIX 253

A-1. TABLE OF CONTENTS FOR THE CD-ROM 253

Mac-OS Section 253

Windows Section 253

A-2. CIRCUITRY FOR SOME FTS CONTROL UNITS 254

LIST OF FIGURES

Figure 1-1. A typical ICP-AES instrument..... 7
Figure 1-2. The processes sample experiences in an ICP-AES analysis..... 8
Figure 1-3. Optical and detection systems of the Perkin Elmer Optima. 10
Figure 1-4. Czerny-Turner Mount. 12
Figure 1-5. Basic Components of a Michelson interferometer..... 14
Figure 1-6. Mg HCL and ICP Spectra showing different spectral lines..... 18
Figure 1-7. NIST ASD Home page and a list of Mg lines. 20
Figure 1-8. Time and Frequency domain description of a sine wave..... 22
Figure 1-9. Aliasing of a 175 Hz sine wave to a 25 Hz sine wave..... 26
Figure 1-10. Aliasing illustrated by Flame emission spectra. 28
Figure 2-1. Optical system for the Fourier Transform Spectrometer..... 44
Figure 2-2. The Plasma-Therm ICP-2500 system. 48
Figure 2-3. Diagnosis for ICP robustness with Mg spectral line ratio. 49
Figure 2-4. Important diagnosis signals for the FTS routine operation..... 51
Figure 3-1. Elements covered by the ICP-AES Spectral Library..... 60
Figure 3-2. Some UV interferograms from the Spectral Library. 63
Figure 3-3. UV spectra for the first row of the transition metals. 64
Figure 3-4. Reference laser apparent wavelength values vs. element. 70
Figure 3-5. Spectral line wavelength errors vs. element. 71
Figure 3-6. Spectral line wavelength errors vs. standard deviation of laser apparent wavelength..... 72
Figure 3-7. Wavelength errors $\Delta\lambda$ vs. wavelength for Fe UV lines. 76
Figure 3-8. Wavelength errors $\Delta\lambda$ vs. wavelength for some "large error" lines. 79
Figure 3-9. Some Ho visible lines with hyperfine structure..... 81
Figure 3-10. Line shape of some Ho lines..... 82
Figure 3-11. Some observed hyperfine structure..... 85
Figure 3-12. Wavelength errors and correction factors for Ar visible lines..... 88
Figure 3-13. Wavelength errors vs. wavelength for La, Cr, Sc, Ce, Y, and Nd..... 89
Figure 3-14. Wavelength errors verse wavelength for all visible lines. 91

Figure 3-15. Wavelength errors vs. wavelength for Nb, Sn, Gd, Hf, Sb and Cu. 94
Figure 3-16. Wavelength errors vs. wavelength for Pb, Pt, and Yb. 96
Figure 3-17. Wavelength errors vs. wavelength for all UV lines. 98
Figure 3-18. Wavelength errors under different standards for Pb, Cu, Sn, and Sb.. 100
Figure 3-19. Wavelength errors of Ag lines calibrated with average apparent reference laser wavelength (632.8438 nm). 103
Figure 3-20. Wavelength errors of Cu lines calibrated with average apparent reference laser wavelength (632.8438 nm). 104
Figure 3-21. Wavelength errors of Co lines calibrated with average apparent reference laser wavelength (632.8438 nm). 105
Figure 3-22. The mean of wavelength errors of spectra calibrated with average apparent reference laser wavelength (632.8438 nm). 107
Figure 3-23. The standard deviation of wavelength errors for spectra calibrated with average apparent reference laser wavelength 108
Figure 3-24. Spectral lines from Gaussian bell shape interferograms. 112
Figure 3-25. Spectral lines from triangular shape interferograms. 113
Figure 3-26. Spectra demonstrate the resolution of the spectral library. 114
Figure 3-27. Ca UV spectrum measured with 1000 and 10,000 ppm solutions 116
Figure 3-28. Cd UV spectrum measured with 1000 and 10,000 ppm solutions 119
Figure 3-29. Ag visible spectrum before and after the removal of argon lines. 120
Figure 3-30. Co visible spectrum before and after the removal of argon lines. 121
Figure 3-31. Zinc visible spectrum before and after the removal of argon lines 122
Figure 3-32. Lines introduced to Zn and Sb spectra by impurity elements. 124
Figure 3-33. Lines introduced to by impurity or counter-ions. 125
Figure 4-1. Boron UV interferogram at different scale. 129
Figure 4-2. Boron UV spectrum and the detailed structure of the two doublets. 130
Figure 4-3. Measuring spectral information with the *SpectroPlot*. 131
Figure 4-4. Beryllium UV interferogram at different scale. 133
Figure 4-5. Beryllium UV spectrum and detailed spectral features. 134
Figure 4-6. Removal of Ar lines in Pd visible spectrum. 136
Figure 4-7. Background subtraction for Ba visible interferogram. 138

Figure 4-8. Ba visible spectra before and after background subtraction. 139
Figure 4-9. Ar lines removed from Ba visible spectrum 140
Figure 4-10. Background subtraction for Ce visible interferogram. 141
Figure 4-11. Ce visible spectra before and after background subtraction. 142
Figure 4-12. Ar lines removed from Ce spectrum 143
Figure 4-13. ICP-AES scanning spectrum for a mixture of seven metal ions..... 144
Figure 4-14. Simulated spectrum of the mixture and the constituent element spectra from the Spectral Library..... 146
Figure 4-15. Comparison of the scanning and the simulated spectra. 147
Figure 4-16. Simulated interferograms of different length for the mixture..... 148
Figure 4-17. Resolution decreased as a result of reduced interferogram length. 149
Figure 4-18. Overview of the constituent elemental spectra. 151
Figure 4-19. Identification of dominant lines for Cd and Zn 153
Figure 4-20. Identification of Cu and Ca after removal of dominant lines. 154
Figure 4-21. Simulated Optima optical windows (sub-array) for P lines..... 158
Figure 4-22. Simulated Optima subarrays 054 and 120 for Pb 160
Figure 4-23. Simulated Optima subarrays 042 and 081 for Pb 161
Figure 4-24. Effect of interfering line intensity change. 162
Figure 4-25. Fe interferes on U analysis..... 165
Figure 4-26. Sinulation of spectral window for Ho 339.898 nm line..... 167
Figure 4-27. Simulation of spectral windows for a scanning spectrometer. 168
Figure 5-1. A prototype user interface for the Spectral Library. 172
Figure 5-2. The user interface of the Spectral Library built on *Origin* 175
Figure 5-3. A line plot for B UV spectrum data in *Origin*. 178
Figure 5-4. Boron UV spectrum displayed in *Origin*. 179
Figure 5-5. ***Data Reader Tools***r. 181
Figure 5-6. Property window for x-axis. 182
Figure 5-7. Select a section of spectrum with ***Data Selector*** tool. 183
Figure 5-8. Plot a section of spectrum with *Extract Worksheet Data* window. 184
Figure 5-9. The parameter control dialog of FFT function. 185
Figure 5-10. The calculation result listing for the FFT. 186

Figure 5-11. The spectra plotted after FFT in *Origin*. 186
Figure 5-12. Extracting amplitude data of a spectrum from a FFT worksheet..... 188
Figure 5-13. ***Set Column Value*** dialog.for wavelength calibration. 189
Figure 5-14. Spectral Library Interface for *Igor Pro*..... 191
Figure 5-15. Loading delimited text data into *Igor Pro*. 193
Figure 5-16. Boron UV interferogram displayed in *Igor Pro*. 194
Figure 5-17. Use cursor and "info box" for precise data readout. 195
Figure 5-18. FFT in *Igor Pro*..... 197
Figure 5-19. Delete Points dialog box. 198
Figure 5-20. FFT option dialog. 199
Figure 5-21.Boron 249 doublet transformed with enhanced resolution. 201
Figure 6-1. UV spectrum and line assignment for NIST SRM 1634d. 205
Figure 6-2. Visible spectrum and line assignment for NIST SRM 1634d..... 206
Figure 6-3. Identification of Ag in SM-20 with spectrum subtraction. 208
Figure 6-4. Spectral line identification for Mn, Fe, and Cr in SM-20. 210
Figure 6-5. Spectral line identification for Cd, V, and Co in SM-20 211
Figure 6-6. Spectral line identification for Zn, Ni, and Cu in SM-20. 212
Figure 6-7.Positive "residual" caused by intensity difference during spectrum subtraction for Mn 267.610 nm line..... 213
Figure 6-8. Ag 243.779 nm line reduced to a "residual" by spectrum subtraction of adjacent strong Ni and Mn lines. 215
Figure 6-9. Ag 241.318 nm line was lost after spectrum over-subtraction. 216
Figure 6-10. A single scan 16k interferogram and spectrum of Cu powder..... 225
Figure 6-11. Cu visible interferogram and spectrum by powder pump-sampling ICP-FTS. 226
Figure 6-12. Ni visible interferogram and spectrum from powder pump-sampling ICP-FTS 227
Figure 6-13. Visible interferogram and spectrum for Ni coated Cu particles from powder pump-sampling ICP-FTS 229
Figure 6-14. Elements in the NIST SRM 2704 Buffalo River Sediment 233
Figure 6-15. Elements in the NIST SRM 1632 Coal..... 235

Figure 6-16. Elements in the NIST SRM 1575 Pine Needle. 237
Figure 6-17. Elements in the Pepper Bush (Japan)..... 239
Figure 6-18. Calibration lines for ICP-FTS for solid mixture TS-6 (matrix SiO_2) sampled with powder pump. 242
Figure 6-19. Calibration lines for ICP-FTS for solid mixture G-7 (matrix Graphite) sampled with powder pump. 243

LIST OF TABLES

Table 2-1. Operation Conditions for the ICP-2500 system 49
Table 2-2. Operation parameters for FTS and data acquisition. 54
Table 2-3. Standard solutions and concentration used. 56
Table 3-1. Calibration of Mg UV Spectrum. 66
Table 3-2. Major spectral lines of Fe in the UV region. 67
Table 3-3. Wavelength accuracy for Fe visible lines (λ in nm) 74
Table 3-4. Wavelength accuracy for Fe UV lines (λ in nm) 75
Table 3-5. Comparison of wavelength errors with different wavelength standards. . 78
Table 3-6. Ho visible lines. 83
Table 3-7. Ho visible line wavelength at lower resolution 84
Table 3-8. Least square fitting results for trend lines (visible lines) 90
Table 3-9. Sub-regions for statistical analysis. 92
Table 3-10. t value calculated for wavelength errors and correction factor k. 93
Table 3-11. Critical t values at confidence level of 95%. 93
Table 3-12. Least square fitting results for trend lines (visible lines) 95
Table 3-13. UV Sub-regions for statistical analysis. 95
Table 3-14. t value calculated for wavelength errors and correction factor k. 97
Table 3-15. Least square fitting results with different standards (UV lines) 99
Table 3-16. Calculated t for comparison of spectral line wavelength values *. 108
Table 3-17. Alias lines found in the spectral library 117
Table 4-1. Spectral line assignment of the scanning spectrum. 156
Table 5-1. Important tools in the *Origin* toolbox. 180
Table 6-1. Elements in the NIST SRM 1643d 204
Table 6-2. Composition of the standard solution. 207
Table 6-3. Spectral lines in the UV spectrum of SM-40 218
Table 6-4. Spectral lines in the visible spectrum of SM-40 219
Table 6-5. Spectral lines in the UV spectrum of SM-50 220
Table 6-6. Spectral lines in the visible spectrum of SM-50 221

Table 6-7. Typical experiment conditions for the ICP-FTS measurement with powder pump sampling. 224
Table 6-8. Spectral line wavelength values for Cu and Ni powder. 228
Table 6-9. Constituent elements of the solid SRMs. 232
Table 6-10. Spectral lines found in NIST SRM 2704 Buffalo River Sediment 234
Table 6-11. Spectral lines found in NIST SRM 1632 Coal 236
Table 6-12. Spectral lines found in NIST SRM 1575 Pine Needle 238
Table 6-13. Spectral lines found in Pepper Bush 240
Table 6-14. Sample uptake for the Powder Pump-ICP-FTS calibration. 241

Chapter 1. Introduction

1.1. Thesis Objective.

Inductively Coupled Plasma – Atomic Emission Spectrometry (ICP-AES) is a powerful analytical atomic spectroscopic method for elemental analysis. Because of its high efficiency, high sensitivity, wide linear dynamic range, and near freedom from chemical interferences, ICP-AES has replaced the traditional volumetric methods and atomic absorption spectrometry and become the method of choice for medium to low level elemental analysis (1-4).

Many advances have been made since the first commercial ICP-AES instrument was introduced to the analytical community in 1974. Over thirty years of research and development have led to a better understanding of the ICP source and the dramatically improved measurement systems for the emission signal (5-22).

In contrast to these substantial advances, research on and development of a comprehensive spectral line database has been slow (23). Except for a few published works (24, 25), currently nearly all authoritative atomic spectral line references are based on arc and spark emission spectra, and thus inadequate for predicting spectral interference in ICP-AES (26-31). In addition, these traditional references are printed wavelength tables omitted much of the information and visual effects that spectra carry.

This research project is designed to provide the analytical community with an interactive spectral library for ICP-AES. It will provide full coverage for all elements in the Periodic Table with genuine ICP-AES data for correct spectral line position

and relative intensity, along with accurate and precise wavelength values available only with a Fourier Transform spectrometer. As this spectral library will be distributed on CD-ROM in common electronic data format, it will also provide unparalleled interactivity and visual effects for any user with a personal computer. As well, this library will contain all the vital information that are lost during the conversion of spectra to wavelength tables, and it will provide an invaluable data source for future work on modeling and simulation for ICP-AES.

1.2. ICP-AES and its Application.

1.2.1. Role of ICP-AES in Elemental Analysis.

In 1992 Velmer A. Fassel wrote that "The most significant event that occurred during the past decades in the field of analytical atomic spectroscopy was the emergence of various atmospheric-pressure, flame-like plasmas as vaporization, atomization, excitation, and ionization sources for analytical atomic spectroscopy. Judged on the basis of their acceptance by the analytical spectroscopy community, by their growth in usage, and by the number of commercial instruments sold, ICPs undoubtedly have had the greatest impact to date." (32)

Indeed, since the introduction of the ICP to the atomic spectroscopy by Stanley Greenfield and Velmer Fassel in 1964 (2, 33), analytical techniques based on the ICP, notably ICP-AES and ICP-MS, have revolutionized trace metal analysis.

Traditionally elemental analysis had been the market of flame atomic absorption, and occasionally spark and arc emission (34). When ultra low detection limits were required, graphite furnace AA was used (6, 7, 34). Although flame AA has the advantage of low cost and ease of operation (35), sample throughput is limited by the inherent weakness of a single element method. Also, because of the relatively low temperature of the excitation source (flame or furnace), chemical interference has been another major problem for atomic absorption methods (9).

For ICP-AES or ICP-MS, the high temperature ICP source (6000 to 10000°C compared to 2000 to 3000°C for AA) provides a much better excitation source (12). At such a high temperature, almost all elements except those with very high

excitation potentials can be vaporized and excited in similar conditions. Thus a uniform experimental condition can often be used for simultaneous multi-element detection with little compromise. This characteristic, together with the advance of solid-state image detection technology that will be discussed in more detail later, has made the ICP-AES the fastest elemental analysis method ever. Varian, one of the leading manufacturers for atomic spectrometers, claims that their Vista CCD simultaneous ICP-AES can analyze 73 elements in 35 seconds (36). Although it is questionable whether this speed can be achieved in practical analyses, it does give a sense of the speed of these state-of-the-art instruments. Considering the number of measurements that an industrial lab performs everyday, the increase in sample throughput and improvement in efficiency translate into huge economic benefits.

The second advantage of the ICP being a high temperature source is that it dramatically reduces chemical interferences. Although it is not true that the ICP has no matrix effects as some early developers hoped, ICP-AES is the technique that is closest to the state of being free from chemical interferences (4, 5, 37). Thus, even though ICP-AES instruments are three to five times more expensive than flame AA, they still became the de-facto standards for elemental analysis and are commonplace in analytical labs around the world.

1.2.2. A Brief Review of Analysis with ICP-AES.

With so many advantages, it is not surprising to find that ICP-AES has found a very wide range of applications. Meyer and Keliher (38) indicated in a survey that, for the first half of year 1990, environmental analysis took 30% of the total publications of atomic spectrometry while biological applications were listed in the

second place with 22%. The third place is food, with 15%, and then agriculture (9%), geological (9%), industrial (9%), and metallurgical (6%). Today, ICP-AES is still the leading method in analysis of agricultural materials (39-50), biological materials (51-66), geological and environmental materials (67-78), metals (79-94), radioactive materials (95-107), waters (108-112), metals speciation and pre-concentration (109, 113-121), applications in process control (79, 97, 122-134), and other newly developed applications (88, 135-148). The scientific research and application development of ICP-AES are constantly reviewed and updated by the Application Update of *Analytical Chemistry* and the Atomic Spectrometry Update (ASU) of the *Journal of Analytical Atomic Spectrometry*.

1.2.3. ICP-AES Remains Competitive.

Admittedly the rapid development of ICP-MS in the past ten years has drawn much attention away from ICP-AES (149-152). ICP-MS shares techniques similar to ICP-AES for excitation and ionization of the analytes but uses a mass spectrometer as the detection system. ICP-MS offers significantly better detection limits, similar efficiency and sample throughput, less complicated spectra, and isotope ratio and isotopic dilution measurement (153-156).

In the recent past, ICP-MS was more difficult to operate and more expensive than either ICP-AES or GFAA. Now with the development of fifth generation instruments, the learning curve for ICP-MS operation has been significantly lowered and the price of the instrument has dropped. Thus any analytical lab with reasonable technical and financial assets should have little problem in affording an ICP-MS.

Will ICP-AES be able to survive such a stiff competition and stay in the main stream of elemental analysis?

The answer is YES.

According to a recent survey by *Analytical Chemistry* on "wet" chemical analysis instrumentation, the market for flame AA has been rapidly declining for the past few years. ICP-AES, although being affected by the rapid development of ICP-MS, remains competitive (22). The competitive edge of ICP-AES over ICP-MS, according to the author, is three fold. Firstly, the price of ICP-AES is considerably lower than that of ICP-MS. Secondly, more industrial standards, e.g. standards from EPA, are based on ICP-AES, and finally, ICP-AES has been accepted by many industries as a proven technology, thus usually it is the old instruments being replaced by new ones rather than the ICP-AES itself being replaced by new technologies.

Certainly none of these reasons would prevent ICP-MS from gaining more ground in elemental analysis in the long run. However, the current market shows that ICP-AES is still the instrument of choice for mid- to low level elemental analysis, with ICP-MS as the instrument of choice for ultra-low level measurements. As the workhorse for analytical laboratories around the world, ICP-AES is, and for the foreseen future, will remain the main force for elemental analysis.

1.3. ICP-AES Instrumentation.

1.3.1. Overview.

In ICP-AES analysis, the sample is usually transported into the instrument as a liquid stream that is converted into an aerosol through nebulization. The sample aerosol is then transported to the high temperature plasma where it is desolvated, vaporized, atomized and/or ionized, and excited (5, 6, 34). The excited atoms and ions emit their characteristic radiation that is collected by a spectrometer that sorts the radiation by wavelength. The radiation is detected and converted into electronic signals that are directly related to concentration information for the analytes. A schematic representation of a typical ICP-AES instrument is shown in Figure 1-1. The processes samples experience in an ICP-AES analysis are shown in Figure 1-2.

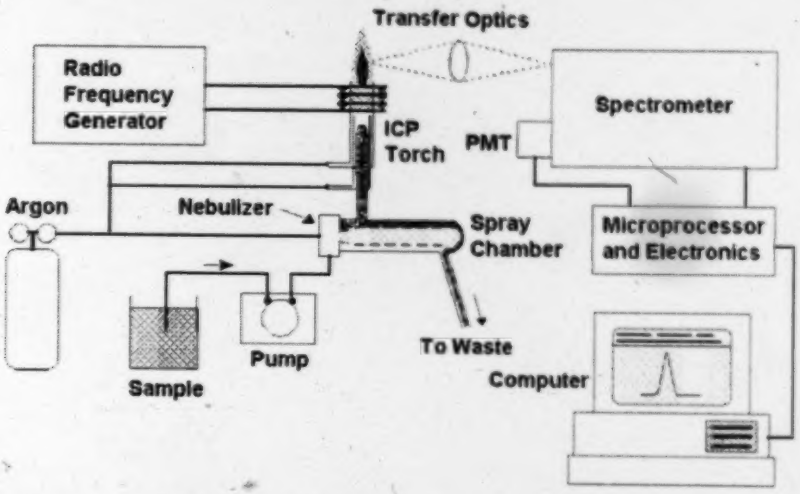

Figure 1-1. A typical ICP-AES instrument. Reprinted with permission from ref(157) © 1997 Perkin-Elmer Corp.

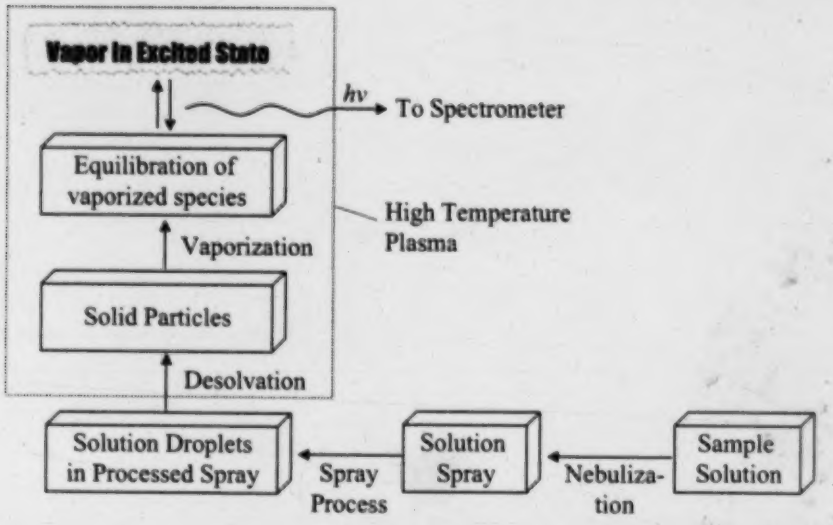

Figure 1-2. The processes a sample experiences in an ICP-AES analysis.

In this section, two types of popular commercial ICP-AES instruments, the simultaneous spectrometer based on an echelle spectrometer and solid-state detection and the more traditional sequential spectrometer based on a monochromator and PMT detection will be discussed in further detail along with Fourier transform spectrometers.

1.3.2. Simultaneous Spectrometer.

The greatest advantage of ICP-AES over atomic absorption is the ability of simultaneous measurement for all elements. This was, however, not fully realized until the introduction of the Optima 3000 by Perkin Elmer in 1993. Even though it was not the first ICP-AES instrument based on a solid-state detection system, it was the Optima that revolutionized the ICP-AES market and, in certain ways, atomic spectroscopy. With the combined power from a high resolution echelle grating (158)

and a Segmented-array Charge-coupled Device (SCD) detector (159) (Figure 1-3), the Optima 3000 provides real simultaneous measurement and can, as it is claimed, measure over 73 elements in less than a minute (160). The Optima offers over 6,000 spectral lines at different wavelengths, with a minimum of 2 to 4 selected ICP emission wavelengths for each element, allowing the flexibility to select lines least affected by line and matrix interference. The Optima also allows multiple wavelength detection for the elements to enhance quality control and increase confidence.

From Figure 1-3 it can be seen that the echelle grating of the Optima produces a 2D echellegram on the detector plane. The subarrays on different positions of the SCD see different portions of the spectrum simultaneously to achieve simultaneous coverage for over 6,000 emission and background wavelengths. As the Optima measures the spectral line emission and adjacent background simultaneously, one can perform real-time background subtraction to improve analytical accuracy and precision.

However, due to the nature of an echelle system, the spectral lines on the Optima detector plane are basically of high diffraction order, and many from different orders of diffraction. Although this would not affect routine analysis in any way, it precludes the possibility for assembly of a spectrum from Optima line intensity data for a given element. In addition, the incomplete wavelength coverage of the SCD detector also excludes this possibility.

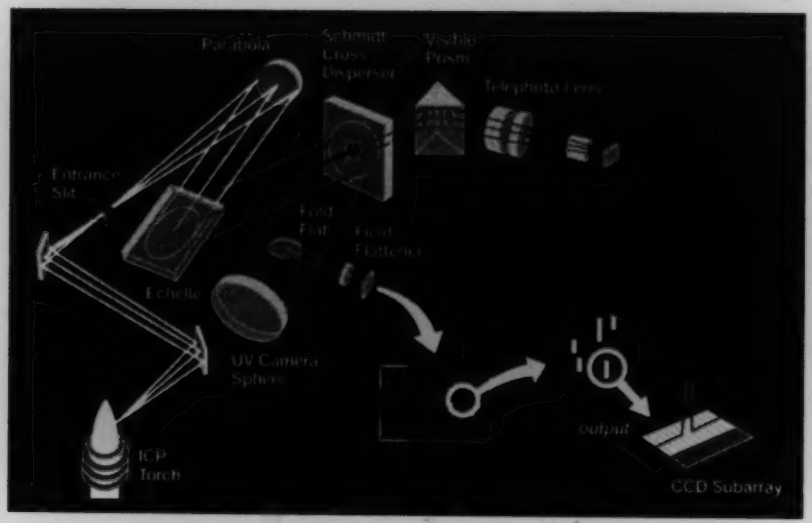

(a) Optical system of Optima 3000

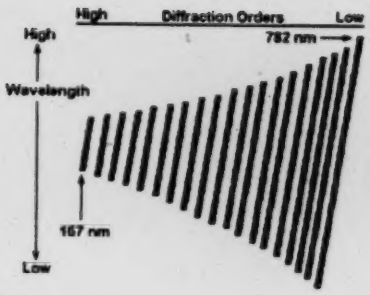

(b) Echellegram

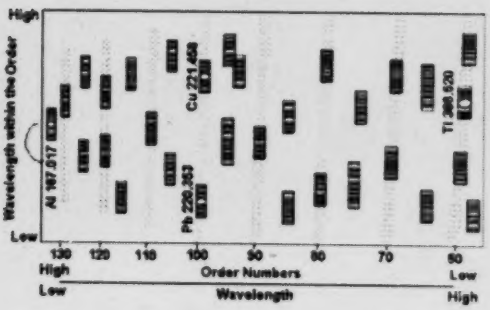

(c) SCD Detector

Figure 1-3. Optical and detection systems of the Perkin Elmer Optima. Reprinted with permission from ref(157) © 1997 Perkin-Elmer Corp..

An interesting design from Spectro is their CIROS CCD ICP-AES product line (161). CIROS stands for CIRcular Optical System, which, instead of an echelle, merges two high-resolution Paschen-Runge polychromators (34) into a single mount. With the so-called UV-Plus technology, CIROS is able to provide continuous first order wavelength coverage from 125 nm to 770 nm with a pixel resolution of 9 picometer. A complete wavelength "scan" from 125 to 770 nm for more than 10,000 emission lines takes less than a second. Currently there is no independent review available for the performance of this instrument. However, light throughput is expected to be improved with the use of first order light, and the stray light may be reduced in a single plane optical geometry, instead of a cross-dispersion system, as is used in echelle systems (162).

1.3.3. Scanning Spectrometer.

Most of the first generation ICP-AES instruments were scanning sequential spectrometers with a monochromator as the wavelength dispersion device. The Czerny-Turner mount (34) (Figure 1-4) was often the optical system of choice.

An example of a newly refined sequential ICP-AES instrument is the Ultima from Jobin Yvon. Introduced at Pittcon '98, the Jobin Yvon Ultima was equipped with a 2400 grooves/mm, 110 × 110 mm in size, ion-etched holographic grating mounted on a one-meter focal length Czerny-Turner mount (22, 163). This system provides high resolution with excellent efficiency over a wide working spectral range. The so-called High Dynamic Detectors (HDD) detection system, which consists of modified PMTs, provides a dynamic range from a single reading of

5×10^{10}, approximately six orders of magnitude more than that of a CCD based detection system.

An interesting aspect of the Ultima is that this instrument is designed to recover the full spectral information lost after the transition of atomic spectroscopy from photographic plates to PMTs. Combined with fast Direct Drive wavelength scanning system and the fast reading HDD detection system, Ultima can virtually create an digital "photographic plate", with enhanced dynamic range, covering a full wavelength range for about 250,000 spectral lines with at least 12 points per peak. If wavelength calibration for the Ultima can be done accurately without too much effort, it could be a very useful tool for ICP-AES fundamental studies.

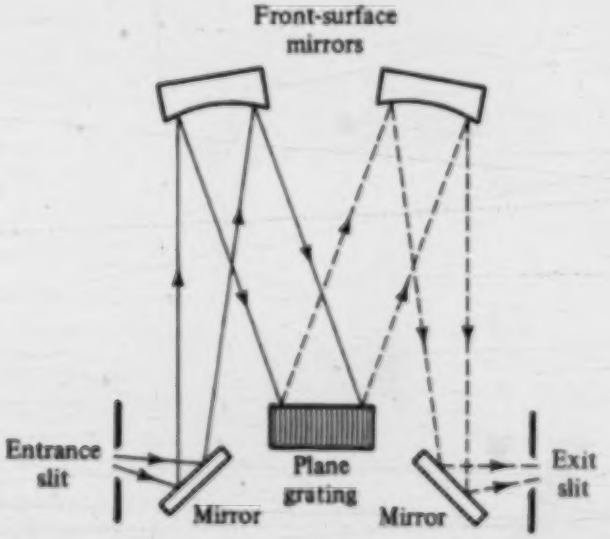

Figure 1-4. Czerny-Turner Mount. Reprinted with permission from ref (34) © 1988 Prentice-Hall, Inc.

1.3.4. Fourier Transform Spectrometer.

In addition to using an image detector or scanning through the wavelength range, an interferometric system (164) is another way to obtain large and continuous wavelength coverage. The Michelson interferometer, using a periodic mirror scan mechanism, provides wavelength and intensity information after Fourier Transformation of the data. Compared to the conventional dispersive instruments, a Fourier transform spectrometer (FTS) has the ability to measure absolute wavelength values with high precision and possibly with high accuracy; it has higher energy throughput and can achieve higher optical resolution; it also has the ability to monitor all spectral information nearly simultaneously for an extended period thus signal averaging can be performed to improve the signal to noise ratio in a measurement (165, 166). The major problems for ICP-FTS not being successful in the market place are the multiplex disadvantage, noise resulting from strong emission lines of the plasma, and the limited dynamic range (167, 168).

The basic components of a Michelson interferometer are shown in Figure 1-5. Radiation from the source falls on a beam-splitter and is split (amplitude-wise) into two beams of equal intensity, one is transmitted towards a fixed mirror and another reflected to a mirror moving at constant velocity. The reflected beams from these two mirrors are recombined at the beam-splitter and emerge as a single beam. At the detector the re-combined beam will form either a constructive or destructive interference pattern, or anything in between, depending on whether the optical path difference of the two constituent light beams is exactly equal to $n\lambda$, or $n\lambda/2$, or in between, respectively, where n is a integer and λ is the source wavelength. With a

monochromatic source, the interferogram observed at the detector is a cosine wave. The frequency of this cosine waveform, or the modulation frequency, depends on the source wavelength and the moving mirror velocity. The amplitude of this waveform is proportional to the intensity of the incident monochromatic radiation. If the incident radiation is polychromatic, each wavelength component will be transformed so that the detector output is the sum of all cosine waveforms from each wavelength component (that is, an interferogram).

Fourier transformation of this composite signal can be used to obtain wavelength/wavenumber domain information, or spectra, from interferograms. The concept of Fourier transformation, and its application in spectroscopy will be discussed in further detail later in this chapter.

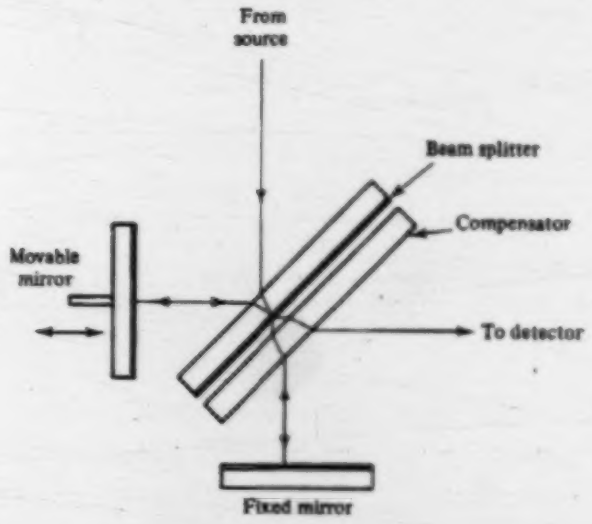

Figure 1-5. Basic Components of a Michelson interferometer. Reprinted with permission from ref (34) © 1988 Prentice-Hall, Inc.

1.4. The Need for ICP-AES Spectral Reference Data

Compared to the traditional atomic spectroscopic techniques like arc and spark emission spectroscopy, ICP-AES has probably received the most attention in terms of fundamental research and application development, which it rightly deserves considering the vast applications ICP-AES still has today and the revolutionary change it brought into elemental analysis (5, 32). It is surprising that, two and a half decades after the introduction of the first commercial ICP-AES instrument and with thousands of published research papers and several books for this technique, the very basic data, the wavelength and intensity values from "real" ICP emission lines, are not readily available, or at least not as readily available as for arc or spark spectral lines.

Everyone understands and agrees that quality reference data are important, from daily life to every field of science and technology. Just as a good dictionary is important for language study, quality reference data for a specific technique are always a key component for all activities related to that technique, and is often important for techniques related to it. For ICP-AES, the reference data, noticeably the wavelength values, intensities, and energy levels are essential to the fundamental understanding and research, essential for the design and manufacture of the commercial instrument, essential for the applications development, and essential for education.

With today's technology, quality reference data are even more important than before (169) as reliable data are the common essential element for modeling and simulation dominated research, for computer aided design and virtual testing, and for

today's industry that is driven by quality and model-based processing and manufacturing. As for analytical atomic spectroscopy, a science where spectral data is common language, it is surprising that reference data for ICP-AES is so sparse compared to other techniques in this field. One would wonder what would be the reasons behind this situation?

One of the facts that might contribute to this situation is that, compared to other techniques, ICP-AES is built upon the vast research and development of other atomic spectroscopic methods such as arc, spark, and glow discharge emission. As the atomic structure, energy levels, and transition probabilities for all elements are well defined by modern physics, one would expect much similarity for the ICP emission compared to the well-known arc or spark spectrum. In other words, as all atomic structures and energy levels are well characterized, ICP emission lines would be predictable. How close is this speculation to the reality?

Let's take Mg as an example. The emission spectra for a magnesium hollow cathode lamp (Mg HCL) and Mg ICP are shown in Figure 1-6. It can be seen that, determined by the atomic energy levels of magnesium, these two spectra share many spectral lines with the same wavelength values. It is also noticed, however, that there are some lines in the Mg HCL spectrum that cannot be found in the Mg ICP spectrum and other lines appear with significantly different relative intensities. In fact, even though the atomic spectral lines are determined by the atomic structure of the element, it is common to see that spectra from different emission sources differ significantly from each other. Thus, even for the same element, an emission

spectrum from one source cannot be assumed to be the same as a spectrum from another source.

The second reason behind this situation might be that the ICP is "too good". For spectroscopists who were accustomed to the tough sources like arc or spark, the ICP discharge is so robust, so easy to use, so interference "free" that there is little room left for concerns. This romantic picture, unfortunately, is not true.

Generally, two major interferences exist in analytical atomic spectroscopy: the chemical interference and the spectral interference. Traditional sources like arc and spark suffer from both interferences and special attention has to be paid in order to obtain accurate results. For ICP, chemical or matrix interference is minimal, and at the early stage of ICP-AES, the spectral lines used were limited and thus spectral line selection was limited to some best characterized lines. With a scanning spectrometer, line selection is generally not a problem as a portion of the spectrum can readily be scanned to assist identifying any potential spectral interference at a particular wavelength. For polychromator direct readers, the line decision process is simple as lines are selected by the manufacturers and cannot be easily changed. However, if spectral interference is suspected at a preset wavelength, that wavelength has to be discarded and these situations can be difficult to recognize. With the advent of the CCD detector based instruments, a broad knowledge of spectral lines becomes very important, sometimes critical, to the successful analysis of real world samples, particularly those with a complex matrix.

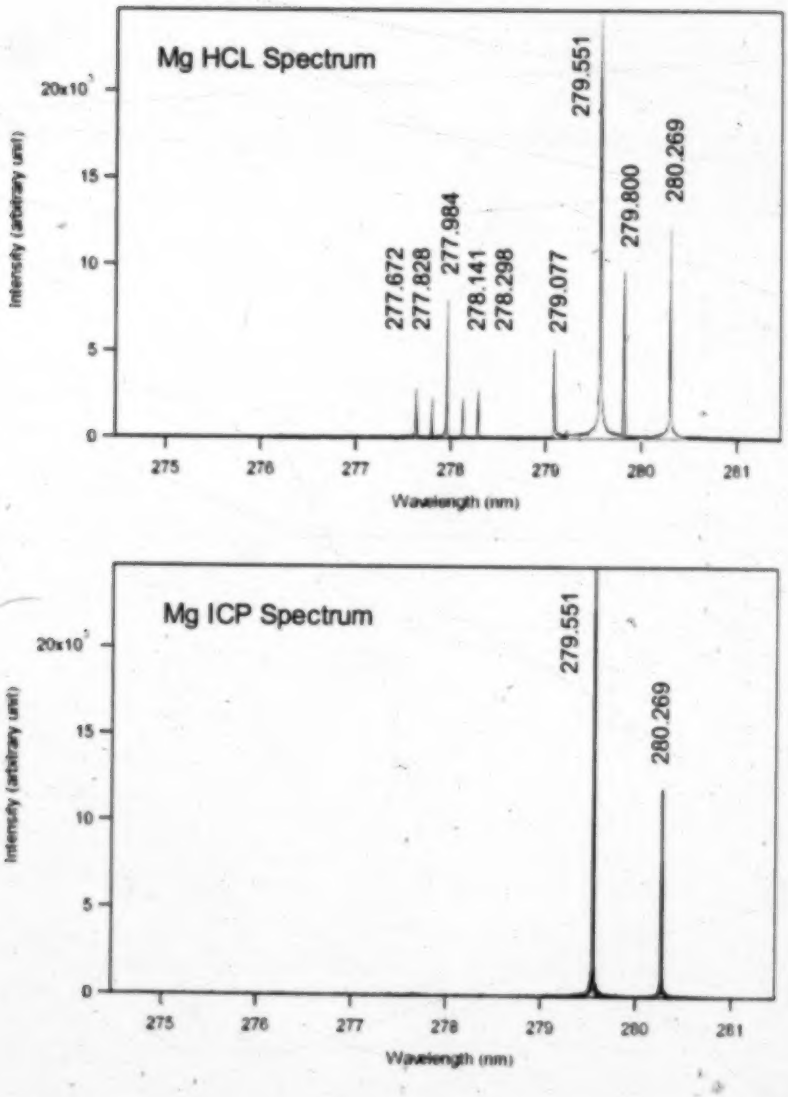

Figure 1-6. Mg HCL and ICP Spectra showing different spectral lines.

The third explanation for this situation is a technical one. Providing a set of complete reference data for atomic spectral lines is by no means an easy task. It is a heavy workload for any single research group or organization. Some attempts have been made to obtain such data during the last two decades, but often these attempts ended with either acquiring data for only some of the elements or collecting only very few major spectral lines (24, 25, 170, 171). NIST started an ambitious program in 1985 to establish an atomic spectral line database for ICP-AES from scratch (172). The first phase of the program was to collect all spectra for all elements with a high-resolution spectrometer at concentrations spanning six orders of magnitude. This portion of the work was done in the early 90's and provided realistic relative intensity information for all spectral lines, which are valuable for line selection, modeling, and simulation. The second projected step was to obtain wavelength "marks" for these spectra with a high resolution ICP-FTS designed at Imperial College (London, England). Combined with accurate wavelengths from ICP-FTS measurements and reliable intensity information from the high-resolution spectrometer, it was believed a high quality, fully ICP-AES based atomic spectral database would be readily available. Spectral data for a few elements resulting from this project appeared on the NIST website in 1995. This first version of the database contained wavelengths and energy levels for approximately 20 elements. Then, from 1997, the process of publishing new data seemed to stop. Instead, compiled data from the original NIST wavelength table (173) and some newly published work were adapted into this database. Now the second version of the database, based on the work from NIST Atomic Spectral Database (ASD) program, covers observed

transitions of 99 elements and energy levels of 52 elements. ASD contains data on about 950 spectra from about 0.1 to 2000 nm, with about 70,000 energy levels and 90,000 lines, 40,000 of which have transition probabilities. The most current NIST-evaluated data associated with each transition are integrated under a single listing, the NIST ASD (Figure 1-7).

It can be seen that now the NIST ASD is basically an electronic version of the modified and updated NIST wavelength table books. Because this original data was used to make up for the slow adoption of the ICP-AES data, ASD is no longer an exclusive ICP-AES database as originally planned. Rather, it is a general reference data for the transition probabilities and energy levels, and, like its predecessor, the valuable graphical representation – the spectra for the elements, have been left out.

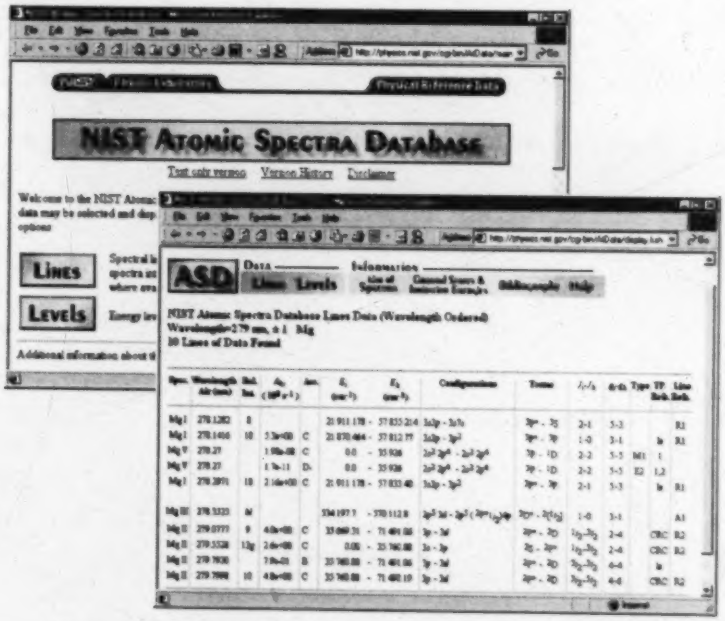

Figure 1-7. NIST ASD Home page and a list of Mg lines.

1.5. ICP-FTS: Solutions for the Spectral Library.

1.5.1. Digital Fourier Transform.

In this section, the concepts and advantages of Inductively Coupled Plasma – Fourier Transform Spectrometry (ICP-FTS) will be presented along with some important aspects of the digital Fourier Transform.

1.5.1.1. Time and Frequency Domains.

Time and frequency domains are two basics of scientific measurements, and the Fourier Transform is the bridge between them (164, 165, 168, 174).

In the time domain, time is used to record the order things happened. As the moving mirror in a Michelson interferometer usually moves at constant velocity and the moving distance is directly proportional to time, distance is sometimes used to substitute for time as the variable for time domain functions.

In the frequency domain, frequency is used to describe the change of other physical properties. For example, a spectrum describes what is the value of amplitude at each frequency point. For spectroscopists, that is the basic meaning of a frequency domain function.

Nearly all real waveforms can be described as being in either the time or frequency domain. Figure 1-8 shows the two representation of a sine wave. On the top is the familiar time domain sine wave, and at the bottom is its frequency domain representation consisting of an amplitude and a phase spectrum. Although the two representations differ visually, they represent a single wave function and, if one of the two is known, the other can be calculated (174).

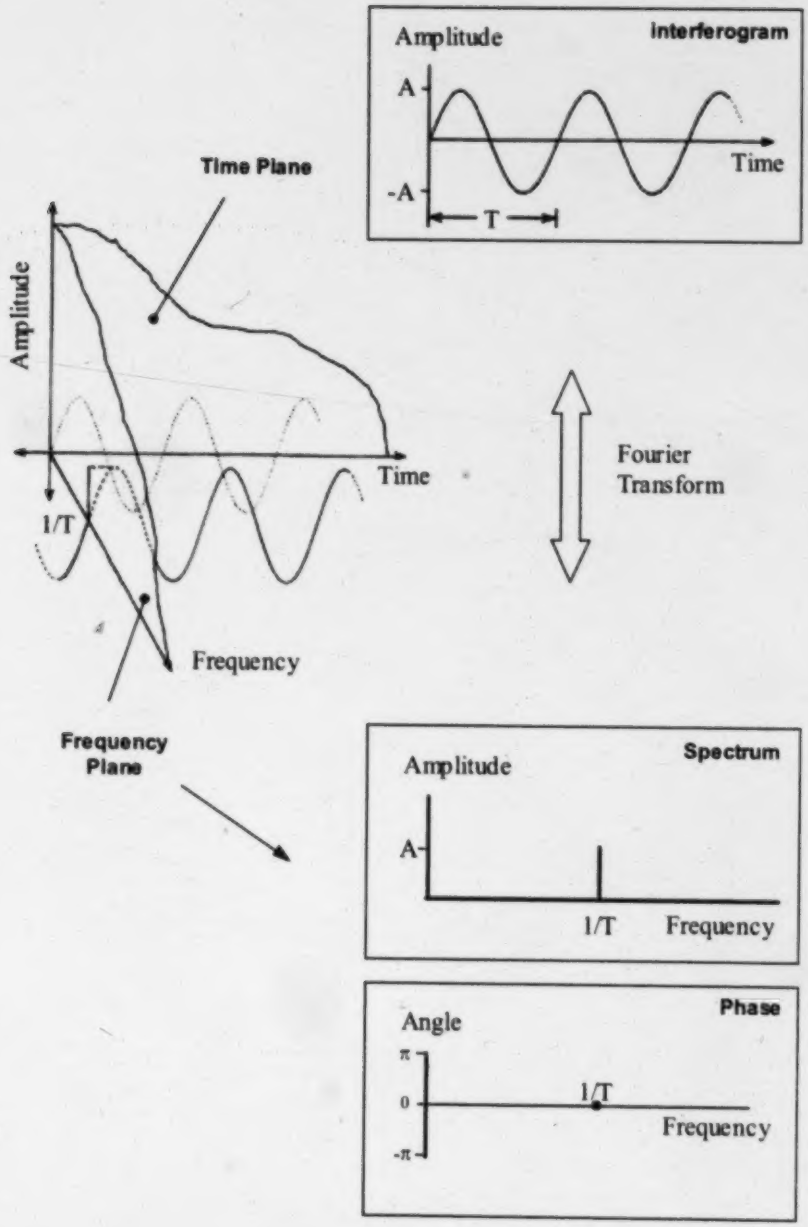

Figure 1-8. Time and Frequency domain description of a sine wave.

This unique relationship between the time domain waveform and the frequency domain spectrum is the foundation of the interferometric measurements, and the mathematical technique to get frequency domain information (including amplitude and phase spectra) and vice versa, is Fourier Transformation (165, 168).

1.5.1.2. Fourier Transformation

In 1822, Jean Baptiste Joseph Fourier proposed that a mathematical series of sine and cosine terms could be used to describe periodic waveforms and allow transformation of physically realizable time domain waveforms to the frequency domain and vice versa (175). The general form of the Fourier series is

$$x(t) = a_0 + \sum_{n=1}^{\infty} (a_n \cos 2\pi f_0 t + b_0 \sin 2\pi f_0 t)$$

Where x(t) on the left of the equation is the time domain function and the function on the right is its frequency domain representation.

However, from a practical point of view, there is no real waveform in spectroscopic measurements that meets the strict mathematical "periodic" requirement that extends from negative infinity to positive infinity. Rather, these "periodic waveforms" only exist in a finite time window. For these types of waveforms, as for all other non-periodic time-domain functions, Fourier analysis can only be performed with the Fourier Integral (165):

$$X(f) = \int_{-\infty}^{\infty} x(t) e^{-2\pi i f t} dt$$

$$x(t) = \int_{-\infty}^{\infty} X(f) e^{2\pi i f t} df$$

The Fourier Transform pair above shows clearly that through Fourier analysis the close relationship between the two representations of a waveform in the time and frequency domain can be established. As will be seen later, this makes it possible to get a spectrum from the time domain waveform, or interferogram, produced by a Michelson Interferometer (165).

1.5.1.3. Digitization Noise and Signal Averaging

In FT spectroscopy, light is modulated to a relatively low frequency analog waveform (e.g. a cosine wave in the time domain) and must be converted to its digital representation before it can be transformed into the frequency domain with Fourier Transformation. Digitization errors refer to the errors introduced by such conversions. They are common to any case involving similar conversion and are not unique to Fourier Transformation (174, 176-178).

The first type of error, *Time Jitter*, is introduced during data acquisition by small errors in the sampling time (or distance). For example, if the sampling time is controlled by a triggering level on a real-world sine wave in which frequency variation and noise components are inevitable, then the sine wave will reach the triggering level slightly sooner, later, or at the same time as for an ideal waveform. This introduces small but not insignificant error on the sampling timing.

For single-shot sampling or digitization, *Time Jitter* is usually not a major problem. If, however, several sweeps of the waveform are required to build up a full complement of samples, the effect of *Time Jitter* is a shifting of some samples on the waveform with respect to other samples. Fortunately, sampling errors from *Time*

Jitter are often random in occurrence and like random noise can be reduced by signal averaging.

The second type of digitization error is *Quantizing Error*, which originates from the finite resolution of the digitizer. That is, when the analog waveform is sampled, the real value often falls in between two adjacent digital levels and has to round off to the closest digital value. Thus instead of getting a smooth line as that of the analog waveform, the digital waveform will look like tiny "stairs" from one digital level to another. The difference between the stepwise digital waveform and the smooth line of the analog waveform is the *Quantizing Error*. As this is determined by the nature of the analog waveform being sampled and the resolution of the digitizer, *Quantizing Error* is not random in nature and thus, by itself, could not be reduced by signal averaging.

Since *Quantizing Error* cannot exceed half a digital level, it is generally small compared to other types of noise. Although using a digitizer with higher digital resolution can reduce *Quantizing Error*, there is always a limit. In practice, *Quantizing Error* can actually be reduced by signal averaging. This nice surprise comes from the fact that additional noise in the process, e.g. additive noise or jitter, can inject a certain level of randomness into the *Quantizing Error* and thus made it possible to reduce it by signal averaging (174).

1.5.1.4. Aliasing

Aliasing is a common phenomenon when under-sampling occurs. Real life examples are from the steady wheels of a horse wagon in a western movie to the backwards-turning electric fan under fluorescent lights. In Fourier Transform spectroscopy, aliasing usually occurs when the wavelength of the light signal falls into the UV-visible range and it introduces some unique and predictable but spurious lines into spectra (168, 179, 180).

Obviously, an exact description of a signal with unrestricted variations can be obtained only if the intervals between sampling points approach zero. For band limited signals, however, there is a finite sampling rate that is sufficient to include all the information in the signal. This sampling rate, as defined by the Nyquist Theorem (174), is twice the frequency of the highest frequency component in the signal to be sampled. If the Nyquist frequency is not satisfied, aliasing will occur. Figure 1-9 shows how a 25 Hz alias is formed when a 175 Hz sine wave is sampled at a 200 Hz sampling rate.(176)

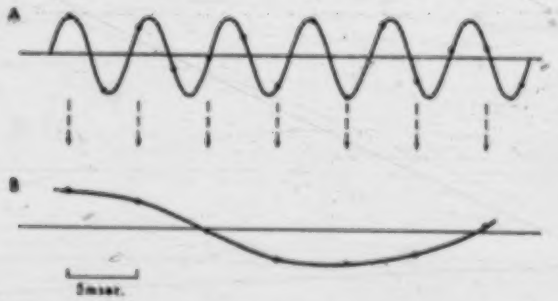

Figure 1-9. Aliasing of a 175 Hz sine wave to a 25 Hz sine wave by undersampling. Reprinted with permission from ref(176) © 1970 American Chemical Society

Most Fourier Transform spectrometers rely on the red HeNe laser that has a wavelength of 632.8164 nm as their sampling reference (164). According to the Nyquist rule, these spectrometers can only correctly sample any signal with a wavelength longer than 1300 nm without aliasing. That is why most commercial FT-IR spectrometers seldom have problems with aliasing. For a UV-Visible FTS spectrometer, as the one used in this project, aliasing will occur for all spectra covered if the base frequency of the red HeNe laser is use for sampling. Even though the alias lines are completely predictable, to separate them from each other and put them in the right position on a wavelength axis is by no means an easy task. Figure 1-10 shows an example of how a spectrum can be folded over due to aliasing (179).

A group of alkali metal spectral lines with wavelength ranging from 670 to 894 nm were sampled at an interval derived from the base wavelength of the 632.8 nm HeNe laser line. For Spectrum (a) the sampling interval was halved so that the interferogram was sampled at intervals of 316.4 nm. All alkali metal lines were properly sampled and no aliasing occurred as they all have wavelengths longer than 632.8 nm. Spectrum (b) was sampled with the base interval of 632.8 nm. In this case the cut-off wavelength is 1266 nm, thus no alkali line was properly sampled according to the Nyquist theorem and all spectral lines fold over along the wavenumber axis. Because of aliasing, the axis is now labeled from right to left for wavenumber in order to show correct wavelength.

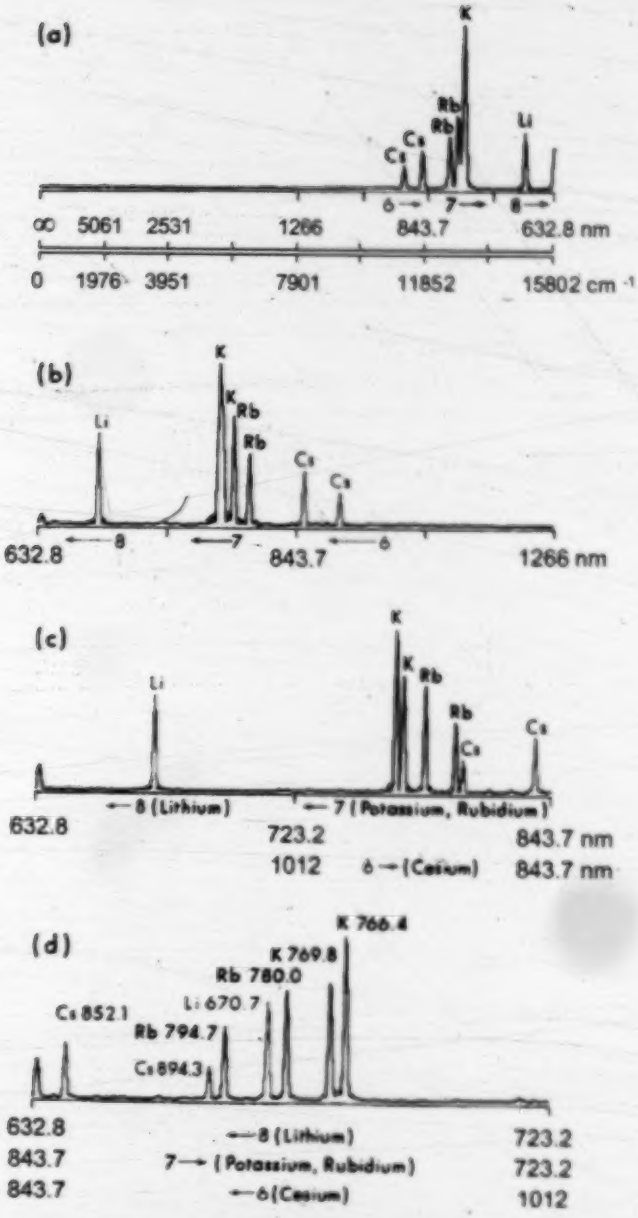

Figure 1-10. Aliasing illustrated by Flame emission spectra sampled at different sampling rate. Reprinted with permission from ref(179) © 1977 America Chemical Society.

The third spectrum, Spectrum (c), was sampled at twice the interval of the HeNe laser or at a sampling interval of 1266 nm. Thus aliasing would occur again for any line with an apparent (i.e. aliased) wavelength longer than 790 nm, that is, the two Cesium lines. When the sampling interval was further reduced to a quarter of the laser base frequency, all spectral lines except that of Li 670.7 nm folded over again on the wavenumber axis as their aliased frequencies were higher than twice of the sampling rate.

It can be seen from Figure 1-10 that, although aliasing lines are predictable and it is not too difficult to assign a correct aliasing region and wavelength, spectra with lines from several different aliasing regions could be misleading and very confusing for inexperienced readers. Thus aliasing should be avoided whenever possible for the spectral library to accommodate users of different levels.

It can also be noticed that, from spectrum (a) to (d), as the sampling frequency decreases, the resolution of the spectrum increased significantly. It is well known that the resolution of the frequency domain spectrum depends on the total length of the waveform in the time domain, that is, the length of the interferograms (179). The total number of points for the data in Figure 1-10 is fixed and at a lower sampling frequency a longer length of interferogram is sampled and thus the higher the resolution. In some cases, if the aliasing lines will not overlap with lines from other regions and thus not cause confusion, this unique property of FTS can actually be used to improve the resolution of a transformed spectrum.

Finally notice the labeling of the frequency (or wavelength) axis. The FTS transformed spectrum has a uniform frequency axis in terms of cm^{-1}. Thus when the

spectrum is displayed in wavelength (nm), the axis is plotted backwards from right to left (a). If aliasing occurs and assuming only one fold over, then the spectrum will be displayed in a "normal" axis direction (left to right) for wavelength (b). As shall be seen later, in this spectral library, all visible spectra are displayed from long wavelength to short wavelength (from left to right), and UV spectra are plotted with short wavelength to long wavelength (from left to right) due to aliasing.

1.5.2. Building the Spectral Library with ICP-FTS.

As a general reference for spectroscopists, the goal for the Spectral Library is to provide full wavelength coverage for ICP-AES with accurate wavelength values and correct intensity information for all spectral lines. The spectra should have reasonably high resolution, high interactivity and accessibility with personal computers. It should also provide all the information carried by spectra that is lost in the wavelength tables.

As discussed before, although state-of-the-art ICP-AES spectrometers have high sensitivity, precision, and stability, they are still not suitable for this task. For sequential scanning spectrometers the major problems are lack of the necessary spectral resolution and difficulty in exact wavelength calibration. For solid state based spectrometers, continuous first order wavelength coverage for the desired wavelength range is not usually available and thus neither of the two popular commercial spectrometers is capable of building the spectral library.

Fourier Transform Spectrometers, on the other hand, are superior in many aspects as instruments of choice for building a spectral library.

It is well known that FTS provides high precision and accuracy for wavelength values for transformed spectra. The wavelength values from a Michelson interferometer depend only on the accuracy of the wavelength of the HeNe reference laser(180), which has been well characterized and its value is highly accurate, reliable, and stable.

The i'th wavenumber value (σ_i) in a spectrum is given by (180):

$$\sigma_i = \frac{i}{N\lambda_{HeNe}}$$

Whereas: σ_i is the wave number of the *i*th datapoint.
N is the total data points in that interferogram.
λ_{HeNe} is the sampling interval measured as reference laser wavelength.

As can be seen from above equation, the wavelength value of each data point in the spectrum is determined only by the relative position of that point in the spectra and the reference laser wavelength value. Thus, at least in theory, the wavelength value for every spectral line is accurate and does not vary line by line.

In practice, however, as the reference laser has to be adjusted so that it is not perfectly perpendicular to the mirrors to avoid feedback of the laser beam into laser cavity, the reference laser wavelength appears slightly different from its actual value. Thus the great wavelength accuracy of FTS might not be achieved directly but the precision remains (168). King and Horlick (181) suggested that the FTS be calibrated for wavelength values for high accuracy work. In this method, several Fe spectral lines with well-known wavelength values were selected. Their observed wavelength values with the FTS were compared with the literature values and the apparent wavelength values of the reference laser can thus be calculated. The average value of the apparent laser wavelength was then used to re-calibrate the Fe spectrum for the

wavelength values of all spectral lines. As the deviation of the laser wavelength is caused by the angle of the laser mounting, under certain experimental condition this deviation should be a constant and thus, once corrected, will re-establish the high wavelength accuracy of the FTS.

In the present work, high-resolution interferograms for 71 elements in the UV and visible regions are collected under optimal experimental conditions. These interferograms are then transformed into corresponding UV and visible spectra for each element. Then the spectra are calibrated according to the method described above and wavelength values of up to the 30 most intense lines in each spectrum are reported and compared to literature values. The full spectral library, including all interferograms and UV and visible spectra are stored on a Mac HFS format CD, and can be accessed with the *SpectroPlot* program developed by Greg King (181). Users with Microsoft Windows based computers can access this library distributed in ASCII text format with any technical graphing software.

Reference

(1) Boumans, P. W. J. M.; Bastings, L. C.; De Boer, F. J.; Van Kollenburg, L. W. J.: *Fresenius' Z. Anal. Chem.* **1978** *291*, 10-19.

(2) Fassel, V. A.: Current and potential applications of inductively coupled plasma (ICP)-atomic emission spectroscopy (AES) in the exploration, mining, and processing of materials; Report IS-M-85 **1976**, 14 pp.

(3) Fassel, V. A.: Inductively coupled plasma-atomic emission spectroscopy: an alternative approach to "flameless" atomic absorption spectroscopy; Report IS-M-62 **1976**, 45 pp.

(4) Fassel, V. A.: *Pure Appl. Chem.* **1977** *49*, 1533-45.

(5) Montaser, A.; Golightly, D. W. Inductively Coupled Plasmas in Analytical Atomic Spectrometry;; VCH Publishers, Inc, 1992.

(6) Beaty, R. D.; Kerber, J. D. *Concept, Instrumentation, and Techniques in Atomic Absorption Spectroscopy*; 1st ed.; Perkin-Elmer Corp.: Norwalk CT, 1993.

(7) Perkin-Elmer: *The Guide to Techniques and Applications of Atomic Spectroscopy*; Perkin-Elmer Corp.: Norwalk CT, 1995.

(8) Olesik, J.: *Anal. Chem.* **1996**, 438A.

(9) De Kersabiec, A. M.; Mermet, J. M.: *Spectra Anal.* **2000** *29*, 11-20.

(10) Djingova, R.; Kuleff, I.: *Trace Met. Environ.* **2000** *4*, 137-185.

(11) Boumans, P. W. J. M.: Inductively Coupled Plasma Emission Spectroscopy In *Chemical Analysis*; Elving, P. J., Winefordner, J. D., Eds.; John Wiley & Sons: New York, 1987; Vol. 90.

(12) Blades, M. W.; Weir, D. G.: *Spectroscopy* **1994** *9*, 14.

(13) Furuta, N.; Horlick, G.: *Spectrochim. Acta, Part B* **1982** *37*, 53.

(14) Maly, K.: *Oesterr. Chem. Z.* **1999** *100*, 36-37.

(15) Evans, E. H.; Chenery, S.; Fisher, A.; Marshall, J.; Sutton, K.: *J. Anal. At. Spectrom.* **1999** *14*, 977-1004.

(16) Fisher, A.; Hill, S. J.: *Induct. Coupled Plasma Spectrom. Its Appl.* **1999**, 71-97.

(17) Greenfield, S.; Foulkes, M.: *Induct. Coupled Plasma Spectrom. Its Appl.* **1999**, 1-34.

(18) Walsh, J. N.: *Mod. Anal. Geochem.* **1997**, 41-66.

(19) Hwang, J. D.; Wang, W. J.: *Appl. Spectrosc. Rev.* **1995** *30*, 231-350.

(20) Horlick, G.; Furuta, N.: *Spectrochim. Acta, Part B* **1982** *37*, 999.

(21) Mermet, J.-M.; Poussel, E.: *Applied Spectroscopy* **1998** *49*, 12A.

(22) Erickson, B.: *Anal. Chem.* **1998** *70*, 211A-215A.

(23) Boumans, P. W. J. M.; Sheeline, A.: Needs for Fundamental data in analytical atomic spectroscopy; Scarborough Ontario Canada **1987**.

(24) Huang, B.; Wang, X.; Yang, P.; Ying, H.; Su, S.; Zhang, Z.; Zhuang, Z.; Sun, Z.; Li, B. *An Altas of High Resolution Spectra of Rare Earth Elements for ICP-AES*; The Royal Society of Chemistry, 2000.

(25) Winge, R. K.; Fassel, V. A.; Peterson, V. J.; Floyd, W. A. *Inductively Coupled Plasma-Atomic Emission Spectroscopy: An Atlas of Spectral Information*; 1st ed.; Elsevier: New York, 1985.

(26) Boumans, P. W. J. M.; Tielrooy, J. A.; Maessen, F. J. M. J.: *Spectrochim. Acta, Part B* **1988** *43B*, 173.

(27) Boumans, P. W. J. M.; Zhuang, H. Z.; Vrakking, J. J. A. M.; Tielrooy, J. A.; Maessen, F. J. M. J.: *Spectrochim. Acta, Part B* **1989** *44B*, 31.

(28) Daskalova, N.; Velichkov, S.; Slavova, P.: *Spectrochim. Acta, Part B* **1996** *51B*, 733-768.

(29) Daskalova, N.; Velichkov, S.; Slavova, P.: *Spectrochim. Acta, Part B* **1992** *47B*, E1595.

(30) Velichkov, S.; Daskalova, N.; Slavova, P.: *Spectrochim. Acta, Part B* **1993** *48B*, E1743-89.

(31) Boumans, P. W. J. M.; Vrakking, J. J. A. M.; Heijms, A. H. M.: *Spectrochim. Acta, Part B* **1988** *43B*, 1365-404.

(32) Fassel, V. A.: Forward In *Inductively Coupled Plasmas in Analytical Atomic Spectrometry*; Montaser, A., Golightly, D. W., Eds.; VCH Publishers, Inc, 1992.

(33) Greenfield, S.; Jones, I. L. I.; C.T.Berry: *Analyst* **1964** *89*, 713.

(34) Ingle, J. D. J.; Crouch, S. R. *Spectrochemical Analysis*; 1st ed.; Prentice-Hall, Inc: Upper Saddle River NJ, 1988.

(35) Walsh, A.: *Anal. Chem.* **1974** *46*, 698A.

(36) Varian *Vista CCD Simulanous ICP-AES Product Brochure*; Varian Australia Pty Ltd, 1998.

(37) Boumans, P. W. J. M.: *Guangpuxue Yu Guangpu Fenxi* **1986** *6*, 26-39.

(38) Meyer, G. A.; Keliher, P. N.: An Overview of Analysis by Inductively Coupled Plasma-Atomic Emission Spectrometry In *Inductively Coupled*

Plasmas in Analytical Atomic Spectrometry; Montaser, A., Golightly, D. W., Eds.; VCH Publishers, Inc, 1992.

(39) Fujikawa, Y.; Satta, N.; Tagami, K.; Yasuda, H.; Uchida, S.; Fukui, M.: *Kyoto Daigaku Genshiro Jikkensho Gakujutsu Koenkai Hobunshu* **1995** *29*, 175-84.

(40) Velez, D.; Ybanez, N.; Montoro, R.: *J. Agric. Food Chem.* **1995** *43*, 1289-94.

(41) Miller-Ihli, N. J.: *J. Agric. Food Chem.* **1996** *44*, 2182-2186.

(42) Liu, W.; Liu, C.; Lu, X.; Yao, Z.; Song, B.: *Fenxi Shiyanshi* **1997** *16*, 90-93.

(43) Liang, S.; Qin, Y.: *Guangpu Shiyanshi* **1997** *14*, 15-18.

(44) Haneklaus, S.; Harms, H.; Nowak, G. A.; Schnug, E.; Wierzbowska, J.: *Chem. Inz. Ekol.* **1999** *6*, 67-75.

(45) Raven, K. P.; Reynolds, J. W.; Loeppert, R. H.: *Commun. Soil Sci. Plant Anal.* **1997** *28*, 237-257.

(46) Liu, S.-y.; Zu, G.-l.; Lin, Y.-k.; Chang, T.-w.; Wang, J.-y.: *Zhonghua Nongye Yanjiu* **2000** *49*, 28-35.

(47) Kampf, N.; Zohar, C.; Nussinovitch, A.: *Biotechnol. Prog.* **2000** *16*, 480-487.

(48) Yasui, A.; Shindoh, K.: *Bunseki Kagaku* **2000** *49*, 405-410.

(49) Wang, J.; Yi, H.; He, C.; Li, H.: *Commun. Soil Sci. Plant Anal.* **1999** *30*, 599-603.

(50) Kronka, E. A. M.; Reis, B. F.: *Quim. Anal. (Barcelona)* **1998** *17*, 15-20.

(51) Brown, A. A.; Halls, D. J.; Taylor, A.: *J. Anal. At. Spectrom.* **1988** *3*, 45R-88R.

(52) Qiu, H.; Liu, J.: *Guijinshu* **2000** *21*, 28-30.

(53) Sanz-Medel, A.: *Tec. Lab.* **1992** *14*, 18-29.

(54) Shibata, Y.: *Jpn. J. Toxicol. Environ. Health* **1996** *42*, 385-401.

(55) Haraguchi, H.; Inagaki, K.; Takeuchi, S.; Arakawa, Y.: *Biomed. Res. Trace Elem.* **1997** *8*, 119-125.

(56) Shao, L.: *Huaxue Shijie* **1999** *40*, 288-290.

(57) Yuan, Z.; Han, S.; Zhu, M.: *Yaoxue Xuebao* **1999** *34*, 475-480.

(58) Frache, R.; Rivaro, P.: *Chem. Processes Mar. Environ., [Int. Sch. Mar. Chem.], 2nd* **2000**, 201-211.

(59) Eilola, K.; Peramaki, P.: *Fresenius' J. Anal. Chem.* **2001** *369*, 107-112.

(60) Zhou, X.; Cheng, F.; Nin, M.: *Guangpuxue Yu Guangpu Fenxi* **2000** *20*, 361-363.

(61) Trynda-Lemiesz, L.; Karaczyn, A.; Keppler, B. K.; Kozlowski, H.: *J. Inorg. Biochem.* **2000** *78*, 341-346.

(62) Szaloki, I.; Braun, M.; Van Grieken, R.: *J. Anal. At. Spectrom.* **2000** *15*, 843-850.

(63) Sun, H.-T.; Liu, Y.-G.; Xu, K.-M.: *Guangpu Shiyanshi* **2000** *17*, 403-405.

(64) Somogyi, G.; Jenei, E.; Szokol, J.; Buris, L.; Buris, L., Jr.; Nagy, D.; Pap, L.: *Pharmazie* **2000** *55*, 239-242.

(65) Reitznerova, E.; Amarasiriwardena, D.; Kopcakova, M.; Barnes, R. M.: *Fresenius' J. Anal. Chem.* **2000** *367*, 748-754.

(66) Qiu, H.-L.; Liu, J.-S.; Hong, Y.: *Guangpu Shiyanshi* **2000** *17*, 416-418.

(67) Sutton, K. L.; Caruso, J. A.: *Induct. Coupled Plasma Spectrom. Its Appl.* **1999**, 245-272.

(68) Jenniss, S. W.; Katz, S. A.; Lynch, R. W.: *ACH - Models Chem.* **1999** *136*, 55-68.

(69) Sturgeon, R. E.: *Commun. Soil Sci. Plant Anal.* **2000** *31*, 1479-1512.

(70) Landsberger, S.; Kaminski, M.; Basunia, M.; Iskander, F. Y.: *J. Radioanal. Nucl. Chem.* **2000** *244*, 35-40.

(71) Jiang, Z.-c.; Hu, B.; Peng, T.-y.; Qin, Y.-c.; Liao, Z.-h.: *Yankuang Ceshi* **2000** *19*, 122-128.

(72) Hirata, S.: *J. Flow Injection Anal.* **2000** *17*, 23-35.

(73) Haraguchi, H.; Inagaki, K.: *Bunseki* **1998**, 494-503.

(74) Niedzielski, P.; Baralkiewicz, D.; Siepak, J.: *Ekol. Tech.* **1996** *4*, 26-30.

(75) Haraguchi, H.; Itoh, A.: *Kikan Kagaku Sosetsu* **1996** *29*, 35-57.

(76) Balaram, V.: *TrAC, Trends Anal. Chem.* **1996** *15*, 475-486.

(77) Vaisanen, A.; Matilainen, R.; Tummavuori, J.: *Fresenius' J. Anal. Chem.* **2000** *367*, 755-760.

(78) Sutherland, R. A.; Tolosa, C. A.: *Environ. Pollut. (Oxford, U. K.)* **2000** *110*, 483-495.

(79) Kim, H. Y.; Lim, H. B.: *Anal. Chim. Acta* **2001** *429*, 145-150.

(80) Danzaki, Y.; Wagatsuma, K.; Syoji, T.; Yoshimi, K.: *Fresenius' J. Anal. Chem.* **2001** *369*, 184-186.

(81) Zhang, G.; Huang, F.; Sun, X.: *Guangpuxue Yu Guangpu Fenxi* **2000** *20*, 71-73.

(82) Yokota, F.; Shimizu, A.: *Bunseki Kagaku* **2000** *49*, 1043-1046.

(83) Yin, G.-P.; Xia, B.-J.; Cheng, X.-Q.; Shi, P.-F.: *Dianyuan Jishu* **2000** *24*, 144-145, 188.

(84) Yang, P.: *Fenxi Shiyanshi* **2000** *19*, 56-58.

(85) Xiong, H.-C.; Hu, B.; Huang, W.-H.; Peng, T.-Y.; Chen, S.-Z.; Jiang, Z.-C.: *Gaodeng Xuexiao Huaxue Xuebao* **2000** *21*, 1647-1650.

(86) Xia, B.-j.; Yin, G.-p.; Shi, P.-f.; Cheng, X.-q.: *Dianchi* **2000** *30*, 198-200.

(87) Tsuchiya, T.; Honjo, T.: *Bunseki Kagaku* **2000** *49*, 895-900.

(88) Shuai, Q.; Qin, Y.; Hu, B.; Xiong, H.; Jiang, Z.: *Anal. Sci.* **2000** *16*, 957-961.

(89) Qin, S.; Bin, H.; Yongchao, Q.; Wanjau, R.; Zucheng, J.: *J. Anal. At. Spectrom.* **2000** *15*, 1413-1416.

(90) Li, W.-c.: *Kuangye (Beijing)* **2000** *9*, 99-103.

(91) Karadjova, I.; Arpadjan, S.; Jordanova, L.: *Fresenius' J. Anal. Chem.* **2000** *367*, 146-150.

(92) Cai, B.; Hu, B.; Jiang, Z.: *Fresenius' J. Anal. Chem.* **2000** *367*, 259-263.

(93) Qiu, H.; Liu, J.; Yang, J.: *Guangpuxue Yu Guangpu Fenxi* **1999** *19*, 70-71.

(94) Qiu, H.; Liu, J.: *Guijinshu* **1999** *20*, 38-41.

(95) Swafford, A. M.; Keller, J. M.: Separation techniques for the clean-up of radioactive mixed waste for ICP-AES/ICP-MS analysis; Report ORNL/TM-12329; Order No. De93012726 **1993**, 29 pp.

(96) Shiraishi, K.: *Hoshasen Igaku Sogo Kenkyusho, [Rep.] NIRS-M* **1999** *NIRS-M-134*, 158-167.

(97) Radhakrishnan, K.; Kulkarni, V. T.; Patwardhan, A. B.; Ramanujam, A.; Page, A. G.: *J. Anal. At. Spectrom.* **1999** *14*, 1889-1892.

(98) Bonchin, S. L.; Gerth, D. J.: *Global '99: \"Nucl. Technol. - Bridging Millennia\", Proc. Int. Conf. Future Nucl. Syst.* **1999**, 1940-1941.

(99) Banba, T.; Hagiya, H.; Tamura, Y.; Senoo, M.; Yonezawa, C.; Carter, P. B.: *Anal. Sci.* **1998** *14*, 389-394.

(100) Giglio, J. J.; Cummings, D. G.; Michlik, M. M.; Goodall, P. S.; Johnson, S. G.: *Nucl. Instrum. Methods Phys. Res., Sect. A* **1997** *396*, 251-256.

(101) Valsami-Jones, E.; Ragnarsdottir, K. V.; Mann, T.; Kemp, A. J.: *Proc. Int. Symp. Geochem. Earth's Surf., 4th* **1996**, 686-689.

(102) Pilon, F.; Lorthioir, S.; Birolleau, J.-C.; Lafontan, S.: *J. Anal. At. Spectrom.* **1996** *11*, 759-764.

(103) Coleman, C. J.; Bibler, N. E.; Ferrara, D. M.; Hay, M. S.: *Ceram. Trans.* **1996** *72*, 467-474.

(104) Chou, F. I.; Lin, S. W.; Lee, C. H.: *Nucl. Sci. J.* **1996** *33*, 200-211.

(105) Kulkarni, M. J.; Argekar, A. A.; Thulasidas, S. K.; Dhawale, B. A.; Rajeswari, B.; Adya, V. C.; Purohit, P. J.; Neelam, G.; Bangia, T. R.; et al.: *Nucl. Technol.* **1994** *106*, 326-33.

(106) Gin, S.; Godon, N.; Mestre, J. P.; Vernaz, E. Y.; Beaufort, D.: *Appl. Geochem.* **1994** *9*, 255-69.

(107) Chou, F. I.; Jang, W. S.; Lee, C. H.; Chen, S. C.; Lee, R. T.; Tsai, C. M.: *Nucl. Sci. J.* **1994** *31*, 274-84.

(108) Huber, L.: *Vom Wasser* **1982** *58*, 173-85.

(109) Kalembkiewicz, J.; Sitarz-Palczak, E.: *Wiad. Chem.* **1999** *53*, 549-561.

(110) Hoffmann, H. J.: *Muench. Beitr. Abwasser-, Fisch.- Flussbiol.* **1981** *33*, 87-100.

(111) Hoffmann, H. J.: *LaborPraxis* **1993** *17*, 44-9.

(112) Oishi, K.; Uchino, K.; Atsuya, I.; Harada, K.: *Hitachi Hyoron* **1994** *76*, 293-8.

(113) Feng, Y.-L.; Narasaki, H.; Chen, H.-Y.; Tian, L.-C.: *Anal. Chim. Acta* **1999** *386*, 297-304.

(114) Heltai, G.; Feher, B.; Jozsa, T.; Percsics, K.: *Magy. Kem. Foly.* **2000** *106*, 201-207.

(115) Li, L.; Xie, M.; Wu, X.; Shun, Z.: *Jaingxi Nongye Daxue Xuebao* **1999** *21*, 546-551.

(116) Lobinski, R.: *Spectrochim. Acta, Part B* **1998** *53B*, 177-185.

(117) Matsuura, H.; Hokura, A.; Haraguchi, H.: *Bunseki Kagaku* **2000** *49*, 397-404.

(118) Mitrovic, B.; Milacic, R.: *Sci. Total Environ.* **2000** *258*, 183-194.

(119) Liang, P.; Li, C.-x.; Qin, Y.-c.; Hu, B.; Jiang, Z.-c.: *Fenxi Kexue Xuebao* **2000** *16*, 300-303.

(120) Schlegel, Đ.: Arsenic speciation analysis by ion chromatography and capillary electrophoresis combined with element-specific detection; UFZ-Ber.5 **1999**, i-ix, 1-151.

(121) Smichowski, P.; Marrero, J.; Ledesma, A.; Polla, G.; Batistoni, D. A.: *J. Anal. At. Spectrom.* **2000** *15*, 1493-1497.

(122) Mermet, J.-M.: *Proc. SPIE-Int. Soc. Opt. Eng.* **1999** *3853*, 15-25.

(123) Zhang, W.; Qian, S.; Yan, Z.: *Pige Keji* **1986**, 23-4.

(124) Von Piechowski, K.; Massop, K.: *Fett Wiss. Technol.* **1988** *90*, 315-19.

(125) Stern, D. A.: *Proc. AESF Annu. Tech. Conf.* **1990** *77th*, 367-78.

(126) Ong, C. C.: *Food Chem.* **1992** *45*, 145-9.

(127) Argentine, M. D.; Krushevska, A.; Barnes, R. M.: *J. Anal. At. Spectrom.* **1994** *9*, 1121-8.

(128) Arniaud, D.; Meyer, G.: *Am. Lab. (Shelton, Conn.)* **1994** *26*, 37.

(129) Coedo, A. G.; Dorado, M. T.; Escudero, E.; Cobo, I. G.: *At. Spectrosc.* **1994** *15*, 78-82.

(130) Hu, Y.; Zhang, Z.; Zheng, J.: *J. Anal. At. Spectrom.* **1994** *9*, 213-16.

(131) Kuz'min, N. M.; Kubrakova, I. V.; Pukhovskaya, V. M.; Kudinova, T. F.: *Zh. Anal. Khim.* **1994** *49*, 199-208.

(132) Costache, M.: *Rev. Chim. (Bucharest)* **1997** *48*, 464-467.

(133) Wang, X.; Zhu, Y.; Lang, R.: *Book of Abstracts, 215th ACS National Meeting, Dallas, March 29-April 2* **1998**, PETR-085.

(134) Telgheder, U.; Pilger, H.; Benninghoff, C.; Pulvermacher, E.: *CLB Chem. Labor Biotech.* **2000** *51*, 217-220.

(135) Wolf, C.; Rosick, U.; Bratter, P.: *Fresenius' J. Anal. Chem.* **2000** *368*, 839-843.

(136) Vela, N. P.; Caruso, J. A.: *J. Biochem. Biophys. Methods* **2000** *43*, 45-58.

(137) Mahan, C.; Bonchin, S.; Figg, D.; Gerth, D.; Collier, C.: *J. Anal. At. Spectrom.* **2000** *15*, 929-935.

(138) Li, Y.-w.; Xhang, Y.-l.; Di, Y.-a.; Liu, X.-d.: *Yankuang Ceshi* **2000** *19*, 63-69.

(139) Do, B.; Alet, P.; Pradeau, D.; Poupon, J.; Guilley-Gaillot, M.; Guyon, F.: *J. Chromatogr., B: Biomed. Sci. Appl.* **2000** *740*, 179-186.

(140) Bocca, B.; Alimonti, A.; Coni, E.; Di Pasquale, M.; Giglio, L.; Bocca, A. P.; Caroli, S.: *Talanta* **2000** *53*, 295-303.

(141) Seubert, A.: *Fresenius' J. Anal. Chem.* **1999** *364*, 404-409.

(142) Salgueiro, A.; Egea, M. A.; Valls, R.; Espina, M.; Garcia, M. L.: *J. Pharm. Biomed. Anal.* **1999** *21*, 611-618.

(143) Pomazal, K.; Prohaska, C.; Steffan, I.; Reich, G.; Huber, J. F. K.: *Analyst (Cambridge, U. K.)* **1999** *124*, 657-663.

(144) Oguma, K.; Kato, K.; Kurashima, Y.; Seki, T.; Ono, A.; Ishibashi, Y.: *Tetsu to Hagane* **1999** *85*, 119-123.

(145) Fuentes, F. J. V.: *Charact. Tech. Glasses Ceram.* **1999**, 3-13.

(146) Yates, D. M.; Joyce, K. J.; Heaney, P. J.: *Appl. Geochem.* **1998** *13*, 235-241.

(147) Tirler, W.; Bloedorn, W.: *LaborPraxis* **1998** *22*, 52,54-56.

(148) Rocha, A. A.; Miekeley, N.; Da Silveira, C. L. P.; Bezerra, M. C. M.: *Quim. Nova* **1998** *21*, 584-589.

(149) Date, A. R.; Gray, A. L.: *Analyst* **1981** *106*, 1255-1267.

(150) Gray, A. L.: *Dyn. Mass Spectrom.* **1978** *5*, 106-113.

(151) Houk, R. S.; Fassel, V. A.; Flesch, G. D.; Svec, H. J.; Gray, A. L.; Taylor, C. E.: *Anal. Chem.* **1980** *52*, 2283-2289.

(152) Horlick, G.; Tan, S. H.; Vaughan, M. A.; Shao, Y.: Inductively Coupled Plasma - Mass Spectrometry In *Inductively Coupled Plasmas in Analytical Atomic Spectrometry*; Montaser, A., Golightly, D. W., Eds.; VCH Publishers, Inc.: New York, 1987, pp 361-398.

(153) Horlick, G.: *JAAS* **1994** *9*, 593-597.

(154) Horlick, G.; Shao, Y.: Inductively Coupled Plasma-Mass Spectrometry for Elemental Analysis In *Inductively Coupled Plasmas in Analytical Atomic*

Spectrometry; Montaser, A., Golightly, D. W., Eds.; VCH Publishers: New York, 1992, pp 551-612.

(155) Horlick, G.; Montaser, A.: Analytical Characteristics of ICPMS In *Inductively Coupled Plasma Mass Spectrometry*; Montaser, A., Ed.; Wiley-VCH, Inc., 1998.

(156) Montaser, A. *Inductively Coupled Plasma Mass Spectrometry*; Wiley-VCH, Inc., 1998.

(157) Boss, C. B.; Fredeen, K. J. *Concepts, Instrumentation and Techniques in Inductively Coupled Plasma Optical Emission Spectrometry*; 2nd ed ed.; Perkin-Elmer, 1997.

(158) Barnard, T. W.; Crockett, M. I.; Ivaldi, J. C.; Lundberg, P. L.: *Anal. Chem.* **1993** *65*, 1225.

(159) Barnard, T. W.; Crockett, M. I.; Ivaldi, J. C.; Lundberg, P. L.; Yates, D. A.; Levine, P. A.; Sauer, D. J.: *Anal. Chem.* **1993** *65*, 1231.

(160) Perkin-Elmer, C. *The Optima 3000 Family of Inductively Coupled Plasma - Optical Emession Spectrometers*; Perkin-Elmer, Corp., 1997.

(161) Spectro *Experience Real ICP Performance - Spectro CIROS CCD*; Spectro, 1999.

(162) Hill, S.; Chenery, S.; Dawson, J.; Evans, E.; Fisher, A.; Price, W. J.; Smith, C. M. M.; Sutton, K. L.; Tyson, J. F.: *J. Anal. At. Spectrom.* **2000** *15*, 763.

(163) Jobin Yvon Emission *Ultima - The Ultimate ICP Analysis*; Jobin Yvon Emission, 1999.

(164) Griffiths, P. R.; Haseth, J. A. *Fourier Transform Infrared Spectrometry*; John Wiley & Sons: New York, 1986.

(165) Horlick, G.: *Anal. Chem.* **1971** *43*, 61A-66A.

(166) Faires, L. M.: *Anal. Chem.* **1986** *58*, 1023A-1034A.

(167) Faires, L. M.: *J. Anal. At. Spectrom.* **1987** *2*, 585-590.

(168) Horlick, G.; Hall, R. H.; Yuen, W. K.: Atomic emission spectrochemical measurements with a Fourier transform spectrometer In *Fourier transform infrared spectroscopy*; Ferraro, J. R., Basile, L. J., Eds.; Acadmic Press: New York, 1982; Vol. 3, pp 37-81.

(169) Rumble, J. J.: The Role of Databases in Modern Analytical Science; New Delhi, India **1998** NIST.

(170) Schierle, C.; Thorne, A. P.: *Spectrochim. Acta, Part B* **1995** *50*, 27-50.

(171) Boumans, P. W. J. M.; Vrakking, J. J. A. M.: *Spectrochim. Acta, Part B* **1986** *41*, 1235.

(172) Salit, M. L.; Travis, J. C.; Winchester, M. R.: *Appl. Opt.* **1996** *35*, 2960-2970.

(173) Phelps, F. M. *MIT Wavelength Tables*; MIT Press: Cambridge MA, 1982.

(174) Ramirez, R. W. *The FFT Fundamentals and Concepts*; Prentice-Hall, Inc.: Englewood Cliffs NJ, 1985.

(175) Alt, G. Encarta® Encyclopedia 2000;; Microsoft Corp.: Redmont WA, 2000.

(176) Horlick, G.; Malmstadt, H.: *Anal. Chem.* **1970** *42*, 1361.

(177) Horlick, G.: *Anal. Chem.* **1972** *44*, 943.

(178) Kelly, P. C.; Horlick, G.: *Anal. Chem.* **1973** *45*, 518.

(179) Yuen, W. K.; Horlick, G.: *Anal. Chem.* **1977** *49*, 1448.

(180) King, G. B.; Todd, B. R.; Horlick, G.: *Spectrochim. Acta, Part B* **1991** *47B*, E333-E352.

(181) King, G. B.; Horlick, G.: *Spectrochim. Acta Electronic* **1991** *47B*, Electronic publication.

Chapter 2. ICP-FTS and Operations

2.1. The UV - Visible FTS instrument.

The Fourier Transform Spectrometer used in this project is a Michelson interferometer built in this laboratory (1). This instrument is specially designed to meet the stringent requirements for the UV-Visible spectral region. This instrument is the result of the work of several generations of students and the latest major re-design and modifications were done by Bruce Todd (2) in the early 90's. This section will discuss the operation principles in further detail.

2.1.1. Optical System.

The heart of the Fourier Transform Spectrometer is a Michelson interferometer. Its optical system consists of five major parts (Figure 2-1): (a) A Plano-convex quartz lens that collimates the incident light from ICP or other light sources. (b) A quartz beam splitter mounted in a specially designed and machined aluminum cube. (c) A fixed mirror on a mount attached to the beam splitter cube. This mount was designed to allow very fine adjustment of the plane angle of the fixed mirror, which is very important for the alignment of the optical system. (d) A moving-mirror assembly which moves back forth at constant velocity. The movement of the mirror is controlled by a sophisticated motion control system with the maximum moving distance of ±2.07 cm. The operation of this motion control system will be discussed in further detail in the next section. (e) An off-axis parabolic mirror reflects the output beam onto a PMT detector through an exit aperture.

The optical system of this instrument has three channels: the main signal channel for the ICP source; a red HeNe laser channel for a cosine reference laser signal for both moving mirror motion control and sample interferogram digitization timing; and a white light channel that provides a sharp signal at the Zero Path Difference (ZPD) position on each sweep of the moving mirror movement (2).

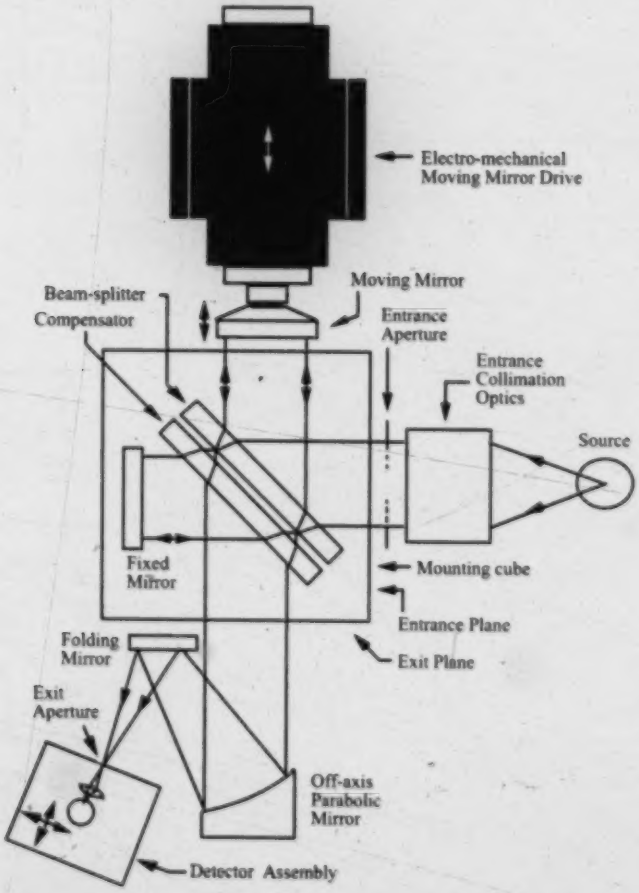

Figure 2-1. Optical system for the Fourier Transform Spectrometer. Reprinted from ref (2) with permission from Elsevier Science.

2.1.2. Drive Motion Control System.

The motion control subsystem for the moving mirror of the FTS is one of the most important and hard-to-build parts of the Michelson Spectrometer. Unlike most other instruments designed for the infrared, the error tolerance for the drive velocity for this UV-Visible FT instrument is much less in order to achieve similar signal-to-noise ratio as that of an FT-IR due to the much shorter wavelength of the signal of interest.

Ideally, the motion control system should provide very constant and vibration-free linear movement in a controlled distance. To achieve this, the moving mirror drive is mounted on an air-bearing drive to reduce vibration. Powered by a strong electro-magnetic coil, it is controlled by two different mechanisms. In "Coarse feedback" controlling mode, the drive is under control of feed back from an auxiliary coil attached to the drive assembly. This control mode provides relatively steady movement of the drive required to lock it into the "Fine feedback" mode in which the velocity of the drive is controlled by a frequency-to-voltage (f-to-v) feedback system.

The velocity of the moving mirror drive is designed to be 0.32 cm/sec, thus the modulation frequency of the HeNe reference laser is 10 kHz. A digital square wave is generated based on the reference laser signal and feeds back into the controlling circuit. If the velocity of the drive varies, the reference laser signal and the feedback will change accordingly. The power of the driving coil is adjusted based on the frequency difference of the reference laser signal and design value either to retard or accelerate the movement.

Moving mirror position control is achieved with fringe counting. When the drive starts moving, it is in "Coarse feedback" mode and moves at maximal distance set by two opto-switches at each end. When instrument operation is switched to the "Fine Feedback" mode, the drive continues moving under "Coarse feedback" control until it reaches the ZPD position and a digital pulse generated by the white light signal triggers fringe counting for the position control. The drive is then said to be "locked" into "Fine Feedback" mode and the moving distance is defined by the number of fringes set by the operator. On the first strike of ZPD after it is locked into "Fine Feedback" mode, the drive is forced to turn around at half the fringe number after it passes the ZPD. Once turned back, the drive is allowed to move the full preset fringe number before it is forced to turn around at the other end. Thus the drive moves at a distance set by the number of fringes across the ZPD symmetrically and generates double-sided symmetric interferograms.

2.1.3. Data Acquisition System.

All interferograms are recorded with PMT detectors. Again the reference laser fringe is used as the digitization clock. The instrument is designed such that the digitization clock rate can be set to one data point per reference laser fringe (1x), or four data points per fringe (4x), or eight points per fringe (8x).

As discussed before, when sampled at 1x, the shortest wavelength can be correctly sampled without aliasing is 1266 nm and thus all UV-Visible spectral lines within the range of 200 to 700 nm will be aliasing and many lines will be folded over multiple times. The spectra for many elements, except for those with only few lines,

will be very complex and thus is not desirable for a spectral library targeted for spectroscopists of all levels.

If the digitization clock rate is set to four data point per laser fringe (4x), all spectral lines with a wavelength longer than 316 nm, which covers the whole visible region, can be correctly sampled without aliasing. The UV lines, however, are still under sampled and aliasing will occur. This problem is resolved by carefully selecting the spectral response of the PMT and using electronic bandpass filters to separate the UV-Visible region into two different spectra (2). For the UV spectra, the Hamamatsu (Hamamatsu Corp., 360 Foothill Rd, Bridgewater, NJ 08807) solar blind P166 is used with electronic bandpass filter set to 21 to 35 kHz, which corresponds to 180 to 300 nm. In this way, even though aliasing still exists and spectral lines are flipped over on the wavelength axis, there is no overlapping between the aliasing UV lines and visible lines since later are not detected. As long as the wavelength axis is correctly labeled, aliasing is transparent to library users.

For the visible region data acquisition is more straightforward with a glass covered 1P21 PMT to filter out UV lines. The electronic bandpass filter was set from 10 kHz to 20 kHz.

2.2. Operation of the Instruments

2.2.1. Operation of the ICP.

The ICP system used in this project is an ICP-2500 from Plasma-Therm Inc. (Route 73, Kresson, NJ 08053. Tel. 609-767-6120). Powered by a HFP 2500D crystal-controlled RF generator operated at 27.12 MHz, this system provides a stable analytical ICP discharge for vertical viewing (Figure 2-2).

Mermet proposed a simple method using the relative intensity ratio of Mg ionic and atomic lines to set the parameters for optimal plasma operation (3). He found that if the intensity ratio of the Mg 280.270 nm line verses Mg 285.213 nm line was about 10, then the plasma was optimal for most analytical work. This method was used to establish the plasma conditions for this project. The typical operation parameters for the ICP 2500 listed in Table 2-1 might be slightly adjusted to achieve this optimal plasma condition. (Figure 2-3).

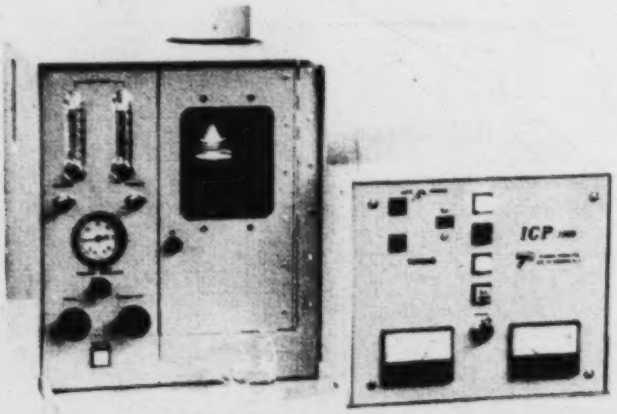

Figure 2-2. The Plasma-Therm ICP-2500 system.

Table 2-1. Operation Conditions for the ICP-2500 system

	Experiment Parameter
Torch	Fassel Type
Injector Gas Flow	0.45 L/min
Intermediate Gas Flow	0.85 L/min
Plasma Gas Flow	13 L/min
Forward RF Power	1.5 kw
Observation Height	15 mm above load coil
Solution uptake rate	1 mL/min

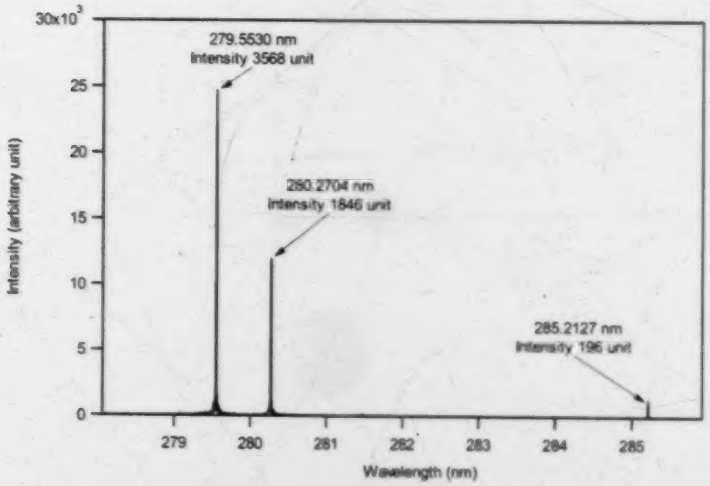

Figure 2-3. Diagnosis for ICP robustness with Mg spectral line ratio.

2.2.2. Operation of the FTS

As for all sophisticated instruments, the operation of the FTS requires considerable skill and experience. Although Todd (4) documented all detailed design principles, diagnosis, and circuitry of the FTS in his thesis, few details were included for routine operation. This inevitably increased the difficulty of the learning process for those new to this instrument. Therefore a brief summary of operation procedures is included here in the hope of lowering the learning curve for future students. This can, however, by no means substitute for reading his thesis. The operation procedures will make sense only to those who have solid knowledge of the instrument.

The rest of the section describes detailed operation procedures for the FTS instrument. Note that scope displays of key operation and diagnostic signals are showed in Figure 2-4.

To start the FTS, first turn on the nitrogen gas tank used for the air-bearing drive. Then turn on the power of the velocity control unit, the drive control unit, white light power, and the white light detector power.

Make sure the air-bearing drive can be moved smoothly by hand. Then turn the switch marked "Mirror" on the front panel of the control unit to "Release" position. This releases the so-called "Crow Bar" and the drive starts moving in the "Coarse feedback mode" or "Mark Time mode", meaning it is controlled by the feed back signal from the auxiliary coil, not by f-to-v control as in "Fine feedback mode".

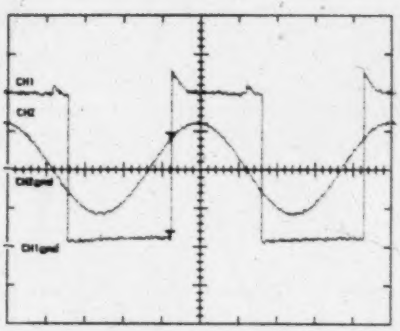

A. Reference laser fringes (analog and digital).

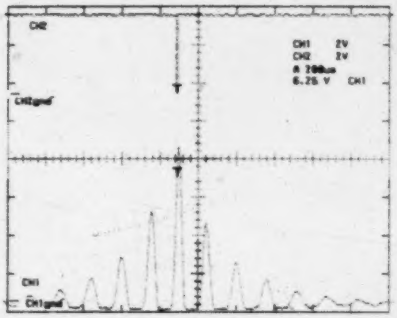

B. White light signals (analog and digital).

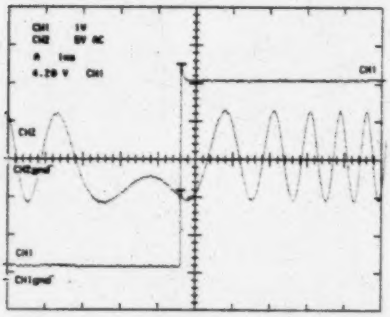

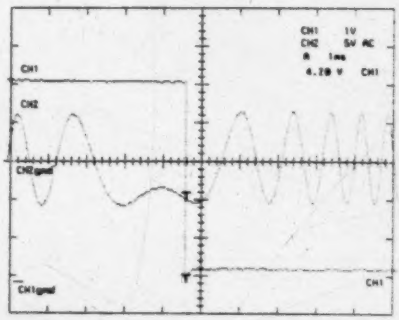

C. Digital signal FWD in analog turn-around brackets.

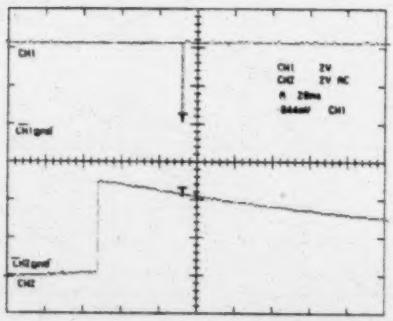

D. FWD and turn-around count-out.

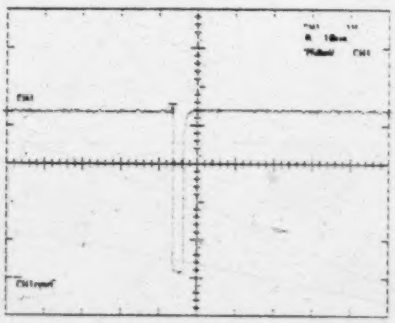

E. N count-out.

Figure 2-4. Important diagnosis signals for the FTS routine operation.

Now one should check the reference laser signal from the test point on the front panel of the velocity control unit. The signal should be a cosine waveform with frequency of about 10 kHz, and peak-to-peak intensity of at least 10 volts (Figure 2-4 A). If this signal is not available or not strong enough, check the laser power, mirror alignment, laser alignment, and the fringe generation unit. For initial adjustment, the gain for the laser fringe should be set to maximum by adjusting a pot inside the fringe generation unit, and reset to about 10 volts at the end of adjustment.

Then the digital FRINJ signal should be checked. Displayed on the same oscilloscope, FRINJ should be in-phase with the analog laser signal. Check fringe generation unit if there is a problem with this signal.

The analog white light signal (Figure 2-4 B) is considerably more difficult to monitor than the laser fringe since it is a transient signal and is much more sensitive to even the slightest misalignment of the mirror. Sometimes use two scopes, an analog one and a digital one will help, and the power to the white light bulb should set to maximum for initial adjustment.

Once the analog white light is available, try to increase its intensity by adjusting the alignment of the fixed mirror. Keep the white light power at maximum and keep aligning the mirror until the central fringe of the analog white light reaches at least 7 volts, which should be the proper trigger level for the digital white light pulse to appear (Figure 2-4 B).

Next, set the fringe counter to a small number, say, 4096, and try to lock the drive movement to fine feedback mode by switching the SCAN/MARK TIME switch to SCAN position. If the drive fails to switch into the fine feedback mode, one

should first try to continue aligning the mirror to get a higher analog white light signal and try to lock it again. If the white light signal reaches 10 volts and the drive still cannot be locked in to fine feedback, then the FRINJ and digital white light pulse should be checked. Remember, however, even though the digital white light pulse can be seen on scope for every scan when the drive is in fine feedback mode, it can only be seen once right after the switch is lifted up into the Mark Time mode. If the drive fails to be locked, one has to reset the switch and try again in order to catch the digital white light signal.

Once the drive is locked into fine feedback mode, it will move back forth around the middle position and the analog white light should be captured by the digital scope easily. One can get almost real time response when adjusting the alignment of the mirror. As the alignment gets better, the intensity of the analog white light signal gets higher and the power supply voltage for the white light can be reduced while keeping the white light central fringe above 7 volts. Then, reset the fringe counter to a large number and measure the frequency of the analog laser fringe. It should be at 10 kHz and be the same on each side of the drive stroke.

Turn on the computer and the counter, and lock the drive into fine feedback. The counter should give a constant reading on every stroke of the drive, with a plus or minus one counting error. The reading will be half of the fringe-count setting multiplied by the clock rate settings. For example, if the fringe count is set to 16384, and the clock rate set to 1, the counter will display 8192; if the clock rate is set to 4, the display will be 32768. Quite often, the counter gives a number close to, but not exactly is, the number expected. This is fine as long as the reading is constant.

If the counting cannot be stabilized to give a constant reading, one should check the turn around signal as outlined by Todd (4). Pay attention to the intensity of the analog reference laser signal and the analog white light signal. At turn-around, the laser signal should not be lower than 8 volts, while at ZPD it should not be too high as to generate false peaks for the digital FRINJ. Todd used the analog laser fringe to monitor the turn-around brackets. This is fine if one is experienced. Actually, using FRINJ to monitor is easier and more intuitive. With the turn-around signal and the FRINJ, one can even observe the number displayed by the counter changing with even a single out-of-the-bracket turn-around.

2.2.3. FTS operation parameters.

The principals and the instrumentation of the UV visible Fourier Transform Spectrometer have been discussed in Chapter 1 and in the previous section. The operation parameters, including those for data acquisition, are listed below.

Table 2-2. Operation parameters for FTS and data acquisition.

Fringe Counted:	32768
DAQ Clock Rate:	4 × HeNe Laser frequency (40 kHz)
Interferogram Length:	131072
Signal scan Average:	32
PMT used:	1P21 for visible and P166 for UV
PMT Voltage:	500 – 650 volts
Amplifier Rising Time:	0.01 ms
Amplifier Gain:	10^4 - 10^5
Bandpass:	10 - 21 kHz (visible), 21 - 35 kHz (UV)

2.3. Solutions.

To assure adequate signal-to-background ratio of the spectra and to avoid possible contamination from impurities, the measurements for the Spectral Library used solutions of individual elements (donated by High-Purity Standards, P. O. Box 30188, Charleston, SC, 29417, Tel 803-556-3411) at a relatively high concentration of 1000 ppm. As turned out, this concentration level was appropriate for most elements in both UV and visible regions to obtain decent spectra that carry information for both major and minor spectral lines.

Some elements with very strong emission lines, e.g. Mg in the UV region, and Ca, Sr, and Ba in the visible region, would saturate the measurement system at such a high concentration. Thus ten times diluted solutions (100 ppm) were used for these elements in corresponding spectral regions. The dilution was made with 2% nitric acid that was prepared with reagent grade nitric acid.

In contrast, other elements, e.g. Ca and P in the UV region, and Cd and Co in the visible region, emit very weakly. Thus 10,000-ppm solutions from SCP Science (2367 Guenette, St. Laurent, Quebec, H4R 2E9, Canada) were used to maintain appropriate signal-to-background ratio. The matrix for all 10,000 ppm solutions was 2% HNO_3 except for P, which was in pure water.

In order to avoid contamination, all standards were stored separately from other standard solutions in the laboratory and strictly used for the current project only. Except for dilutions stated above, they were used directly without further treatment.

Table 2-3. Standard solutions and concentration used.

	material for preparing solution		Density	Matrix	Element
Element	Compound / Format *	Purity (%)	(g/ml)	Acid (%)	Conc. (μg/ml)
Ag		99.999	1.0016		
Al		99.999	1.0143		
As		99.999	1.0136		
Au		99.99	1.0079	HCl (2%)	
B	Boric Acid	99.99	1.0018	H_2O	
Ba	Carbonate	99.99+	1.0137		100 (vis)
Be		99.5	1.0190		
Bi		99.999	1.0119		
Ca	Carbonate	99.99	1.0118		10,000 (UV) 100 (vis)
Cd		99.999	1.0117		10,000 (vis)
Ce	Oxide	99.99	1.0128		
Co		99.998	1.0113		10,000 (vis)
Cr		99.999	1.0115		
Cs	Carbonate	99.999	1.0055	HNO_3 (1%)	
Cu		99.999	1.0146		
Dy	Oxide	99.99	--		
Er	Oxide	99.99	1.0123		
Eu	Oxide	99.99	--		
Fe		99.99	1.0151		
Ga		99.999	1.0135		
Gd	Oxide	99.99	1.0090		
Ge		99.999	1.0069	Oxalic (5%)	
Hf		99.9+	1.0526	HNO_3 (2%)**	
Hg		99.998	1.0091		
Ho	Oxide	99.99	1.0138		
In	Ammonium Hexachlororidate	99.99	1.0212	HCl (10%)	
Ir		99.999	1.0075		
K	Nitrate	99.999	1.0073	HNO_3 (1%)	
La	Oxide	99.99	1.0152		
Li	Carbonate	99.999	1.0006	HNO_3 (1%)	
Lu	Oxide	99.99	1.0150		
Mg		99.99	1.0126		100 (UV)
Mn		99.99	1.0103		
Mo		99.999	1.0141		
Na	Sodium Nitrate	99.999	1.0102	HNO_3 (1%)	

* Pure metal is used to prepare the solution if not specified.
** HNO_3 (2%) is the matrix if not specified.

Table 2-3. Standard solutions and concentration used. (Continuing)

Element	Source for preparing solution		Density	Matrix	Conc.
	Compound / Format	Purity (%)	(g/ml)	Acid (%)	(μg/ml)
Nb		99.95	1.0270		
Nd	Oxide	99.99	--		
Ni		99.999	1.0122		
Os	Ammonium Hexachloroosminum	99.99	1.0043	HNO_3 (10%)	
P	Ammonium Dihydrogen Phosphate	99.95	1.0022	HNO_3 (0.05%)	10,000 (UV)
Pb		99.995	1.0134		
Pd		99.99	1.0422	HNO_3 (5%)	
Pr	Oxide	99.99	1.0119		
Pt		99.99	1.0040	HCl (5%)	
Rb	Carbonate	99.99+	1.0111		
Re		99.99+	--		
Rh	Ammonium Hexachlororhodium	99.99	1.0219	HCl (10%)	
Ru	Ammonium Hexachlororuthenium	99.9+	1.0214	HCl (10%)	
S	subboiling sulfuric acid	99.999	0.997*	H_2O	
Sb		99.999	1.0267	HNO_3 (5%)**	
Sc	Oxide	99.99	1.0157		
Se		99.99+	1.0548		
Si	Sodium Silicate	99.99	1.0046*	H_2O	
Sm	Oxide	99.99	--		
Sn		99.998	1.0133	HNO_3 (2%)**	
Sr	Carbonate	99.99	1.0117		100 (vis)
Ta		99.98	1.0082	HNO_3 (2%)**	
Tb	Oxide	99.99	1.0124		
Te		99.99	--	HCl (10%)	
Th	Oxide	99.99	1.0507		
Ti		99.99	1.0112	HNO_3 (2%)**	
Tl		99.999	1.0111		
Tm	Oxide	99.99	--		
U	Oxide	99.968	1.0118		
V	Ammonium Metavanadate	99.99	1.0136		
W		99.99	1.0118		
Y	Oxide	99.99	1.0122		
Yb	Oxide	99.99	1.0536		
Zn		99.999	1.0089		
Zr		99.84	1.0124		

Reference

(1) Horlick, G.; Yuen, W. K.: *Applied Spectroscopy* **1978** *32*, 38.

(2) Todd, B. R.; Horlick, G.: *Spectrochim. Acta, Part B* **1991** *47B*, E353-E370.

(3) Mermet, J. M.: *Analytica Chemica Acta* **1991** *250*, 85-94.

(4) Todd, B. R.: The design and characterization of a Fourier Transform spectrometer for the ultraviolet and visible regions of the spectrum; Ph. D., University of Alberta, Edmonton Alberta, 1989.

Chapter 3. The ICP-AES Spectral Library

In the first part of this chapter the practical aspects of the Spectral Library, including the content, organization, and accessibility will be discussed. Then more in-depth discussions will be given to the important measures of spectra qualities in the Spectral Library, such as spectral line resolution, line wavelength calibration and accuracy, and noise and its control.

3.1. Introduction to the Spectral Library

As stated in the thesis objective (Section 1-1), the Spectral Library is built for Inductively Coupled Plasma Atomic Emission Spectrometry (ICP-AES). It is intended to include emission spectra for all seventy elements that can be determined with an argon based ICP-AES (Figure 3-1). However, some of the elements have lines too weak to be detected with FTS, and thus their spectra might be incomplete.

In its simplest form, the Spectral Library has two spectra and two interferograms to cover UV and visible regions, respectively, for each element. The UV spectrum runs from 158 to 316 nm, with the effective wavelength coverage from about 200 to 316 nm as spectra were acquired at atmospheric pressure without inert gas purging. The visible spectra range is from 316 to 632 nm for the ASCII text version. For the Mac version, the spectra goes further form 316 nm to infinity (i.e. 0 cm^{-1}), but the effective wavelength coverage is the same as for its text counterpart.

In its complete form, the Spectral Library contains two to four spectra for the UV region for one element: an interferogram and a corresponding spectrum; or an

interferogram, a background interferogram, a background subtracted interferogram, and a corresponding spectrum.

For the visible region, the complete set for an element can contain up to seven different spectra: an interferogram and a corresponding spectrum (Spectrum A); a background interferogram and the spectrum (Spectrum B); a background-subtracted interferogram and the corresponding spectrum (Spectrum C). The last spectrum is one with background Ar lines further cleared. This was usually the result of subtraction of Spectrum B from Spectrum C, but sometimes was the result of Spectrum A minus Spectrum B.

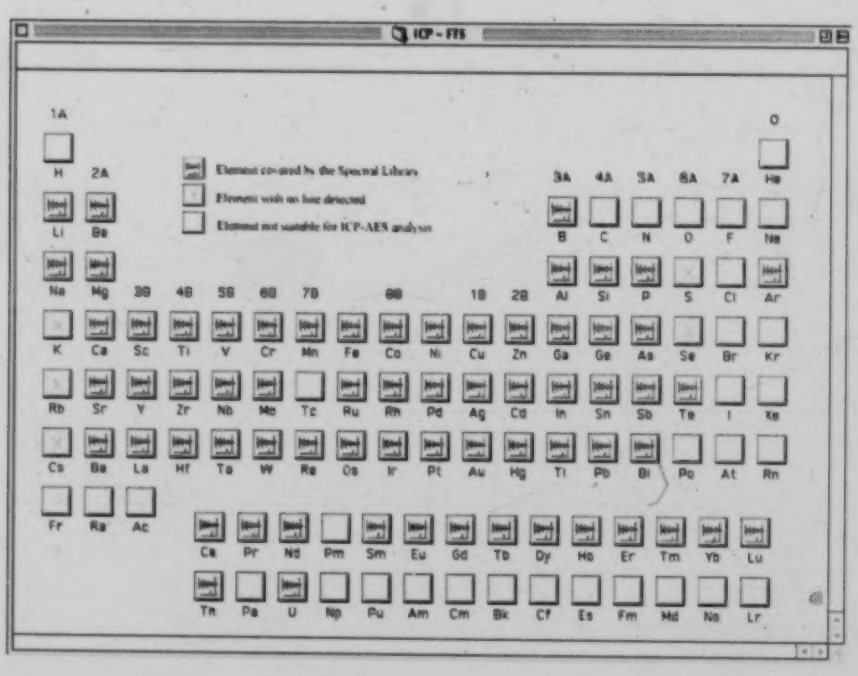

Figure 3-1. Elements covered by the ICP-AES Spectral Library.

In the *SpectroPlot* (1) binary file format, each spectrum takes about 650 KB disk space, and an interferogram takes 1.2 MB. Total 142 spectra (71 for UV and 71 for visible) require 90 MB disk space with an additional 180 MB required for the interferograms. The complete library has about 800 data files and needs 760 MB disk space. In ASCII text format, the size of the files is even larger. A calibrated spectrum is 1.1 MB in size, and the interferogram 2.1 MB. A Library containing only spectra and interferograms for every element takes 450 MB.

Currently there are only a few media available to store such a huge amount of data. Among them, CD-ROM provides a most convenient and cost-effective way for storing and distribution. Because such a format is read-only, it also provides the added security to prevent accidental change to the library data files.

The Spectral Library CD-ROM currently is available in either Macintosh HFS format or in ISO 9660 format. The Macintosh HFS CD-ROM (2, 3) is accessible solely on personal computers running Apple Computer's MacOS. The *SpectroPlot* program is included for viewing and manipulating the spectral data, which are stored in *SpectroPlot* binary file format for faster execution.

The ISO 9660 format CD-ROM (2, 3) provides access to the Spectral Library for the majority of personal computers running Microsoft Windows. Unix or Linux users with CD-ROM drives that support the ISO 9660 standard will also be able to access the library. Data files on the ISO 9660 CD-ROM are in tab delimited ASCII text format and contain wavelength and intensity values for the spectra. Unfortunately, there is no dedicated user interface available at this time for viewing and manipulating the spectral data under Microsoft Windows or Unix/Linux. Some

commercially available technical graphics package, such as Microcal Origin or WaveMetrics Igor Pro, can be used for this purpose. However, users will have to purchase them separately. Popular spreadsheet programs such as Microsoft Excel are not powerful enough to handle the large data sets offered in the Spectral Library.

In order to give the readers a general idea of the Spectral Library, a few interferograms and spectra are presented in Figures 3-2 and 3-3. The data files for these spectra and all others covered by the Spectral Library can be obtained by contacting the University of Alberta research group.

3.2. Wavelength Calibration

Wavelength accuracy is one of the greatest advantages of Fourier Transform Spectrometry (FTS), since in FTS the wavelength is solely, in theory, determined by the reference laser wavelength. As the laser wavelength is usually determined with very high accuracy, the wavelength values from FTS should have high precision and accuracy.

In practice, however, this might not be the case. As discussed in Chapter 1, beam divergence, which results from imperfect collimation of incident light and imperfect alignment of the reference laser and main channel optics, usually results in a slight shift in the wavelength values obtained. Thus the great wavelength accuracy of the FTS might not be achieved directly but the high wavelength precision still remains for a well-adjusted system. For spectroscopic studies that require ultra-high wavelength accuracy, wavelength calibration for the FTS is a convenient way to achieve the accuracy promised by this technique.

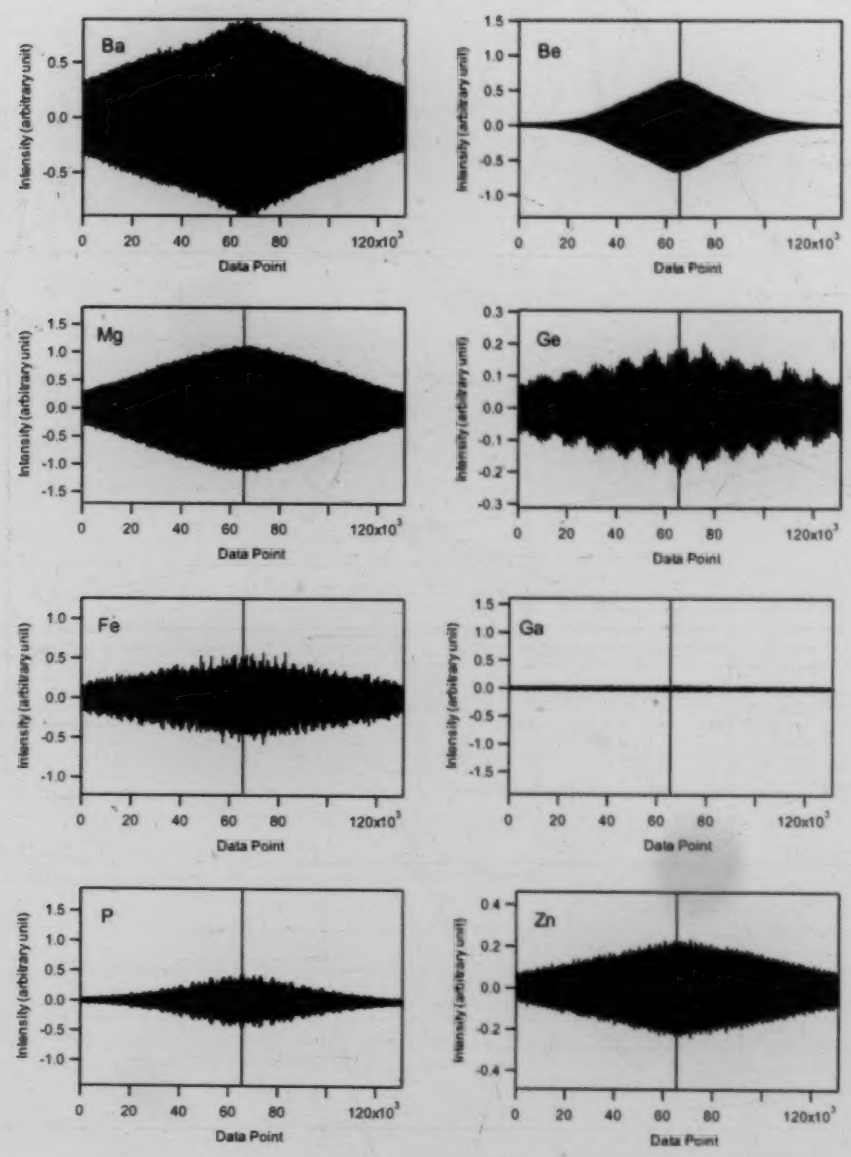

Figure 3-2. Some UV interferograms from the Spectral Library.

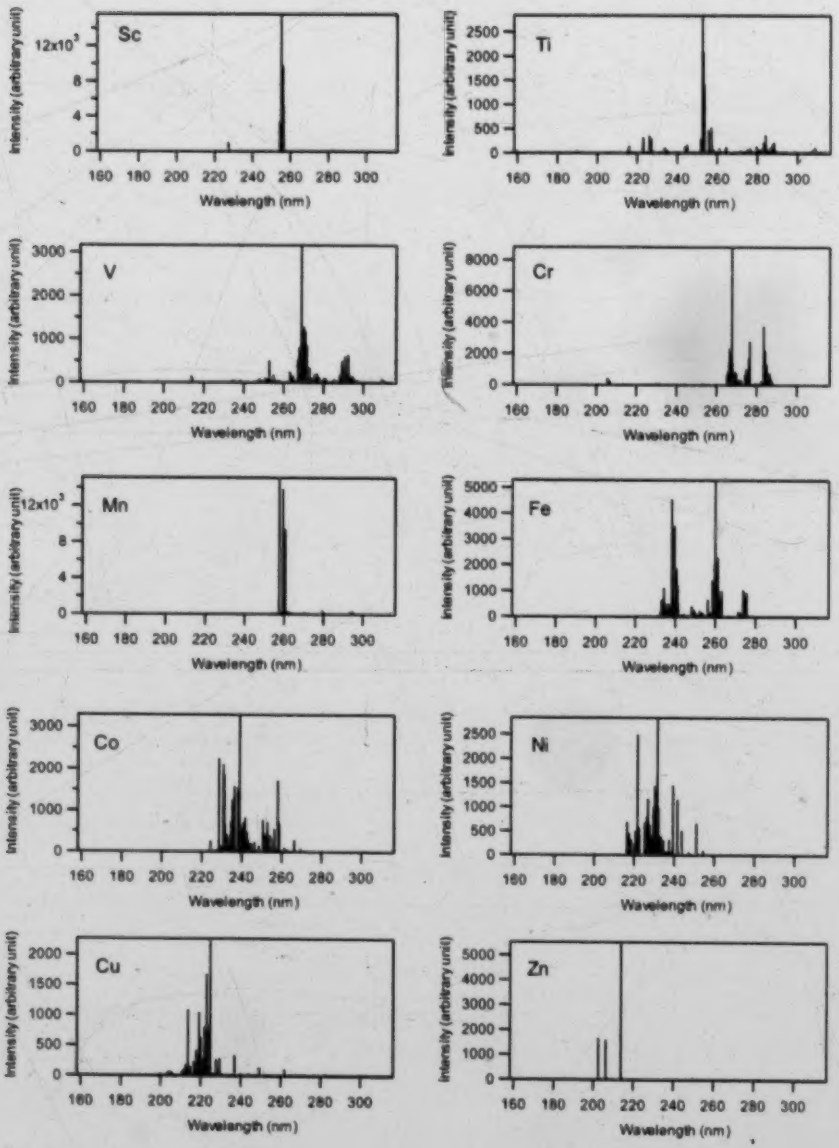

Figure 3-3. UV spectra for the first row of the transition metals.

3.2.1. Calibration of the Spectra

As discussed in Chapter 1, all factors that affect the wavelength accuracy of the FTS can be summarized into one parameter called "reference Laser Apparent Wavelength" or λ_{LAW}. With this concept, the FTS spectra can be easily calibrated or recalibrated to achieve high wavelength accuracy (4).

As an example, Table 3-1 shows the steps for calibration of an Mg UV spectrum with *SpectroPlot* and *Excel* spreadsheet. The primary calibration standards are the wavelength values from Zaidel's "Tables of Spectral Lines" (5).

3.2.2. Major Spectral Lines of the Elements

For each spectrum in the Spectral Library, up to 30 spectral lines of the highest intensity were used to establish calibration. The measured wavelength values and peak relative height (ratio of peak height and that of the dominant line in the spectra) are listed in a tabular form, as illustrated with Fe lines in Table 3-2. The λ_{LAW} value, the value of *reference Laser Apparent Wavelength* for that spectrum, is given in the heading of the table. For example, λ_{LAW} value for the spectrum listed in Table 3-2 is 632.8438, as listed under the "Measured value" heading. The literature values are obtained from reference (5), the relative height values are calculated from the original amplitude values. By comparing the relative height from the spectral library and that from the literature, one can get information about relative intensity changes when the source is switched from spark or arc to the ICP as Zaidel's intensity values are from spark and arc sources.

Table 3-1. Calibration of Mg UV Spectrum.

Step	Action
1	Open Mg UV interferogram from *SpectroPlot*, and transform it to an amplitude spectrum and zero-fill it 8 times.
2	Calibrate the spectrum with the reference laser's standard wavelength 632.81646 (6).
3	Use "Find Peaks..." feature of *SpectroPlot* to get the information for the desired peaks, including wavelength and amplitude. The threshold was set to a value such that up to 30 lines could be found in a spectrum.
4	In *Excel*, calculate reference laser apparent wavelength for each spectral line $\lambda_{laser,\ apparent}$ according to the following equation: $$\lambda_{\text{laser, apparent}} = \frac{\lambda_{\text{line, lit}}}{\lambda_{\text{line, measured}}} \cdot \lambda_{\text{laser, standard}}$$ where $\lambda_{line,\ lit}$ is the Zaidel's wavelength value of that particular line. $\lambda_{line,\ measured}$ is the wavelength reported by *SpectroPlot*. $\lambda_{laser,\ standard}$ = 632.81646 nm is laser's standard wavelength.
5	The mean value and the standard deviation of $\lambda_{laser,\ apparent}$ are calculated for all lines in the spectrum. The mean value of $\lambda_{laser,\ apparent}$ is the Laser Apparent Wavelength λ_{LAW} for this spectrum.
6	Use the calculated λ_{LAW} to re-calibrate the spectrum with *SpectroPlot*, and use "Find Peaks ..." to get the wavelength values for each line.
7	In *Excel*, calculate the wavelength error $\Delta\lambda = \lambda_{line,\ measured} - \lambda_{line,\ lit}$ for each spectral line. Notice the values of $\lambda_{line,\ measured}$ have changed from Step 4 since the spectrum has been recalibrated. The error absolute value $\Delta\lambda_{abs}$ of a particular line is the absolute value of its wavelength error.
8	The mean of the wavelength error and the error absolute value for all calibrated spectral lines over each spectrum are calculated. They are called "average wavelength error" $\Delta\lambda_{err}$ and "average absolute error" $\Delta\lambda_{abs,\ err}$, respectively.

Table 3-2. Major spectral lines of Fe in the UV region.

Measured value			Lit. value			
$\lambda_{632.8438}$ (nm)	H (%)	Line	λ (nm)	H (%)	Δλ (pm)	$\Delta\lambda_{abs}$ (pm)
233.2804	11.7	II	233.280	12.5	0.4	0.4
234.3498	24.7	II	234.349	17.5	0.8	0.8
234.8308	10.1	II	234.830	6	0.8	0.8
236.4831	9.3	II	236.483	10.5	0.1	0.1
238.2040	83.5	II	238.207	75	-3.0	3.0
238.8632	16.1	II	238.863	15	0.2	0.2
239.5627	61.9	II	239.560	50	2.7	2.7
239.9244	17.1	II	239.924	18	0.4	0.4
240.4885	35.8	II	240.488	50	0.5	0.5
240.6665	15.5	II	240.668	16	-1.5	1.5
241.0522	21.6	II	241.052	15	0.2	0.2
241.1068	9.7	II	241.107	11	-0.2	0.2
241.3310	8.8	II	241.331	11	0.0	0.0
256.2535	12.0	II	256.253	15	0.5	0.5
258.5878	28.2	II	258.588	32.5	-0.2	0.2
259.8368	35.2	II	259.837	32.5	-0.2	0.2
259.9398	100.0	II	259.940	100	-0.2	0.2
260.7086	29.6	II	260.709	32.5	-0.4	0.4
261.1876	41.6	II	261.187	40	0.6	0.6
261.3823	17.3	II	261.382	16	0.3	0.3
261.7617	11.8	II	261.762	16	-0.3	0.3
262.5667	14.7	II	262.567	22	-0.3	0.3
262.8296	13.3	II	262.829	16	0.6	0.6
263.1043	19.0	II	263.105	27.5	-0.7	0.7
263.1327	19.1	II	263.132	27.5	0.7	0.7
273.9546	18.1	II	273.955	37.5	-0.4	0.4
274.6480	10.8	II	274.648	21	0.0	0.0
274.6985	8.8	II	274.698	19	0.5	0.5
274.9321	15.6	II	274.932	30	0.1	0.1
275.5737	18.0	II	275.574	37.5	-0.3	0.3

The last two columns in the table list the wavelength error $\Delta\lambda$ and the absolute values $\Delta\lambda_{abs}$ in picometers for the spectral lines. These are the primary measures of wavelength accuracy. The data for all calibrated spectral lines in the library can be found on the CD-ROM in Adobe Acrobat PDF format. Interested readers can refer to it for further detail.

3.3. Spectral Line Wavelength Accuracy

As discussed before, wavelength calibration of the FTS in this work was done through the concept of *reference Laser Apparent Wavelength*, or λ_{LAW}. The accuracy of the calibration result can be measured through the spectral line wavelength error $\Delta\lambda$. In this section, the trends of wavelength accuracy (or inaccuracy) and the possible reasons will be discussed in further detail.

3.3.1. Overview

From the calibration procedure given in Table 3-1, it can be seen that the divergence of the λ_{LAW} value from its true value reflects the overall effects of all factors that affect the wavelength accuracy. Thus the λ_{LAW} value of a spectrum is the measure of the degree of inaccuracy imposed by the instrument at the time of measurement. Scatter of these values among elements would be a measure of the overall stability of the instrument with respect to wavelength accuracy. The laser apparent wavelength λ_{LAW} values for each spectrum plotted against the elements are shown in Figure 3-4 for the visible (top) and UV region (bottom), respectively. It can be seen that with few exceptions, all λ_{LAW} values fall into a 10 picometer range from 632.8400 to 632.8500 nm, with an average value for the visible region being

632.8445 ± 0.0027 nm and for UV region 632.8432 ± 0.0024 nm. The values for the visible region increase slightly as the atomic number increases. Currently there is no explanation readily available for this increase. However, as the standard deviation of the λ_{LAW} values apparently increased for the heavy elements, there might not even be an actual increase in the wavelengths. The values for the UV spectra are less scattered and show no apparent trend.

To see how the λ_{LAW} value affects the spectral line wavelength errors, the mean of the line wavelength errors for each spectrum, $\Delta\lambda_{err}$, along with that for the wavelength error absolute values, $\Delta\lambda_{abs,\ err}$, were plotted against the elements (Figure 3-5) for the visible and the UV region, respectively. It can be seen that $\Delta\lambda_{err}$ values stay almost constantly close to zero for nearly all the elements for both visible and UV regions. The $\Delta\lambda_{abs,\ err}$ values remain roughly in a two-picometer range with an average error at about one picometer.

Finally, these values were plotted against the standard deviation of the apparent reference laser wavelength of that spectrum for all spectra (Figure 3-6). Apparently, the standard deviation of the apparent reference laser wavelength exerts little effect on $\Delta\lambda_{err}$ values, as they remain constantly close to zero for most elements. The $\Delta\lambda_{abs,\ err}$ values do increase as the standard deviation of the apparent reference laser wavelength increases. Least square curve fitting for both UV and visible regions gave similar results. The slope of the curve is about 0.3 and R^2 about 0.6. That is, if the standard deviation of λ_{LAW} increases by one picometer, the mean of the wavelength error absolute values $\Delta\lambda_{abs,\ err}$ would increase 0.3 pm.

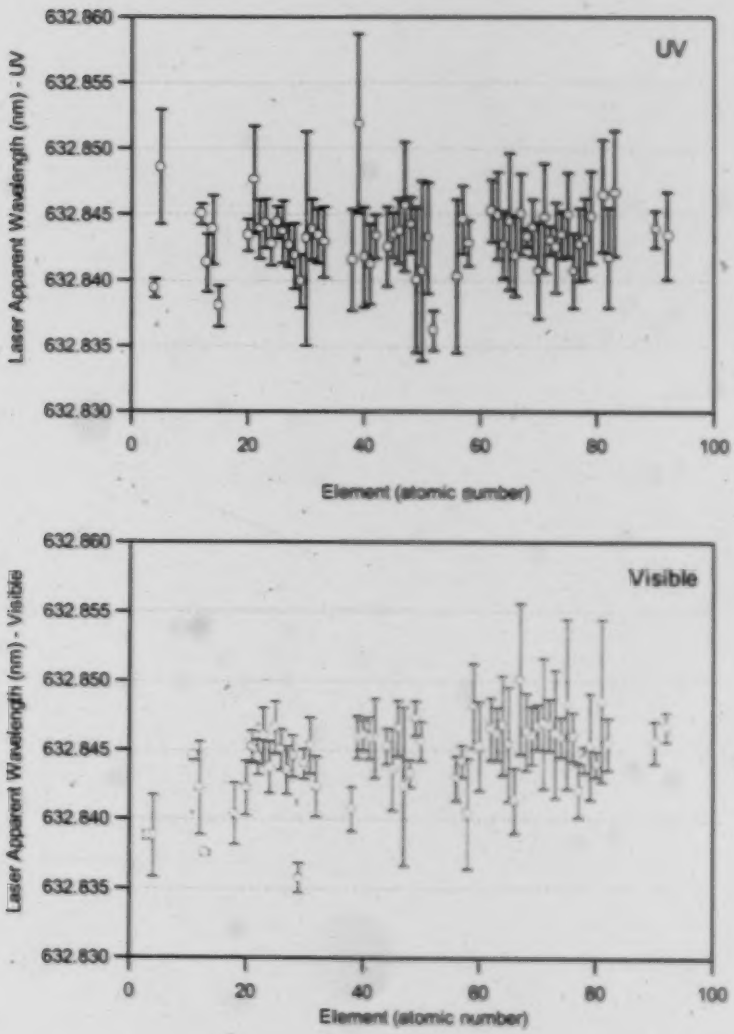

Figure 3-4. Reference laser apparent wavelength values for UV and visible region.

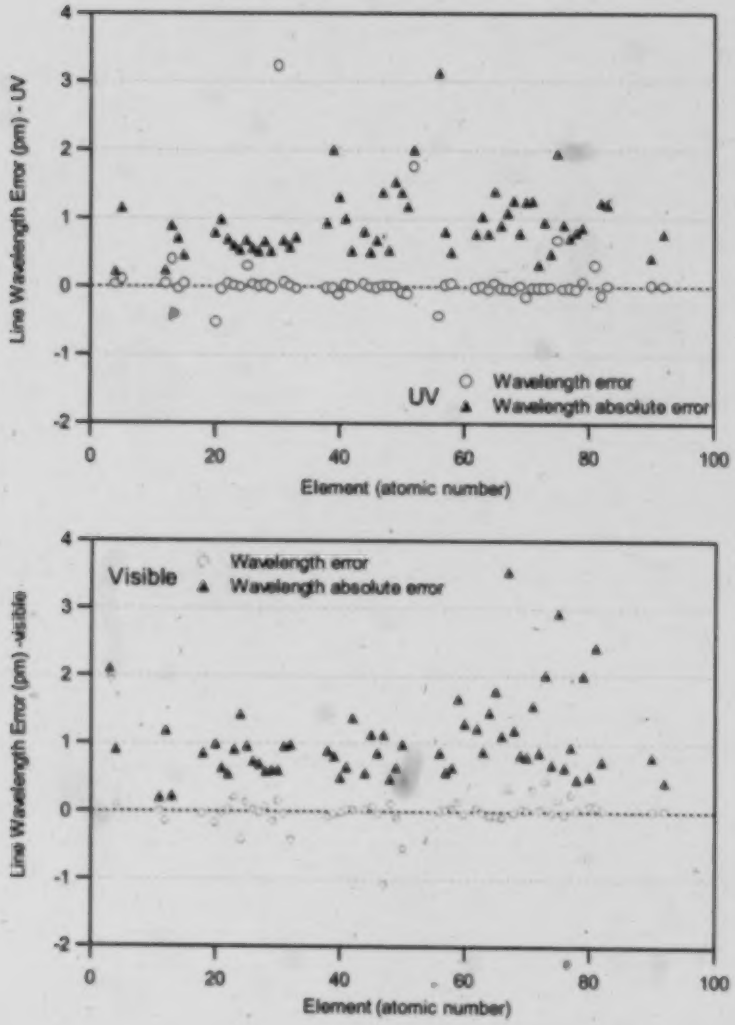

Figure 3-5. Spectral line wavelength errors ($\Delta\lambda_{err}$ and $\Delta\lambda_{abs,\ err}$) for UV and visible regions.

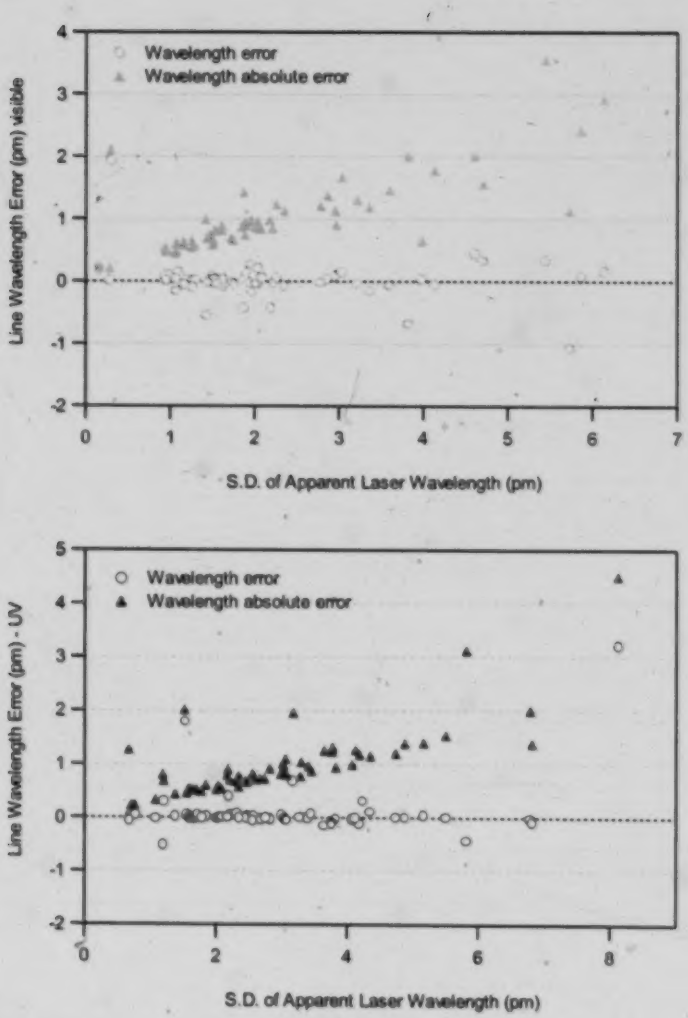
Wavelength error
Wavelength absolute error
Line Wavelength Error (pm) visible
S.D. of Apparent Laser Wavelength (pm)
Wavelength error
Wavelength absolute error
Line Wavelength Error (pm) - UV
S.D. of Apparent Laser Wavelength (pm)

Figure 3-6. Spectral line wavelength errors ($\Delta\lambda_{err}$ and $\Delta\lambda_{abs.\ err}$) vs. standard deviation of laser apparent wavelength.

3.3.2. A Close Look at Wavelength Accuracy.

In the previous section the trends of the wavelength accuracy were discussed with respect to Zaidel's wavelength values, but how accurate are the spectral line wavelengths of an element? What might happen to spectral lines that have significantly larger errors in wavelength? These will be discussed in this section.

First the spectral lines from iron were examined. Iron is an element common in everyday life, and is one of the most studied elements. Iron lines are well known with highly accurate and reliable wavelength values. Therefore, any quality work in wavelength measurement should not show significant discrepancy for Iron spectral line wavelengths.

Tables 3-3 and 3-4 list the calibrated spectral lines for Fe in the visible and UV regions, respectively. In these two tables, $\lambda_{measured}$ is the wavelength calibrated in the current study, λ_{Zaidel} is the wavelength quoted from Zaidel's wavelength table (5), and λ_{Thorne} is the wavelength reported by A. P. Thorne in a relatively recent work (7) in which Thorne and co-worker measured the spectral lines for 35 elements emitted from ICP with a high resolution FTS (0.1 cm^{-1}).

It can be seen that, the measured wavelength values, which were based on Zaidel's wavelength data, are generally in excellent agreement with Thorne's wavelength values. When compared to Zaidel's wavelengths, the mean for the wavelength error absolute values $\Delta\lambda_{abs.\ err}$ for the visible region is 0.7 pm, with a standard deviation of 0.9 pm, while compared to Thorne's wavelength, this value decreased to 0.6 pm, and standard deviation decreased to 0.7 pm.

Table 3-3. Wavelength accuracy for Fe visible lines (λ in nm)

Line	$\lambda_{measured}$	λ_{Zaidel}	$\Delta\lambda$ (pm)	λ_{Thorne}	$\Delta\lambda$ (pm)
I	356.5390	356.538	1.0	356.5380	1.0
I	357.0101	357.010	0.1	357.0099	0.2
I	358.1199	358.119	0.9	358.1194	0.5
I	360.8855	360.886	-0.5	360.8860	-0.5
I	361.8774	361.876	1.4	361.8769	0.5
I	363.1464	363.147	-0.6	363.1464	0.0
I	364.7849	364.785	-0.1	364.7844	0.5
I	371.9928	371.994	-1.2	371.9935	-0.7
I	373.7140	373.713	1.0	373.7132	0.8
I	374.5570	374.556	1.0	374.5561	0.9
I	374.8261	374.827	-0.9	374.8262	-0.1
I	374.9489	374.949	-0.1	374.9486	0.3
I	375.8221	375.823	-0.9	375.8234	-1.3
I	376.3797	376.379	0.7	376.3790	0.7
I	376.7199	376.719	0.9	376.7193	0.6
I	381.5836	381.584	-0.4	381.5842	-0.6
I	382.0432	382.043	0.2	382.0427	0.5
I	382.5886	382.588	0.6	382.5882	0.4
I	382.7819	382.782	-0.1	382.7823	-0.4
I	383.4233	383.422	1.3	383.4223	1.0
I	384.0437	384.044	-0.3	384.0438	-0.1
I	384.1051	384.105	0.1	384.1049	0.2
I	385.9917	385.991	0.7	385.9911	0.6
I	388.6275	388.629	-1.5	388.6282	-0.7
I	404.5803	404.582	-1.7	404.5814	-1.1
I	406.3601	406.360	0.1	406.3593	0.8
I	407.1750	407.174	1.0	407.1741	0.9

Table 3-4. Wavelength accuracy for Fe UV lines (λ in nm)

Line	$\lambda_{measured}$	λ_{Zaidel}	$\Delta\lambda$ (pm)	λ_{Thorne}	$\Delta\lambda$ (pm)
II	233.2804	233.280	0.4	233.2799	0.5
II	234.3497	234.349	0.7	234.3494	0.3
II	234.8307	234.830	0.7	234.8302	0.5
II	236.4831	236.483	0.1	236.4836	-0.5
II	238.2039	238.207	-3.1	238.2036	0.3
II	238.8631	238.863	0.1	238.8628	0.3
II	239.5627	239.560	2.7	239.5624	0.3
II	239.9244	239.924	0.4	239.9240	0.4
II	240.4885	240.488	0.5	240.4880	0.5
II	240.6664	240.668	-1.6	240.6660	0.4
II	241.0521	241.052	0.1	241.0518	0.3
II	241.1068	241.107	-0.2	241.1067	0.1
II	241.3309	241.331	-0.1	241.3309	0.0
II	256.2535	256.253	0.5	256.2534	0.1
II	258.5877	258.588	-0.3	258.5875	0.2
II	259.8368	259.837	-0.2	259.8368	0.0
II	259.9398	259.940	-0.2	259.9394	0.4
II	260.7086	260.709	-0.4	260.7086	0.0
II	261.1876	261.187	0.6	261.1875	0.1
II	261.3823	261.382	0.3	261.3824	-0.1
II	261.7617	261.762	-0.3	261.7617	0.0
II	262.5667	262.567	-0.3	262.5667	0.0
II	262.8296	262.829	0.6	262.8292	0.4
II	263.1043	263.105	-0.7	263.1046	-0.3
II	263.1326	263.132	0.6	263.1322	0.4
II	273.9545	273.955	-0.5	273.9547	-0.2
II	274.6480	274.648	0.0	274.6483	-0.3
II	274.6985	274.698	0.5	274.6981	0.4
II	274.9320	274.932	0.0	274.9320	0.0
II	275.5737	275.574	-0.3	275.5736	0.1

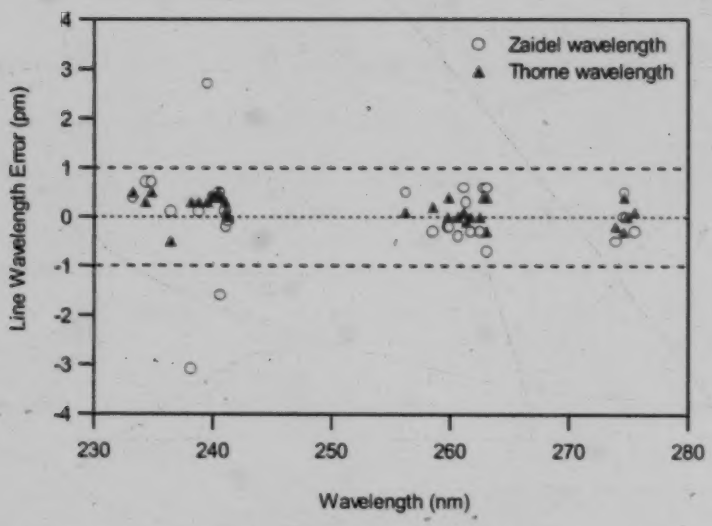

Figure 3-7. Wavelength errors $\Delta\lambda$ vs. wavelength for Fe UV lines.

The spectral lines in the UV region show even better agreement with Thorne's wavelengths. All line wavelength error absolute values decreased to or below 0.5 pm. The three lines with large wavelength errors (based on Zaidel's values), Fe II 238.207 (with error -3.1 pm), Fe II 239.560 (error 2.7 pm), and Fe II 240.668 (error -1.6 pm), now have error values at 0.3, 0.3, and 0.4 pm respectively, close to the precision limit of current instrument (0.3 pm). The decrease in wavelength errors can be clearly observed in the plot of wavelength error vs. wavelength for iron (Figure 3-7).

To further investigate this phenomenon, spectral lines with wavelength error absolute values $\Delta\lambda_{abs}$ greater than 2 pm were chosen and compared to the wavelengths reported by Thorne. The results for 34 lines that had Thorne's wavelength values available are listed in Table 3-5, and the error values verse wavelength plot is given in Figure 3-8.

From the data it can be seen that, among all 34 lines, 18 lines have error less than 1 pm when compared with Thorne's wavelength; 9 lines have errors equals to or great than 1 pm but less than 2 pm; and only 7 lines still have errors greater than 2 pm.

Among the 7 lines that have errors greater than 2 pm, 3 yttrium lines showed clear bias on wavelength error and should be readily corrected with re-calibration (which is not possible when using Zaidel's wavelength as standard). In fact, the laser apparent wavelength for yttrium UV spectrum is 632.8519 nm, significantly larger than the average value for the UV region (632.8432 nm). The difference in line wavelength calculated from these two laser wavelength is 3.3 pm at 240 nm.

For all 34 lines, the mean of line wavelength error absolute values $\Delta\lambda_{abs,\,err}$ was 2.9 ± 3.3 pm when using Zaidel's wavelength as standard, and was 1.2 ± 1.7 pm when using Thorne's wavelength as standard. If the three yttrium lines were not counted, the mean value of the line wavelength error absolute values $\Delta\lambda_{abs,\,err}$ was increased to 3.1 ± 3.5 pm using Zaidel's wavelength as standard, and decreased to 1.0 ± 1.3 pm using Thorne's.

This inter-comparison indicates that some minor errors are present in the Zaidel compilation and that overall it is not as precise a set of values as those that can be obtained using modern FTS instruments. However, this is not the whole story as will be seen in the next section.

Table 3-5. Comparison of wavelength errors with different wavelength standards.

Line	Height (%)	$\lambda_{measured}$	λ_{Zaidel}	$\Delta\lambda$ (pm)	λ_{Thorne}	$\Delta\lambda$ (pm)
Ag	64.4	241.3201	241.318	2.1	241.3188	1.3
Al	14.4	265.2478	265.243	4.8	265.2481	-0.3
B	1.5	208.8910	208.893	-2.0	208.8889	2.1
Bi	34.2	222.8228	222.825	-2.2	222.8213	1.5
Ce	54.0	429.6692	429.667	2.2	429.6679	1.3
Cr	4.1	318.0695	318.073	-3.5	318.0700	-0.5
Cr	20.0	319.7056	319.712	-6.4	319.7081	-2.5
Cr	8.7	320.9183	320.921	-2.7	320.9184	-0.1
Cr	0.0	321.7393	321.744	-4.7	321.7403	-1.0
Cr	6.4	434.4481	434.451	-2.9	434.4517	-3.6
Fe	83.5	238.2039	238.207	-3.1	238.2036	0.3
Fe	61.9	239.5627	239.560	2.7	239.5624	0.3
Mg	20.1	382.9339	382.930	3.9	382.9349	-1.0
Mn	100.0	344.2003	344.198	2.3	344.1985	1.8
Mo	100.1	379.8272	379.825	2.2	379.8253	1.9
Pb	100.0	220.3533	220.351	2.3	220.3531	0.2
Pb	16.9	283.3048	283.307	-2.2	283.3056	-0.8
Sb	11.5	206.8351	206.833	2.1	206.8361	-1.0
Sb	100.0	252.8510	252.854	-3.0	252.8510	0.0
Sc	5.9	227.3128	227.310	2.8	227.3109	1.9
Si	3.1	263.1281	263.131	-2.9	263.1283	-0.2
Sn	10.8	248.3401	248.344	-3.9	248.3407	-0.6
Sn	53.8	283.9969	283.999	-2.1	283.9978	-0.9
Sr	0.4	460.7309	460.733	-2.1	460.7333	-2.4
V	27.3	271.5659	271.568	-2.1	271.5655	0.4
V	44.2	371.5460	371.548	-2.0	371.5466	-0.6
Y	2.2	239.8106	239.814	-3.4	239.8067	3.9
Y	100.0	242.2223	242.219	3.3	242.2187	3.6
Y	8.6	246.0593	246.062	-2.7	246.0556	3.7
Y	34.8	417.7528	417.755	-2.2	417.7529	-0.1
Zn	27.0	206.2006	206.191	9.6	206.2000	0.6
Zn	100.0	213.8580	213.856	2.0	213.8575	0.5
Zr	13.7	255.0738	255.071	2.8	255.0744	-0.6
Zr	83.2	257.1456	257.142	3.6	257.1457	-0.1

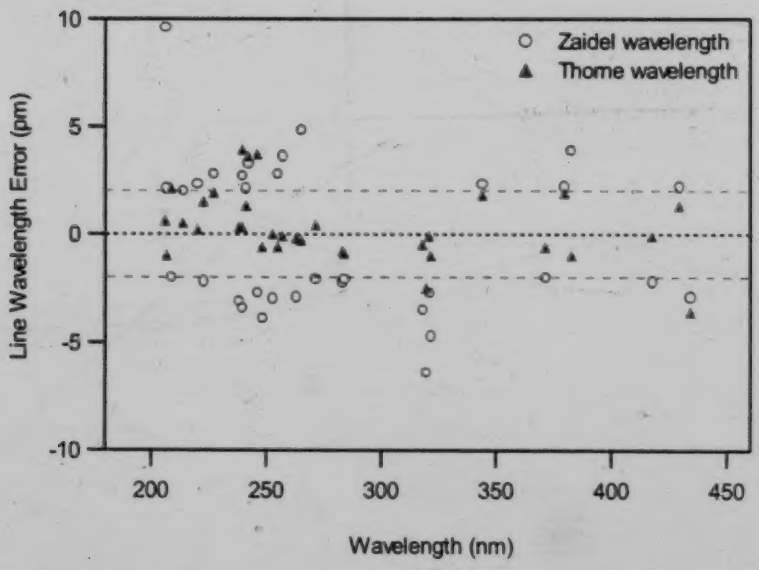

Figure 3-8. Wavelength errors $\Delta\lambda$ vs. wavelength for some "large error" lines.

3.3.3. Line Hyperfine Structure and Wavelength Accuracy

Obviously the wavelength accuracy of a measurement is dependent on the resolution of the instrument used. If the spectral lines have hyperfine structure that cannot be resolved, or not fully resolved by the instrument, the wavelength accuracy of the measurement will certainly be affected. This is one of the reasons accounting for many troublesome lines in current study.

The Ho visible spectrum, for example, is one of the worst cases for wavelength accuracy. The mean of the wavelength error absolute is 3.5 ±5.6 pm, considerably larger than the average. Close examination revealed many doublets or even triplets, not fully resolved, in the spectrum (Figure 3-9). Ultra-high-resolution spectroscopic studies have shown that hyperfine structure exist for these lines, as

shown in Figure 3-10. Often it is these lines that are responsible for the largest error in wavelength values reported from our spectra.

As can be seen in Table 3-6, which lists the calibrated Ho visible lines, the wavelengths reported by *SpectroPlot* and the calculated error, and the wavelength at the center of the lines and the calculated error, that the wavelength accuracy is much "improved" when the wavelength of the center of the peak is used for calculation. This suggests that a lower resolution spectrum would be more "compatible" with the Zaidel's wavelength values. Table 3-7 compares the wavelength errors for normally measured wavelengths and those from a lower resolution spectrum (interferogram length 16384 reference laser fringe, theoretical resolution 1.93 cm^{-1}, compared to 0.97 cm^{-1} of the regular spectra in the library). It was found that some of the largest errors in wavelength have been reduced, but some originally small errors have been enlarged due to the reduced resolution and overall there was not much improvement. Nevertheless, the mean in wavelength errors did reduced from 3.5 to 3.2 pm, and standard deviation from 5.6 to 4.1 pm.

Hyperfine structure is by no means a unique property of Ho spectral lines. It was also observed for some Re and Th UV lines (Figure 3-11), and many, if not all, of the rare earth elements. This is inevitably one of the major factors contributing to the wavelength differences between different studies, as the instruments used for different measurement seldom have similar resolving power.

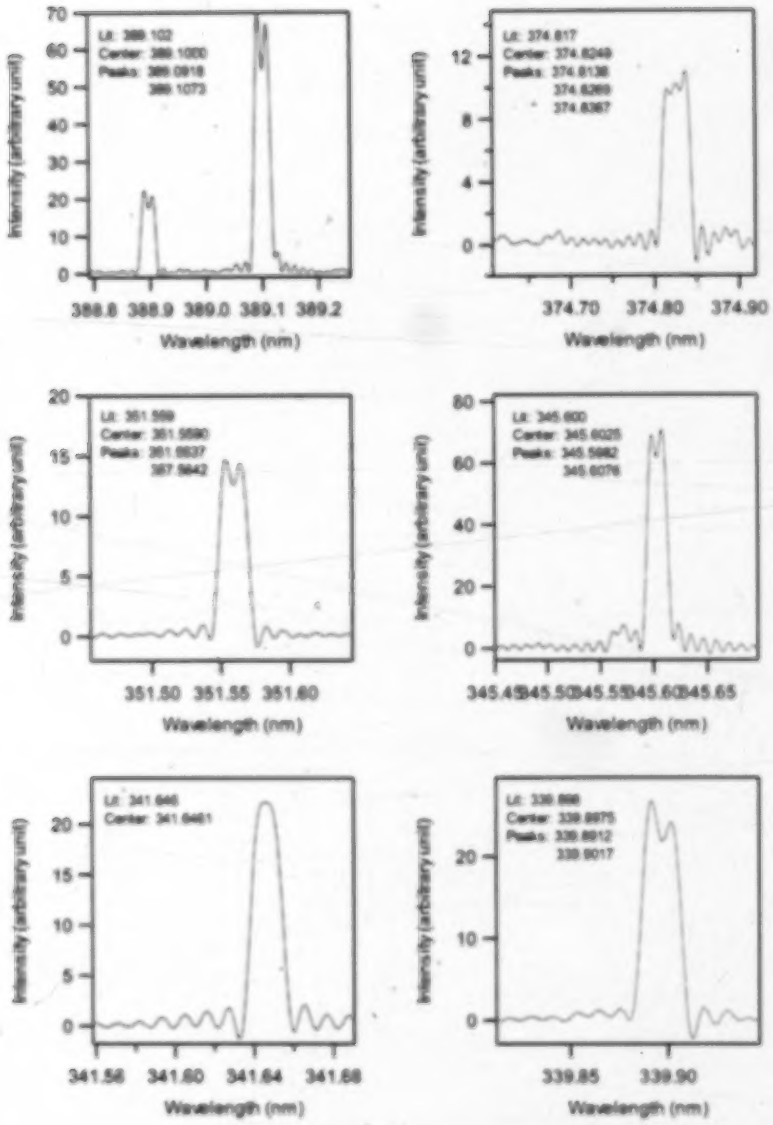

Figure 3-9. Some Ho visible lines with hyperfine structure.

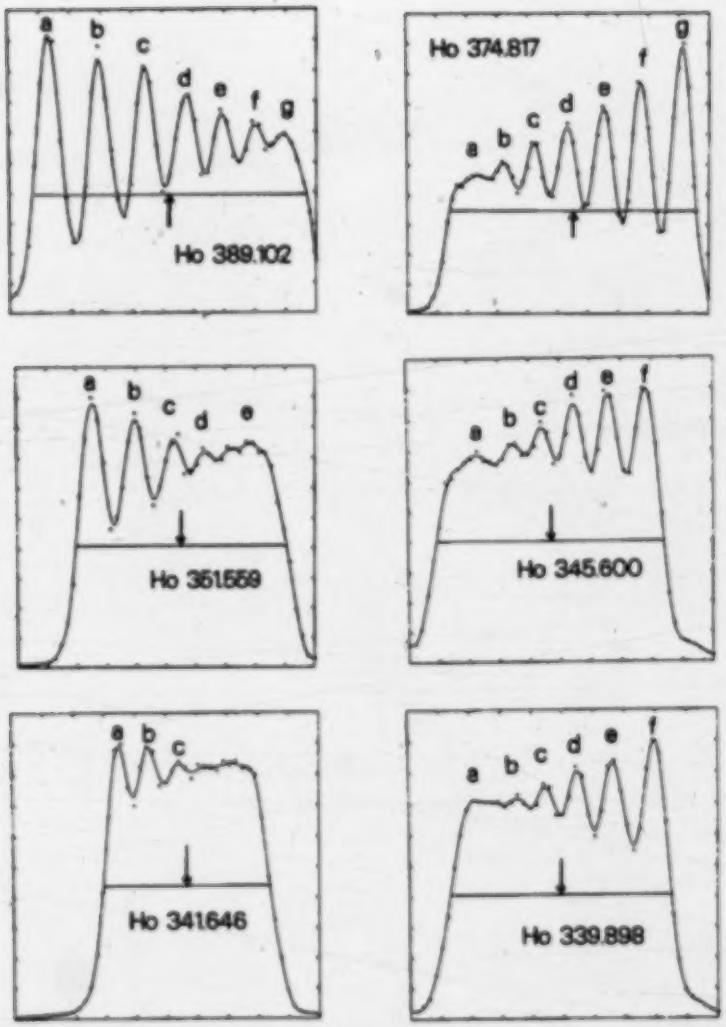

Figure 3-10. Line shape of some Ho lines. Reprinted from ref (8) with permission from Elsevier Science.

Table 3-6. Ho visible lines.

Line	Height (%)	λ_{Zaidel} (nm)	$\lambda_{measured}$ (nm)	Error (pm)	$\lambda_{Peak\ center}$ (nm)	Error (pm)
II	37.8	339.898	339.8905	-7.5	339.8975	-0.5
II	31.3	341.646	341.6461	0.1		
II	11.0	342.534	342.5377	3.7	342.5335	-0.5
II	14.6	342.813	342.8095	-3.5	342.8109	-2.1
II	20.2	345.314	345.3126	-1.4		
	10.9	345.570	345.5708	0.8		
II	100.0	345.600	345.6068	6.8	345.6025	2.5
II	10.3	346.197	346.1961	-0.9		
II	8.9	347.391	347.3966	5.6	347.3915	0.5
II	31.7	347.426	347.4242	-1.8	347.4301	4.1
II	38.1	348.484	348.4839	-0.1		
II	17.1	349.476	349.4860	10.0	349.4810	5.0
II	20.7	351.559	351.5530	-6.0	351.5590	0.0
II	19.3	354.605	354.6031	-1.9		
II	15.6	374.817	374.8359	18.9	374.8249	7.9
I	58.2	379.675	379.6750	0.0		
I	90.2	381.073	381.0740	1.0		
II	9.6	381.325	381.3192	-5.8	381.3270	2.0
II	8.9	383.751	383.7591	8.1	383.7519	0.9
II	11.9	384.386	384.3886	2.6		
II	17.7	385.407	385.4048	-2.2	385.4092	2.2
II	16.6	386.168	386.1656	-2.4	386.1727	4.7
II	31.6	388.896	388.8885	-7.5	388.8966	0.6
II	98.1	389.102	389.0910	-11.0	389.1000	-2.0
II	7.9	390.568	390.5675	-0.5		
II	80.9	404.544	404.5472	3.2		
II	14.2	406.509	406.5079	-1.1		
II	9.7	433.713	433.7122	-0.8		
II	16.3	435.673	435.6724	-0.6		
II	9.6	442.056	442.0586	2.6		
II	10.7	447.764	447.7641	0.1		
II	16.7	462.910	462.9121	2.1		

Table 3-7. Ho visible line wavelength at lower resolution

Line	Height (%)	λ_{Zaidel} (nm)	$\lambda_{measured}$ (nm)	Error (pm)	$\lambda_{Low\ Resolution}$ (nm)	Error (pm)
II	37.8	339.898	339.8905	-7.5	339.8961	-5.6
II	31.3	341.646	341.6461	0.1	341.6461	0.0
II	11.0	342.534	342.5377	3.7	342.5335	4.2
II	14.6	342.813	342.8095	-3.5	342.8123	-2.8
II	20.2	345.314	345.3126	-1.4	345.3126	0.0
	10.9	345.570	345.5708	0.8	345.5701	0.7
II	100.0	345.600	345.6068	6.8	345.6033	3.5
II	10.3	346.197	346.1961	-0.9	346.1961	0.0
II	8.9	347.391	347.3966	5.6	347.3937	2.9
II	31.7	347.426	347.4242	-1.8	347.4286	-4.4
II	38.1	348.484	348.4839	-0.1	348.4854	-1.5
II	17.1	349.476	349.4860	10.0	349.4823	3.7
II	20.7	351.559	351.5530	-6.0	351.5590	-6.0
II	19.3	354.605	354.6031	-1.9	354.6038	-0.7
II	15.6	374.817	374.8359	18.9	374.8274	8.5
I	58.2	379.675	379.6750	0.0	379.6759	-0.9
I	90.2	381.073	381.0740	1.0	381.0730	1.0
II	9.6	381.325	381.3192	-5.8	381.3270	-7.8
II	8.9	383.751	383.7591	8.1	383.7528	6.3
II	11.9	384.386	384.3886	2.6	384.3894	-0.8
II	17.7	385.407	385.4048	-2.2	385.4092	-4.4
II	16.6	386.168	386.1656	-2.4	386.1736	-8.0
II	31.6	388.896	388.8885	-7.5	388.8948	-6.3
II	98.1	389.102	389.0910	-11.0	389.0991	-8.1
II	7.9	390.568	390.5675	-0.5	390.5685	-1.0
II	80.9	404.544	404.5472	3.2	404.5480	-0.8
II	14.2	406.509	406.5079	-1.1	406.5068	1.1
II	9.7	433.713	433.7122	-0.8	433.7108	1.4
II	16.3	435.673	435.6724	-0.6	435.6744	-2.0
II	9.6	442.056	442.0586	2.6	442.0619	-3.3
II	10.7	447.764	447.7641	0.1	447.7675	-3.4
II	16.7	462.910	462.9121	2.1	462.9105	1.6

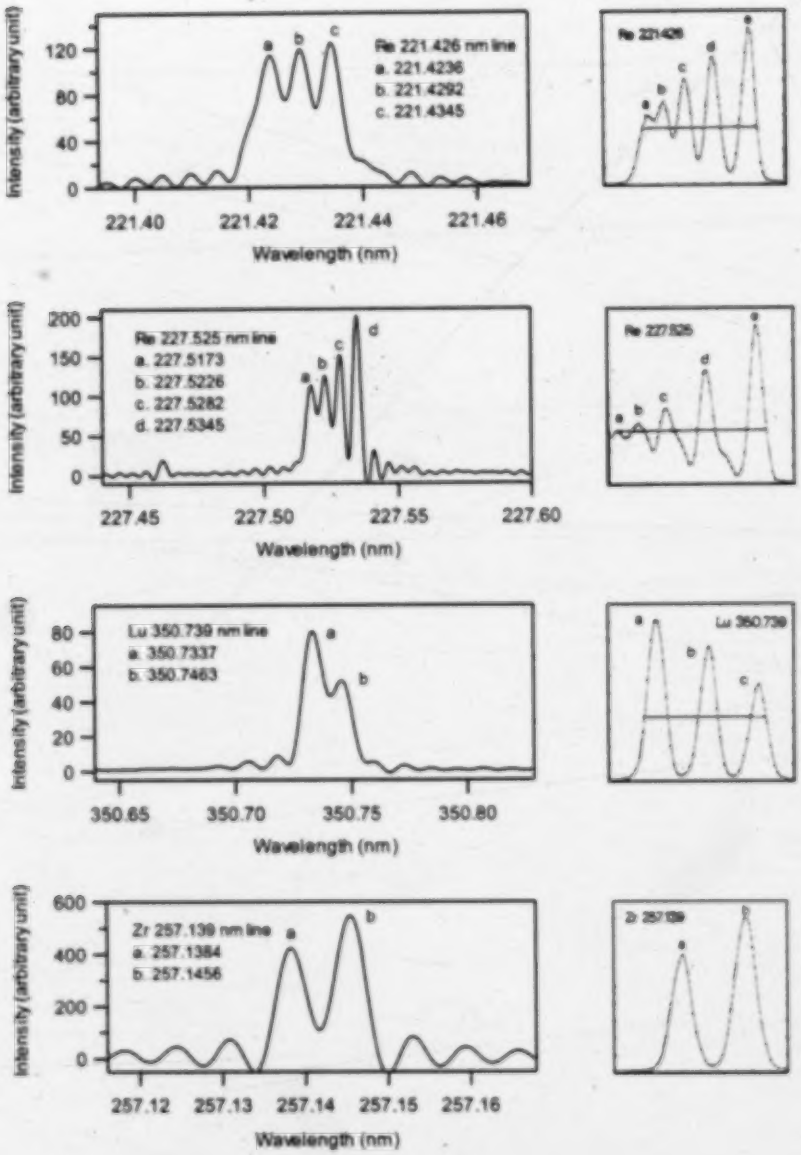

Figure 3-11. Some observed hyperfine structure. The line structures on the right are reprinted from ref(8) with permission from Elsevier Science.

3.3.4. Wavelength Bias in FTS Measurement

Another concern about the FTS measurement is whether the wavelength accuracy of FTS is wavelength dependent, or, in other words, if the FTS measurement has wavelength bias. Previous work(9) showed that, in ICP, the band broadening and position shifts usually occur in the order of 0.01 to 0.03 cm^{-1}. Therefore, they should not be of major concern by the analytical chemists since this level of resolution is not routinely available with normal spectrometers (10). Salit and co-workers (11) measured the wavelength of Ar ionic lines in the visible region with an upgraded version of a Chelsea FT-500 UV-visible FTS (designed by Blackett Laboratory, Imperial College of London). They observed apparent wavelength bias for both Ar and Hg lines. The correction factor k and the wavenumber had a fairly good linear relationship. The least square curve-fitting of the scanned k - σ plot gave the following relationship:

$$k = 2 \times 10^{-11}\sigma + 1.889 \times 10^{-7}$$

Where k is the wave number correction factor and σ is the wave number in cm^{-1}. At 20000 cm^{-1} or 500 nm, k equals to 5.9×10^{-7}, and the wave number shift is about 0.012 cm^{-1}. When the wavelength decreased from 500 to 350 nm, the value of correction factor increased about 30%.

This type of wavelength bias, even if exists, will not be a major concern for the Spectral Library, since the error level is far beyond the resolution of the library and thus will not be noticed. Nevertheless, it is still worthwhile to have a look at the wavelength bias issue of the Spectral Library.

Argon visible lines provided a convenient source for the examination of the instrumental wavelength dependence. Their wavelength errors were plotted against corresponding wavelength (Figure 3-12, top). It can be seen that, although there is no definite linear relationship, there is a trend that the wavelength errors decrease as the wavelength increases. Least square curve fitting gives a slope of –0.034, or 3.4 pm change in wavelength error per 100 nm change in wavelength, R^2 equals 0.48. The same trend was observed when Thorne's Ar wavelength values were used. The slope for the least square fitted line was –0.037, and R^2 is 0.43.

For comparison, a correction factor k verses wavenumber plot is also included (Figure 3-12, bottom). It can be seen that it shows the same trend as that by the wavelength error verse wavelength. In fact, the plot itself looks like the wavelength error plot with a 180-degree rotation.

Next, visible spectra of La, Y, Cr, Sc, Ce, and Nd were selected to investigate further the possible wavelength bias. The only criteria for selecting these spectra was that they had spectral lines spread out over a large wavelength span, so the wavelength bias, if it exists, would be easily noticed.

From Figure 3-13 it can be seen that the wavelength errors are generally scattered in a ±5 pm range. No wavelength dependency of either the magnitude or the degree of scattering of the errors could be observed. Least square fitting generally gave R^2 values less than 0.05 for these plots, so there was no definite linear relationship between the errors and the wavelength. The slopes for the trend lines were generally less than 0.01. That is, even if there were a change in wavelength error, it would be less than 1 pm per 100-nm wavelength change.

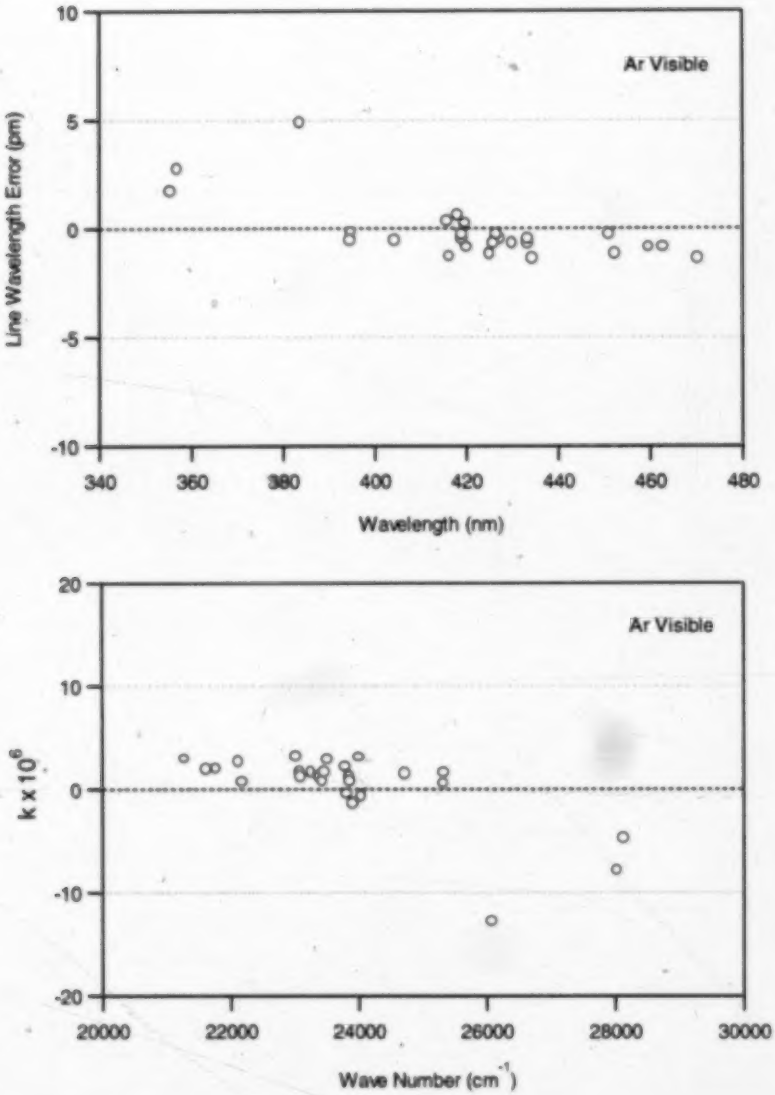

Figure 3-12. Wavelength errors and correction factors for Ar visible lines.

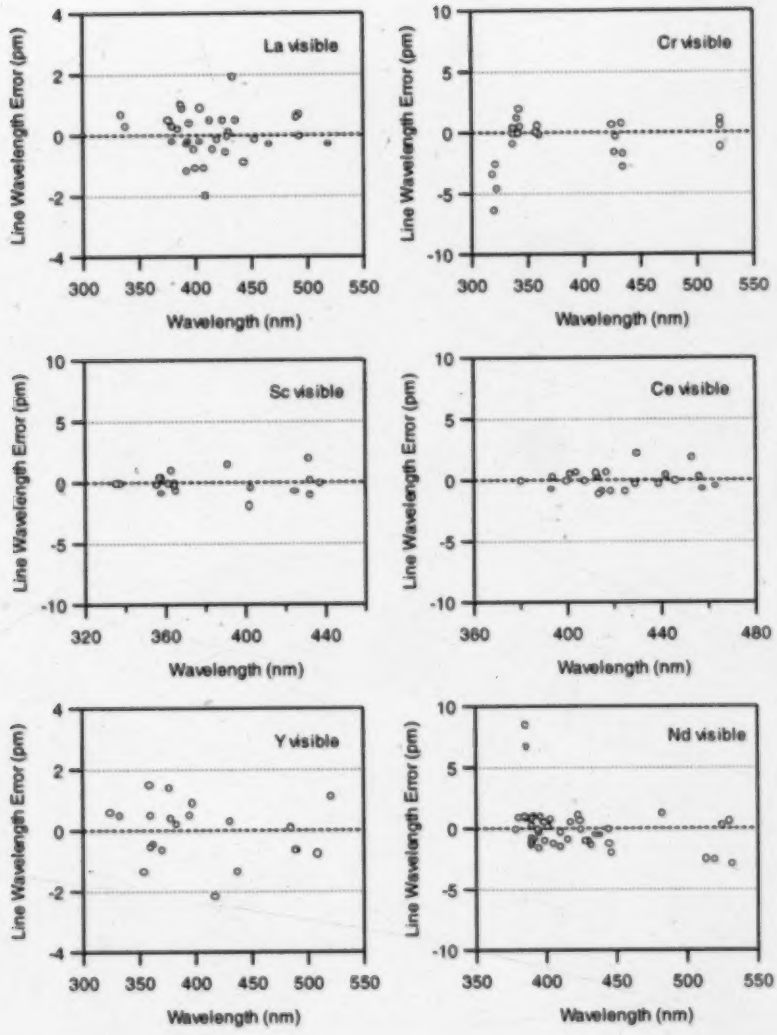

Figure 3-13. Wavelength errors vs. wavelength for La, Cr, Sc, Ce, Y, and Nd.

Wavelength errors for all calibrated spectral lines in the visible region were then plotted against their wavelength value. These should provide even more solid evidence for the possible wavelength bias, or for no wavelength bias. Figure 3-14 shows that about one thousand data points scattered in a ± 10 pm region, with majority within ± 2 pm. The points are distributed roughly symmetrically about the zero error line all the way along the wavelength axis. There is no visual indication for any wavelength related scattering pattern change.

The slope for the trend line for this plot is 0.0002 with R^2 of 0.00004. That is, for every 100 nm change in wavelength, the wavelength error would increase 0.02 pm. As this was way below the precision level of the current spectrometer, it should be considered as zero in order to be meaningful. Therefore, on the given level of resolution and accuracy, there was no wavelength bias observed.

To eliminate any further doubt, the visible region was divided into four sub-regions for statistical analysis. The wavelength range of these sub-regions, the number of lines they cover, and the mean and standard deviation for wavelength errors and k values are listed in Table 3-9.

Table 3-8. Least square fitting results for trend lines (visible lines)

Element	Slope	Intercept	R^2
Ce	0.0032	-1.3229	0.0073
Cr	0.0078	-3.8273	0.0661
La	-0.0005	0.2012	0.0006
Nd	-0.0157	6.5562	0.01106
Sc	2×10^{-8}	-0.0572	5×10^{-9}
Y	-0.0032	1.2415	0.0378

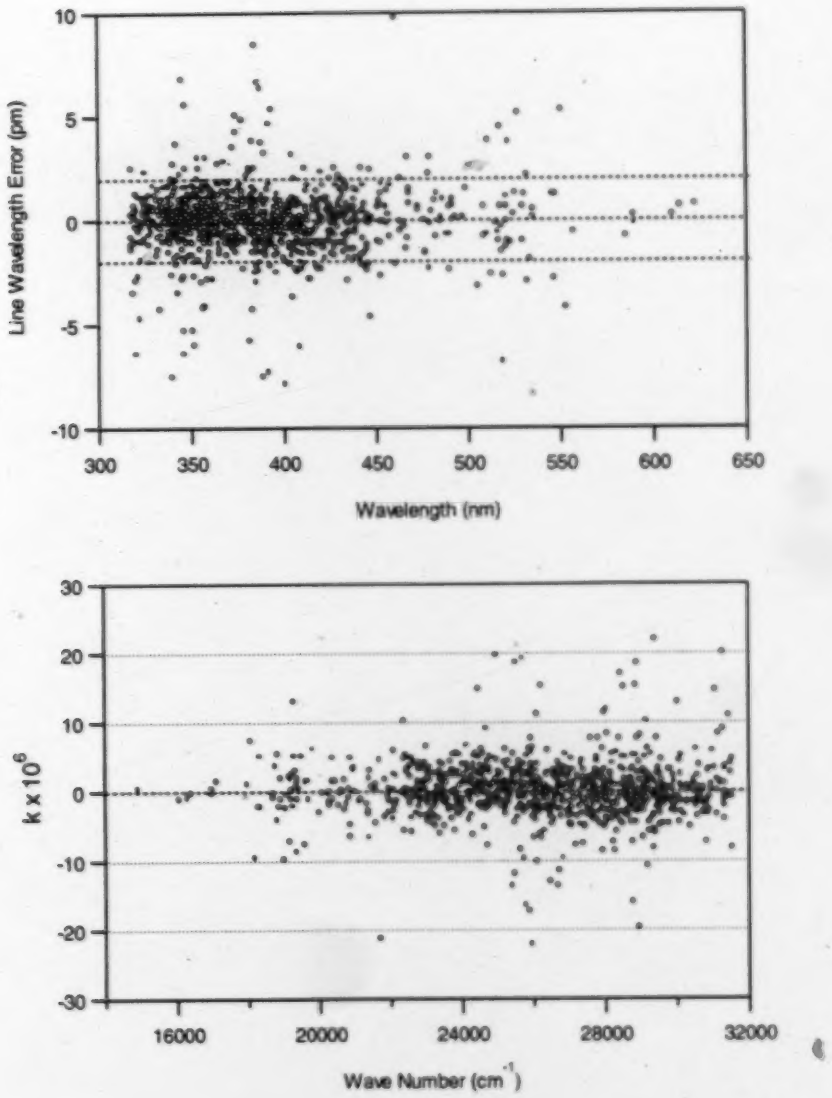

Figure 3-14. Wavelength errors verse wavelength for all visible lines.

Table 3-9. Sub-regions for statistical analysis.

Sub-Region	Wavelength (nm)	Number of Lines	Wavelength Error Mean (pm)	Wavelength Error SD (pm)	Correction factor k	SD of k
1	316-350	228	-0.04167	1.54483	0.13534	4.58701
2	350-400	390	0.05205	1.61280	-0.14274	4.29112
3	400-500	290	-0.12276	1.48225	0.31602	3.44265
4	500-630	47	-0.03617	2.28648	0.07833	4.33644

The idea behind this analysis was simple. Remember each spectrum in the library was calibrated with a single laser wavelength, and by definition, if systematic wavelength bias existed, the wavelength errors would be different for lines at different wavelength. The mean value of the wavelength errors of different sub-regions would also be different. This could be tested with Student t tests, and the results were listed in Table 3-10. It can be seen that, between sub-region 1 (316-350 nm) and any other sub-regions, the t values were always less than the critical value of t at confidence level of 95%. This means the wavelength errors in region 1 were not significantly different from any other sub-regions. The analysis results for correction factor k gave similar results. Similarly, the t values for tests between any two sub-regions were always less than t critical values. Thus the wavelength errors showed no significant difference between any two sub-regions. That is, by definition, no wavelength bias.

The UV region, however, had a slightly different picture. Spectra of nine elements, Cu, Sn, Nb, Gd, Hf, Sb, Pt, Pb, and Y, were selected by the same criteria for selecting visible spectra. The wavelength errors vs. wavelength plots for Cu, Sn, Nb, Gd, Hf, and Sb (Figure 3-15) showed no clear trend for wavelength bias,

although one might suspect that there is a small wavelength dependency as suggested by the slope of the trend line, which varied from –0.05 to about -0.01 (Table 3-12).

The three plots for Pb, Pt, and Yb in Figure 3-16, however, showed a fairly good linear relationship between the wavelength error and the wavelength, and all R^2 values were above 0.6. The slopes suggested an average 3 to 5 pm change in wavelength error per 100-nm change in wavelength. The all-lines-plot for the wavelength error vs. wavelength in the UV region (Figure 3-17) indicated a slight tilting of the trend line, with the larger errors occurring at the low wavelength end. The slope of the trend line was –0.0128 with R^2 at 0.0374.

Table 3-10. t value* calculated for wavelength errors and correction factor k.

Sub-region		2	3	4
1	$t_{wavelength}$ *	-0.7159 (494)	0.6037 (480)	-0.0158 (55)
	t_k	-0.7448 (452)	0.4949 (411)	-0.0814 (70)
2	$t_{wavelength}$		1.4646 (651)	0.2569 (52)
	t_k		-1.5457 (676)	-0.0331 (58)
3	$t_{wavelength}$			-0.2512 (53)
	t_k			-0.3579 (56)

* The values for Student t and degree of freedom (in parenthesis) were calculated as

$$t_{cal} = \frac{\bar{x}_1 - \bar{x}_2}{\sqrt{s_1^2/n_1 + s_2^2/n_2}} \qquad \text{Degree of Freedom} = \frac{\left(s_1^2/n_1 + s_2^2/n_2\right)^2}{\frac{\left(s_1^2/n_1\right)^2}{n_1+1} + \frac{\left(s_2^2/n_2\right)^2}{n_2+1}} - 2$$

Table 3-11. Critical t values at confidence level of 95%.

Degree of freedom	∞	450	250	200	150	70	60	50
t value	1.645	1.652	1.655	1.656	1.657	1.669	1.673	1.680

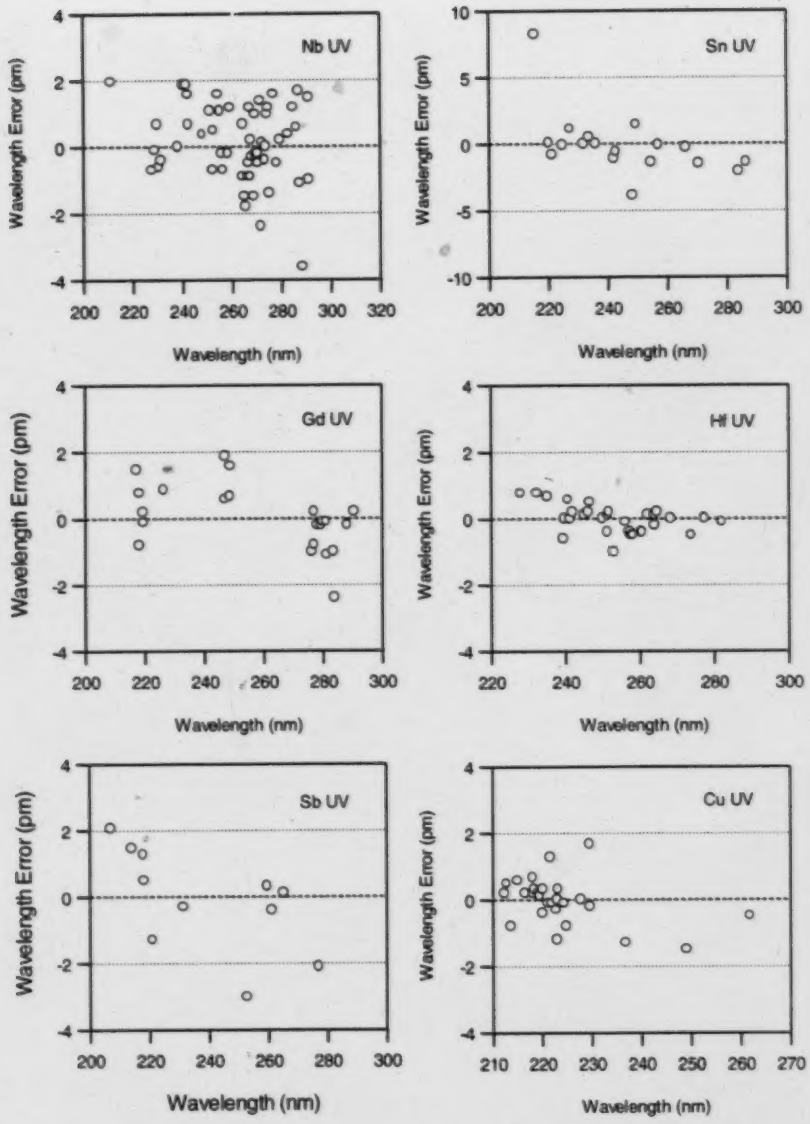

Figure 3-15. Wavelength errors vs. wavelength for Nb, Sn, Gd, Hf, Sb and Cu.

The statistical analysis for the wavelength errors at different sub-regions of the spectrum seems to further confirm the existence of a small wavelength bias. The mean of the wavelength errors in the first sub-region (200-230 nm) is significantly different from any one of the other four sub-regions. That of the second and third sub-regions (230-250 and 250-265 nm respectively) are also significantly different from that in the last sub-region (280-316 nm) above 95% confidence level (Table 3-14). Student t test for correction factor k values gives similar results.

Table 3-12. Least square fitting results for trend lines (visible lines)

Element	Slope	Intercept	R^2
Nb	-0.0190	5.01	0.072
Cu	-0.0272	6.06	0.168
Sn	-0.0502	14.1	0.264
Hf	-0.0159	4.01	0.236
Gd	-0.0195	5.05	0.301
Sb	-0.0386	9.09	0.387
Pt	-0.0314	8.00	0.629
Pb	-0.0550	13.7	0.717
Yb	-0.0451	11.5	0.868

Table 3-13. UV Sub-regions for statistical analysis.

Sub-Region	Wavelength (nm)	Number of Lines	Wavelength Error Mean (pm)	Wavelength Error SD (pm)	Correction factor k	SD of k
1	200-230	155	0.6834	1.90	-3.111	8.74
2	230-250	240	0.0112	1.27	-0.0547	5.27
3	250-265	225	-0.0533	1.23	0.2119	4.82
4	265-280	243	-0.1601	1.14	0.5865	4.20
5	280-316	99	-0.3039	1.15	1.0673	4.00

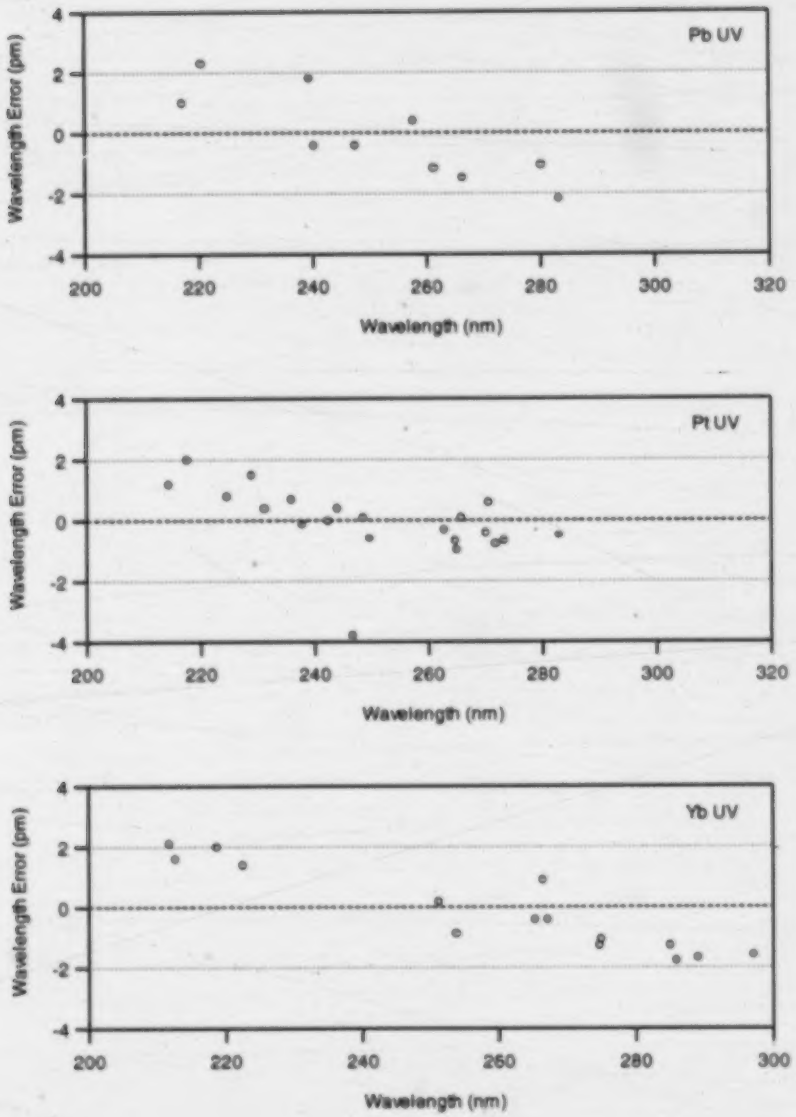

Figure 3-16. Wavelength errors vs. wavelength for Pb, Pt, and Yb.

Table 3-14. t value calculated for wavelength errors and correction factor k.

Sub-region		2	3	4	5
1	$t_{wavelength}$ *	3.8745 (243)	4.2539 (243)	4.9780 (226)	5.1545 (253)
	t_k	-3.9191 (228)	-4.3050 (220)	-4.9198 (200)	-5.1664 (234)
2	$t_{wavelength}$		0.5731 (464)	1.1657 (476)	2.2278 (203)
	t_k		-4.3050 (465)	-4.9198 (457)	-2.1303 (241)
3	$t_{wavelength}$			0.9528 (457)	1.7549 (202)
	t_k			-0.8934 (447)	-1.6615 (226)
4	$t_{wavelength}$				1.0540 (182)
	t_k				-0.9937 (192)

* Number in bracket is degree of freedom.

Before jumping to a conclusion, however, one might want to consider other facts. Figure 3-7 in Section 3.3.2 shows that when Thorne's wavelengths were used as standards, the wavelength errors of Fe were significantly changed in both magnitude and distribution pattern. What about the elements considered here?

The wavelength errors vs. wavelength plots for Pb, Cu, Sb, Sn were shown in Figure 3-18. It was clear that, when using Thorne's wavelengths as standards, the wavelength errors for lines of all four elements were reduced, and the degree of scatter decreased. The slope of their trend lines changed so much that there was no apparent wavelength dependency noticeable (Table 3-15).

This raises an interesting question: what caused the observed wavelength bias for these elements?

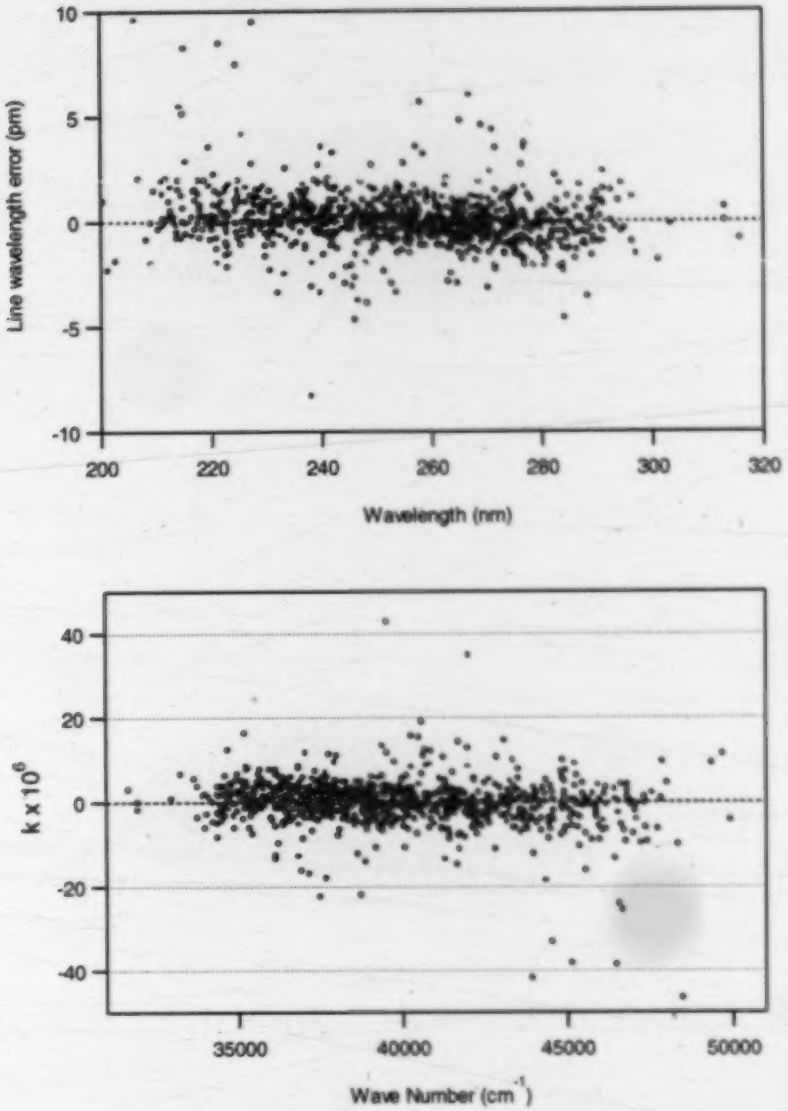

Figure 3-17. Wavelength errors vs. wavelength for all UV lines.

One of the possibilities is that FTS may have an inherent wavelength bias. However, this is supported neither by theory nor by experimental results. Although Salit (11) reported observed wavelength bias, his work was done at much higher resolution, the reported bias was at 0.001 pm level. Besides, his single point calibration experiment, in which the wavelength of a visible laser and its first harmonics in the UV were measured, indicated no sign of wavelength bias. Thus they suspected the literature wavelengths were not accurate.

Thorne's wavelength values were obtained with high resolution FTS and they did not observe any wavelength dependency of correction factors. As discussed before, the results from this research basically shows no wavelength dependency when compared with Thorne's wavelengths. Therefore, it is not likely that FTS is at the root of the problem, albeit a small problem.

Another possibility is the inaccuracy of the literature wavelength values for some spectral lines. However, as Pb, Cu or Sn are common elements, their wavelength values should have been well characterized and this level of error should not exist. Apparently further studies are needed to clarify this problem.

Table 3-15. Least square fitting results with different standards (UV lines)

	Zaidel wavelength			Thorne wavelength		
Element	Slope	Intercept	R^2	Slope	Intercept	R^2
Cu	-0.0272	6.06	0.168	-0.0036	0.093	0.0096
Sn	-0.0582	14.2	0.264	-0.0078	1.02	0.201
Sb	-0.0386	9.09	0.387	0.0094	-2.03	0.111
Pb	-0.0550	13.7	0.717	-0.0137	3.19	0.296

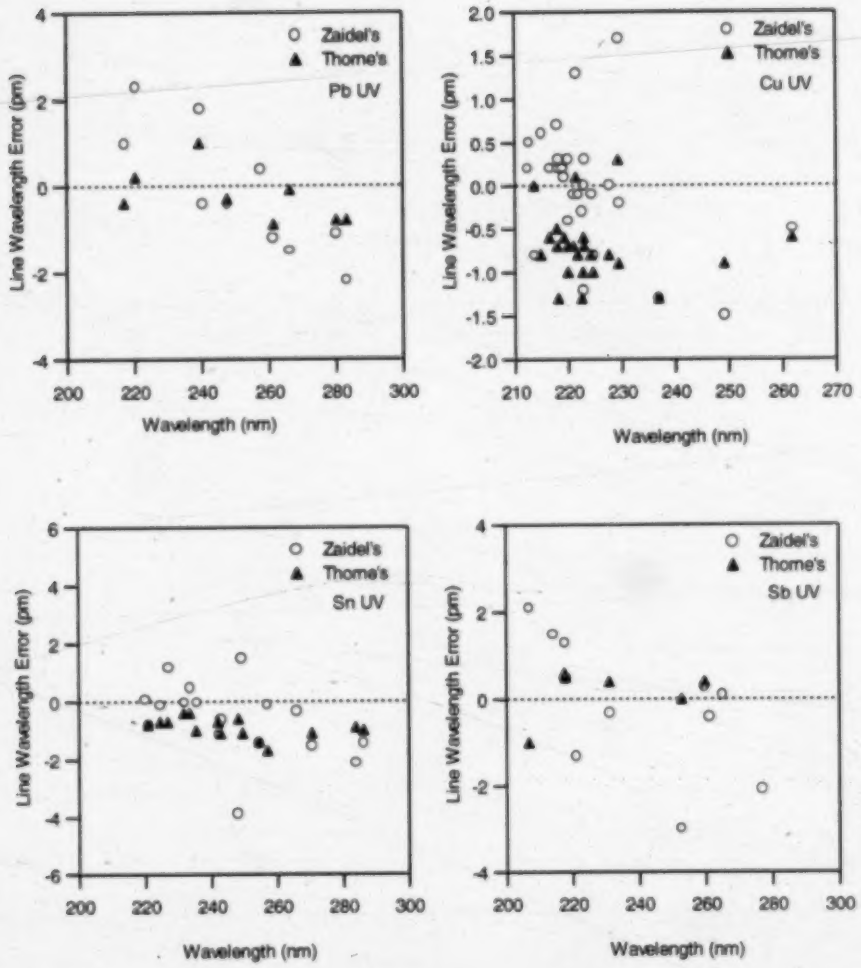

Figure 3-18. Wavelength errors vs. wavelength under different wavelength standards for Pb, Cu, Sn, and Sb..

3.3.5. Calibration with Average Laser Wavelength

As discussed throughout this section, the reference laser apparent wavelength provides an excellent way to obtain accurate wavelength values with this instrument by having a separate λ_{LAW} with each spectrum. Alternatively, these spectra can be calibrated with the average of the *reference Laser Apparent Wavelength* values to simplify the calibration process, although this approach might sacrifice the fine touch of the calibration and compromise the wavelength accuracy.

That said, calibration of spectra with a single laser wavelength is still worth trying due to a number of reasons. First, the primary cause that introduces inaccuracy into FTS wavelength measurements is the misalignment of the reference laser, the mirrors, and the optical system. For a properly installed and adjusted system, the degree of misalignment should be fairly consistent, and so then the apparent reference laser wavelength. Secondly, the wavelength inaccuracy introduced by the finite-size aperture should also be fairly consistent because in all ICP measurements only one set of aperture and lens combination was used, and the ICP position is usually fixed. Thus the homogeneity of luminance on the aperture would be roughly the same, and the variation should be small.

The spectral line wavelength errors of Ag, Co, and Cu spectra calibrated with element specific reference laser apparent wavelength, and that calibrated with average reference laser apparent wavelength are compared in Figures 3-19 to 3-21. The Ag specific laser wavelength $\lambda_{LAW,\,AgUV}$ = 632.8456 nm, so when the spectrum was recalibrated with the average laser wavelength $\lambda_{LAW,\,UV}$ = 632.8438 nm, the line wavelength values decreased uniformly with little change in the scattering pattern.

The error absolute values for lines with positive errors decreased while for those with negative errors increased. The overall result is a shift of the mean of the line wavelength errors from zero to –0.69 pm, the mean of the line wavelength error absolute values increased from 1.38 to 1.41 pm, and the standard deviation was not changed (1.81 verse 1.82).

The Cu lines, on the other hand, shifted towards the positive side in wavelength, as all wavelength errors were positive after re-calibration, the mean of the wavelength error and their absolute values both increased noticeably from –0.03 and 0.51 to 1.36 pm, respectively. The standard deviation decreased slightly from 0.72 to 0.69. With $\lambda_{LAW,\,CoUV}$ = 632.8426 nm, The Co lines showed a more complex situation with moderate increase in the mean values of wavelength error ($\Delta\lambda_{err}$ from -0.01 to 0.45) and wavelength error absolute ($\Delta\lambda_{abs,\,err}$ from 0.51 to 0.62). The standard deviation decreased from 0.64 to 0.62.

The effect of calibration with an average laser wavelength $\lambda_{LAW,\,UV}$ can be seen more clearly from the plot of the mean values (calculated for each individual spectrum) for all the elements (Figure 3-22). Instead of remaining at or very close to zero, the mean values of the line wavelength error $\Delta\lambda_{err}$ now scattered in a 3 pm range centered at zero, representing the bias of wavelength error of each spectrum.

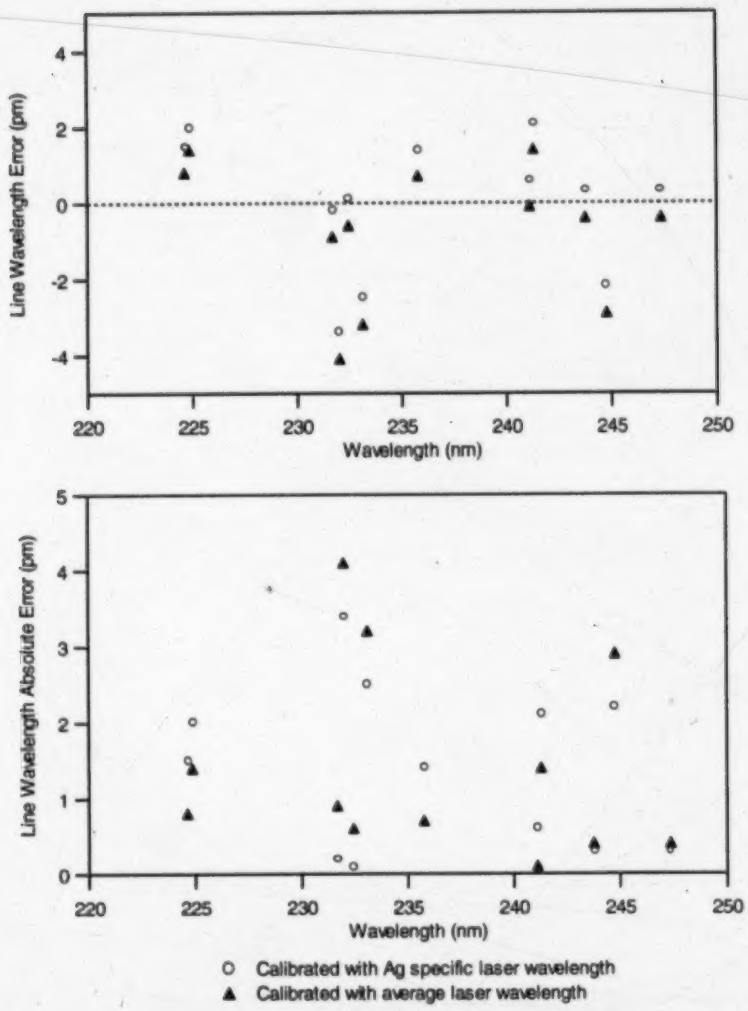

Figure 3-19. Wavelength errors of Ag lines calibrated with average apparent reference laser wavelength (632.8438 nm).

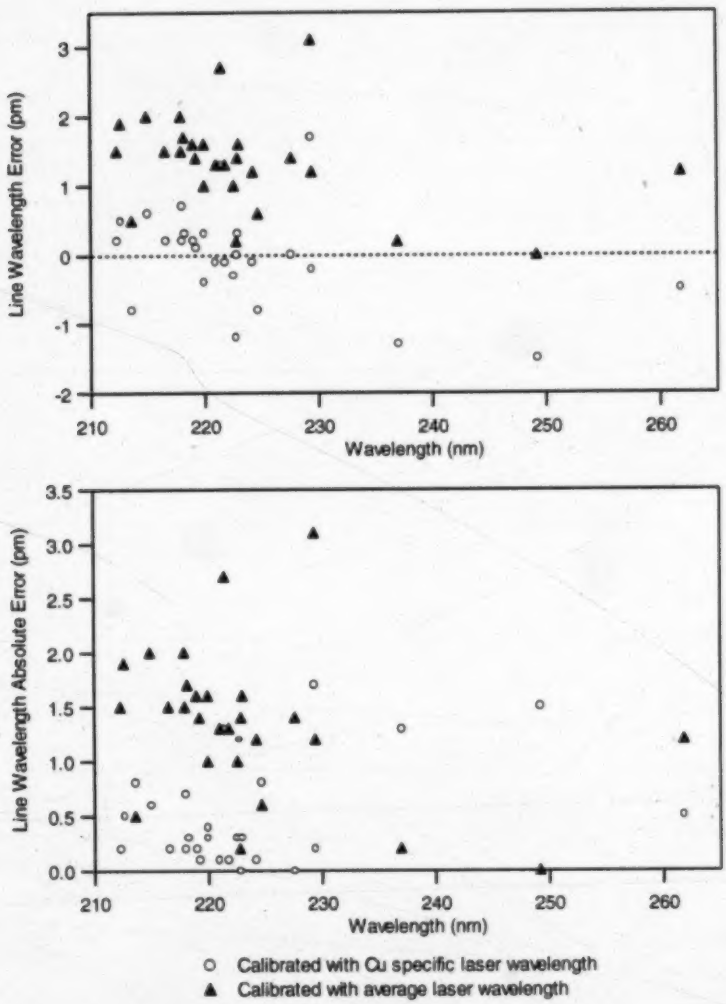

Figure 3-20. Wavelength errors of Cu lines calibrated with average apparent reference laser wavelength (632.8438 nm).

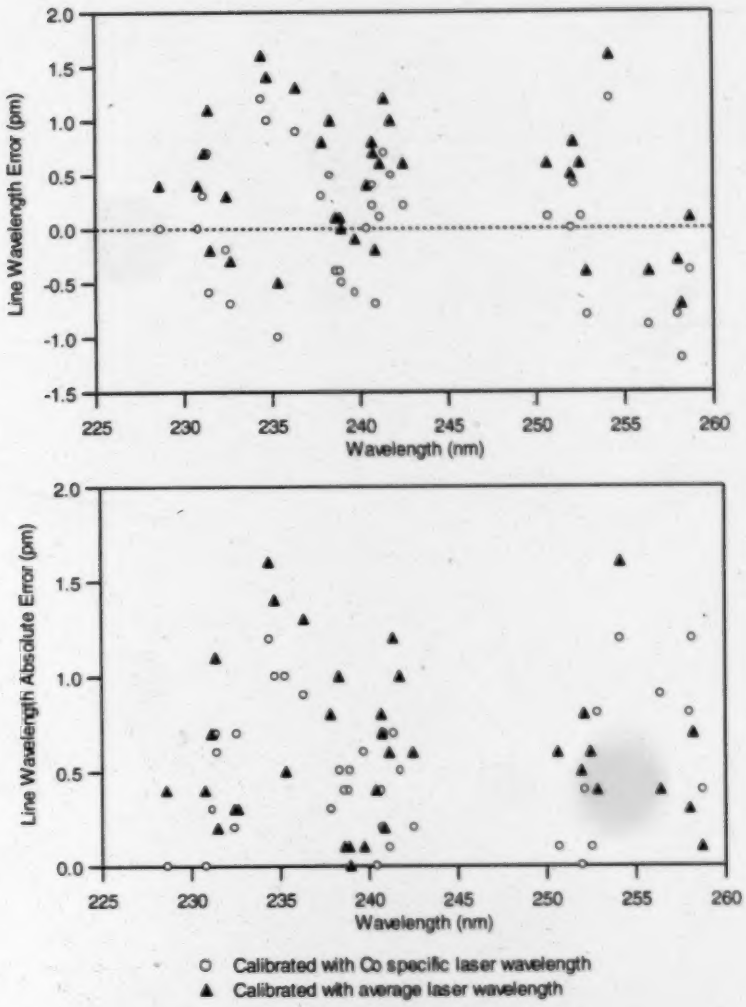

Figure 3-21. Wavelength errors of Co lines calibrated with average apparent reference laser wavelength (632.8438 nm).

The mean of the wavelength error absolute values $\Delta\lambda_{abs.\,err}$ (calculated for each individual spectrum) seems less affected by the re-calibration. Although the change was significant (calculated t was 3.17, compared with the critical value of 2.661 at 99% confidence level), the average value of $\Delta\lambda_{abs.\,err}$ only increased moderately from 1.05 ± 0.92 to 1.26 ± 1.02 pm, about 20%.

The standard deviation of the wavelength errors in each spectrum remains virtually unchanged for nearly all elements (Figure 3-23). This was expected since linear calibration should not change the degree of scattering of data points.

The above discussion defined, semi-qualitatively, the effects of wavelength calibration with the average apparent laser wavelength. But how exactly this affects the wavelength accuracy? Is there any difference between the wavelength values calculated from element specific laser wavelength, and those from average laser wavelength?

For Cr, Mn, Fe, Co, Ni, and Cu, the Student t values between the spectral line wavelength values calculated from element specific laser wavelength, from average laser wavelength, and from literature, termed as $\lambda_{specific}$, $\lambda_{average}$, and λ_{lit}, respectively, were calculated and listed in Table 3-16.

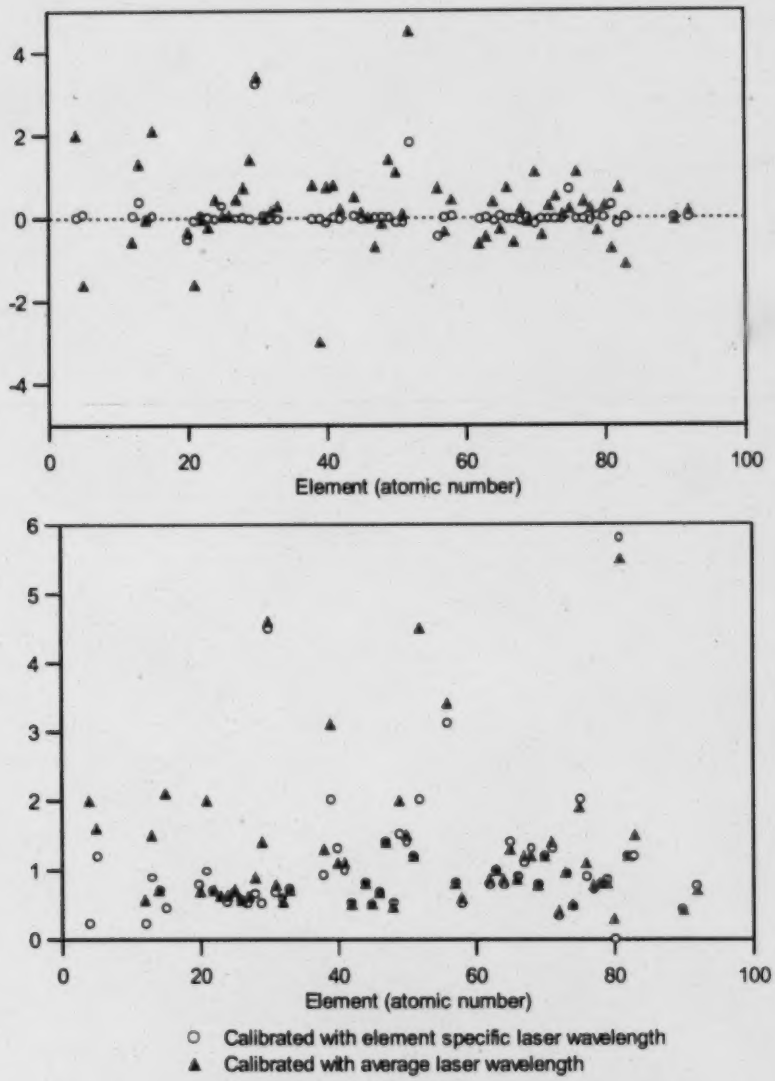

Figure 3-22. The mean of wavelength errors of spectra calibrated with average apparent reference laser wavelength (632.8438 nm).

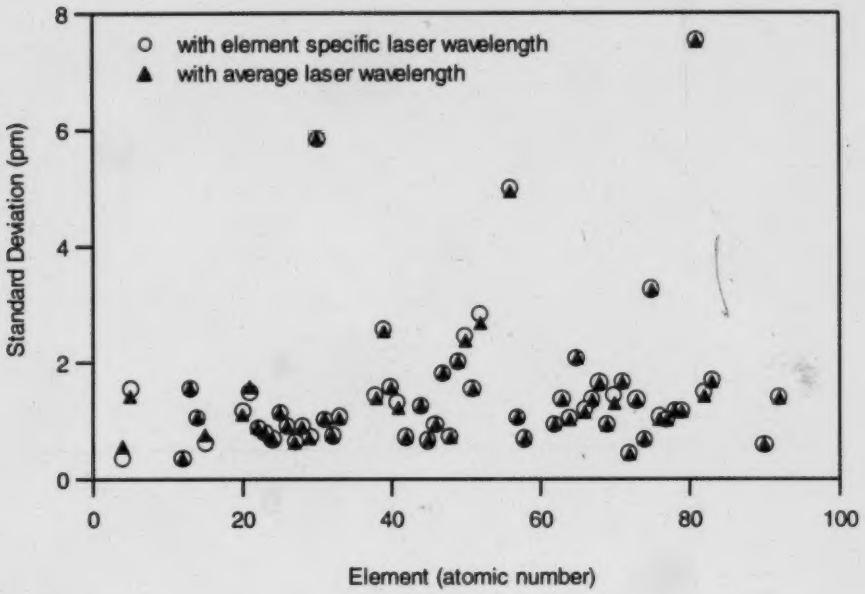

Figure 3-23. The standard deviation of wavelength errors of spectra calibrated with average apparent reference laser wavelength (632.8438 nm).

Table 3-16. Calculated t for comparison of spectral line wavelength values *.

Element	lines	λ_{LAW} (nm)	$\lambda_{specific}$ vs. λ_{lit}	$\lambda_{average}$ vs. λ_{lit}	$\lambda_{specific}$ vs. $\lambda_{average}$
Cr	25	632.8427	0.1113	-3.107	-22.41
Mn	20	632.8444	-0.2108	-1.653	21.92
Fe	29	632.8437	-0.1201	-0.3453	-4.098
Co	34	632.8426	0.1062	-4.266	-53.86
Ni	33	632.8418	-0.0774	-4.7821	6.0402
Cu	26	632.8399	0.1888	-10.16	-81.70

* $\lambda_{specific}$ was the line wavelength calculated with element specific laser wavelength, $\lambda_{average}$ was that with average laser wavelength, and λ_{lit} was Zaidel' wavelength.

As a general rule, $\lambda_{specific}$, the spectral line wavelength values calculated with element specific laser wavelength, showed no significant difference from the literature values (t from 0.07 to 0.21, less than the critical value which is around 2); $\lambda_{average}$, the spectral line wavelength values calculated with average laser wavelength were usually different from the literature values, unless, of course, the laser wavelength value for the specific element is sufficiently close enough to the average value, as in the case of Fe where $\lambda_{LAW, FeUV}$ = 632.8437 nm compared to $\lambda_{LAW, UV}$ = 632.8438. There was definite difference between the $\lambda_{specific}$ and $\lambda_{average}$, with t value generally greater than 4.

As discussed at the beginning of this section, calibration of the spectral library with an average apparent laser wavelength would certainly deteriorate the wavelength accuracy, as many aspects of misalignment or mis-collimation would have to be left uncompensated in this way. Therefore the average value of the apparent laser wavelength, 632.8438 nm, is recommended only if no element specific laser wavelength is available and it should be used only for work not requiring a high degree of wavelength accuracy. On the bright side, however, although the spectral line wavelength calibrated with average laser wavelength showed significant difference from literature values, the error introduced by doing so was only an extra 0.2 pm on average, compared to the original error of 1.05 pm. This demonstrated the excellent long-term stability of the present FTS system.

3.4. Spectral Line Shape and Resolution

Resolution is one of the most important measures of a spectrometer and of the quality of a spectrum. Full Width at Half-Height (FWHH) is one of the most commonly used definitions for resolution.

The spectral line shape profile, and thus the FWHH is significantly affected by any apodization function(s) applied to the interferogram, either intentionally applied mathematical functions or that imposed by the instrument. In fact, any measured interferogram, owing to its finite length, is the convolution of the real interferogram and at least a boxcar apodization function, which would result in a sinc function line profile. A triangular function, on the other hand, gives a $sinc^2$ line shape profile. Ref (12) lists the eight most commonly used apodization functions and the FWHH of the transformed spectral lines.

Instrumental apodization, or self-apodization, results from incident bean divergence, or imperfect collimation of the incident beam. It provides a means for direct observation of the instrumental effects on the line shape. Qualitatively, the interferograms in the spectral library can be roughly classified as three types: (1). Interferograms with a broad bell shape and a central burst intensity comparable in intensity to the wings. Examples include the UV interferograms of B, Mg, Si, Co, P, and the visible interferogram of Be. (2) Triangular shaped interferograms with a strong central burst. Ba and Zn in the UV, and Ba and Sr in the visible are examples. (3) Interferograms with a very strong central burst and low amplitude wings. These usually belong to the elements with either very rich lines or very weak lines in the

region measured. The apodization effects, either from the instrument or by band broadening mechanisms, are hard to discern directly from these interferograms.

The interferometer superimposed an apodization function on the interferograms of the first type, so their envelopes decayed much faster than the calculated Gaussian bell shape (Figure 3-24). Among them, the Mg interferogram decayed slower than that of Be and B. Its envelope resembled much more the envelope determined by a truncated Gaussian function. This probably meant it was less affected by the instrumental apodization. As a result, the widths of Mg lines were significantly narrower than that of Be or B (Figure 3-24).

In practice, instrument manufactures simply demonstrate the resolving power of their instruments by showing the separation of two adjacent spectral lines. Figure 3-26 shows the separation of some spectral lines using the spectra from the library and that with commercial instruments. It can be seen that the resolution of the spectra in the Spectral Library is comparable to or better than some of the-state-of-the-art instruments. The Cd 228.802 and As 228.812 nm lines can be resolved by the Jobin Yvon Ultima spectrometer, but not by Perkin-Elmer Optima (not shown). The simulated spectrum from the Spectral Library shows nearly base line resolution for these two lines. The Cu 213.598 and P 213.618 nm lines separated by the Varian Vista are completely baseline resolved in the simulated spectrum.

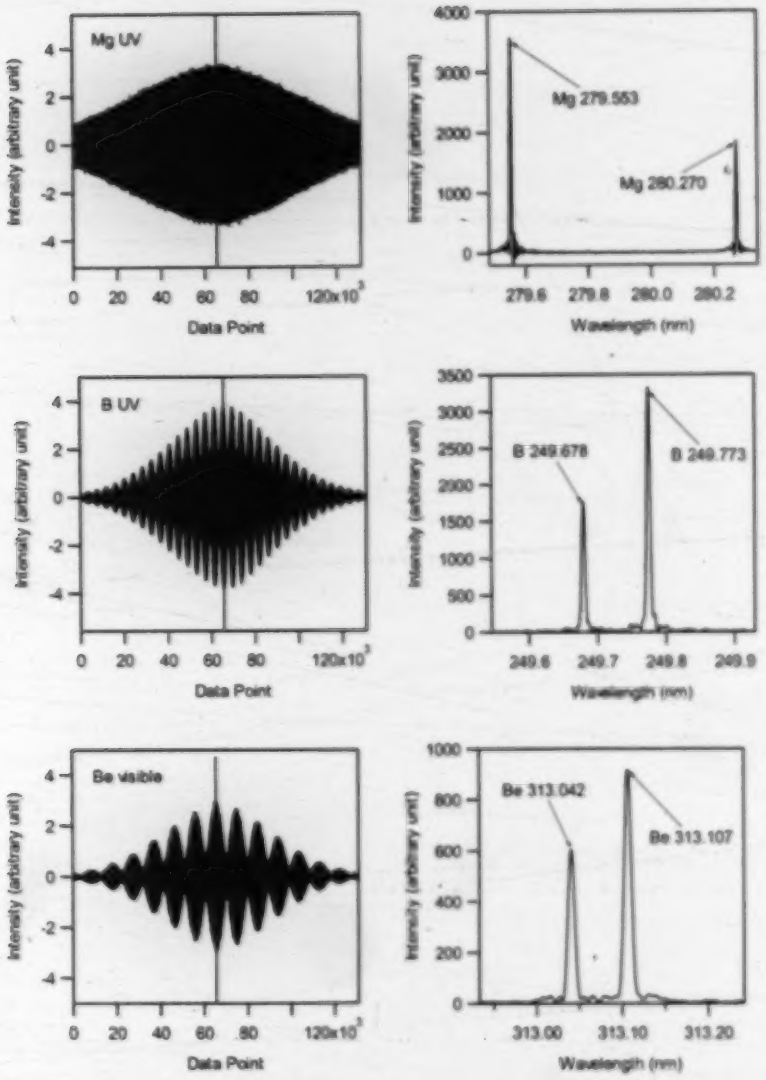

Figure 3-24. Spectral lines from Gaussian bell shape interferograms.

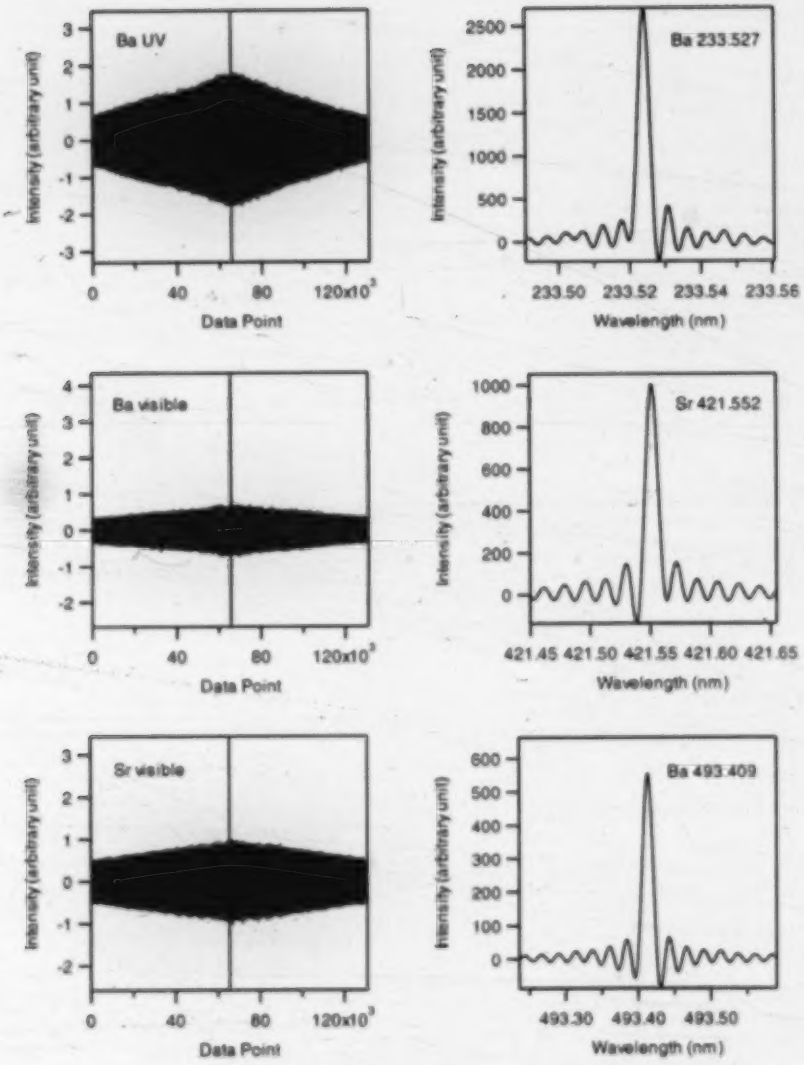

Figure 3-25. Spectral lines from triangular shape interferograms.

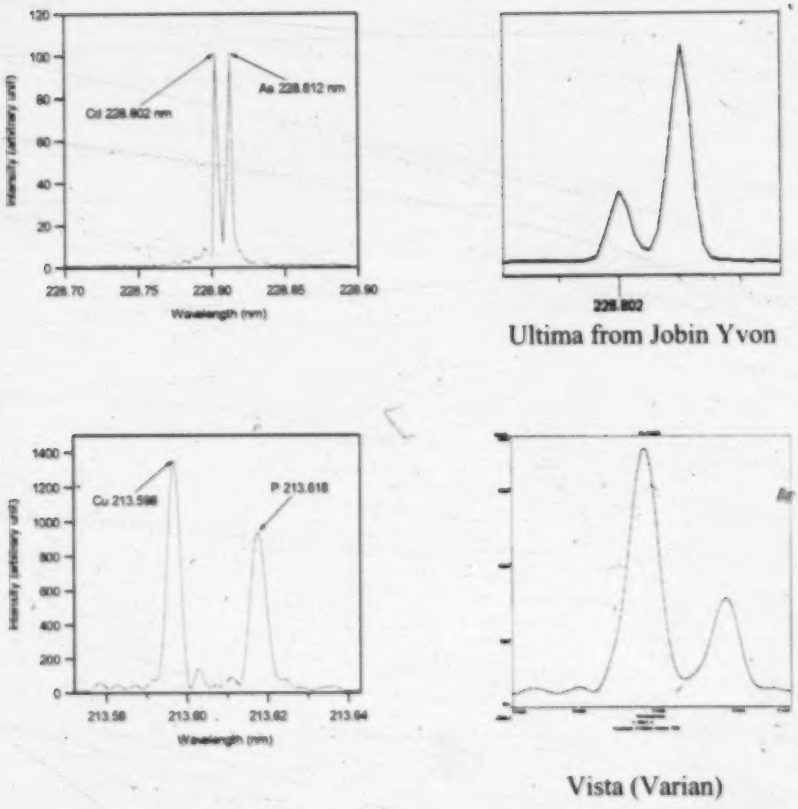

Figure 3-26. Spectra demonstrate the resolution of the spectral library. See text for details.

3.5. Control of Spectral Quality.

While all spectra were acquired using single element solutions, in certain cases, spectral quality in term of interfering lines may compromise the quality of certain spectra. The most common sources of problems in this area were aliasing and the Ar background.

3.5.1. Alias Lines.

As discussed before, alias lines are the result of undersampling of the spectrum. They usually occur in the UV and visible region where the sampling frequency has to be much higher than the reference laser frequency to meet the Nyquist's criteria. In theory, no alias lines should be observed in the spectra according to current experiment design. However, the PMT (both P166 and 1P21) and the electronic bandpass filter did not have a perfect clear cut at the dividing wavelength (316 nm) around which many elements emit strongly. Some very strong lines "penetrated" the wavelength filtering system made by the combination of PMT and bandpass filter and appeared as alias lines.

Figure 3-27 shows an example of this problem. Two spectra were collected for 1,000 ppm and 10,000 ppm solutions of Ca using the UV spectra measurement conditions. The visible region alias of the Ca 396.8445 nm and the Ca 393.3645 lines are actually more intense than the weak Ca UV lines. The situation is improved by running the 10,000 ppm solution, as the intense ground state ion lines will experience self-absorption in the plasma at this concentration level. Thus they are preferentially absorbed and the UV lines can now be readily observed.

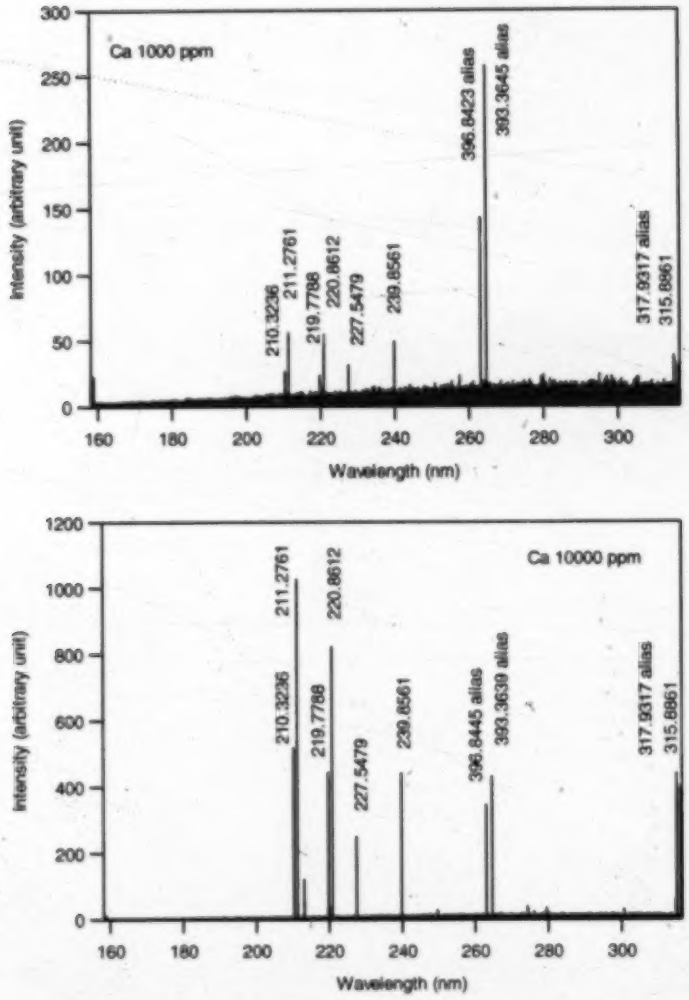

Figure 3-27. Ca UV spectrum measured with 1000 ppm (top) and 10,000 ppm solutions

Table 3-17 lists all alias lines found in the spectra of the library. These should at least be the majority of the alias lines. It is possible, however, some low intensity ones were missed.

Table 3-17. Alias lines found in the spectral library

Element	H%	λ_{alias}	λ_{true}	line	λ_{lit}	$\Delta\lambda$
Al	6.7	325.0705	308.2155	I	308.215	0.5
Al	12.5	323.0946	309.2711	I	309.271	0.1
Al	1.9	323.8901	309.2843	I	309.284	0.3
Be	100.0	319.8701	313.0423	II	313.042	0.3
Be	65.9	319.8029	313.1067	II	313.107	-0.3
Cr	9.5	321.1147	311.8642	II	311.864	0.2
Cr	17.2	320.9326	312.0366	II	312.036	0.6
Cr	25.5	320.4460	312.4975	II	312.494	3.5
Cr	4.3	320.0553	312.8699	II	312.869	0.9
Cr	4.8	319.2233	313.6691	II	313.668	1.1
Cr	4.5	318.1403	314.7218	II	314.722	-0.2
Fe	12.2	332.2136	302.0645	I	302.064	0.5
Hf	30.7	319.4314	313.4716	II	313.472	-0.4
Mg	46.4	364.4916	279.5527	I	279.553	-0.3
Mg	44.1	363.2792	280.2701	I	280.270	0.1
Mg	20.4	355.2989	285.2124	II	285.213	-0.6
Mn	27.7	343.4954	293.3068	II	293.306	0.8
Mn	48.8	342.6427	293.9314	II	293.930	1.4
Mn	77.7	341.3075	294.9211	II	294.921	0.1
Mo	9.3	344.8308	292.3393	II	292.339	0.3
Mo	8.3	343.8474	293.0499	II	293.048	1.9
Mo	10.7	324.4733	308.7623	II	308.763	-0.7
Mo	8.6	320.7618	312.1998	II	312.200	-0.2
Mo	25.6	319.6512	313.2592	I	313.259	0.2
Mo	9.4	317.5720	315.2821	II	315.282	0.1
Nb	9.9	330.7608	303.2764	II	303.277	-0.6
Nb	9.4	327.0628	306.4534	II	306.453	0.4
Nb	70.9	319.8392	313.0789	II	313.078	0.9
Nb	26.3	318.3276	314.5409	II	314.540	0.9
Nb	100.0	316.5050	316.3408	II	316.340	0.8
Ni	7.5	334.4369	300.2492	I	300.249	0.2
Ni	4.8	333.2645	300.2005	I	300.200	0.5
Ni	11.0	328.6379	305.0823	I	305.082	0.3
Ni	12.5	322.9467	310.1563	I	310.155	1.3
Ni	5.9	322.9121	310.1882	I	310.188	0.2
Ni	8.7	319.4930	313.4101	I	313.411	-0.9
Ca	32.5	263.1025	396.8445	II	396.847	-2.5
Ca	39.6	264.6550	393.3639	II	393.367	-3.1
Ca	43.6	314.9260	317.9317	II	317.933	-1.3

3.5.2. Ar lines

As the plasma is an Ar based plasma, it is not surprising that Ar lines are the primary or even dominant lines for many visible spectra in the library. In the simplest situation it may be sufficient to run the element at a higher concentration. This is illustrated for the visible spectrum of Cd in Figure 3-28. With the 10,000 ppm solution in contrast to the 1000 ppm solution the Cd visible lines are clear.

Another way to handle the Ar problem is by spectral subtraction. The library contains a full complementary set of Ar background spectra measured at the same time as that for each element. According to how a spectrum is affected by the Ar lines in it, the visible spectra in the Spectral Library can be divided into three different groups: (1) Ar lines exist in the spectrum but do not mix with lines from the element, as for the Ag visible spectrum (Figure 3-29). In this case, removal of Ar lines was not critical, although showed an improvement to the quality of the spectrum. (2). Ar lines exist in the spectrum and are mixed with element lines with comparable intensity, as in the Co visible spectrum (Figure 3-30). In this situation, line recognition is rather difficult and spectrum subtraction gives a clean Co spectrum without Ar lines present, and thus significantly improves its quality. (3). In the worst case, Ar lines become the dominant lines in the whole spectrum and bury all element lines into the jungle (Figure 3-31). In this case, the only way to get a clean spectrum is to remove Ar lines and this is crucial to the quality of the Zn spectrum. Unfortunately, some Ar line residue remained in the Zn spectrum due to the overwhelming intensity difference before subtraction.

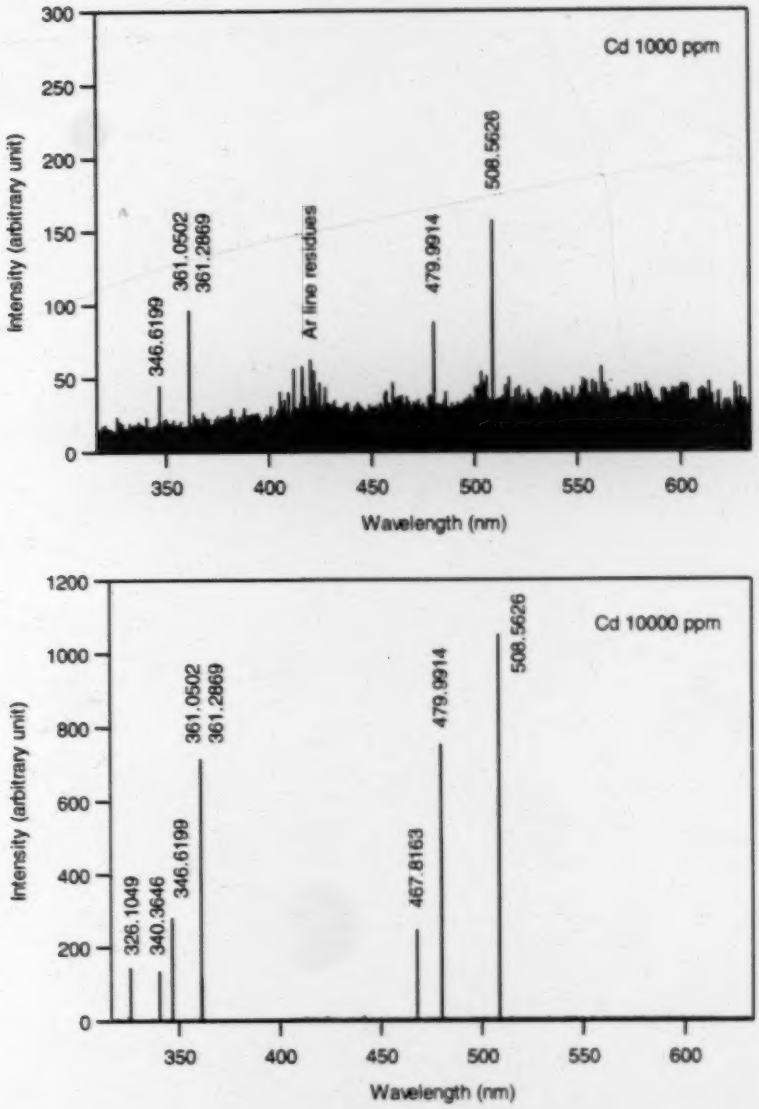

Figure 3-28. Cd UV spectrum measured with 1000 ppm (top) and 10,000 ppm solutions

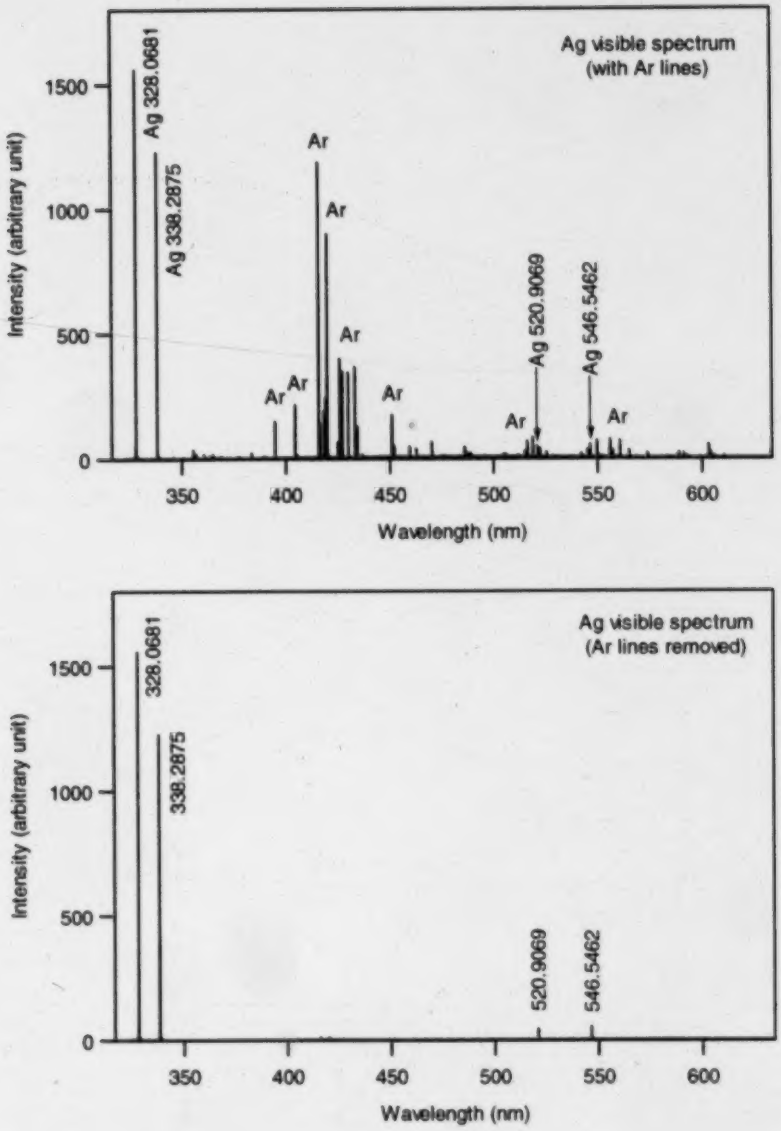

Figure 3-29. Ag visible spectrum before and after the removal of argon lines.

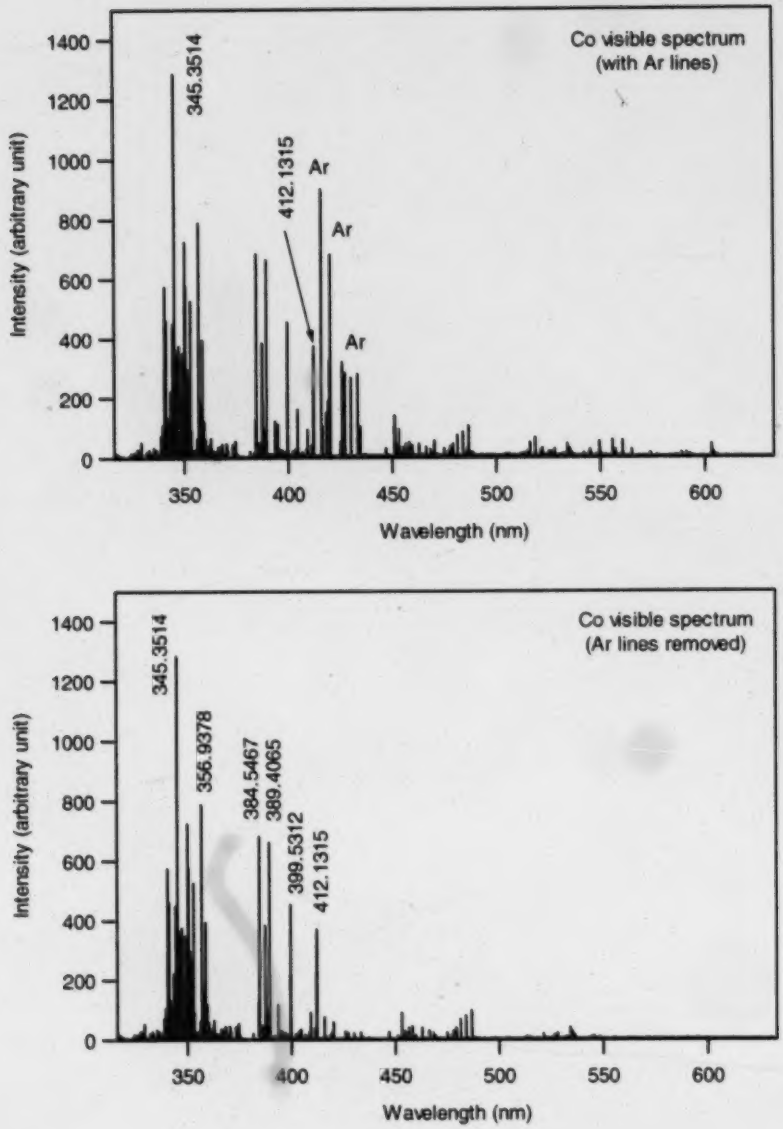

Figure 3-30. Co visible spectrum before and after the removal of argon lines.

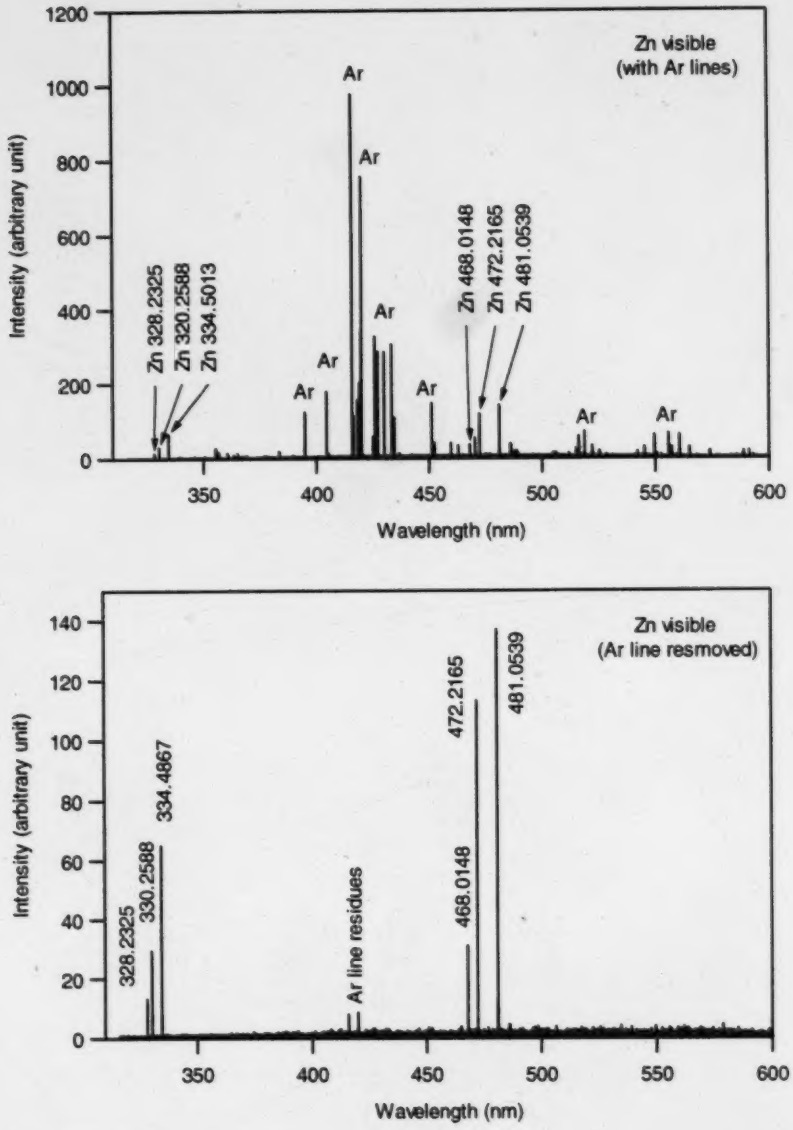

Figure 3-31. Zinc visible spectrum before and after the removal of argon lines.

3.5.3. Lines from Other Sources

Other than the situations discussed above, there are still a few sources of extra lines in a spectrum. King and Horlick (4) discussed the spurious "spectral" lines and features introduced by the modulation of the emission source and interferogram sampling errors. These lines are usually found in vicinity of strong spectral lines, and decrease as the square root of the number of scans on interferogram signal averaging.

Careful readers might have noticed the lines at the end of the spectra. They are the modulated power line frequency and its harmonics.

Finally, although special precautions had been taken during the study, the lines from impurities still showed up. For example, apparently trace boron somehow got into the Zn solution and thus two boron lines showed up as weak lines (Figure 3-32, top). A few silicon lines (either from the torch or a true impurity) found their way into the UV spectrum of Sb (Figure 3-32, bottom). The worst case of this problem is the present of Ca lines as dominant lines in the visible spectrum of Rh (Figure 3-33, top).

Counter-ions that come with the element of interest could be a problem sometimes, as can be seen in the Si visible spectrum (Figure 3-33, bottom). The standard solution of Si is the aqueous solution of high purity sodium silicate. As the Si lines in the visible region are quite weak, it is not a surprise to see the sodium doublet dominating the spectrum. In fact, three out of four lines in this spectrum are sodium lines, leaving this spectrum looking more like a sodium visible spectrum than that of silicon.

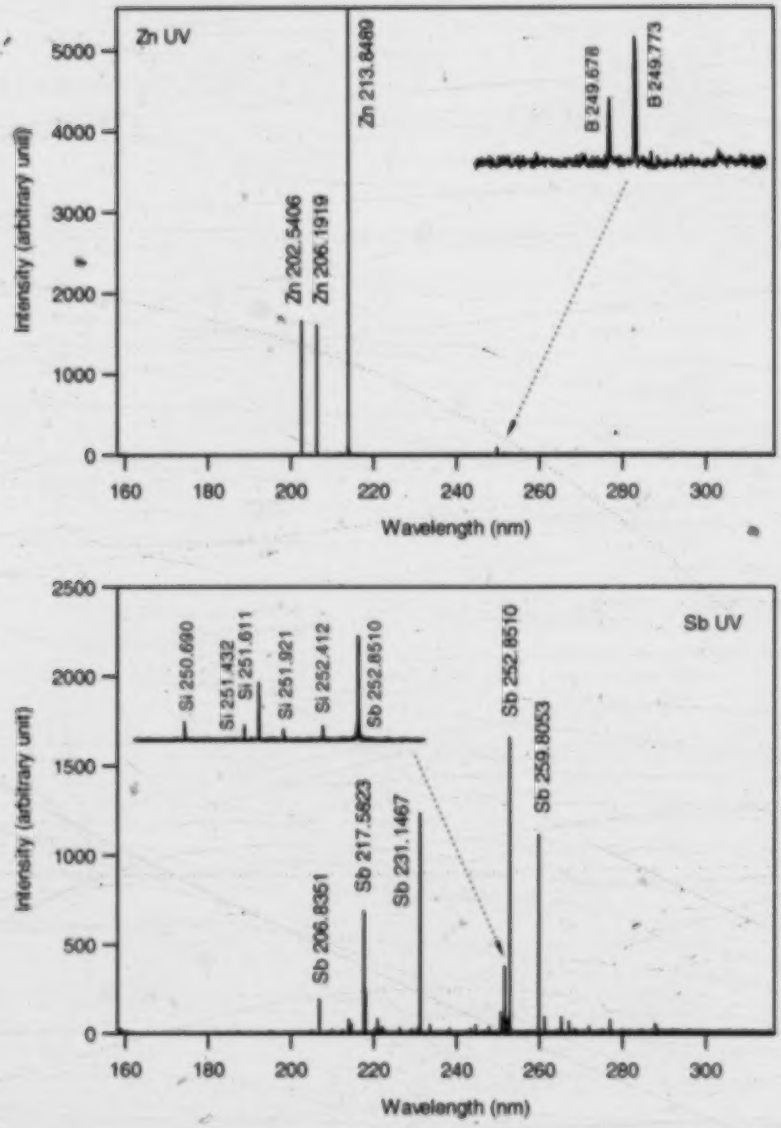

Figure 3-32. Lines introduced to Zn and Sb spectra by impurity elements.

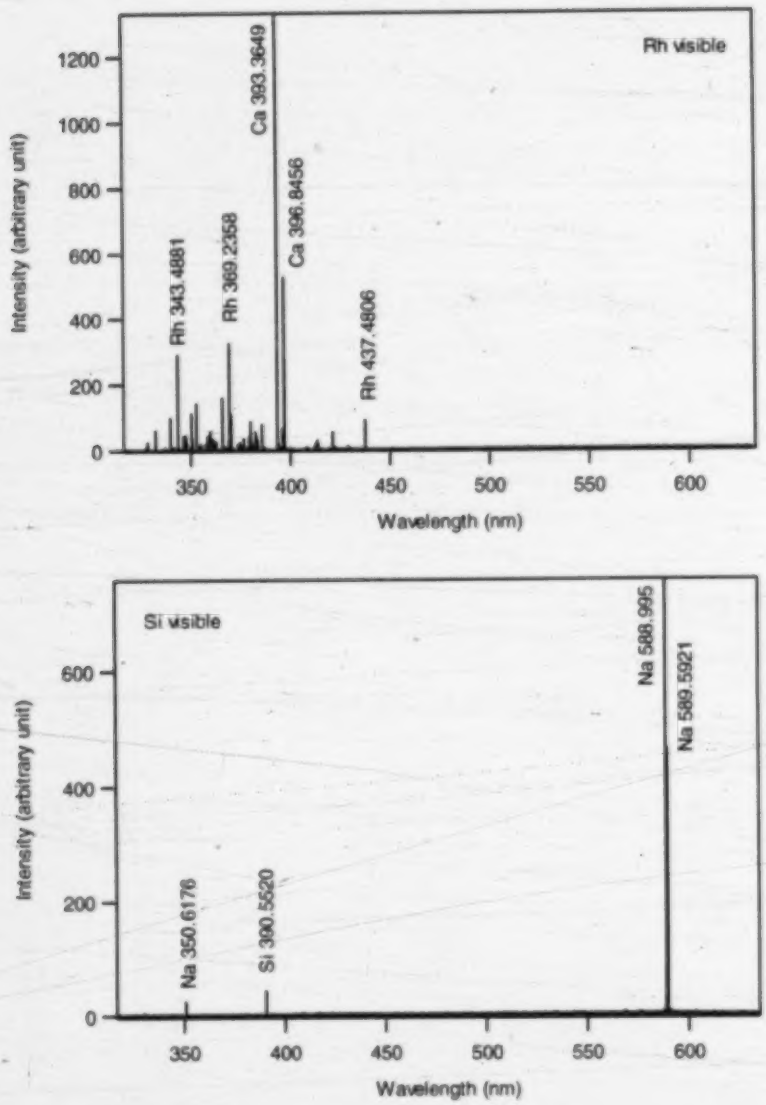

Figure 3-33. Lines introduced to by impurity or counter-ions.

Reference

(1) King, G. B.; Horlick, G.: *Spectrochim. Acta, Part B* **1991** *47B*, E353-E370.

(2) Pahwa, A. *The CD-Recordable Bible*; Eight Bit Books: Wilton CT, 1994.

(3) Astarte GmbH *Toast CD-ROM Pro User's Manual*; Astarte GmbH: Karlstrube Germany, 1994.

(4) King, G. B.; Todd, B. R.; Horlick, G.: *Spectrochim. Acta, Part B* **1991** *47B*, E333-E352.

(5) Zaidel, A. N.; Prokof'ev, V. K.; Raiskii, S. M.; Slavnyi, V. H.; Shreider, E. Y. *Tables of Spectral Lines*; IFI/Plenum: New York, 1970.

(6) Lide, D. R. ***CRC Handbook of Chemistry and Physics***; CRC Press, 1996.

(7) Schierle, C.; Thorne, A. P.: *Spectrochim. Acta, Part B* **1995** *50*, 27-50.

(8) Boumans, P. W. J. M.; Vrakking, J. J. A. M.: *Spectrochim. Acta, Part B* **1986** *41*, 1235.

(9) Ingle, J. D. J.; Crouch, S. R. *Spectrochemical Analysis*; 1st ed.; Prentice-Hall, Inc: Upper Saddle River NJ, 1988.

(10) Manning, T. J.; Winefordner, J. D.; Palmer, B. A.; Hof, D. E.: *Spectrochim. Acta, Part B* **1990** *45*, 1031-1042.

(11) Salit, M. L.; Travis, J. C.; Winchester, M. R.: *Appl. Opt.* **1996** *35*, 2960-2970.

(12) Griffiths, P. R.; Haseth, J. A. *Fourier Transform Infrared Spectrometry*; John Wiley & Sons: New York, 1986.

Chapter 4. Some Applications for the Spectral Library

Compared to the published spectral data, the Spectral Library from this research project provides some important advantages. Firstly, this Spectral Library is one of a few atomic spectroscopic data sets that provides complete coverage (i.e. Full spectra) for the elements with spectral lines exclusively from ICP-AES. It also provides spectral line intensities for the ICP discharge, which is important for interference considerations. Secondly, this Spectral Library has superior wavelength accuracy that is inherited from the FTS. The overall average wavelength error of the Spectral Library was no greater than 1.05 pm when compared with literature data and this number could be, in part, attributed to sources other than the inaccuracy of the current research work, as, for example, variation in the accuracy of comparative wavelength sources. The third advantage comes from the interactive format of the Spectral Library. A fully computer interactive Spectral Library results in a revolutionary change in the way spectral data can be used.

As such, it is expected that the Spectral Library will find a wide range of applications in both industrial and academic environments. This chapter will introduce a few applications based on the Spectral Library. Considering the nature of this project, it should not be surprising that these applications are mainly from an academic point of view, more real world applications from industries are expected once the spectral library gains wider acceptance and availability.

4.1. Interactive ICP-AES Spectral Data

Traditionally, the reference data for spectroscopy are presented in either a tabular or graphics format, both printed on paper. Tabular form wavelength tables can convey information about wavelength, intensity, line energy and others in a relatively compact-sized publication. The graphics format, or spectrum, on the other hand, provides readers with a much better visual sense of the spectral lines. It can preserve nearly all information from any spectral measurement, including spectral line wavelengths, absolute and relative intensities, line shape and width, background noise and distribution, signal-to-noise ratio, etc., almost a perfect illustration of the old saying "a picture is worth a thousand words". This does not, of course, come without a price. With the rich spectral features of the ICP, displaying even a relatively small spectral range on a printed publication at a scale that is comfortable to human eyes means a large publication volume. Thus nearly all published spectra have been printed with tight page layout with little detail available or detail of very short spectral region. Instead of providing many features promised by the graphic format, readers often encounter a discouraging experience in locating specific lines and reading off the intensity values, in addition to the missed details of spectral line shape and width information.

With the help of personal computers, the Spectral Library overcomes most of the problems for displaying spectra that once facing either the tabular wavelength table or the printed spectra. Next, the Boron UV spectrum will be used as an example to illustrate these advantages. Please remember, however, this thesis itself is a printed publication, and thus has limitations on presenting the power of an interactive

spectral library. Readers are strongly urged to experience this power with a personal computer and the enclosed data CD-ROM.

The beat pattern of a Boron UV interferogram (Figure 4-1) is clear evidence of a simple spectrum dominated by a strong doublet. The full-scale spectrum (Figure 4-2) has the appearance containing two lines. Both these lines are, in fact, doublets. In the spectral library with either *SpectroPlot* or other commercial software, to view the details of the two doublets (Figure 4-2, top) is one effortless step. Spectral line wavelength values, intensities, line width and shapes, and background noise level are all readily observable or easy to evaluate (Figure 4-3).

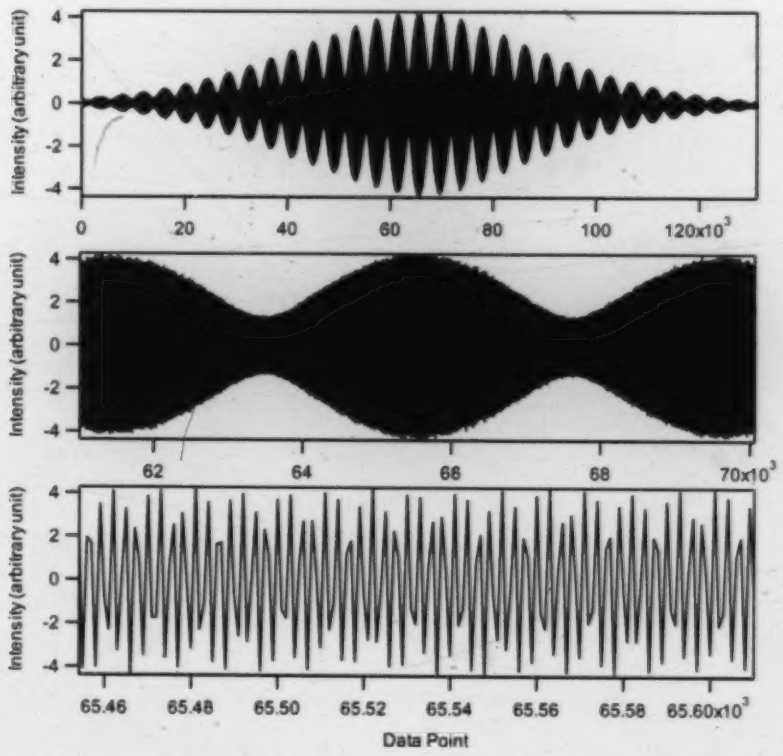

Figure 4-1. Boron UV interferogram at different scale.

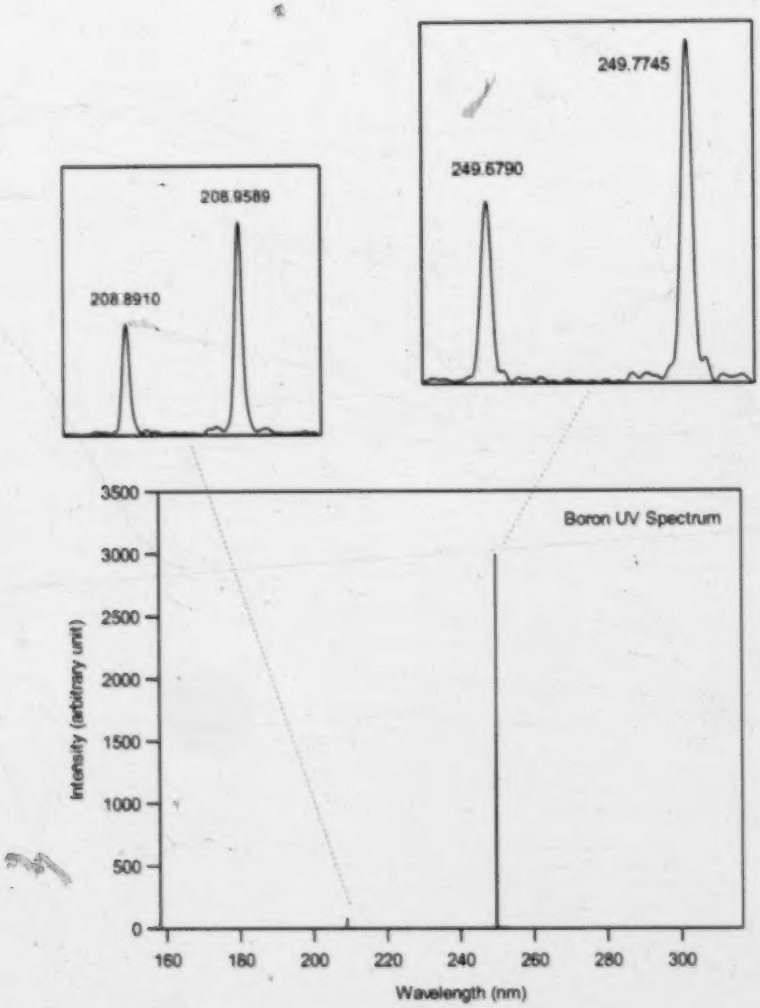

Figure 4-2. Boron UV spectrum and the detailed structure of the two doublets.

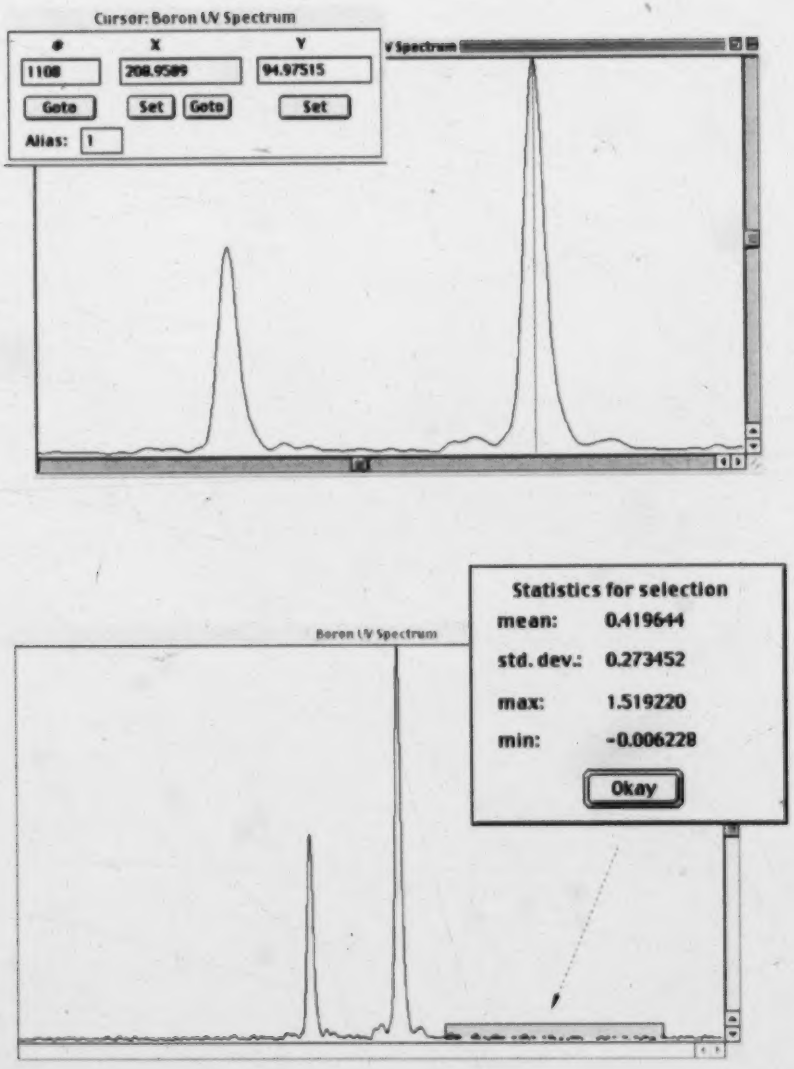

Figure 4-3. Measuring line wavelength, intensity, and background noise with the *SpectroPlot*.

Beryllium has a relatively simple UV spectrum, too. Its interferogram has a flattened Gaussian bell shape, providing no clues about the spectral features of the spectrum. The expanded views, however, revealed regular beat patterns that suggest the existence of a doublet or doublets (Figure 4-4).

There are four spectral features readily recognizable in a printed beryllium UV spectrum (top of Figure 4-5): one dominant line and three weak lines. The enlarged spectrum of "line 1" indicates that the dominant line is a single spectral line centered at 249.8607 nm (Figure 4-5). As shown in Figure 4-5, "Line 2" at 249.457 nm is a closely spaced doublet with lines centered at 249.4576 and 249.4730 nm and separated by 4.6 pm. They are close to being baseline resolved. "Line 3" is a closely spaced triplet; with a high intensity central line at a wavelength of 265.0618 nm, with two weaker lines as shoulders and separated just enough to be full peaks. "Line 4" is two well-resolved spectral lines at 313.0426 and 313.1070 nm. In a single broad coverage spectrum such detail is not readily apparent.

Tabular wavelength tables would certainly be able to list all information for wavelengths and intensities, but they would also certainly miss the information of line shape and width and overall spectral character which is hard to imagine based on information provided only by wavelength tables. With the Spectral library and *SpectroPlot*, all this information is readily available. If desired, tabular wavelength tables are readily generated from the spectrum with *SpectroPlot*, as described in Chapter 3.

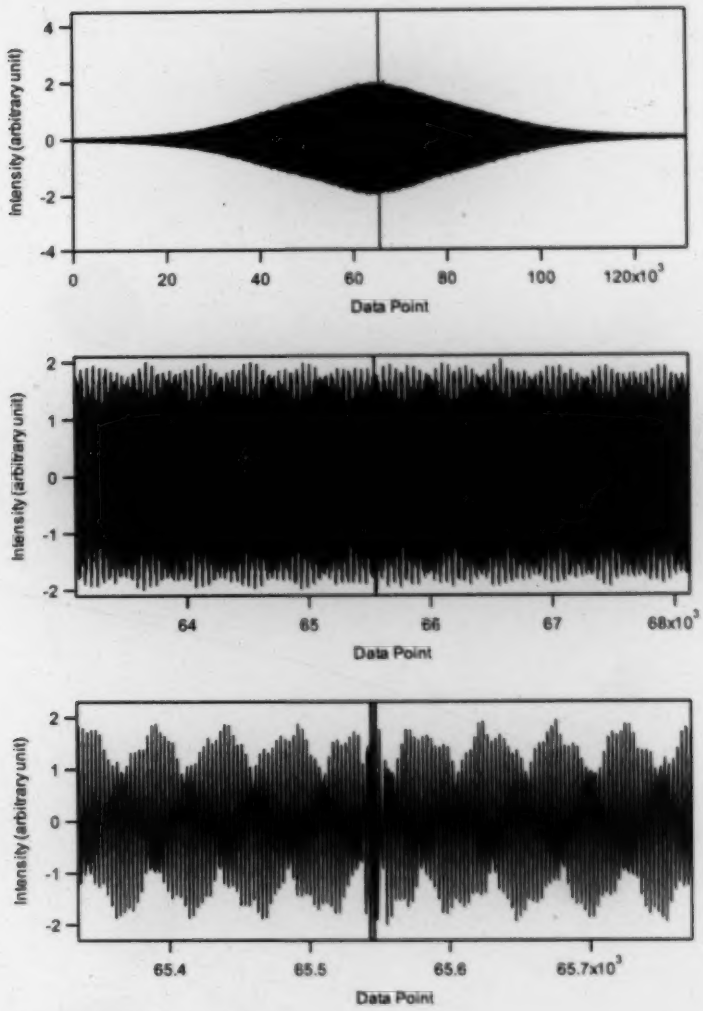

Figure 4-4. Beryllium UV interferogram at different scale.

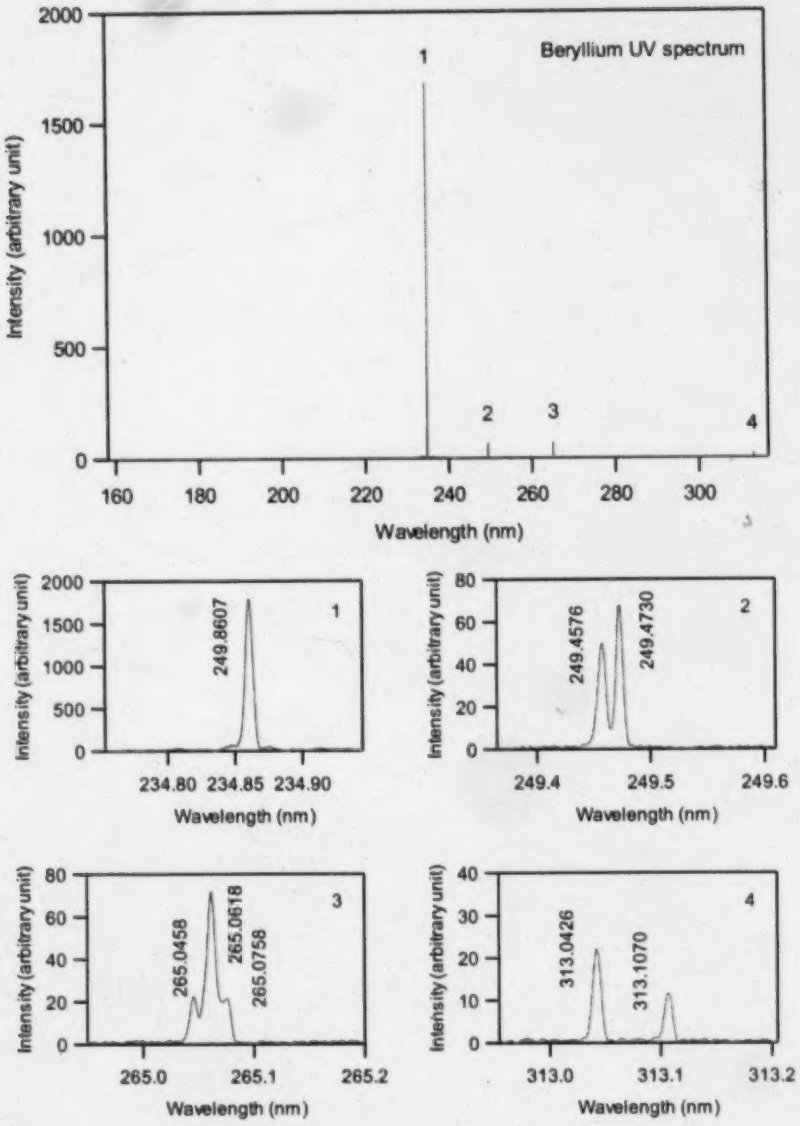

Figure 4-5. Beryllium UV spectrum and detailed spectral features.

4.2. Removal of Argon Lines with Spectra Subtraction.

Spectra subtraction has long been used for background subtraction and other spectroscopic applications. However in FTS, spectra subtraction does not always work, since a slight change in mirror movement or even a counting error results in a shift of the digitization position on the real continuous interferogram and thus introduces a phase difference between two different interferograms or spectra. If spectra subtraction is performed between such two spectra, it usually results in a derivative shaped line residue, often at incorrect wavelengths and causes confusion with other real lines (1).

If, however, the spectra are collected from a stable instrument under carefully controlled experimental conditions, subtraction can be done with reasonable success. For example, argon lines are always present in the visible spectra and it is desirable to remove these lines to get a clear view of the spectra of the elements, as has been done for the Spectral Library. More examples of subtraction for FTS qualitative measurements can be found in Chapter 6.

It was found from experiment that the most effective way to remove argon lines from the visible spectra was intensity-matched subtraction of a background spectrum from the original spectrum containing both element lines and argon lines. As illustrated in Figure 4-6, subtraction using interferograms could usually reduce the intensity of the argon lines, but not eliminate them as shown with the Pd spectrum (middle). However, for exactly the same data, subtraction of spectra gave excellent results (lower spectrum).

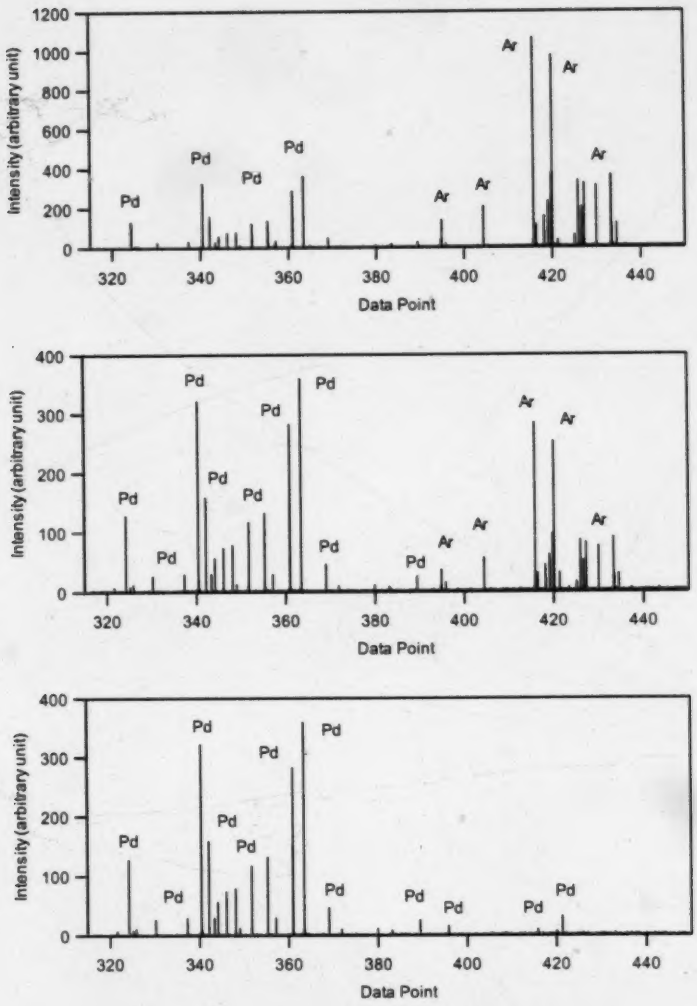

Figure 4-6. Removal of Ar lines in Pd visible spectrum.

Top: original Pd spectrum with no background subtraction.
Middle: spectrum obtained from background subtraction on interferogram
Bottom: spectrum obtained from background subtraction on spectrum

Why, in general, spectrum subtraction performed using interferograms was less effective than using spectra is not known. There are, however, two possible reasons. First, all interferograms in the Spectral Library were the average of multiple signal scans, tiny moving mirror position errors sometimes accumulated and shifted the position (only a single data point) of the interferogram central fringe. This would certainly affect the effectiveness of the subtraction.

Another reason might be related to the intensity difference for the element spectrum and the background spectrum. When subtraction is done with spectra, this difference can be compensated with relative ease by intensity matching. For interferograms, however, to compensate spectral line intensity directly is very difficult as the lines are modulated, along with background lines and features.

As a general rule, effective subtraction with interferograms could be achieved only if the argon lines were weak compared to the element lines. For example, the background interferogram (Figure 4-7 middle) was subtracted from the acquired Ba visible interferogram (top) to remove Ar lines. From Figure 4-8 it can be seen that Ar lines are relatively weak in the Ba visible spectrum; and after subtraction of an Ar interferogram, all Ar lines were removed (Figure 4-9).

The Ce visible spectrum, however, turned out to be an exception to this rule. Argon lines are actually quite strong in the Ce visible spectrum, but the removal of argon lines through interferogram subtraction was almost complete. Close examination showed that the central fringe of the Ce visible and the background interferogram matched each other almost perfectly, and the symmetry was actually improved after subtraction.

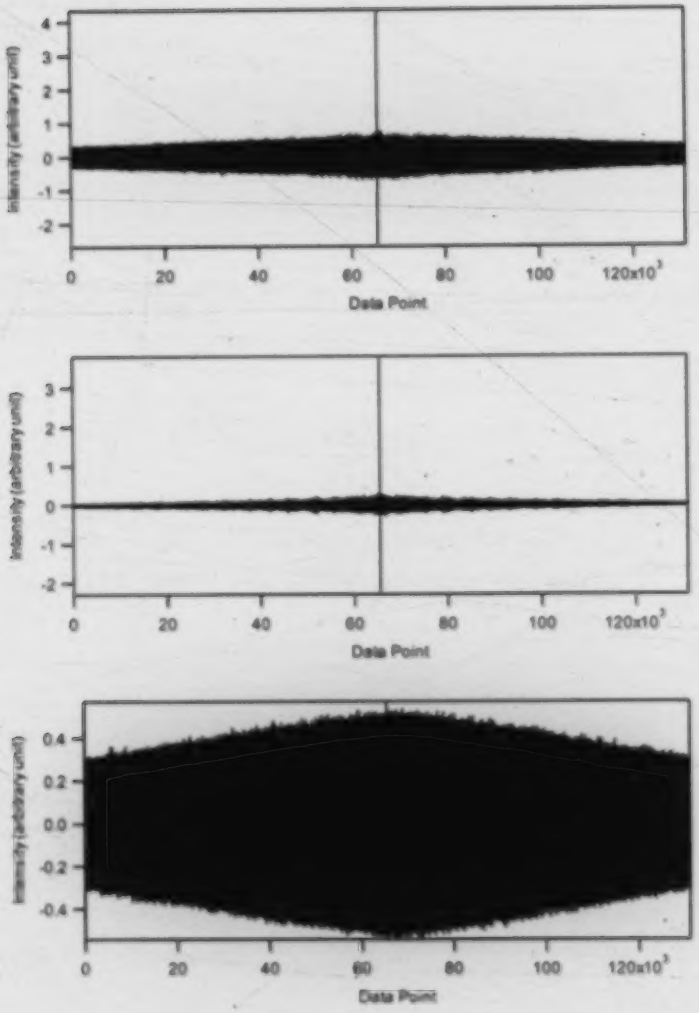

Figure 4-7. Background subtraction for Ba visible interferogram.

Top: original Ba visible interferogram.
Middle: visible interferogram for background.
Bottom: Ba interferogram after background subtraction.

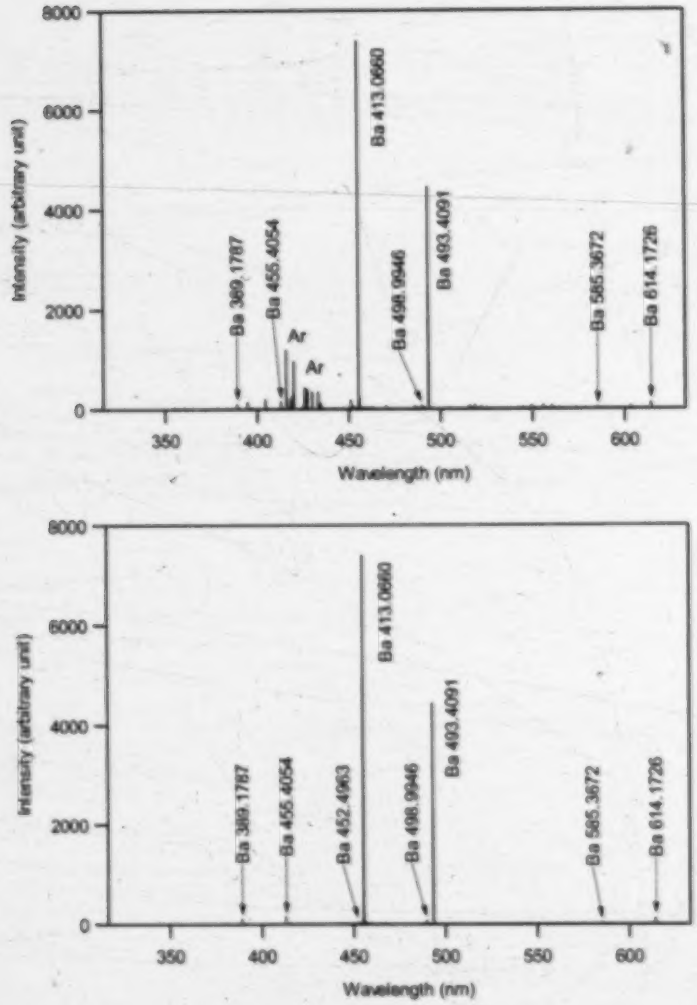

Figure 4-8. Ba visible spectra before (top) and after (bottom) background subtraction.

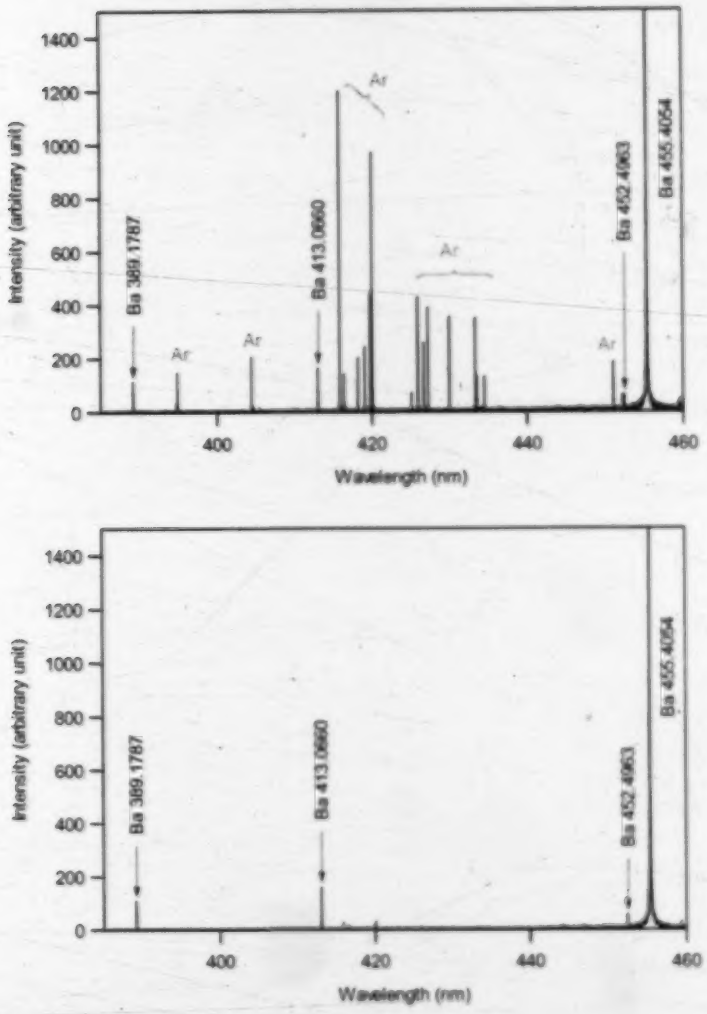

Figure 4-9. Expanded view of Figure 4-8. Ar lines removed from Ba visible spectrum

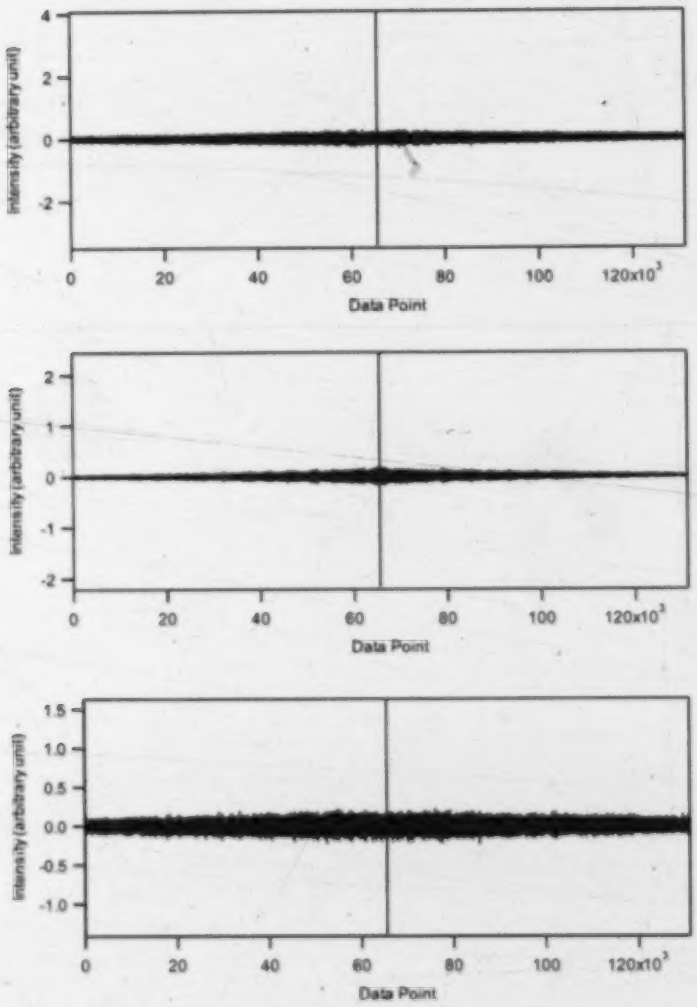

Figure 4-10. Background subtraction for Ce visible interferogram.

Top: original Ce visible interferogram.
Middle: visible interferogram for background.
Bottom: Ce interferogram after background subtraction.

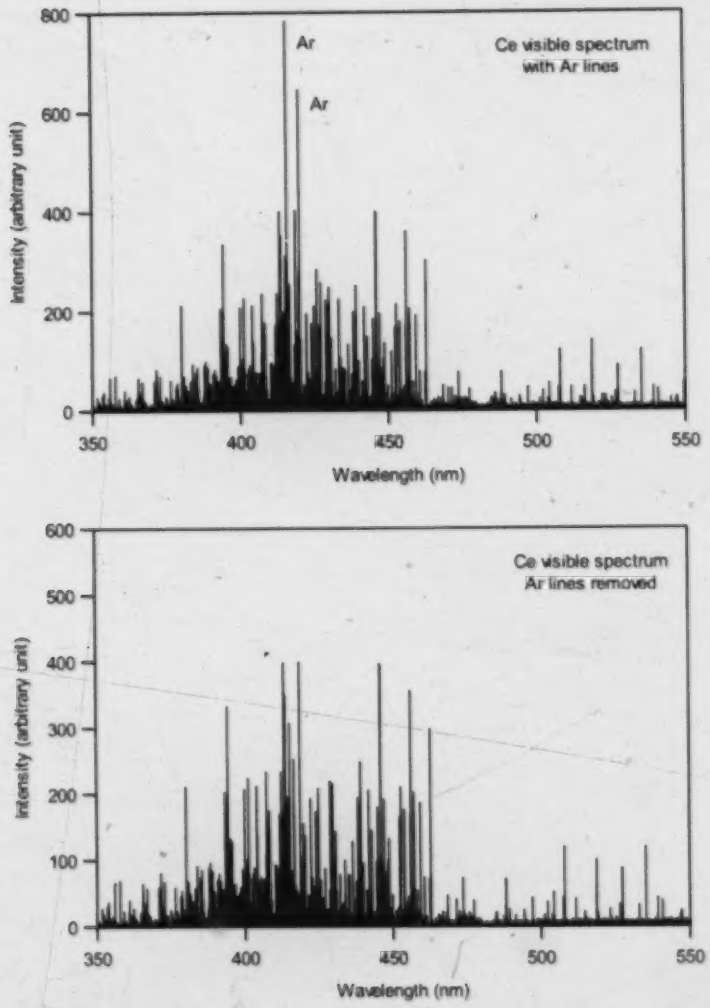

Figure 4-11. Ce visible spectra before and after background subtraction.

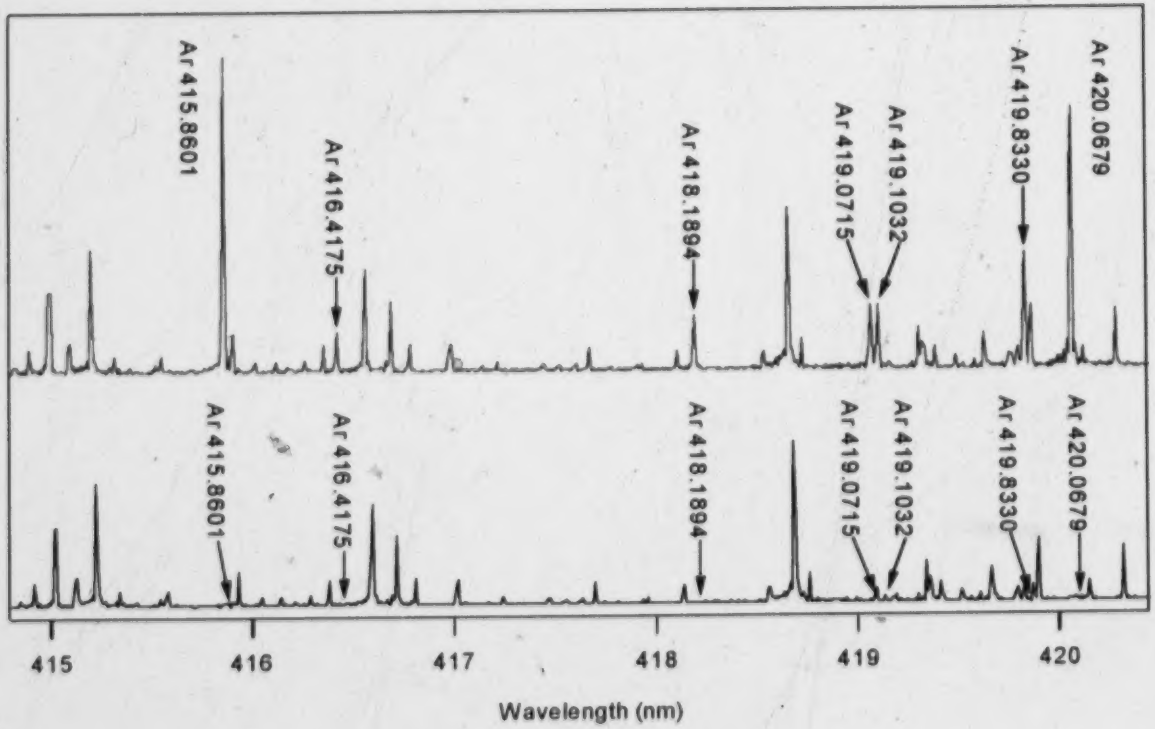

Figure 4-12. Ar lines were removed with Ce interferogram subtraction.

4.3. Scanning Spectrum Simulation and Spectral Line Identification

4.3.1. The Objective of the Simulation

In a student lab for an analytical spectroscopy course, students are asked to collect an ICP-AES UV spectrum with a one-meter scanning spectrometer for a solution containing 10 ppm of Al, Ca, Cd, Cu, Mg, Mn, and Zn. The spectrum covers the wavelength range from 210 to 230 nm (See Figure 4-13) and students need to calibrate the spectrum and identify major lines. Apparently this is not a complicated case; the only difficult time for the students was to identify the lines with a wavelength table and the wavelength values available from their measured scan. In this section it will be shown that the scanning spectrum can be easily simulated with the Spectral Library, and the lines can be identified with great ease in a software "experiment".

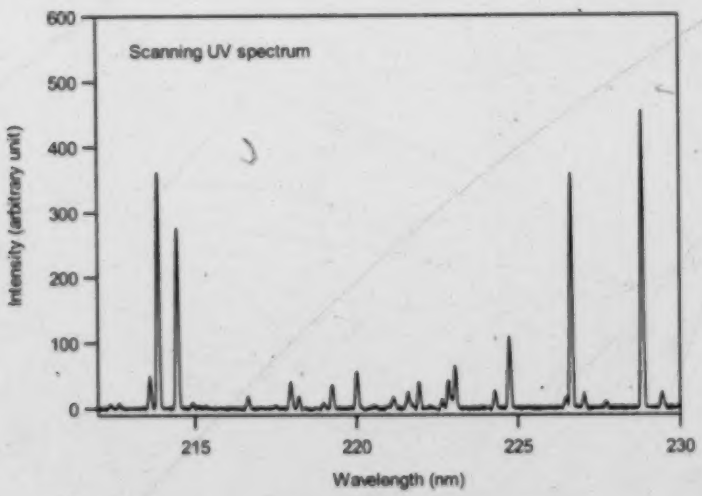

Figure 4-13. ICP-AES scanning spectrum for a mixture of seven metal ions.

4.3.2. Spectrum Simulation and Resolution Control

The UV spectra of the seven constituent elements were obtained from the Spectral Library CD-ROM and a simulated UV spectrum for the mixture was obtained with spectrum addition (Figure 4-14). All spectra were taken directly out of the library without any wavelength re-calibration or intensity matching. Spectral addition could be easily done on a point-by-point bases with the "vector arithmetic ..." function of the *SpectroPlot* (2), or, if it is under Microsoft Windows on IBM-PC, with *Origin* or *Igor Pro* as described in Chapter 5.

The 210 to 230 nm region of the simulated spectrum is compared to the scanning one in Figure 4-15. It can be seen that these two spectra are very similar to each other in terms of line position and distribution. For most lines the relative intensities were similar, but line 2 and 3 had reversed intensity order in the scanning spectrum compared to the simulated spectrum. The major difference between these two spectra was the resolution. The Full Width at Half Maximum (FWHM) of the spectral lines in the scanning spectrum were noticeably larger, and some lines in the scanning spectrum appeared as two lines in the simulated one, presumably due to better resolution.

Utilizing the processing features of *SpectroPlot*, the resolution of the spectra in the Spectral Library can be easily controlled to match the resolution of any instrument that has lower resolution than the Spectral Library. This is illustrated in Figures 4-16 and 4-17.

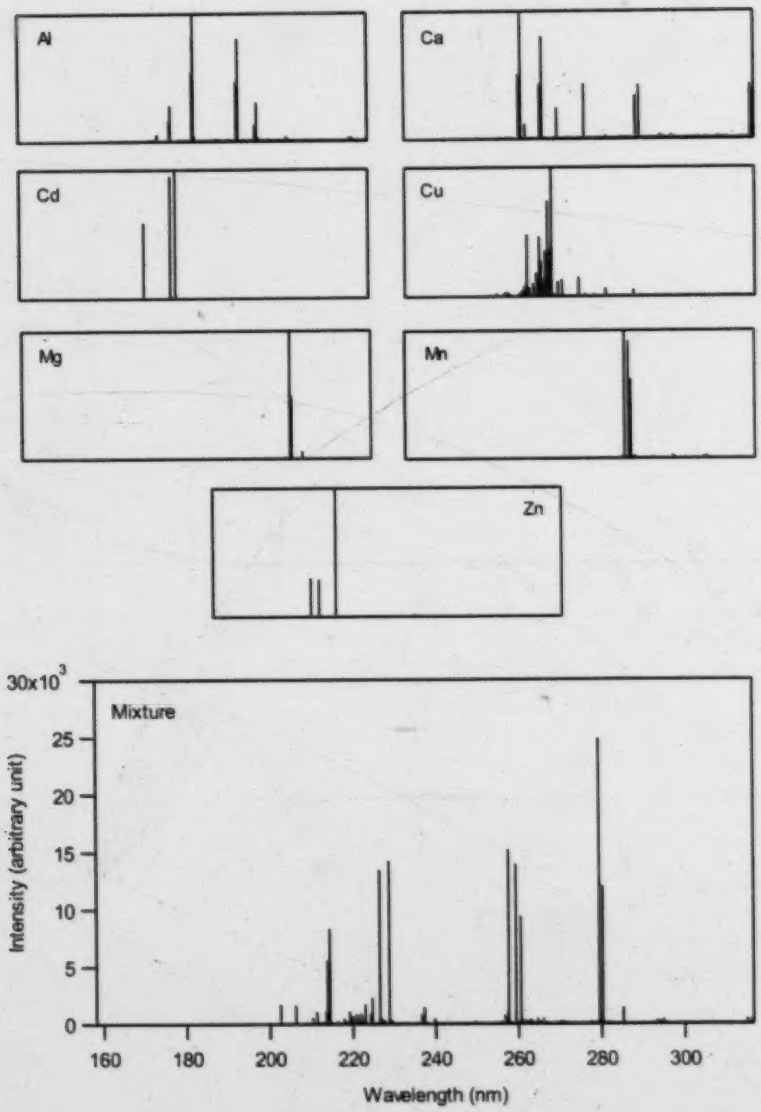

Figure 4-14. Simulated spectrum of the mixture and the constituent element spectra from the Spectral Library

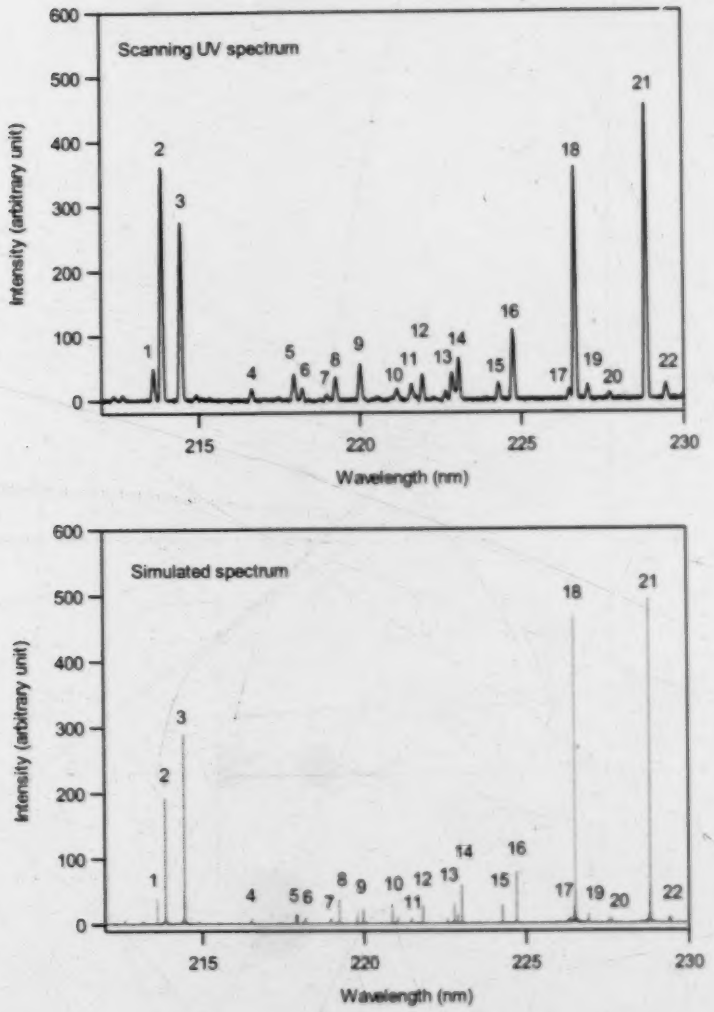

Figure 4-15. Comparison of the scanning and the simulated spectra.

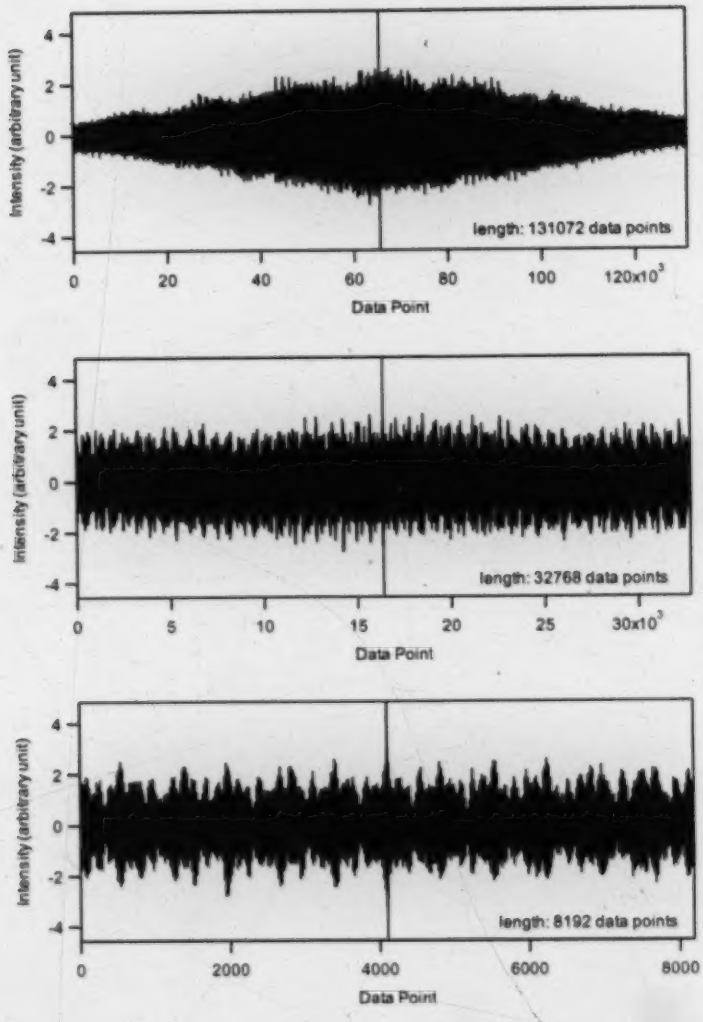

Figure 4-16. Simulated interferograms of different length for the mixture

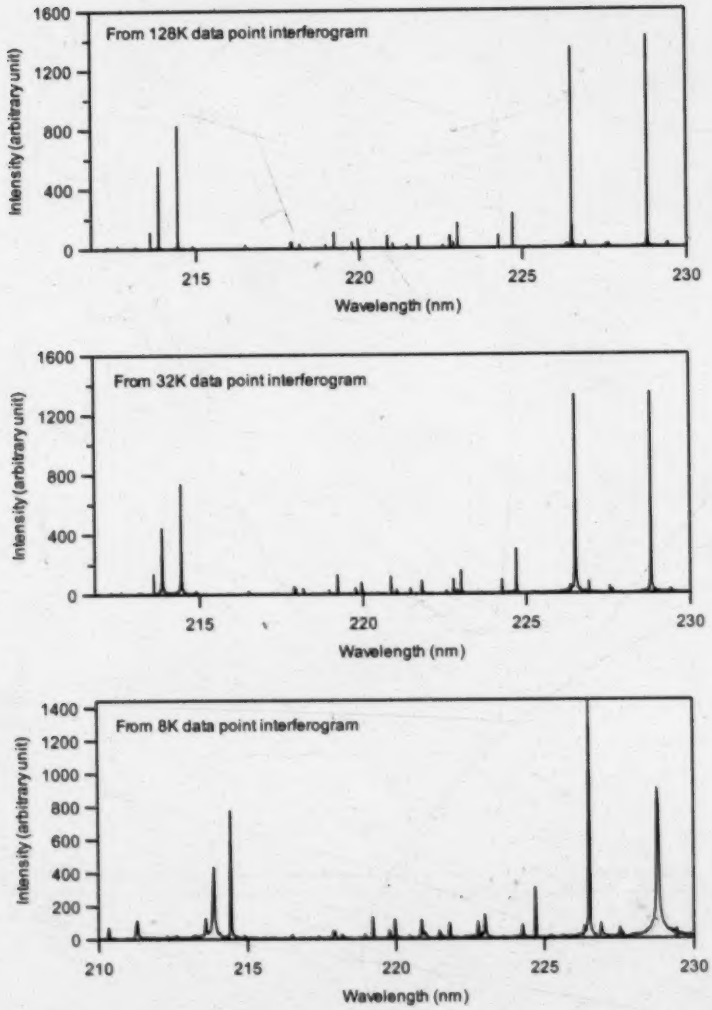

Figure 4-17. Resolution decreased as a result of reduced interferogram length.

Figure 4-16 shows examples of interferograms of different length, measured in data points. The top one is the full-length interferogram of the simulated mixture. Its length, or the optical retardation it represented, could be calculated as follows:

$$\text{Length} = 131072 \times 632.8438 \times 10^{-7} / 4 = 2.0737 \text{ cm}.$$

The interferogram in the middle of Figure 4-16 has 32768 data points or 0.5184 cm long, and the bottom one 8192 data points or 0.1296 cm. The theoretical resolution of the spectra transformed from these interferograms would be 0.9644 cm^{-1}, 3.858 cm^{-1}, and 15.43 cm^{-1}, respectively. The width of the spectral lines increased noticeably, as shown in Figure 4-17.

4.3.3. Identification of Spectral Lines

It can be seen from Figure 4-15 that, the simulated spectrum established a one to one relationships for most of its spectral lines with the scanning spectrum, except for line 9 and 20 for which the simulated spectrum had two lines each and the scanning spectrum had only one. Thus the line identification process for the scanning spectrum could be done with the line identification for the simulated one. Of course, one could always record the wavelength of each spectral line to be identified and check against the value in a wavelength table. Instead, a graphical identification method will be illustrated here utilizing the spectra from the Spectral Library.

The first step for identification was to identify the dominant lines. For this purpose, the 210 to 230 nm region of the constituent elemental spectra were present and compared with the simulated spectrum (Figure 4-18).

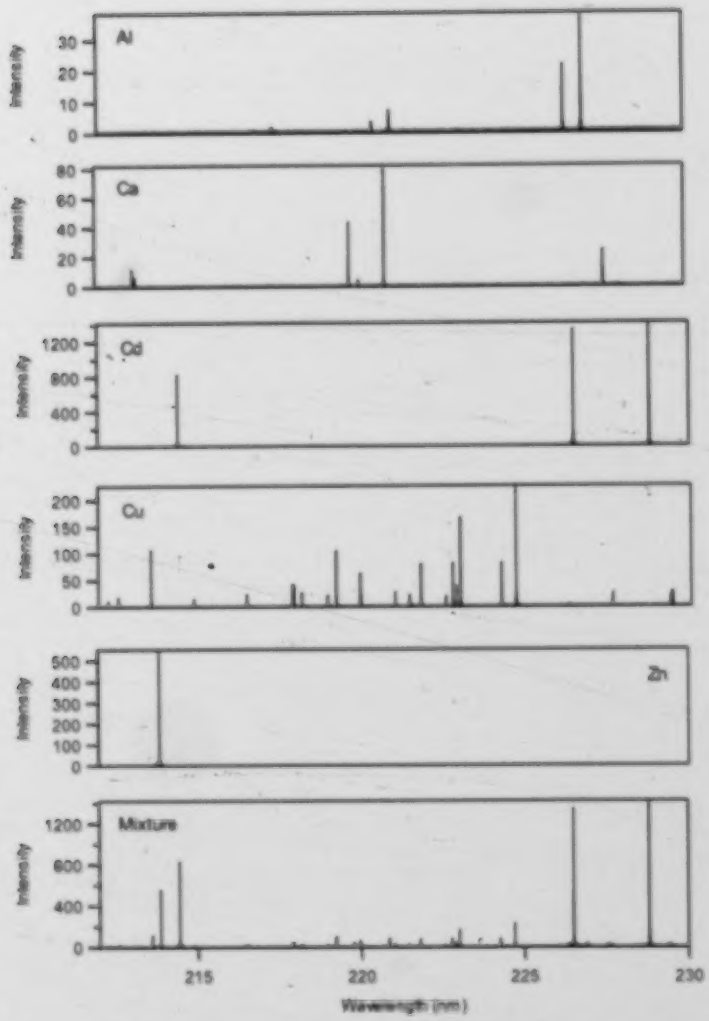

Figure 4-18. Overview of the constituent elemental spectra.

A quick visual inspection of the mixture spectrum and the constituent spectra (Figure 4-18) suggested that lines 21, 18, and 3 were probably Cd lines, and line 3 was a Zn line. Thus the next step would be the confirmation of these lines.

As shown in Figure 4-19, the Cd spectrum (210-230 nm region) was first subtracted from the spectrum of the mixture (top). Lines 3, 18, and 21 were removed after the subtraction and thus they could be identified as Cd lines.

Now that the spectrum of the mixture lost three dominant Cd lines, line 2, which was suspected to be a Zn line, became dominant (Figure 4-19, bottom). To confirm its identity, the Zn spectrum was subtracted from this spectrum and line 2 was removed. Thus line 2 could be identified as a Zn line.

After the removal of Cd and Zn lines, line 1, 14, 16, and spectral features at about 218 to 225-nm region became dominant. The elemental spectra showed that Cu lines had a similar line distribution and expected to be the major source. After the removal of Cu spectrum from the mixture spectrum, line 1 and most spectral lines in the region from 218 to 225, including line 14, 16 disappeared (Figure 4-20, top), and this confirmed that they were Cu lines. It was also noticed that lines 9 and 20 had two lines at each position before the subtraction and only one left after subtraction. This suggested that they were probably not pure, that is, they all contained Cu component and at least one more component from another element.

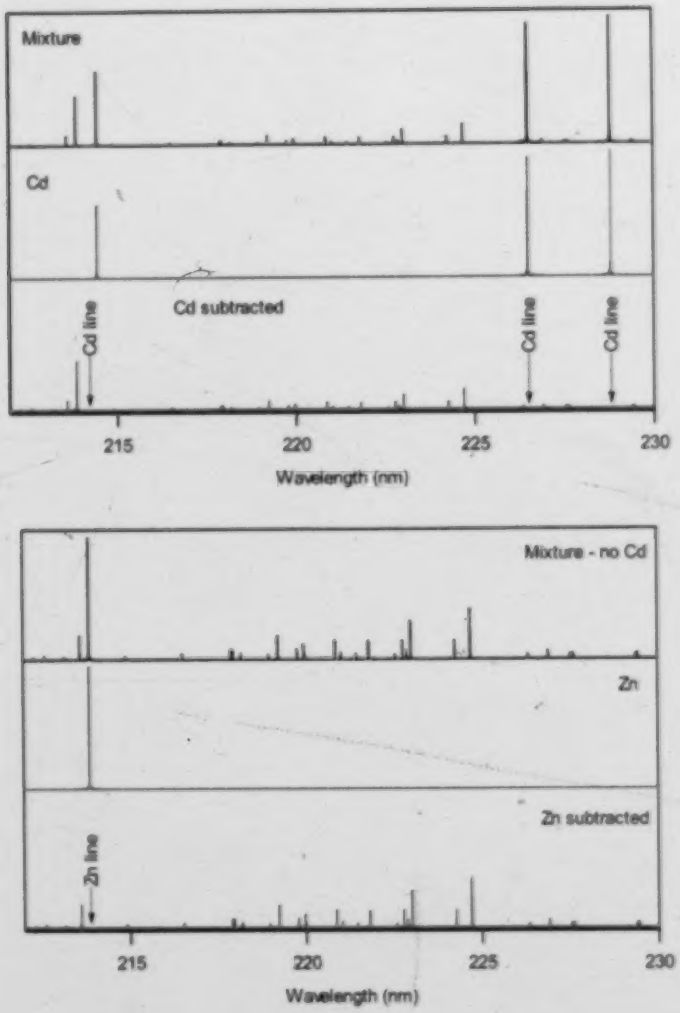

Figure 4-19. Identification of dominant lines with spectrum subtraction for Cd (top) and Zn (bottom).

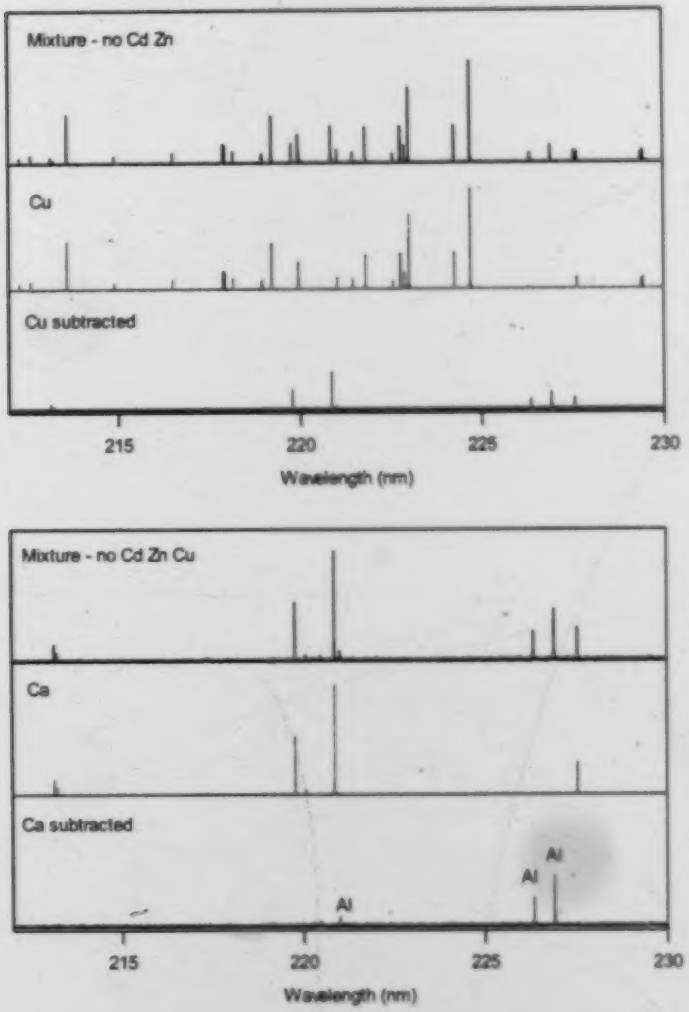

Figure 4-20. Identification of Cu and Ca after removal of dominant lines.

After the removal of the Cu lines, the spectrum became very simple, only 5 lines at 9, 10, 17, 19, and 20 remained. Among them, 9, 10, and 20 were removed after the subtraction of Ca lines (Figure 4-20, bottom), and 17 and 19 were from Al. A complete assignment of these lines, alone with their wavelength values, is given in Table 4-1.

It can be seen that the wavelength values for the scanning spectrum obtained by a student differ quite significantly from literature values but were the best the experiment could provide. Some lines can have errors as large as 0.1 to 0.2 nm. This created considerable difficulties for the students to identify these lines. With such large wavelength errors and no visual assistance from spectra of constituent elements, it could be very hard to decide the identity of these lines. It is under this situation that the graphic method showed great advantage over the traditional wavelength tables, and significantly simplified the spectral line identification process. For the simple task of assigning each line to the elements, one does not even have to know the wavelength of those lines in the element spectra. All one needs is the spectral region of the spectrum to be analyzed and, of course, the Spectral Library. For a more complete analysis of the spectrum that involves identification and measurement of the wavelength, graphical analysis splits a complex problem into a series simple tasks. As spectral lines for one element are always listed in wavelength tables in a clear and orderly fashion, once the spectral lines are assigned to the element, their literature wavelength values can be located with confidence. This not only speeds up the analysis process, but also improves the accuracy.

Table 4-1. Spectral line assignment of the scanning spectrum.

No.	$\lambda_{scanning}$ (nm)	Intensity (%)	Element	Line	$\lambda_{Library}$ (nm)	$\lambda_{Lit.}$ (nm)	$\Delta\lambda$ (nm)
1	213.596	10.9	Cu	II	213.5972	213.598	-0.001
2	213.856	79.5	Zn	I	213.8580	213.856	-0.002
3	214.446	60.7	Cd	II	214.4402	214.441	0.006
4	216.636	4.1	Cu	I	216.5092	216.509	0.127
5	217.966	8.8	Cu	II	217.9402	217.940	0.026
6	218.206	4.0	Cu	I	218.1723	218.172	0.034
7	218.986	1.9	Cu	II	218.9622	218.962	0.024
8	219.256	7.8	Cu	II	219.2261	219.226	0.030
9	220.016	12.2	Ca	II	219.7788	219.779	0.237
			Cu	I	219.9583	219.958	0.058
10	221.156	3.8	Ca	II	220.8612	220.861	0.295
11	221.616	5.3	Cu	I	221.4593	221.458	0.157
12	221.946	8.4	Cu	II	221.8099	221.810	0.136
13	222.856	8.5	Cu	I	222.7768	222.778	0.079
14	223.056	14.1	Cu	I, II	223.0083	223.008	0.048
15	224.286	5.8	Cu	II	224.2609	224.261	0.025
16	224.736	23.8	Cu	II	224.6992	224.700	0.037
17	226.476	3.4	Al	I	226.3463	226.346	0.130
18	226.656	78.9	Cd	II	226.5022	226.502	0.154
19	227.046	5.0	Al	I	226.9095	226.910	0.136
20	227.706	1.4	Cu	II	227.6250	227.625	0.081
			Ca	I	227.5479	227.547	0.158
21	228.846	100	Cd	II	228.8026	228.802	0.043
22	229.456	5.3	Cu	II	229.4358	229.436	0.020

4.4. Assessment of Spectral Interference.

4.4.1. Simulation of Optima Spectral Windows

As discussed in Chapter 1, the Perkin-Elmer Optima uses a segmented charge coupled device (SCD) as a detector and detects each spectral line with a group of pixels on the detector called optical windows, or subarrays. According to the dispersed echelle diffraction pattern, the optical windows are arranged in a way that each subarray covers a small wavelength range and detects one specific chosen line of an element. A total 224 optical windows cover 224 lines for 71 elements that can be determined with ICP-AES.

Although the subarrays were carefully arranged to minimize interference, inevitably one cannot completely avoid spectral interference. Solid knowledge of spectral features in each optical window will definitely improve the quality of any measurement with the Optima.

Using similar methods as in the last section, the spectral windows of the Optima can be easily simulated with the Spectral Library. Figure 4-21 shows the two windows for phosphorous and a few common elements (Zn, Co, Fe, Si) that might interfere with the analytical lines. It can be seen that subarray 038 was set for the P 213.618 nm line, and, for the four common elements, there are no lines that can be found in this window from these elements. Therefore, this line should be free from interference under normal condition.

For subarray 044, however, things are different. In addition to the analytical line of P 214.914, two other lines, Cu 214.887 and Nb 214.953, are also present.

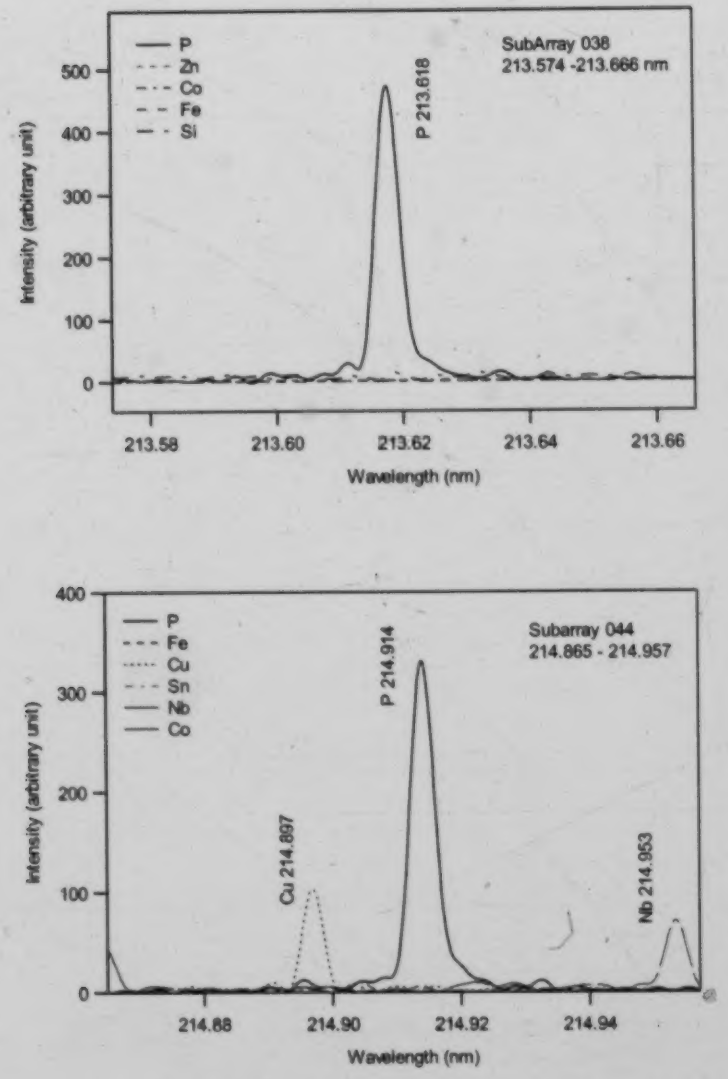

Figure 4-21. Simulated Optima optical windows (sub-array) for P lines.

Since Nb does not commonly exist in samples in high concentration, and the Nb 214.953 nm line is quite far away form the P line, Nb will not likely interfere. Cu, on the other hand, is quite common in nature and often exists in high concentration. If the relative intensity of the two elements and the resolution of the instrument are both similar to that shown in Figure 4-21, then Cu will not interfere. If, however, the instrument has lower resolution, or the sample has a heavy Cu matrix, then the possibility of Cu interference on the P 214.914 nm line does exist. In that case, the P 213.618 nm line should be used for analysis, or at least the results from both windows should be compared in order to find possible interference.

As another example, the optical windows for Pb are shown in Figure 4-22 and Figure 4-23. Among these four windows, subarrays 054 and 120 showed no interfering line from the common elements listed; but in the other two windows, the Mo 217.014 nm line is close to the Pb 216.999 nm line in subarray 042, and the Co 261.436 nm line is close to the Pb 216.999 nm line in subarray 081. Therefore, if a sample contains Mo or Co, the results from these two windows should be used with caution.

The effect of intensity change for an interfering line on the analytical line is shown in Figure 4-24. This figure simulates the subarray 016 for the boron doublet. It can be seen that the Ir line overlaps with B 208.893 nm line and Mo with B 208.959 nm line. The intensity of the Ir and Mo lines increase to twice, five times, and ten times of that in the first spectrum in this simulation, while the intensity of the boron lines remains unchanged. Both these elements can then constitute a series interference.

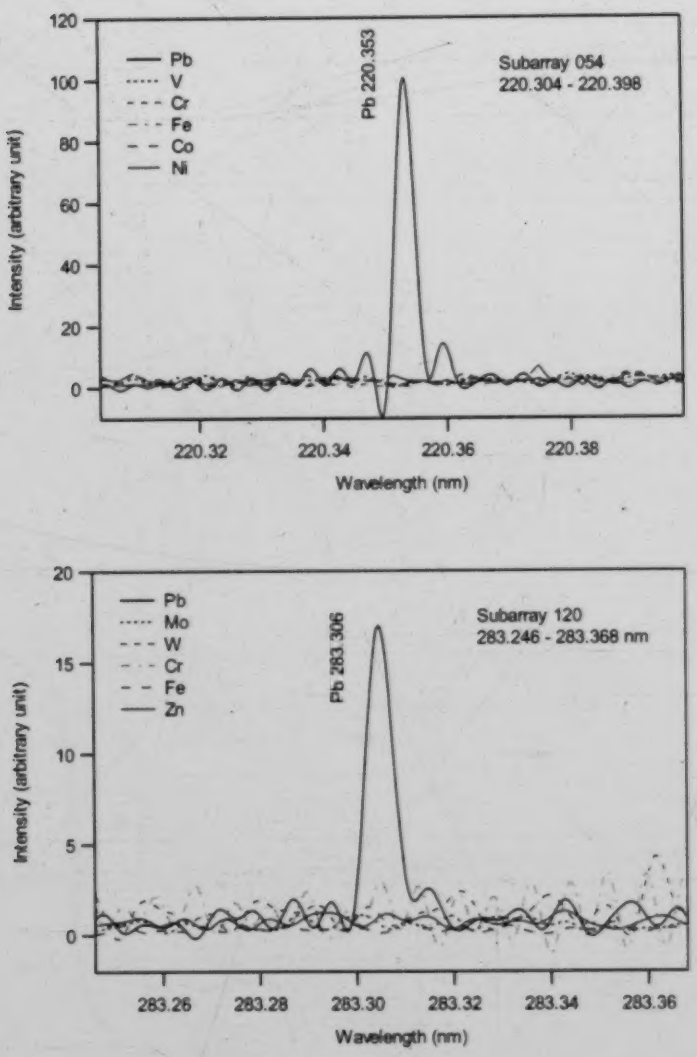

Figure 4-22. Simulated Optima subarrays 054 and 120 for Pb

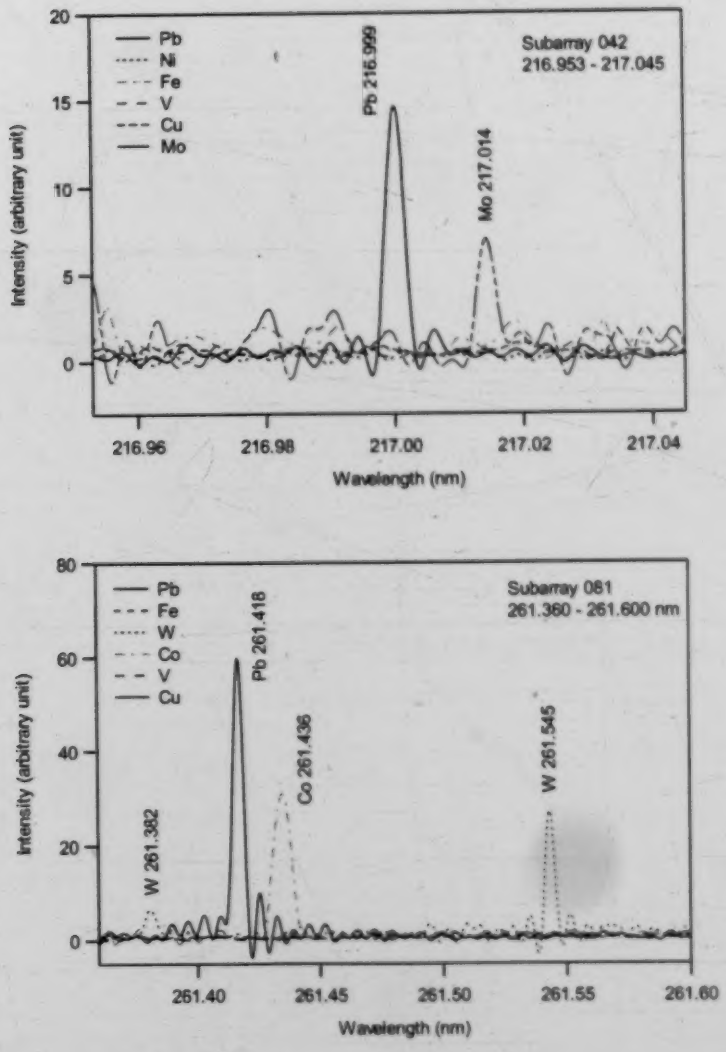

Figure 4-23. Simulated Optima subarrays 042 and 081 for Pb

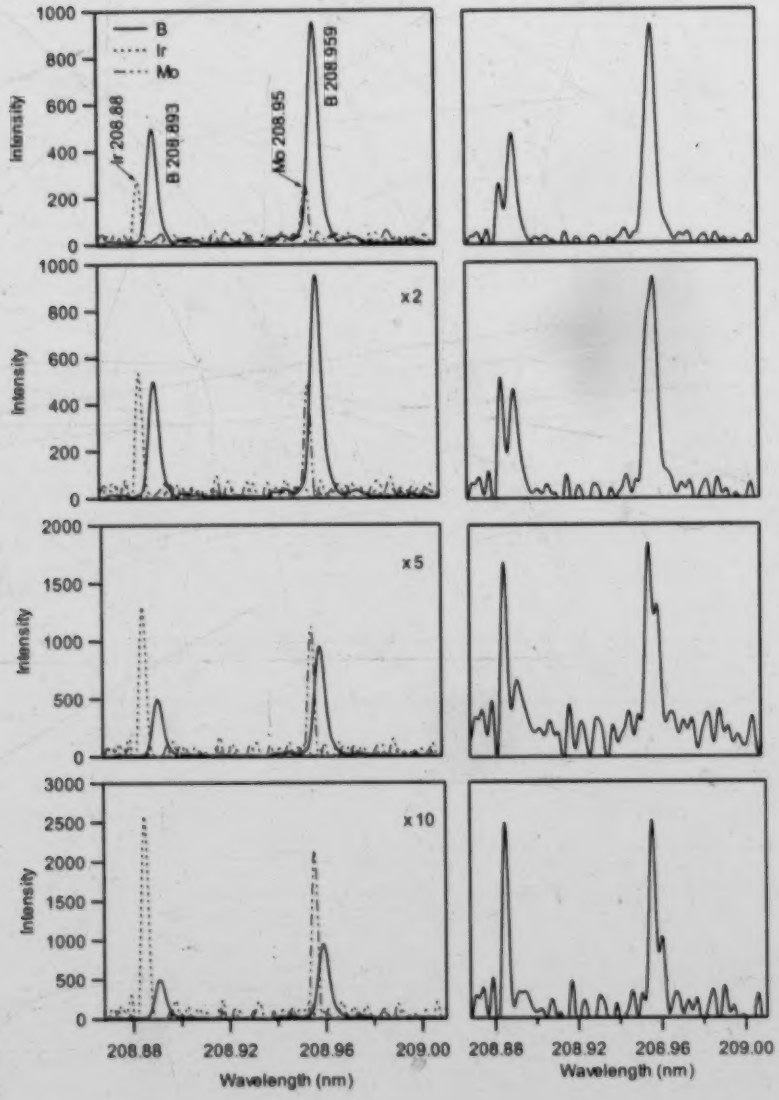

Figure 4-24. Effect of interfering line intensity change.

The total spectra, which are the summation of all spectral traces on the left column in Figure 4-24, are shown on the right column. It can be seen that in the two low intensity spectra (top), the Ir line is partially separated from the B 208.893 nm line, but could still have a strong interference effect. The Mo line totally overlaps the B 208.959 nm line and cannot be resolved. At higher levels of interferent (bottom two spectra), there is a significant overlap. Even if the peak-fitting algorithm of the Optima system software can successfully separate B and Mo, the error of the measurement of B is expected to be large.

To be fair, the developers of the Optima have done a good job in terms of line selection. This does not mean, however, that the instrument is foolproof or the analysts can be worry-free, as discussed in the previous examples. In practice, there have been reports that the determination of uranium with the Optima gave positive errors when iron was present. This can also be easily explained with the simulated optical windows (Figure 4-25).

For uranium, the spectral line at 385.958 nm is the dominant line and thus usually selected as the analytical line. This is fine if iron concentration is low in the sample. However, for many real world samples iron is usually present in concentrations considerably higher than that of uranium in the sample. In some cases iron is added to the sample as an internal standard or spike for QA/QC purposes. In such situations relying only on the result from the U 385.958 nm line could be erroneous, as the Fe 385.991 nm line might interfere with the analysis (top).

This problem should not be too difficult to solve as the Optima provides four subarrays for uranium lines. As indicated by Figure 4-25, three subarrays for uranium, subarray 194, 198, and 217 showed no iron line in the windows when the iron line in subarray 244 showed higher intensity than the dominant uranium line. As iron is very common in practice, one should use the second dominant line at 409.014 nm for uranium determinations to avoid interference. If for some reasons the result from line 385.958 has to be used, the result from other subarrays should also be monitored and compared. In this way, the positive error in the determination of uranium introduced by iron interference should be avoided.

4.4.2. Interference of Rare Earth Elements

It is well known that trace rare-earth elements (REE) are difficult to determine with ICP-AES due to the richness of their spectral features and chemical similarities. Spectral interference of REEs have been investigated intensively by several groups. Recently Huang and associates (3) studied the interference of Sm and Dy on 33 spectral lines of 15 REEs. Their used a high-resolution spectrometer to scan a spectral region from 0.1 nm below to above the center wavelength of each analytical line, and recorded the spectra of the Sm, Dy, and the element of interest. These spectra, prepared as Windows *PaintBrush* pictures and stored on disks, presented detailed spectral information on the environment of the spectral lines, and they can also be simulated with the Spectral Library.

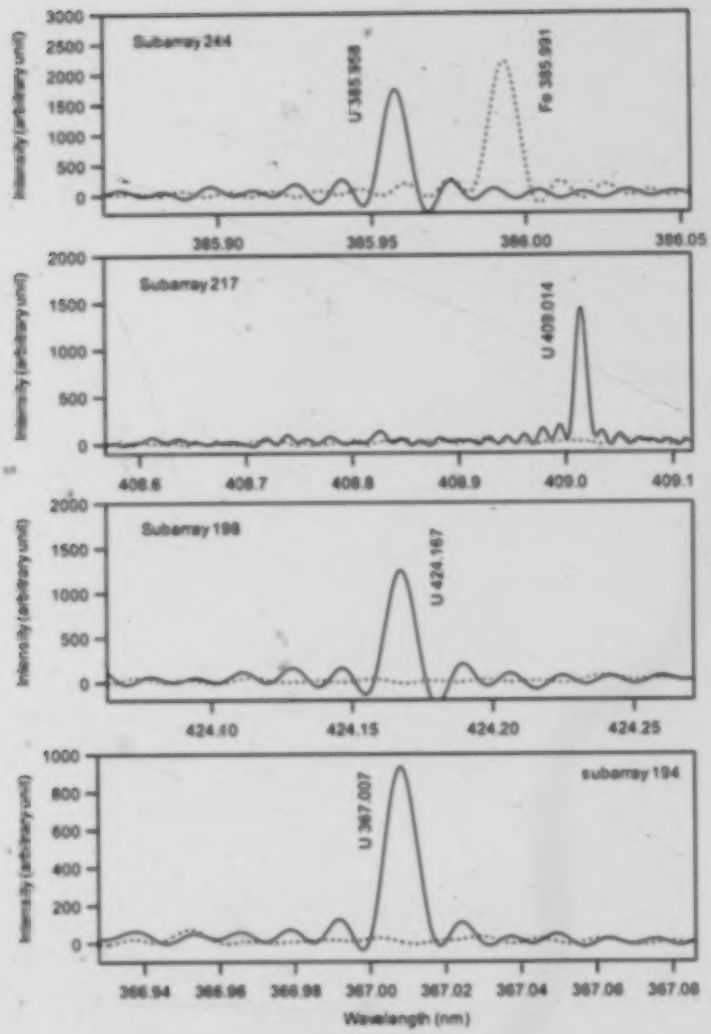

Figure 4-25. Fe interferes on U analysis. This can be avoided by choose any of the other three lines.

Figure 4-26 shows a simulated spectrum for the Ho line at 339.898 nm, along with the spectrum provided by Huang et al (3) (note log amplitude scale for their spectra). It can be seen that these two spectra are quite similar in terms of line position and relative intensity. Three out of four Dy lines and four of five Sm lines reported by Huang can be found in the simulated spectrum. It was clear that the Dy 338.882 line would certainly interfere with the Ho 339.898 line, and Sm 339.876 and 339.936 nm lines might also interfere. Other lines should not be major problems if similar resolution and relative intensities were kept.

The simulated windows for another six lines are shown in Figure 4-27, along with Huang's results. It can be seen that for the Y line at 370.030 nm, all three Dy lines reported by Huang can be found in the simulated spectrum, while only one out of five reported Sm lines could be found. It seems that the signal to noise ratio of the simulated spectra is rather low in this case, and some of the low intensity lines are buried in the background noise. A similar result was observed for the Y 324.228 nm line. In the spectral region from 324.128 to 324.328 nm, only two strong Sm lines were observed along with the analytical line, while none of the spectral feature of Dy could be clearly identified as lines (Figure 4-27b).

For lanthanum, there was no Dy or Sm lines could be found around La 333.749 and 398.852 nm lines; but one out of three Dy lines and all Sm lines were located around La 408.672 nm. For the Ho 345.600 nm line, only one intense Dy line could be found at 345.656 nm, but none of the four Sm lines reported by Huang.

From above discussion it can be seen that the simulation of high-resolution REE spectra with the Spectral Library achieved moderate success. It would certainly

be beneficial if the signal-to-noise ratio had been higher, most of the interfering lines were identified with simulation. This demonstrates the application and value of the Spectral Library in rather complicated situations.

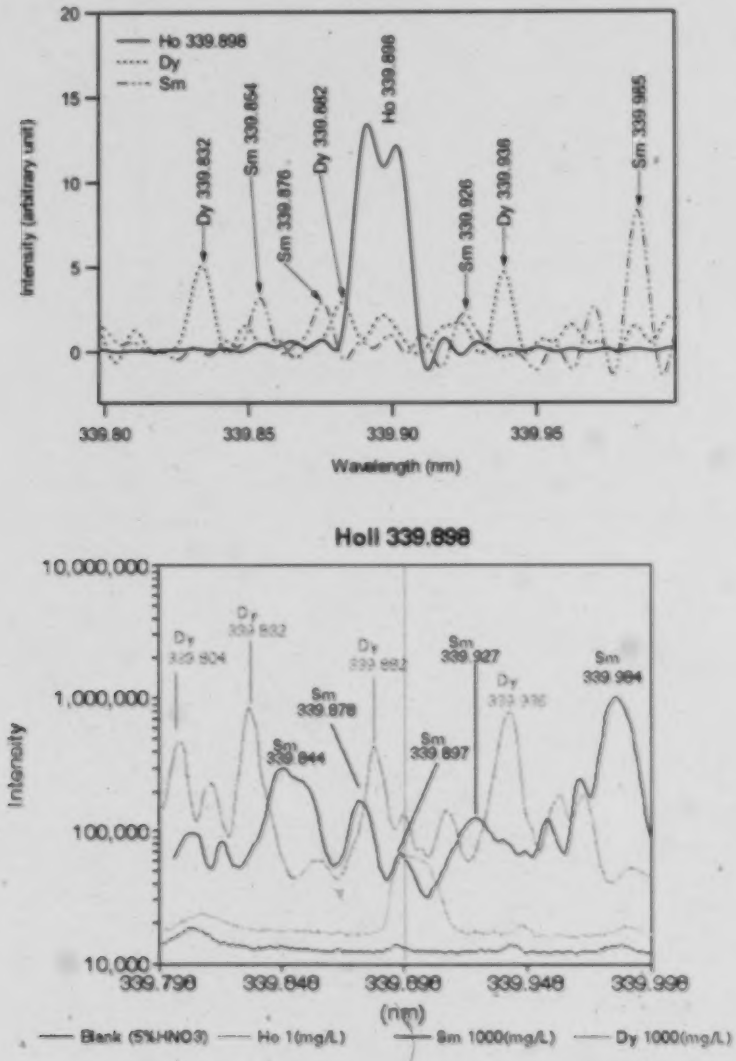

Figure 4-26. Simulation of a spectral window for Ho 339.898 nm line. The lower spectrum was obtained with a scanning spectrometer.

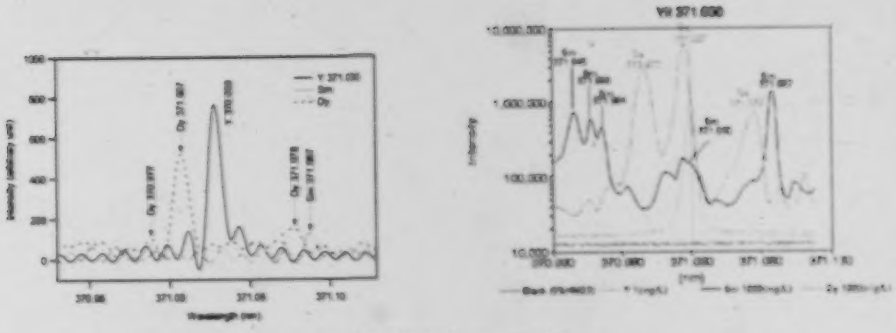

(a). Y 371.030 nm window

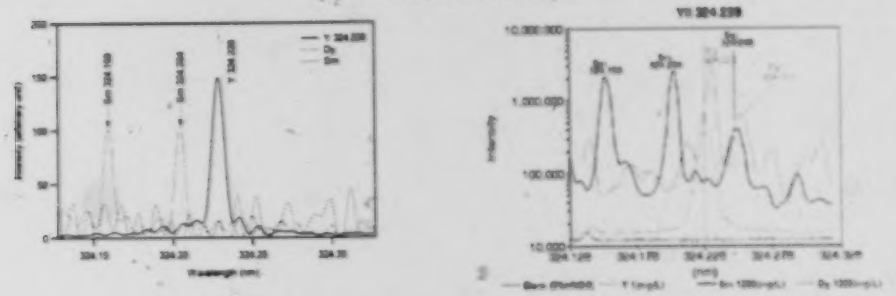

(b). Y 324.228 nm window

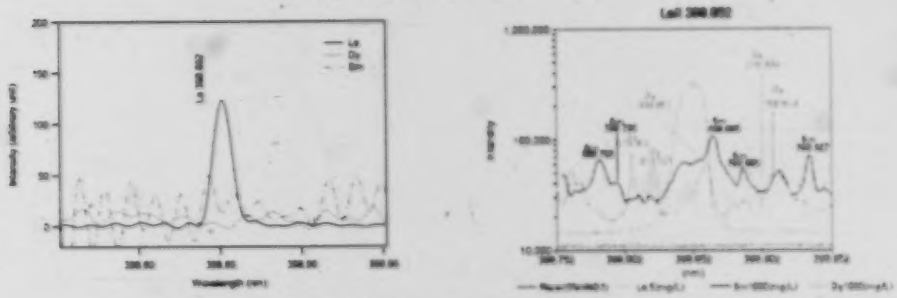

(d). La 398.852 nm window

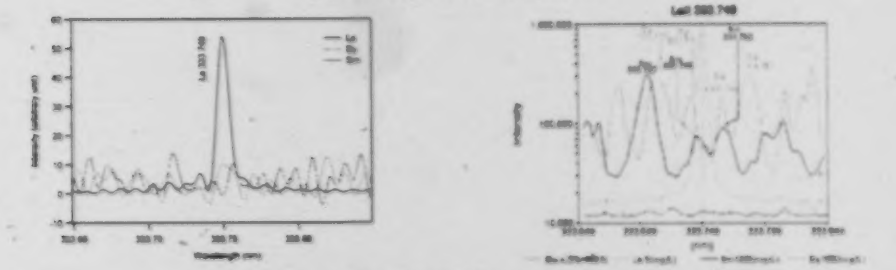

(c). La 333.739 nm window

Figure 4-27. Simulation of a 2 nm spectral windows (left) for a scanning spectrometer (right).

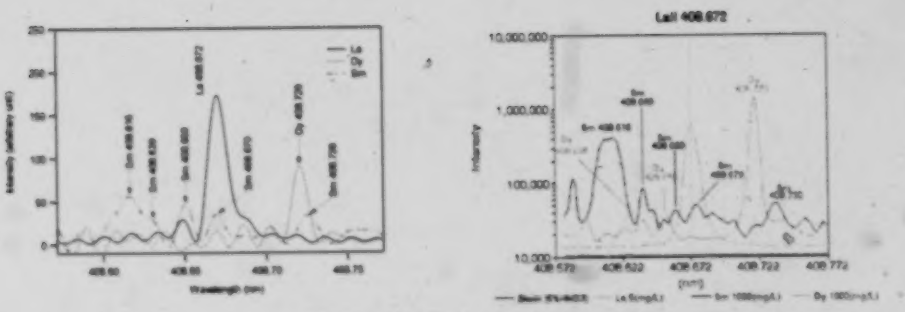

(e). La 408.672 nm window

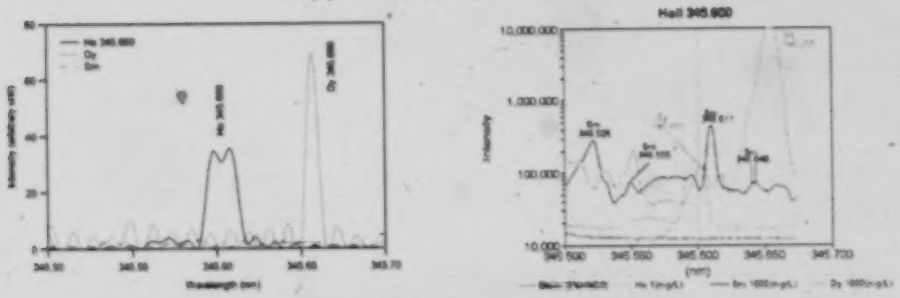

(f). Ho nm 345.600 Window

Figure 4-28. Simulation of a 2 nm spectral windows (left) for a scanning spectrometer (right).

Reference

(1) Griffiths, P. R.; Haseth, J. A. Fourier Transform Infrared Spectrometry; John Wiley & Sons: New York, 1986.

(2) King, G. B.; Horlick, G.: Spectrochim. Acta, Part B 1991 47B, E353-E370.

(3) Ying, H. Y., Pengyuan; Zhang, Zhigang; Gu, Sheng; Wnag, Xiaoru; Huang, Benli (Chem. Dept., Xiamen Univ., Xiamen 361005, Peop. Rep. China).: Guangpuxue Yu Guangpu Fenxi 1998 18, 559-564.

Chapter 5. The Spectral Library for Microsoft Windows Platform

The ICP-AES Spectral Library developed in this project was based on the *SpectroPlot* program (1) that can only be run on Apple Computer's Macintosh system. This chapter describes the preliminary development of the Spectral Library for the more popular Microsoft Windows system.

5.1. Developing Spectral Library for Windows Platform.

5.1.1. The Need.

Apple Computer's Mac OS and Microsoft Windows are two popular operating systems that are used by most personal computers today (2). Although they utilize different technologies and handle technical issues with different approaches, both OSs can be traced back to Xerox's pioneer work on the *Alto* (3). Built at the Palo Alto Research Center (PARC) of Xerox Corporation in the early 70s, *Alto* was the world's first personal computer based on the Graphical User Interface (4, 5). Traditionally Mac OS is regarded as the leader in graphics technologies, particularly before the middle 90's (6-8). Thus it is not surprising that most of the early software for spectroscopy, which relied heavily on graphics, was developed on the Macintosh. *SpectroPlot* (1), the Mac program the Spectral Library relies on, is a good example of such a development.

Today, although Apple Macintosh still excels in intensive graphical processing, the difference in performance is quickly diminishing as a result of rapid

advances in both the Windows operating system and PC hardware (2). As well, Apple Macintosh has never enjoyed the popularity of Microsoft Windows, which now runs on most personal computers and has become the *de facto* standard for the personal computer industry (9). It is important, therefore, to realize that being able to run on Windows will be vital to the general acceptance and success of the Spectral Library. Microsoft Windows is now, and will be for the foreseeable future, the dominant operating system for most people and most industries. For the Spectral Library to be accepted by these people and industries, making it accessible for Windows PC is as important as building its spectroscopic content. Otherwise, the Spectral Library might just stay in the ivory tower forever and never reach the outside world.

5.1.2. Design Guidelines for the User Interface

Clearly, a good user interface is very important to the acceptance of any software program. For the Spectral Library that contains vast amounts of information, a clear and intuitive user interface will be even more crucial as one should never expect all users to be experts of Fourier Transform Spectroscopy, or not even experts for personal computers. A poorly designed user interface will only drive away, or even worse, drown the users in an ocean of spectral data, and eventually bury the otherwise useful work of the Spectral Library.

For the Spectral Library, the user interface should provide direct and easy access to all elements that have spectra in the Spectral Library. A periodic table form is preferred. Figure 5-1 shows a prototype interface designed with Microsoft Visual Basic. A control array of 103 Command Buttons provides the gateways to the spectra

and interferograms of all elements. The buttons for those elements that do not have spectra available are disabled and will not response to a mouse click.

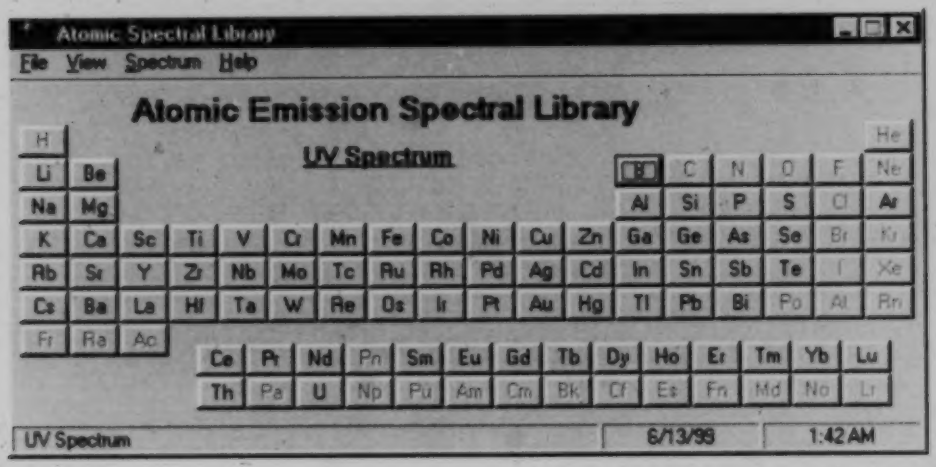
Atomic Spectral Library
File View Spectrum Help
Atomic Emission Spectral Library
UV Spectrum
H
He
Li Be
B C N O F Ne
Na Mg
Al Si P S Cl Ar
K Ca Sc Ti V Cr Mn Fe Co Ni Cu Zn Ga Ge As Se Br Kr
Rb Sr Y Zr Nb Mo Tc Ru Rh Pd Ag Cd In Sn Sb Te I Xe
Cs Ba La Hf Ta W Re Os Ir Pt Au Hg Tl Pb Bi Po At Rn
Fr Ra Ac
Ce Pr Nd Pm Sm Eu Gd Tb Dy Ho Er Tm Yb Lu
Th Pa U Np Pu Am Cm Bk Cf Es Fm Md No Lr
UV Spectrum
6/13/99
1:42 AM

Figure 5-1. A prototype user interface for the Spectral Library.

Through this user interface, users should be able to open and display spectra and interferograms for both the visible and UV regions and it is desirable to have the ability to display two or more spectra or interferograms of one element at the same time. If possible, the basic display window should provide all the functionality of *SpectroPlot*, which has been optimized to fit spectroscopists needs better than any existing user interface, including expensive commercial technical graphing packages.

In addition to access to the spectra, the Spectral Library interface should also provide access to a wavelength table for each element with accurate wavelength values for intensive lines in the visible and UV regions. *SpectroPlot* has a build-in function to list wavelength and intensity for spectral lines on the fly, so it is able to generate such a table on demand. The problem is, however, the accurate wavelength

values require zero filling (a Fourier data processing operation). Thus, a list of accurate and proven lines will be more convenient for spectral line selection.

To assist in spectral line selection and spectral interference identification, the library should provide a means to display cross-reference for spectral interference. For example, for each listed spectral line, provide a list of all possible spectral lines from other elements in a wavelength window centered at the wavelength value of the spectral line under investigation. Such list would alert users to potential spectral interference problems.

Finally but importantly, the Spectral Library interface should provide a fast and correct algorithm to perform Fourier transforms like *SpectroPlot*. This is very important as it is the only way to get spectra from the interferograms and vice versa, and, as has been seen in the pervious chapters, this is also necessary for resolution control of the spectra and thus important for spectrum simulations.

5.1.3. Some Comments on the Interface Development

It should be noted that the previous section is only a guideline for the development of the interface for the Spectral Library. Currently not all features desired or listed were developed or are being developed. Initial attempts to develop the interface from scratch with Microsoft *Visual Basic* had been hindered by the limitation of the development tool and thus a Spectral Library based on commercial graphic software had been developed and will be presented in the next sections. It is the author's feeling that, however, if the interface will ever be developed from ground up, *Visual C++* combined with Microsoft *Foundation Class Library* (MFC) will be more adequate for the job (10). While *Visual Basic* is good at building a user

interface and dealing with a relational database, MFC is much more powerful and efficient when dealing with intensive graphics and large data sets, which is the case for the Spectral Library interface development.

An alternative to this is the graphing libraries (11). Graphing libraries are software components developers can use in their daily development to simplify the development process for graphing. They allow one to create many different styles of graphs in a similar fashion, but much simpler, to using the Windows Graphics Design Interface (GDI). Graphing libraries contain thousands of lines of necessary GDI code to create one's graphs, freeing one from the time-consuming task of developing and debugging one's own GDI-based code. One can also incorporate these libraries into almost any application that supports calling a dynamic linking library or an *ActiveX* control component.

Commercial graphing libraries are available from several software companies and can be used with either *Visual Basic* or C++. Among their products, Pinnacle Publishing's *Graphics Server* provides the most features and most sophisticated capabilities (11, 12). This is a solid, proven package with superior documentation and fine performance. It has made its way into many commercial applications over time. *Graphics Server* is currently at version 5.5 for $499 (US). If it is used, much coding work can be saved for both graphing and data process functions since it comes with a long list of functions including FFT. Since it will handle all graphing tasks, there is no need to worry about the performance of *Visual Basic*.

5.2. Spectral Library Based on *Origin*.

5.2.1. The Spectral Library Interface

Origin™ is a scientific graphing and data analysis program developed by OriginLab Corporation (formerly Microcal, Inc. One Roundhouse Plaza, Northampton, MA 01060, USA) and runs on Microsoft *Windows* (13). A time-limiting working demo of *Origin* can be downloaded free from their web site (http://www.originlab.com).

To provide a convenient way for readers to access the ICP spectra and interferograms in the ICP-AES Spectral Library, a user interface has been built under *Origin* for the Microsoft *Windows* platform (Figure 5-2). Although not a requirement to use the library, it is certainly helpful for readers to have a basic knowledge of the Microsoft *Windows* operating system and *Windows* applications.

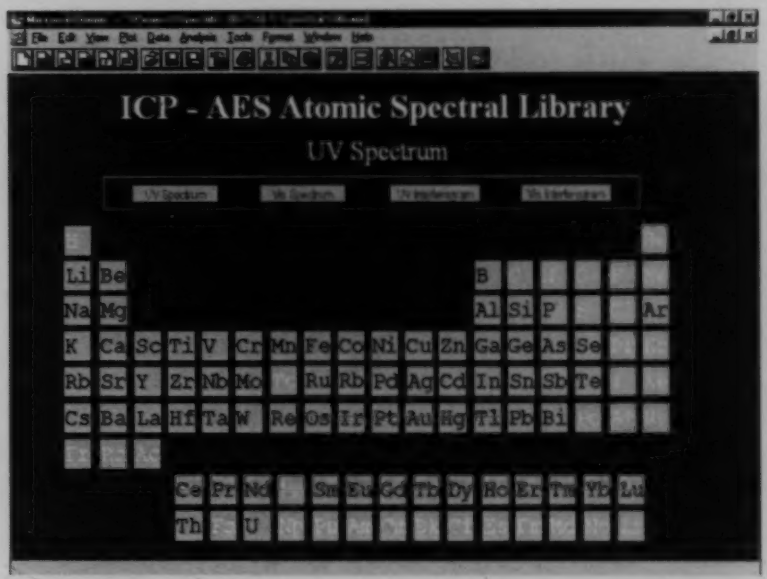

Figure 5-2. The user interface of the Spectral Library built on *Origin*™

The interface of the Spectral Library consists of three main areas. The Title, the spectrum types selection, and the element selection.

On top of the page is the title of the spectral library. The spectrum type selection is achieved by a click on one of the four buttons that are labeled "UV Spectrum", "Visible Spectrum", "UV Interferogram", or "Visible Interferogram", respectively. By default, the spectrum type was set to "UV Spectrum" as indicated by the subtitle of the Spectral Library. In this case, the spectrum for any element accessed will be the UV spectrum for that element. To access visible spectra or interferograms, users can simply click on the corresponding button, e.g. "UV Interferogram", then the subtitle will change to "UV Interferogram", indicating now the UV interferogram is being accessed.

The selection of the elements is accomplished through a collection of buttons arranged in periodic table style. The black symbol on a button indicates the Spectral Library has spectra and interferograms for that element, and the grayed-out symbol on the button indicates that there is neither spectra nor interferograms available, or the element could not be determined by ICP-AES.

Once the spectra or interferograms are opened in *Origin*, they can be viewed and manipulated in many ways as discussed in the following section. It should be noticed, however, that the Spectral Library was developed for an early version of *Origin*, *Origin* Version 4.1. Thus there might be some differences from the current version, but the operation principles should remain the same.

The *Origin* project that contains the user interface is named as SpecLib.opj and stored in folder "Origin" on the companion CD.

5.2.2. Viewing the Spectra

5.2.2.1. Display Spectra in Origin

The easiest way to view spectra or interferograms in *Origin* is to display the spectra or interferograms from the Spectral Library user interface discussed in the previous section. To do that, the user can first load the interface by opening the *Origin* project SpecLib.opj, and then select the spectra type and element.

Alternatively, readers can access the Spectral Library directly from *Origin*. To do this, start *Origin* and a blank worksheet will appear. Click on **File**: **Import** on the menu, and then select **ASCII**. Choose the CD-ROM drive (usually drive D) in the *File Open* window and open folder *spectra*. All spectra for one element are saved in a sub-folder named with the element symbol.

For example, to view the ICP-AES UV spectrum for boron, import file Buvsp.txt in D:\spectra\B folder, and data will appear in two columns once the importing process is finished. The data in column A (marked as *x* by default in *Origin*) is the wavelength value for a spectrum, or data point for an interferogram, and that in column B (marked as *y*) is intensity in arbitrary unit for both spectra and interferograms. To display the spectrum, highlight these two columns on the worksheet and click on the **Plot** on the menu bar, and then select **Line**. A line plot will be displayed in a new window named Graph1 (Figure 5-3).

By default *Origin* plots large data set with the *speed mode* turned on. That is, it omits some data points as it plots. This increases display speed but may causes distortion in the displayed spectrum. To avoid this problem, one should open up the *Page Control* window by clicking on **Format: Page**; then clear the **speed mode**

check box in the *Display Preferences* group, and change the *View* to *Window view* in the *Page* group. Once the OK button is clicked, *Origin* will automatically redraw the window with all data points.

Next the label of the axis should be changed to make the plot meaningful. Double click on the label "X axis title" to get the *Text Control* dialog and change the text from "X axis title" to "Wavelength (nm)" for a spectrum or "Data Point" for an interferogram. Then double click on the x-axis and, in the *X Axis* dialog box, set the scale from 150 to 320 for UV spectra, 300 to 700 for visible spectra, and 0 to 132000 for interferograms, respectively. Similarly, the label of the y-axis should be changed to "Intensity", and the scale range set appropriately. Finally, select the menu **Window: Rename**, click on the *Label* item on the dialog box and enter a name. A properly displayed and labeled boron UV spectrum is shown in Figure 5-4.

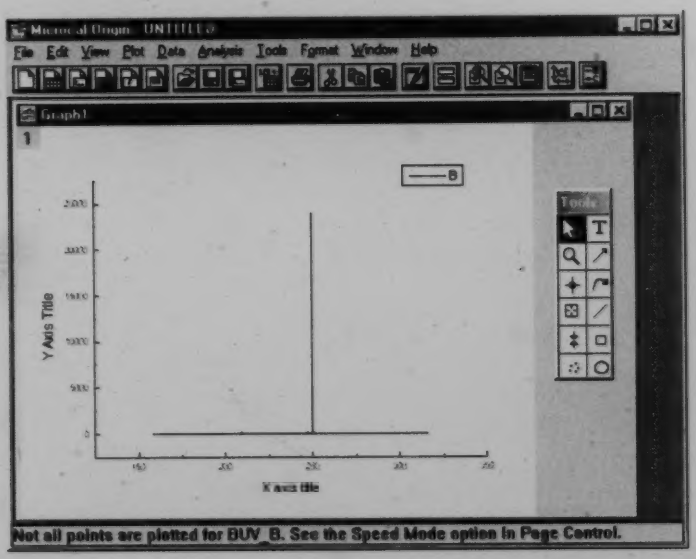
File Edit View Plot Data Analysis Tools Format Window Help
Graph1
1
B
Tools
Y Axis Title
X Axis Title
Not all points are plotted for BUV_B. See the Speed Mode option in Page Control.

Figure 5-3. A line plot for B UV spectrum data in *Origin*.

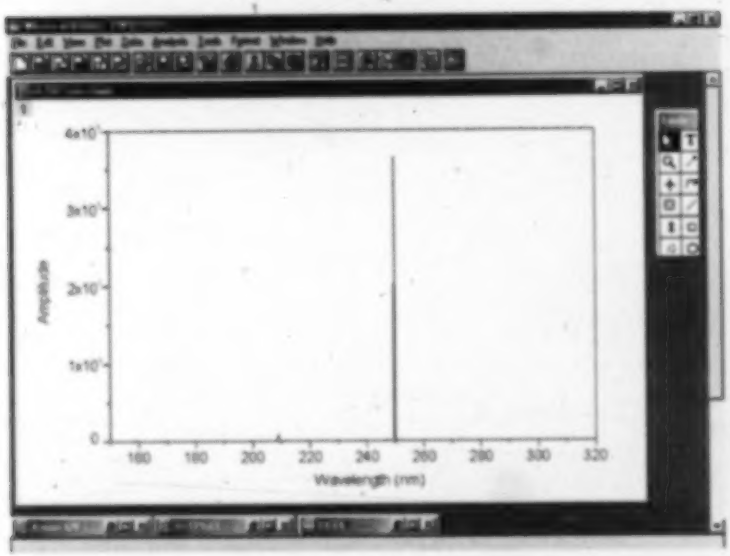

Figure 5-4. Boron UV spectrum displayed in *Origin*.

5.2.3. Viewing Spectra in Detail

Origin provides some useful tools for viewing and manipulating data and spectra. These tools provide convenience and interactivity for users and distinguish the Spectral Library from the traditional printed ones. Collectively these tools are called the "toolbox" in *Origin* and can be accessed by clicking **Tools: Toolbox** on the menu bar. Some of the most important tools are listed in Table 5-1, along with some short descriptions of the tools and their usage. Other tools in the toolbox, like *Text* tool, *straight arrow* tool, *curved arrow* tool, etc, are similar to those in popular presentation software. Although they can be very useful in labeling spectra, they will not be discussed here. Consult the *Origin* manual for further details.

Table 5-1. Important tools in the *Origin* toolbox.

Name	Icon	Primary function
Enlarger Tool		Magnify a portion of a data plot.
Data Reader		Obtain the x, y coordinates value of a data point only.
Screen Reader		Obtain the x, y coordinates value of any point on the graph page.
Data Selector		Select a segment of a data plot for subsequent operation.

5.2.3.1. Reading Information for Spectral Lines

Data Reader is a more useful tool for viewing spectra data than that of *Screen Reader*. It is used to determine the XY coordinates of a point on a data plot. To access the ***Data Reader*** tool, click on the tool and then click on the data point you want to read. It might be necessary for the reader to try several times before a data point can be located. Once a data point is located, a red crosshair will appear at that point, and the point number and x, y value will appear beneath the graph window title bar (Figure 5-5). The crosshair can be moved with the left and right keys, or be dragged to a new location using the mouse.

Screen Reader tool can be used to determine the X and Y coordinates of any point on the graph page. It does not trace the spectral line as the ***Data Reader*** tool. To use the ***Screen Reader*** tool, click on the tool and then click anywhere in the graph window. The XY coordinates appear beneath the graph window title bar. Use either the mouse or the arrow keys to move the crosshair pointer.

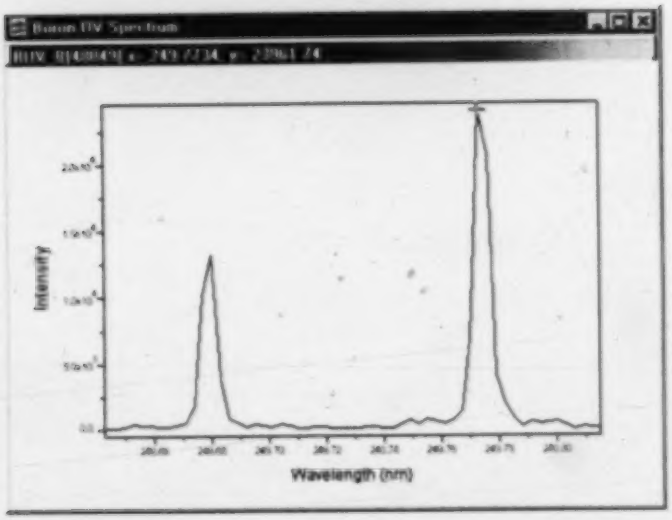

Figure 5-5. ***Data Reader Tools.*** Notice the information in the title bar.

5.2.3.2. Viewing a Section of Spectrum with *Enlarger tool*

Enlarger tool can be used to magnify a portion of a data plot. The spectrum can be zoomed both vertically (intensity axis) and horizontally (wavelength axis). By properly using the *enlarger tool*, a portion of the spectrum can be displayed.

To do this, first click on the *Enlarger tool*, then with the mouse button held down, drag a rectangle around the portion of the data plot one wants to enlarge. When the mouse is released, the axes rescale to show only the selected data. This is the simplest way to view a portion of a spectrum.

To re-display the entire data plot, double-click on the Enlarger tool. The axes revert to their original scale. If the Ctrl key is held down when the rectangle is being drawn, the selected graph will be displayed in a new window.

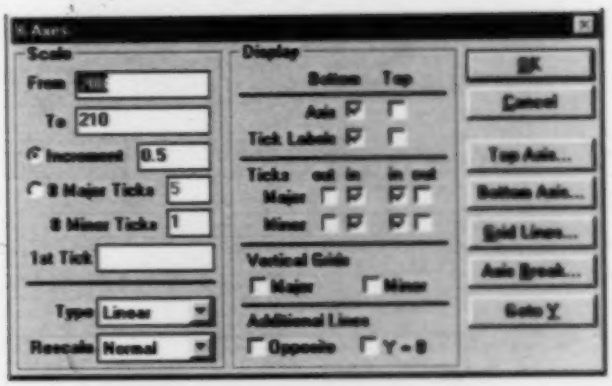

Figure 5-6. Property window for x-axis.

5.2.3.3. Viewing a Section by Changing the Axis Scale

Similar to many graphical plots, the spectrum displayed in *Origin* can be viewed more closely by expanding the scale of axis. For example, double clicking on the X-axis of the spectrum will bring up a property window for the axis (Figure 5-6). Enter the desired wavelength range in the "*from*" and "*to*" boxes and click the *OK* button. The spectrum for the specified wavelength range will be displayed. For small peaks, one can perform a similar operation on the Y-axis to get a better view.

5.2.3.4. Viewing a Section the *Data Selector* Tool

Data Selector is another useful tool provided by *Origin*. It can be used to change the display range of the active data plot without affecting other plot instances or the worksheet display range (Figure 5-7).

To do this, click on the ***Data Selector*** tool in the Toolbox. Data markers appear at both ends of the active data plot. Click and drag the markers along the X-axis with the mouse to mark the data segment of interest. Release the mouse button when the marker displays at the desired data point. Alternatively, use the left and

right arrow keys to select a marker. Then hold down the Ctrl key and press the left or right arrow keys to move the selected marker to the desired data point. The data point number, wavelength value, and intensity can be read out from beneath the title bar of the graph window. Apparently this method is much slower than using the mouse, but it allows one to reach the exact data point of interest and thus have precise control of what data range is selected. Once the data markers are in position, click on the *Data Selector* tool again or press the ENTER key. Then select **Data: Set Display Range**. All spectra except the selected portion will be hid from view.

To reset the display range of the data plot back to the original range, select **Data: Reset to Full Range**.

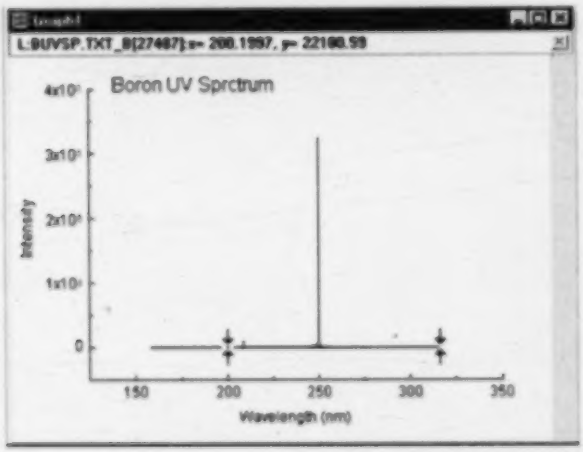

Figure 5-7. Select a section of spectrum with ***Data Selector*** tool.

5.2.3.5. Duplicate a Section of a Spectrum

Due to the vast amount of information a full-range spectrum carries, sometimes it is more efficient or accurate to view and manipulate a specific section of the spectrum, and this can also be done in *Origin*.

To display a section of a spectrum, first extract necessary data points from the data series by selecting **Analysis: Extract Worksheet Data**. Figure 5-8a shows such a window to extract data points from 31750 to 31877. A click on the **Do it** button will extract these data points from current data set to a new worksheet named **Data1**, It can be plotted in the same way as described before to obtain a portion of the spectrum containing only 128 data points (Figure 5-8b).

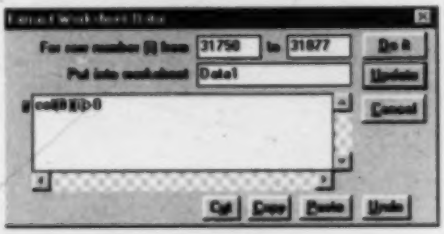

(a)

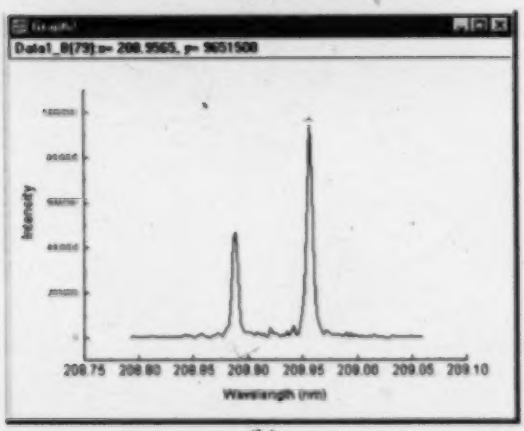

(b)

Figure 5-8. Plot a section of spectrum by extracting data with the *Extract Worksheet Data* window.

5.2.4. Fast Fourier Transform in Origin.

The interferograms in the Spectral Library can be transformed into spectra with the built-in fast Fourier transform (FFT) function of *Origin*. To perform a fast Fourier transform on the active data plot, select menu **Analysis: FFT**. This opens the FFT parameter control dialog (Figure 5-9).

There are two tabs in this window. On the *Operation* tab the *forward FFT* and *Amplitude* spectrum should be selected for transformation from interferograms to spectra. On the *Settings* tab, users can accept default settings for routine operation. The so-called *Windows Method* provides five choices for apodization functions that *Origin* builds in. In most cases, rectangular or boxcar apodization is sufficient to avoid distortion in the spectra, in some cases, other functions can slightly improve spectral line shapes transformed. For interferograms from the Spectral Library, the sampling interval should always set to 1.

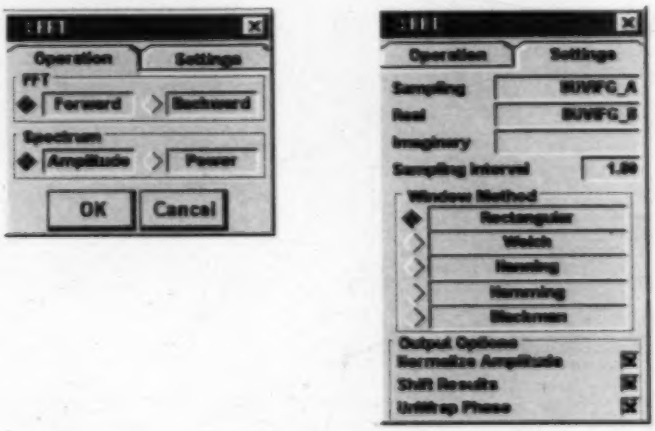

Figure 5-9. The parameter control dialog of FFT function. See text for details.

After the calculation for the FFT, *Origin* saves all results to a new worksheet called FFT1 (Figure 5-10), and displays a line plot of sample amplitude versus sampling frequency along with the phase spectrum.

Depending on the *Shift Result* option checked or not in the FFT setting dialog, the spectrum from the FFT calculation will be displayed differently. A non-shifted spectrum is the one with both positive (real) and negative (imagery) part displayed, and the shifted one displays only the real spectrum (Figure 5-11). Apparently, for atomic spectrum, only the real spectrum should be kept.

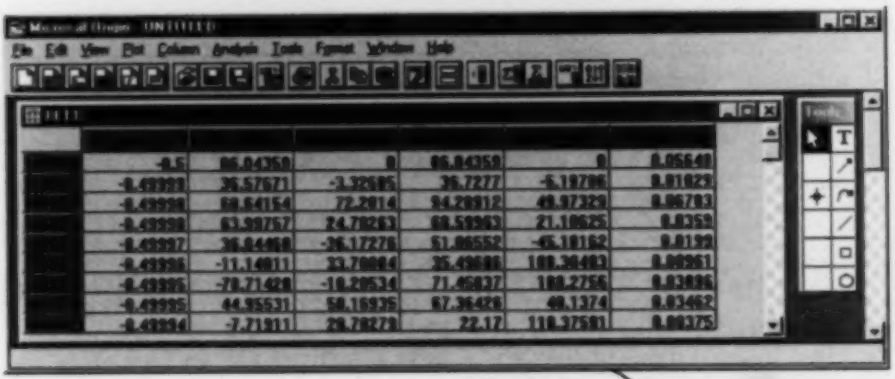

Figure 5-10. The calculation result listing for the FFT.

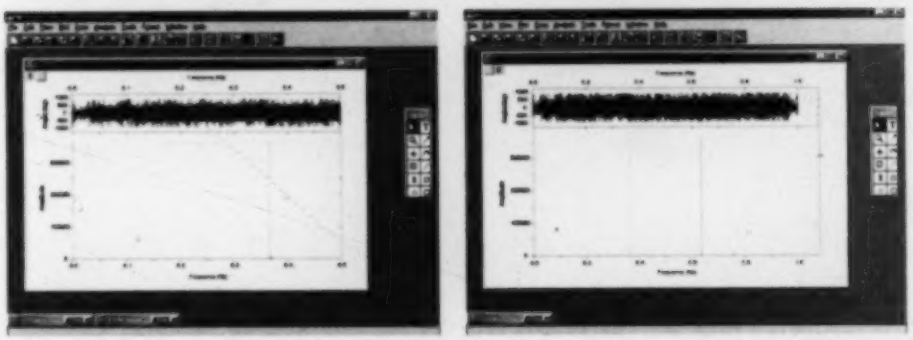

(a) (b)

Figure 5-11. Spectra plotted after FFT in *Origin* (a) with result shift. (b) Without "shift result" checked.

5.2.5. Wavelength Calibration in Origin.

After FFT of the interferograms or to correct wavelength shifting in the spectrum, wavelength calibration or recalibration is often necessary for Spectral Library users to obtain accurate wavelength values for spectral lines.

5.2.5.1. Extraction of Amplitude Data for Wavelength Calibration

As *Origin* saves both the real and imagery parts of the FFT, the first step to calibrate the wavelength for spectra calculated from interferograms by *Origin* is to extract the real spectrum from the FFT results using the method for extraction of a section of a spectrum.

To do this, first remove all columns except r(Y) in the FFT window (Figure 5-10), then highlight column r(Y) and select menu **Analysis: Extract Worksheet Data**. A dialog box similar to Figure 5-12 will appear. Type in row number from 65537 to 131072 if the data is shifted, or from 1 to 65536 if it is not; and enter [i]>0 in the criteria box and then press **Do it** button (Figure 5-12). All data in the specified range will be extracted into the new worksheet that will contain one column and 65536 rows of data, which is the amplitude values of the spectrum. The wavelength can then be calculated from the data points as discussed later in this section.

For spectra loaded directly from the Spectral Library, the extraction step described in this section is not necessary and should not be performed, as only the real spectrum is included.

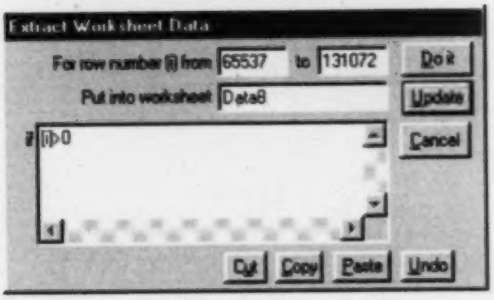

Figure 5-12. Extracting amplitude data of a spectrum from an FFT worksheet.

5.2.5.2. Wavelength Calibration and Re-Calibration

The wavenumber of a data point in a spectrum transformed from an interferogram is given by:

$$\sigma_n = \frac{n}{N \cdot \lambda_{heNe} / n_i}$$

or

$$\lambda_n = \frac{1}{\sigma_n} = \frac{N\lambda_{HeNe}}{(i-1)\cdot n_c} \qquad (5\text{-}1)$$

Whereas: σ_n is the wavenumber at n data point; N is the number of total data points in the interferogram; n is the number of a data point and n= 0, 1, 2,..., N-1; λ_{HeNe} is the wavelength of the He-Ne reference laser used for the interferometer, n_c is the clock rate for data sampling, and i is the row number of an *Origin* worksheet and i = n+1.

This holds true, however, only if no alias occur. The spectra in this library are all sampled at 4 × HeNe laser clock rate, so the visible spectra can be calibrated directly with the above equation. The UV spectra, on the other hand, all fall into alias region one (1). Thus the wavelength calibration is more complicated.

It is easy to see that in alias region one

$$n = (N-1) - n_{obs} = (N-1) - (i-1) = N-i$$

Thus the wavelength is given by:

$$\lambda_n = \frac{1}{\sigma} = \frac{\lambda_{HeNe}}{(1 - i/N) \cdot n_c} \qquad (5\text{-}2)$$

For wavelength calibration or re-calibration, highlight column A or the wavelength column and then select **Column: Set Column Values** from the menu bar (Figure 5-13). In the formula box enter Equation (5-1) for a visible spectrum or Equation (5-2) for a UV spectrum and use N=131,072, n=i-1, and n_c=4.. The recommended apparent wavelength value for the reference laser for all spectra is 632.6438 nm. This value should be accurate enough in most cases. For wavelength critical calculation, the apparent wavelength value for that particular spectrum should be used instead. This value can either be looked up from the wavelength table (PDF files) supplied with the Spectral Library, or be calculated with other external wavelength standards as discussed earlier in the thesis (14).

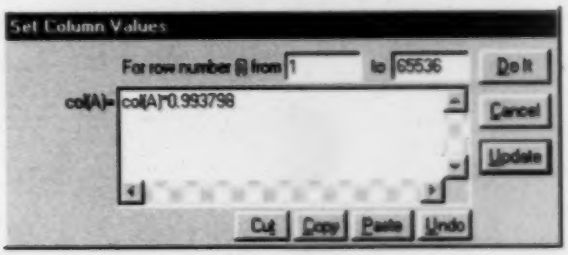

Figure 5-13. ***Set Column Value*** dialog for wavelength calibration in *Origin*.

5.3. Spectral Library Based on WaveMetrics' *Igor Pro*

WaveMetrics' *Igor Pro* is a powerful graphing, data analysis, and programming tool for scientists and engineers. It has been known and used for several years by Macintosh users, but is relatively new to the Windows world.

5.3.1. Strength and Weakness of *Igor Pro*

For users in the scientific and engineering area, *Igor Pro* provides considerable and often unique capacity. This includes: (1). The ability to handle large datasets with support for many different data formats common to the scientific and engineering field. (2). Powerful data analysis including precision data reading, Fourier transformation, curve fitting, and smoothing. (3). Publication-quality graphing including support for charting, drawing, annotations, and layout design. It also supports high-resolution graphics export in the formats of PICT, BMP, Enhanced Metafile, PNG, and Encapsulated PostScript files. (4). Programmability with built-in C style programming language.

The weakness of *Igor Pro*, however, are also obvious. Mastering *Igor Pro* is by no means an easy task. With its rich features and rather confusing interface design, naive users can easily get lost. Although it is supposed to be a Windows program, some essential operations (modifying a data array, for example) are still executed with a DOS style command line. To make things worse, *Igor Pro* uses a terminology system that is so different from popular Windows applications, even a veteran Windows user will have a hard time navigating through it.

Nevertheless, the strengths of *Igor Pro* far overweigh its weaknesses in spectroscopic applications. In the next few sections, the essential steps for display and manipulation of spectra and interferograms with *Igor Pro* will be introduced, along with some discussions on Fourier transformation and wavelength calibration. Readers who have no previous experience with *Igor Pro* are strongly urged to read at least the first chapter of the *Igor Pro* "Getting started" manual before proceeding.

5.3.2. Viewing Spectra or Interferograms with *Igor Pro*

To provide easy access for the spectra and interferograms in the Spectral Library from *Igor Pro*, a user interface with similar design principle and operation to that in *Origin* has been developed (Figure 5-14). Similar to that developed for *Origin*, this interface is also based on the Periodic Table. The type of the spectra can be selected with a pull-down menu underneath the Spectral Library title; and the spectra for each element can be access with a click on the command button labeled with the symbol of the element.

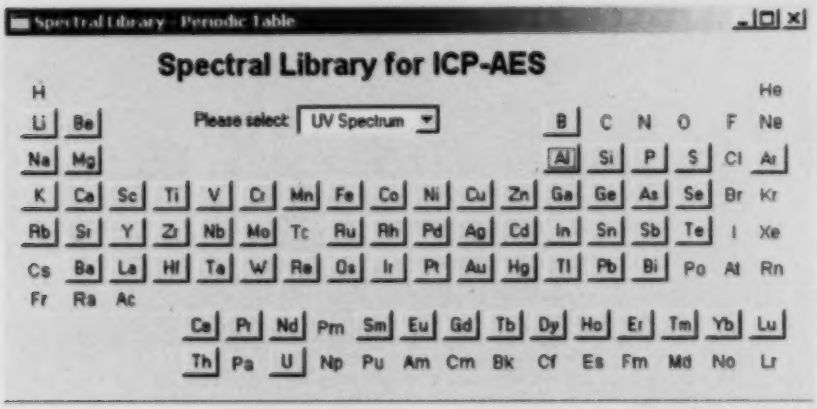
Spectral Library - Periodic Table
Spectral Library for ICP-AES
Please select: UV Spectrum
H
He
Li Be
B C N O F Ne
Na Mg
Al Si P S Cl Ar
K Ca Sc Ti V Cr Mn Fe Co Ni Cu Zn Ga Ge As Se Br Kr
Rb Sr Y Zr Nb Mo Tc Ru Rh Pd Ag Cd In Sn Sb Te I Xe
Cs Ba La Hf Ta W Re Os Ir Pt Au Hg Tl Pb Bi Po At Rn
Fr Ra Ac
Ce Pr Nd Pm Sm Eu Gd Tb Dy Ho Er Tm Yb Lu
Th Pa U Np Pu Am Cm Bk Cf Es Fm Md No Lr

Figure 5-14. Spectral Library Interface for *Igor Pro*.

Alternatively, users can load spectra from the Spectral Library directly from *Igor Pro*. The boron interferogram will be used as an example to illustrate the necessary steps to display and manipulate spectra and interferograms; and the boron UV spectrum will be used to illustrate precise data reading.

When dealing with *Igor Pro*, it is important to understand the meaning of "wave" as it is used in the program. Essentially, an *Igor Pro* "wave" is an array of data, normally displayed in a column in a database table, a spreadsheet, or a delimited text file. To *Igor Pro*, every spectral library file contains two waves: one is data point (for interferograms) or wavelength (for spectra), and another is intensity. When loading a wave, *Igor Pro* loads it directly into memory leaving no visual clue of the existence of the wave, unless it is put into a table or a graph window.

To load spectra directly from *Igor Pro*, first start the program; a table and the command window are displayed by default. Select the **Data** menu, then **Load Waves**: **Load Delimited Text** ... (Figure 5-15a), a *File Open* dialog will appear. In this dialog, select UV\B\Buvifg.txt on the CD-ROM drive and click on *Open*. Enter "Data Points" for the name of wave0 and "intensity" for wave1 in the next dialog window and check "Make Table" check box to display the imported data.

Next, click on **Windows: New Graph** to display the *New Graph* dialog (Figure 5-15b). Select "Intensity" for "Y wave" on the left-hand side window, and "Data Point" for the "X wave" on the right-hand side. Click on **Do It** to display the spectrum.

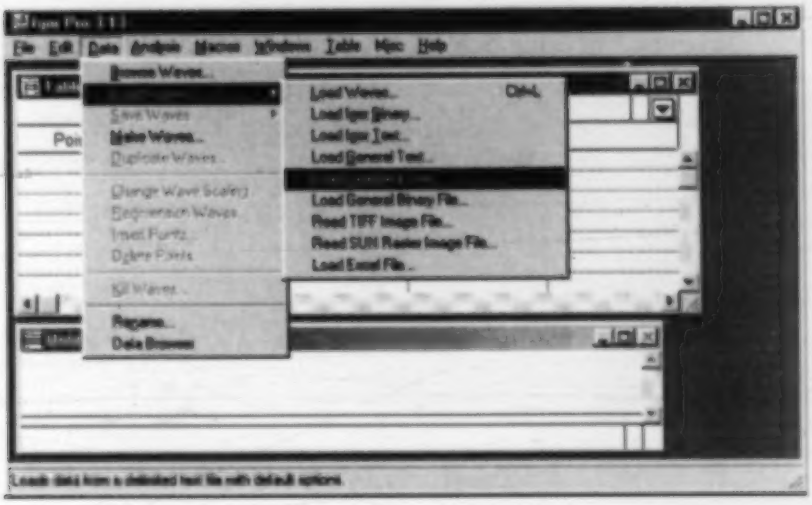

(a)

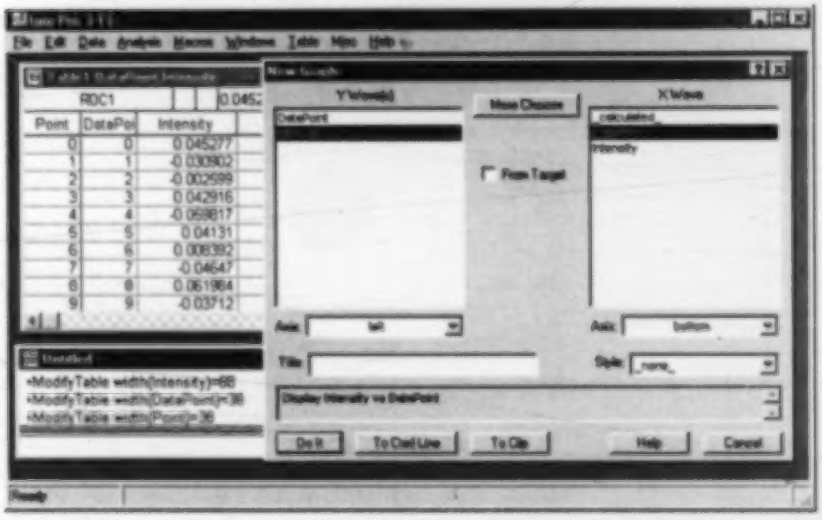

(b)

Figure 5-15. Loading delimited text data from the Spectral Library into *Igor Pro*

To label the axis, click on **Graph: Label Axis** to open up a *Label Axis* dialog. Enter "Intensity" in the "Axis Label" box for the "Left" Axis and "Data Point" for "bottom" axis. Click on **Do It** when done.

To zoom in or zoom out a displayed spectrum is simple. Draw a square with the mouse pointer on where you want the center of view. Then a click anywhere inside that area will bring up a pop-up menu. It shows six options (Figure 5-16): *Expand* will zoom in both directions and make the selected area full view. *Horizontal Expand* will keep current Y scale expand in X direction only. *Vertical Expand* keeps current X scale and expands Y scale only. *Shrink*, *Horizontal shrink*, and *vertical shrink* have similar meaning except they are zooming out. Click on **Graph: Autoscale Axis** will reset the view to its original full view state.

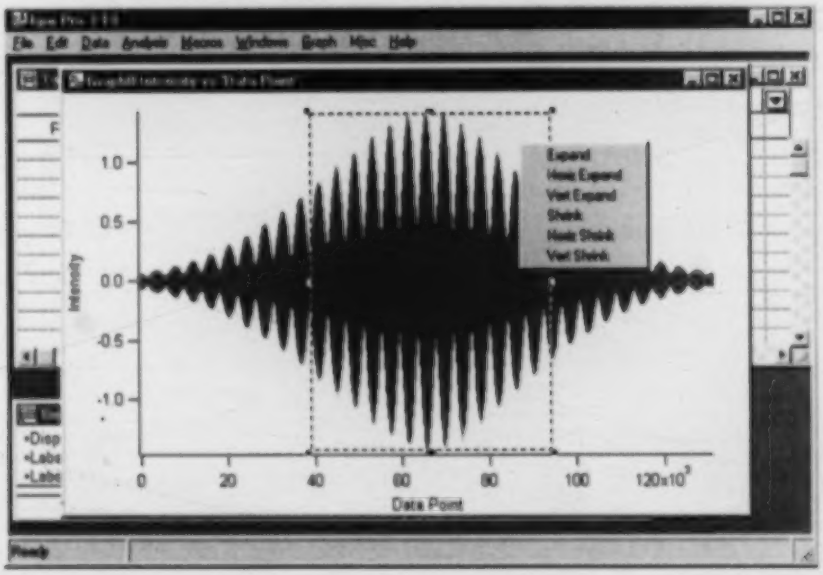

Figure 5-16. Boron UV interferogram displayed in *Igor Pro* with center area selected for zooming.

After zooming in a small portion of a spectrum, one can get a precise readout of any data point in view. Figure 5-17 shows using both cursors to readout the wavelength of the boron 249 nm doublet. To do this, first zoom in at 249 nm, then with the graph window as current, click **Graph: Show Info**. The "Info Box" will show up at the bottom of the graph. Click on one cursor (⊕ for cursor A and ⊠ for B) and drag it to the desired point. The readout area shows the point number, X coordinate and Y coordinate for the point the cursor is on. In Figure 5-17, cursor A is at data point 48017 with wavelength at 249.6801 nm and intensity 13191.79. These data are identical to that reported by *SpectroPlot*. Please note that the cursor will not work if the draw layer is activated. If the cursor cannot be dragged to the data point, clicking on **Graph: Hide Tools** will usually fix the problem.

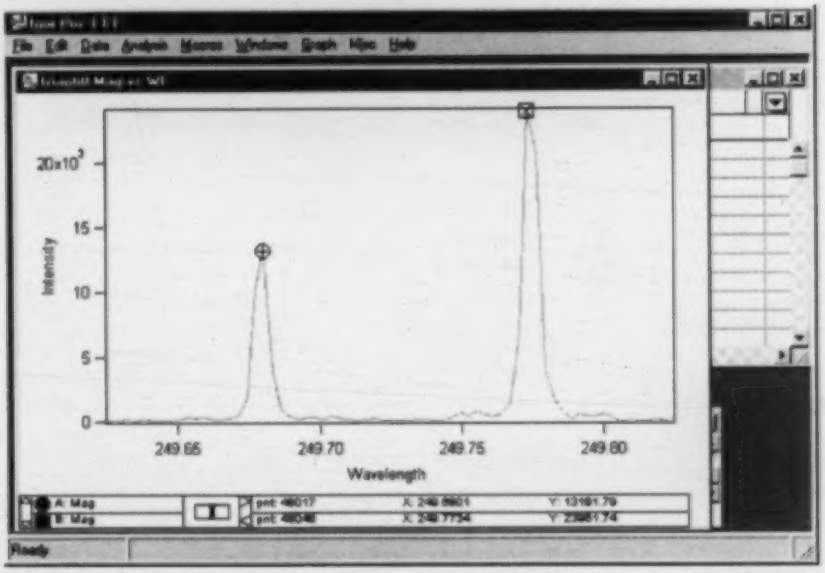

Figure 5-17. Use cursor and "info box" for precise data readout.

5.3.3. Fourier Transform and Wavelength Calibration

Igor Pro uses the Fast Fourier Transform (FFT) algorithm to compute a Discrete Fourier Transform (DFT). Starting from version 3.0, it uses a prime factor multi-dimensional algorithm, which allows the FFT to work on nearly any number of data points, instead of being restricted to a power-of-two number of data points.

The FFT operation replaces the content of original interferogram with the DFT results. One should duplicate the original data before computing the FFT if the original data is to be preserved.

To transform an interferogram, first load it into *Igor Pro*. In order to watch the change *Igor Pro* will make, display both the *DataPoint* and *Intensity* in a table and plot the interferogram as in Figure 5-18a. Notice there are three columns of data in the table: the first column is the index given by *Igor Pro*; the others are *DataPoint* and *Intensity* respectively.

Now click on **Analysis: Fourier Transform** ...to open up the FT dialog. Choose the wave *intensity* and *forward* operation, then click on **Do it**. Once the FFT is done, both the real and imaginary values are listed in the table, and the plot for this complex spectrum is shown in Figure 5-18b.

In most cases, however, human eyes prefer an amplitude spectrum instead of a complex one. The amplitude of a complex spectrum is given by:

$$\text{Amplitude} = (\text{real}^2 + \text{imaginary}^2)^{1/2}$$

In *Igor Pro*, this value can be calculated from the command line by entering the following two lines of command, one line at a time:

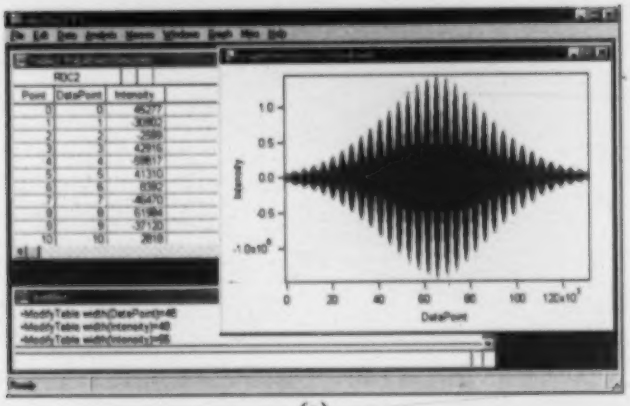

(a)

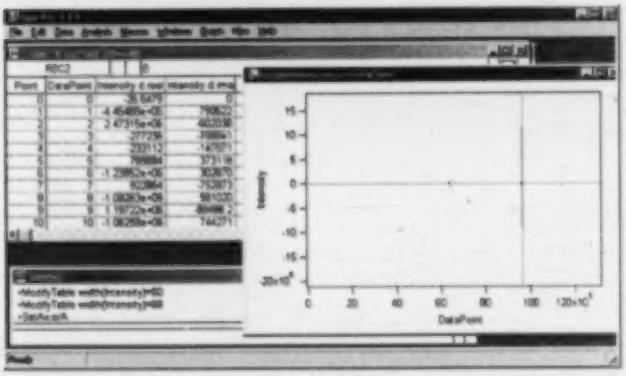

(b)

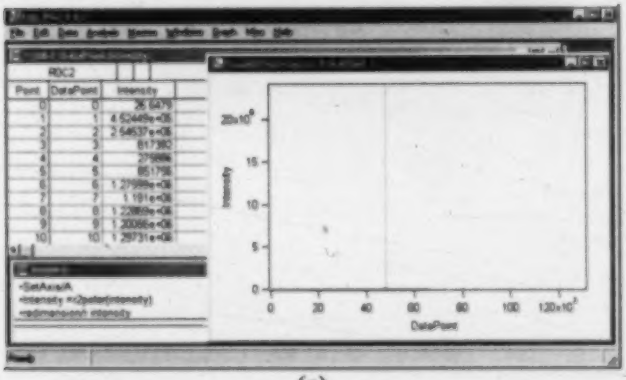

(c)

Figure 5-18. FFT in *Igor Pro*: (a) Boron UV interferogram (b) Complex spectrum from the *Igor Pro* FFT and (c) amplitude spectrum obtained with command line function.

```
Intensity = r2polar(Intensity)
Redimension/R Intensity
```

The first line calculates the amplitude and phase of *Intensity* from real and imaginary value and assigns the value back to *Intensity*. The second line drops the imaginary part and keeps the amplitude only.

As the wave *Intensity* lost half of the data points after the FFT, the data points in the wave *DataPoint* should also be cut in half in order to maintain a correct spectrum. Click on **Data: Delete Points** ... to open the dialog box. Select *DataPoint* in the Wave windows on the right, enter 65536 for the first point to be deleted, and 65536 for the total number of points to be deleted (Figure 5-19).

Next, a wavelength calibration similar to that described previously has to be performed using equation (5-2). Enter the following at the command line:

```
DataPoint=632.8432/4/(1-DataPoint/131072)
```

Then double click on the x-axis label *DataPoint* to bring up the *Label Axis* window and rename the x-axis as *Wavelength (nm)*. This completes the whole Fourier transformation process from an interferogram to a spectrum, and gives a spectrum that is similar to what is stored in this spectral library.

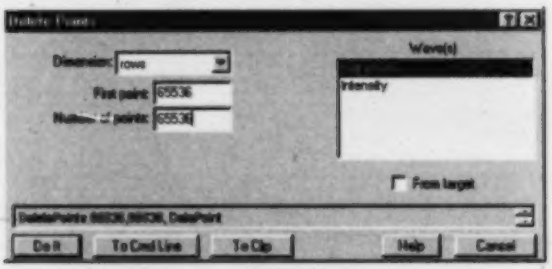

Figure 5-19. Delete Points dialog box.

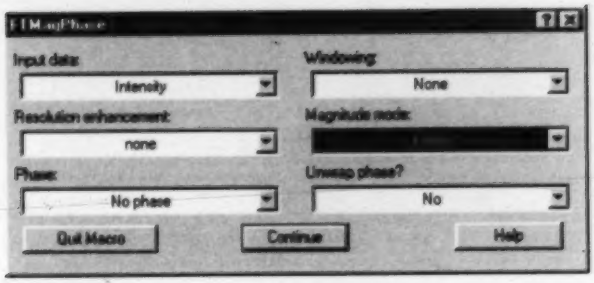

Figure 5-20. FFT option dialog.

5.3.4. Advanced FFT Operation

The above procedure for transformation of an interferogram to a spectrum is tedious. Fortunately, *Igor Pro* comes with some external procedures that significantly simplify the FFT process. One of these procedures is called "FTMagPhase". Its application will be illustrated in this section.

Assume that the boron UV interferogram has been loaded into an *Igor Pro* experiment. Open up the procedure window by clicking **Windows: Procedure Window** and enter the following line:

```
#include <FTMagPhase>
```

When the procedure window is closed, the procedure will be compiled and loaded automatically. Then open the dialog named *FTMagPhase* (Figure 5-20) by clicking on the **Macro: FTMagPhase**. There are several options available for the FFT through this dialog, as discussed below.

Input data is the data on which the FFT will be performed. For all interferograms in the Spectral Library, intensity is the one to choose.

Windowing determines the apodization function that will be applied to the data before FFT. Actually only the Hanning function is available in this macro.

Resolution enhancement provides higher resolution spectra through zero filling, or zero padding as called by *Igor Pro*. User can choose not to zero-fill, or zero-fill up to 32 times for the interferogram. Unfortunately, zero filling is not available for the spectra that have already been transformed; an action that can be done easily in *SpectroPlot*.

Magnitude of the transformed spectra can be expressed either in a linear scale or in dB units, as can be selected in the *magnitude* listbox.

Igor Pro can calculate phase information, and save it in a wave called, e.g. *Intensity_Phase*, where *Intensity* is the name of the data being transformed. Phase information can be in either radians or degree units.

The FFT operation with this macro turned on is simple and intuitive. With the resolution enhancement option available, it can also provide better line shape and more accurate wavelength values (Figure 5-21).

As mentioned at the beginning of this section, *Igor Pro* is a very powerful program with many features available, either as internal functions accessible at a command line, or as external procedures through the procedure window. Complete descriptions of these functions are out of the scope of this thesis. Interested users are referred to the three-volume manuals that accompanying the program for further information. Development based on *Igor Pro* is also possible either with its built-in programming language, or through external procedures that can be written in C.

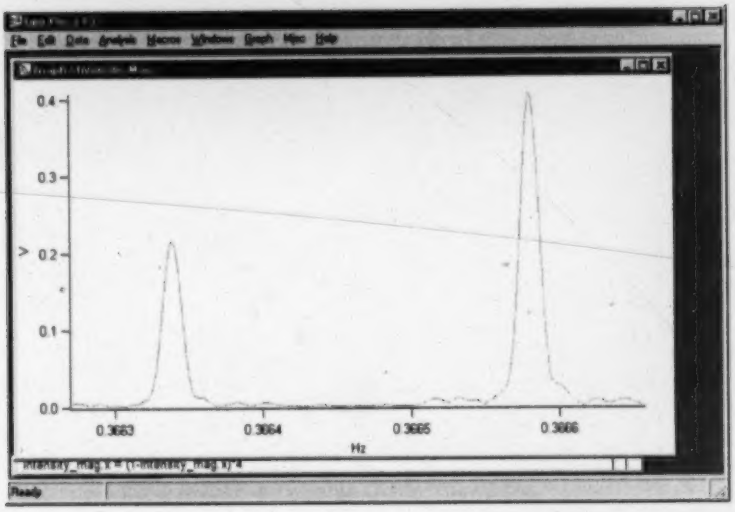

Figure 5-21. Boron 249 doublet transformed with enhanced resolution.

Reference

(1) King, G. B.; Horlick, G.: *Spectrochim. Acta, Part B* **1991** *47B*, E353-E370.

(2) Greenia, M. W. *History of Computing: An Encyclopedia of the People and Machines that Made Computer History*; Cd-Rom Only edition ed.: Lexikon Services, 2001.

(3) Hiltzik, M. *Dealers of Lightning : Xerox Parc and the Dawn of the Computer Age*; Harperbusiness, 2000.

(4) Freiberger, P.; Swaine, M. *Fire in the Valley: The Making of the Personal Computer*; 2nd edition ed.; McGraw-Hill Professional Publishing, 1999.

(5) Smith, D. K.; Alexander, R. C. *Fumbling the Future : How Xerox Invented, Then Ignored, the First Personal Computer*; iUniverse.com, 1999.

(6) Levy, S. *Insanely Great: The Life and Times of MacIntosh, the Computer That Changed Everything*; Reissue edition ed.; Penguin USA, 2000.

(7) Carlton, J.; Kawasaki, G. *Apple: The Inside Story of Intrigue, Egomania, and Business Blunders*; Harperbusiness, 1998.

(8) Kawasaki, G. *The Macintosh Way*; 1st Edition ed.; Scott, Foresman, 1990.

(9) Stross, R. E. *The Microsoft Way: The Real Story of How the Company Outsmarts Its Competition*; Perseus Press, 1997.

(10) Prosise, b. J. *Programming Windows With MFC*; 2nd ed.; Microsoft Press, 1999.

(11) Sipe, S. E. Graphing Libraries In *PC Magazine*, 1998.

(12) Spencer, K.; *Microsoft Internet Developer* **1999**.

(13) Oldenburg, K.; Sweedler, J.: *Anal. Chem.* **1998** *70*, 200A-201A.

(14) King, G. B.; Todd, B. R.; Horlick, G.: *Spectrochim. Acta, Part B* **1991** *47B*, E333-E352.

Chapter 6. Measurement of Mixtures with ICP-AES-FTS

The results for ICP-AES-FTS measurements for some spectrochemical standards, as well as for some standard reference materials from the National Institute of Standards and Technology (NIST, 100 Bureau Drive, Gaithersburg, MD 20899-0001, USA) are discussed in this chapter. Although application of the Spectral Library will be utilized wherever feasible, most experiments are designed to test the measurement ability of the FTS itself.

6.1. Qualitative Measurement of Aqueous Mixtures

6.1.1. NIST Water Standard

NIST Standard Reference Material (SRM) 1643d is a standard for water analysis. It is prepared from high purity reagents by the NIST Analytical Chemistry Division. The certified mass concentration for 26 elements and non-certified mass concentration for 4 elements are listed in Table 6-1.

Two ICP-AES-FTS spectra were acquired for the SRM 1634d, one for the UV region, and one for the visible region. The length of the interferograms is 32768 reference laser fringes with 32 signal-scan-average. Other parameters were the same as for all spectra in the Spectral Library (Chapter 2).

It can be seen from Figure 6-1 that in the UV region, Mg is the only dominant element for the whole spectrum. With intensity at over 8000, the Mg 279.553 nm line is more than a hundred times more intense than the strongest lines of all other elements, the Si 251.611 nm line. The only element other than Mg and Si that

appeared in this spectrum is barium, which has strong lines at 230.424 and 233.527 nm and a relatively high concentration of 506.5 ppb. All other elements, either have no strong emission in this region (Na, Ca, and K), or a low concentration (ppb or lower), or both, and cannot be identified in this spectrum. In many ways this measurement illustrates the so-called multiplex disadvantage of FTS in the UV region.

The visible spectrum (Figure 6-2) shows almost exactly the same trend. At a high concentration of 31.04 ppm, the strong Ca lines at 393.367 and 396.847 nm are over a hundred times more intense than any other lines in the spectrum.

6.1.2. Qualitative Measurement of Multi-element Solutions

Three spectrochemical standard solutions from VHG Labs, Inc. (One Dundee Park, Andover, MA 01810, Tel 617-470-2892) are measured with the ICP-FTS. The matrix and the constituent ions for each solution are listed in Table 6-2. Each element has a concentration of 100 ppm.

Table 6-1. Elements in the NIST SRM 1643d with concentration (ppm) **(1)**

Element	Conc.	Element	Conc.	Element	Conc.
Ca	31.04	Cd	0.00647	Se	0.01143
Mg	7.989	Cr	0.01853	Ag	0.001270
Na	22.07	Co	0.02500	Sr	0.2948
K	2.356	Cu	0.0205	Tl	0.00728
Al	0.1276	Fe	0.0912	V	0.0351
Sb	0.0541	Pb	0.01815	Zn	0.07248
As	0.05602	Li	0.01650	Bi*	0.013
Ba	0.506.5	Mn	0.03766	Ru*	0.013
Be	0.01253	Mo	0.1129	Te*	0.001
B	0.1448	Ni	0.0581	Si*	0.0027

* uncertified concentration.

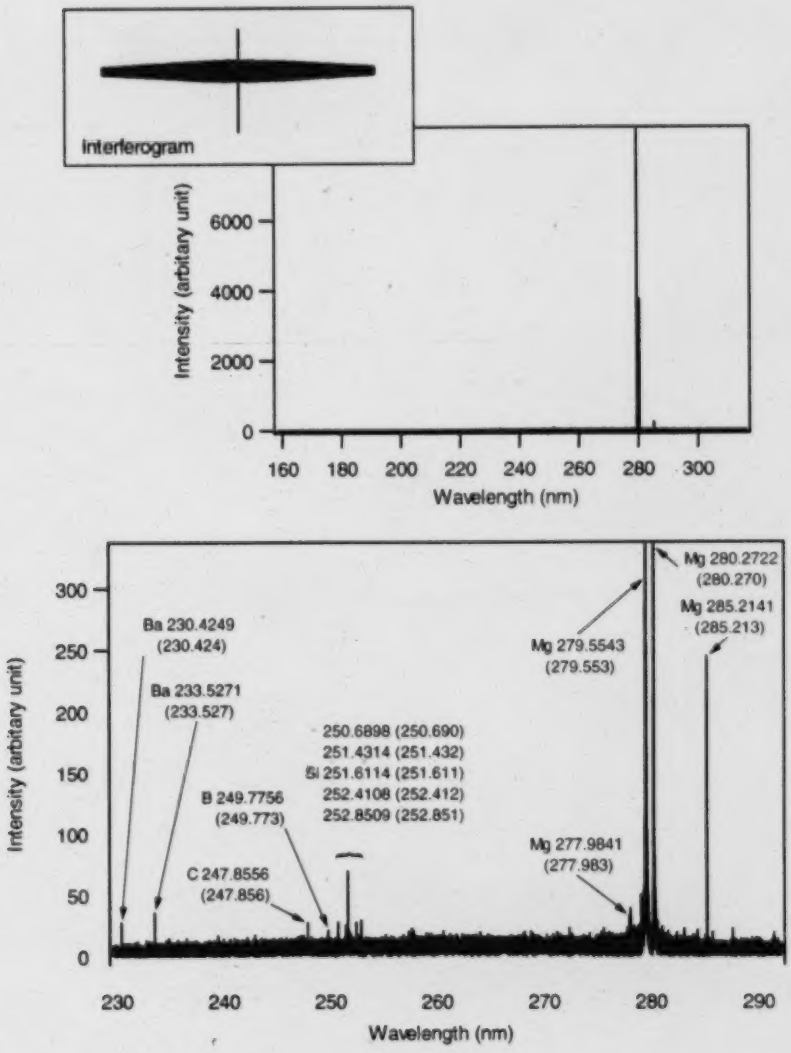

Figure 6-1. UV spectrum and line assignment for NIST SRM 1634d.

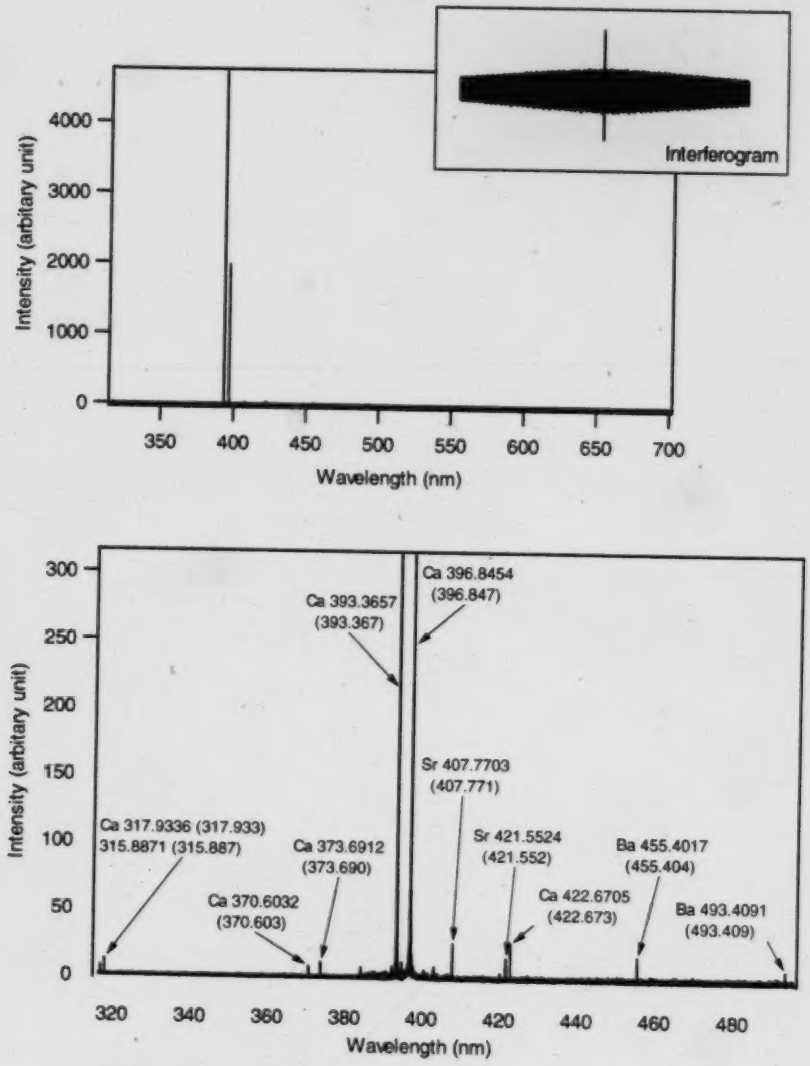

Figure 6-2. Visible spectrum and line assignment for NIST SRM 1634d.

Table 6-2. Composition of the standard solution.

Solution	Matrix	Element	Conc.(ppm)
SM-20	20% HNO_3	V, Cr, Mo, Fe, Co, Ni, Cu, Zn, Ag, Cd	100
SM-40	20% HCl	Au, Ir, Os, Pt, Pd, Re, Rh, Ru	100
SM-60	10% HNO_3	Sc, Y, La, Ce, Pr, Nd, Sm, Eu, Gd, Tb, Dy, Ho, Er, Tm, Yb, Lu	100

The "graphic identification" of Ag spectral lines in the visible spectrum of SM-20 is illustrated in Figure 6-3. This method uses spectrum subtraction with single element spectra from the spectral library to identify spectral lines of interest. The method itself is similar to that used in Chapter 4 for illustration of the applications of the Spectral Library. The spectrum of the original sample is, however, no longer a simulated spectrum that is made from the spectral library. Instead, it is from a real sample solution and acquired by the FTS.

Figure 6-3 consists of three spectra. The one on the top is the visible spectrum of SM-20. The middle is the spectrum of Ag from the spectral library. Subtraction the Ag spectrum from the SM-20 spectrum gives the third spectrum on the bottom. The two Ag 328 nm lines in the visible spectrum of SM-20 (Figure 6-3 top) disappeared after spectral subtraction of the Ag visible spectrum. This confirms the existence of silver in the solution.

Figures 6-4 to 6-6 has nine groups of spectra arranged in the same manner as that in Figure 6-3. They illustrate the stepwise spectrum subtraction for aother nine elements. For clarity, the spectra cover the wavelength range from about 200 to 300 nm range but are not labeled. The subtraction starts with the most intense lines of the

SM-20 UV spectrum, the Mn triplet at about 260 nm. From the first group of spectra it can be seen that the Mn triplet disappeared after the subtraction.

The top spectrum in the second group is essentially the same spectrum as that at the bottom of the previous group, except the intensity is adjusted to the full-scale, so many weak lines can now be seen. In this spectrum the Fe lines are the dominant ones. After the subtraction, two groups of lines at around 238 nm and 259 nm all removed, provide evidence for the existence of Fe in the original spectrum.

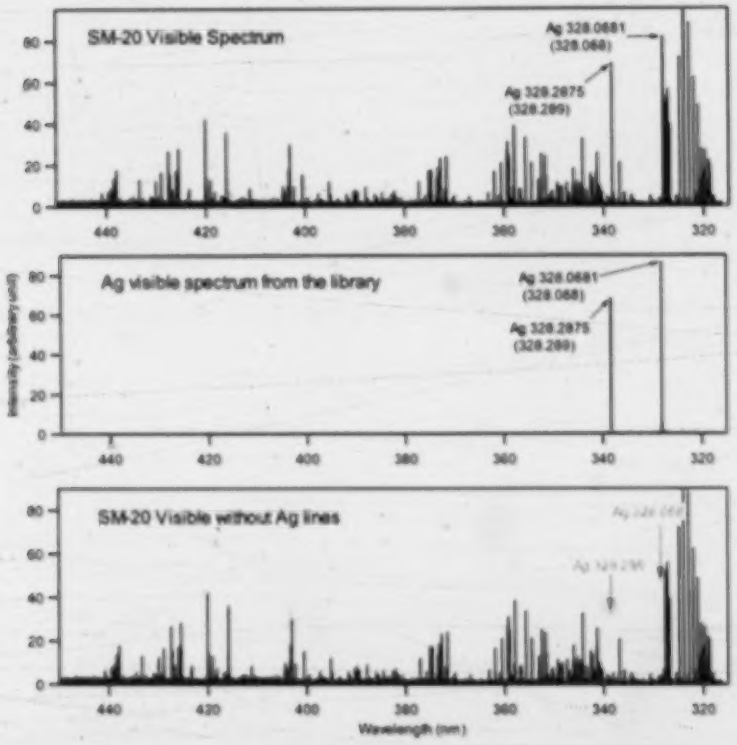

Figure 6-3. Identification of Ag in SM-20 with spectrum subtraction. See text for details.

The rest of the groups of spectra are for Cr, Cd, V, Co, Zn, Ni, and Cu, respectively and in that order.

It is found that, for easy identification, it is necessary to over-subtract the element spectra from the spectrum of the original mixture. Quite often, a small difference in the position where the waveform is sampled exists between the SM-20 spectrum and that of the individual element. This leads to an intensity difference for a particular data point, and, sometimes it is not possible to compensate for every data point that outlines a particular peak with a single intensity match. As a result, the unmatched intensity will become a positive "residual" after the spectrum subtraction at an incorrect wavelength value. Some of the "residuals" of the strong lines can actually be much more intense that the weak lines in the spectrum and generate great confusion for sub-sequential identification. As a rule of thumb, the intensity of the elemental spectra should be at least three times higher than that of the mixture for spectrum subtraction.

Spectrum over-subtraction can sometimes lead to incorrect conclusions if it is not used with caution. This is particularly true when the dominant lines of an element are relatively weak and are close to strong lines in the spectrum of the mixture, as is true for Ag lines in SM-20.

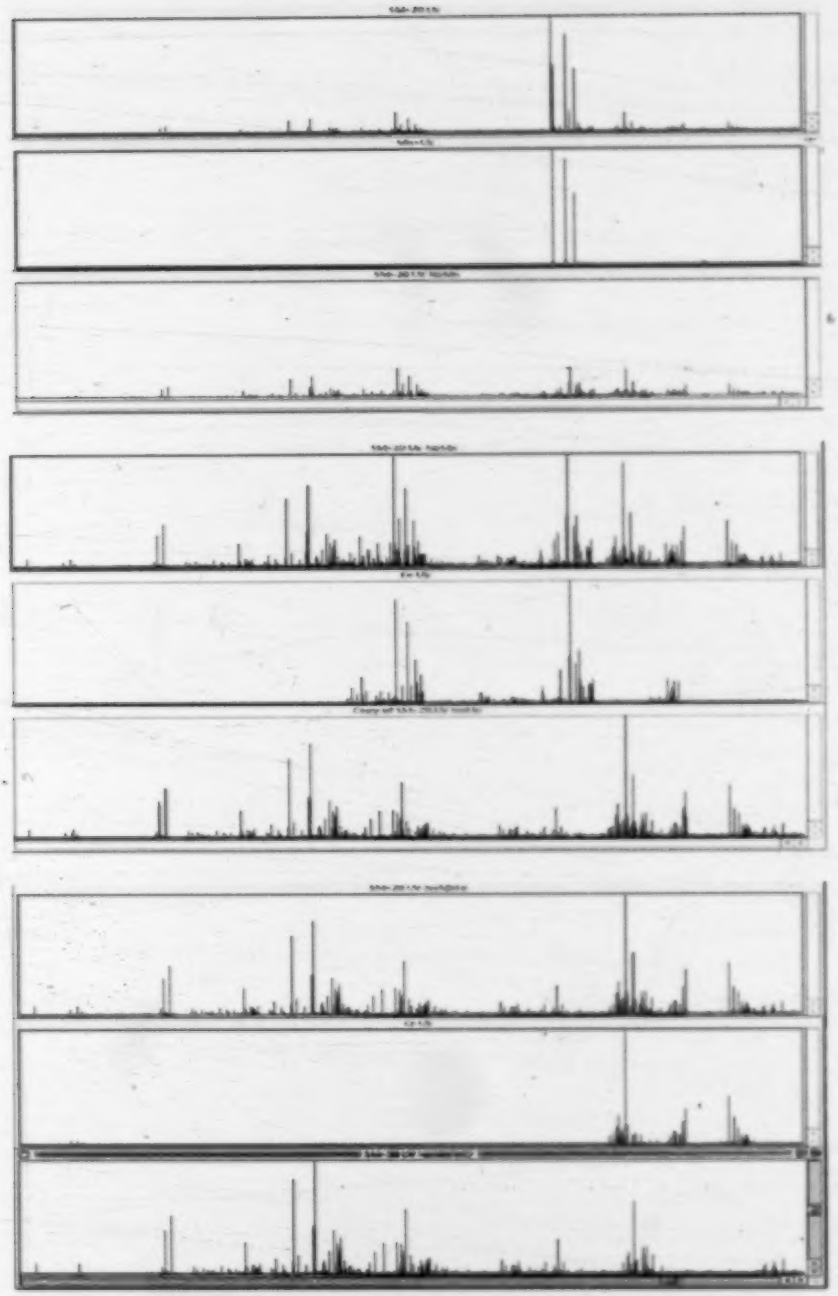

Figure 6-4. Spectral line identification for Mn, Fe, and Cr with spectrum subtraction for SM-20. See text for discussion.

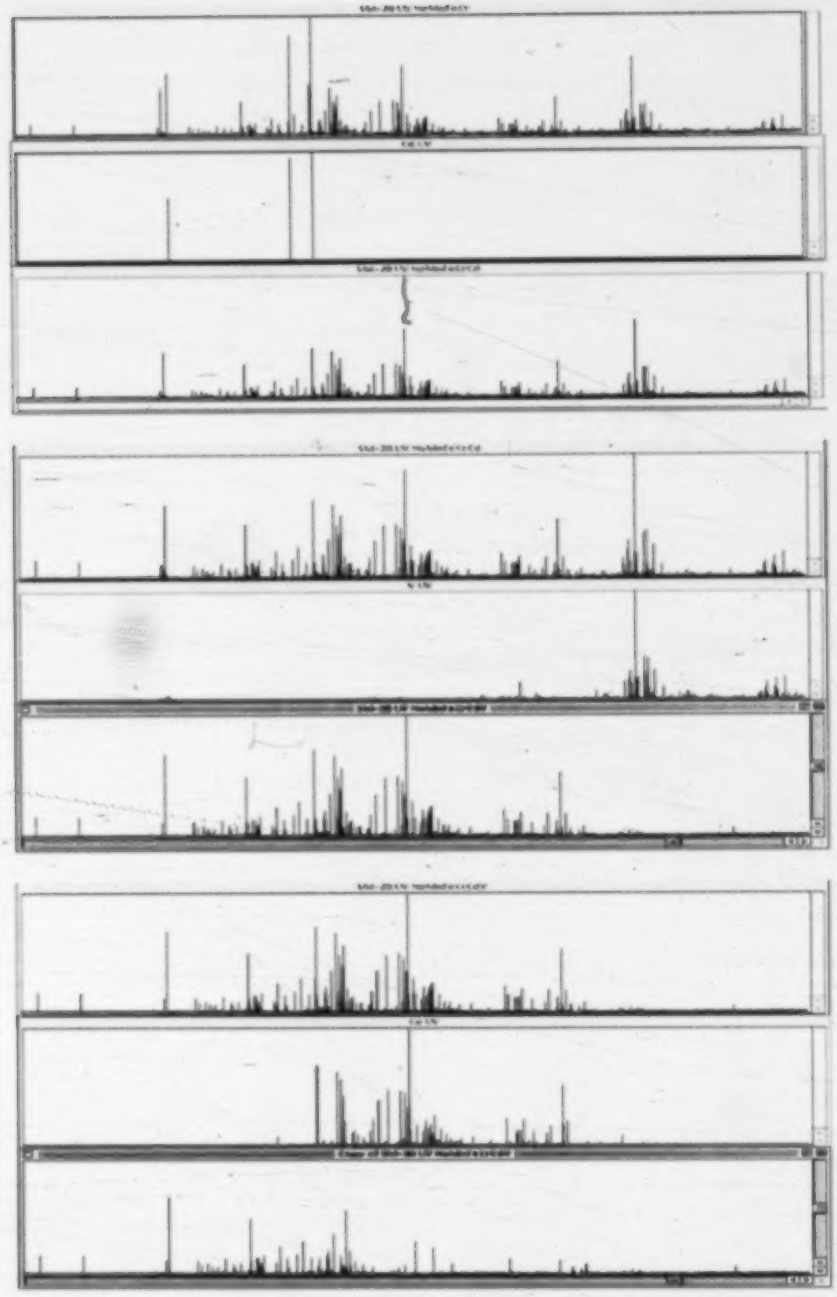

Figure 6-5. Spectral line identification for Cd, V, and Co with spectrum subtraction for SM-20. See text for discussion

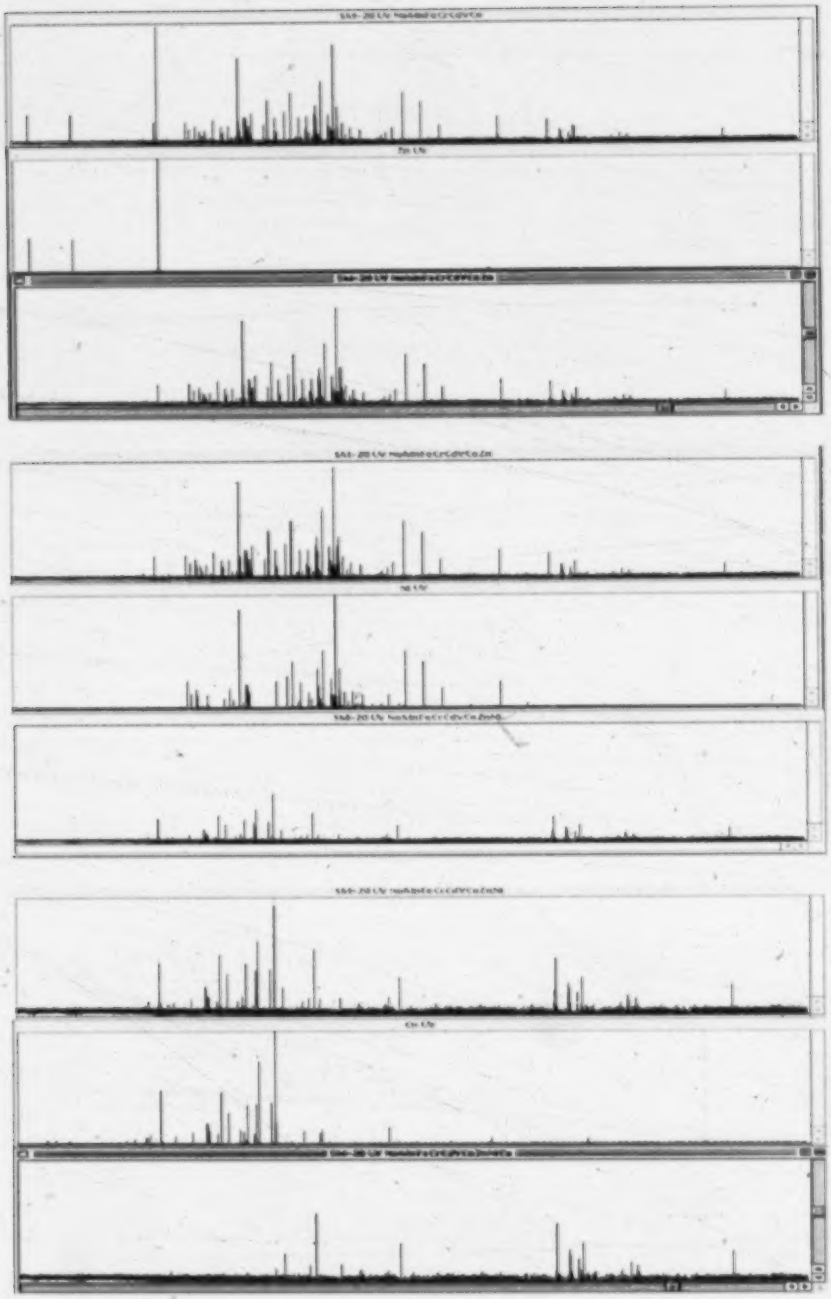

Figure 6-6. Spectral line identification for Zn, Ni, and Cu with spectrum subtraction for SM-20. See text for discussion

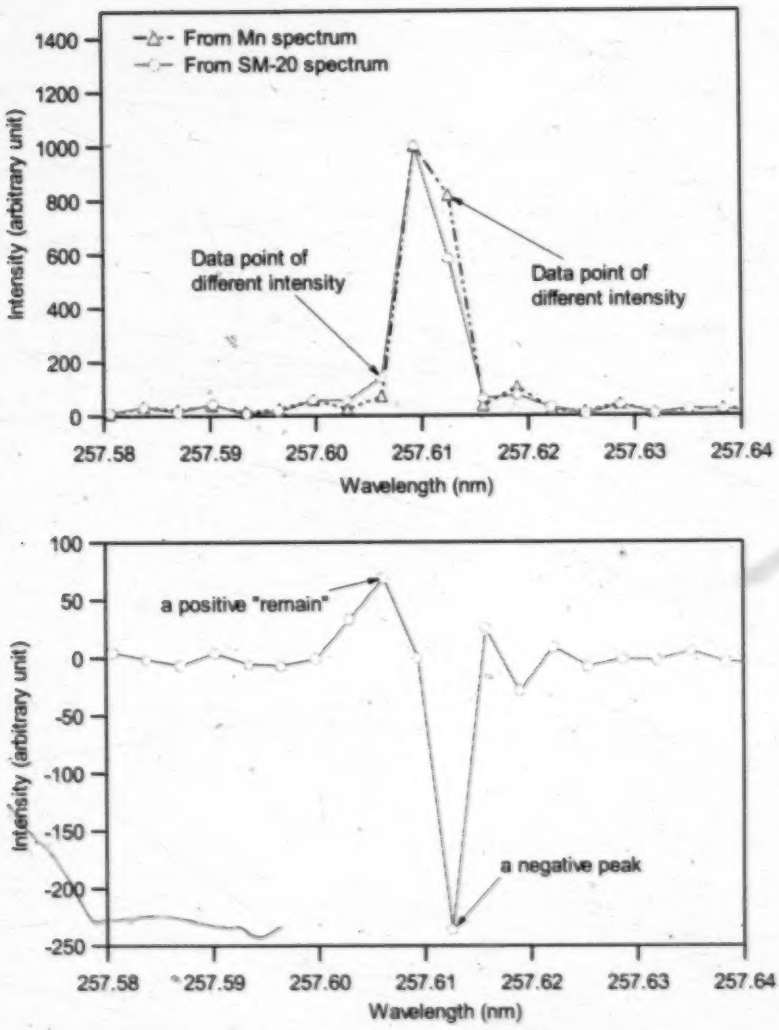

Figure 6-7. Positive "residual" caused by the intensity difference during spectrum subtraction for Mn 267.610 nm line.

Figure 6-8 shows the Ag 243.779 nm line in the spectrum of SM-20 before and after the spectrum subtraction. Ag 243.779 is the dominant line in the UV for this element but it is relatively weak compared to lines from others. Before the subtraction it can be identified in the spectrum of the mixture (top). After the spectrum subtraction (for both Ni and Mn) the intensity of the Ag line was reduced, possibly by both Ni 243.789 and Mn 243.791 nm lines. The net result is that the reduced signal at 243.779 nm is no longer useful for Ag identification.

Figure 6-9 shows similar situation for the Ag 241.318 nm line, which is even less intense than the 243.779 nm line. It is barely noticeable even in the spectrum before subtraction and quite close to a Fe line with medium intensity. This line completely disappeared and looked like a "residual" after the Fe spectrum subtraction (bottom).

Alternatively, the spectral lines can be identified line by line using *SpectroPlot* to search for lines one at a time. Although more time-consuming, this method provides detailed wavelength and intensity information about the spectral lines. The spectrum of the mixture was zero-filled eight times to provide more accurate wavelengths, and the amplitude was normalized to 100 for the most intense line. Then, for each element that is present in the solution, up to five of the most intense peaks are checked at the literature wavelength position. If found, the wavelength and intensity are recorded (Table 6-3).

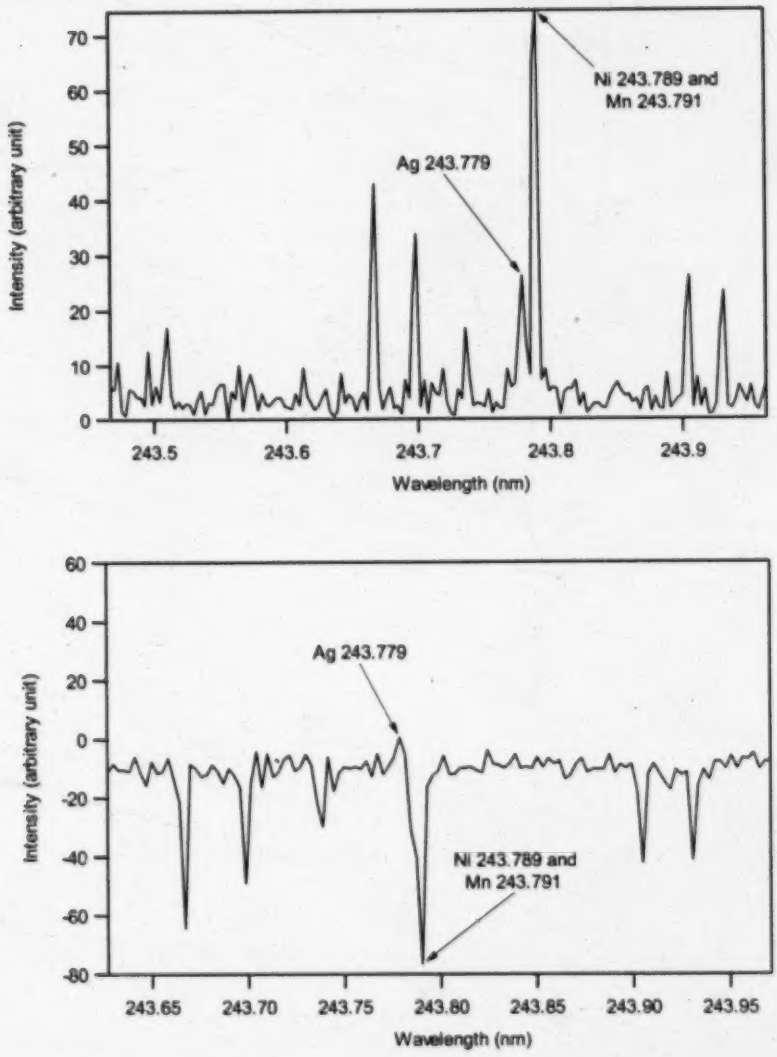

Figure 6-8. Ag 243.779 nm line in the SM-20 UV spectrum (top) is reduced to a "residual" by the spectrum subtraction of adjacent strong lines for Ni and Mn (bottom).

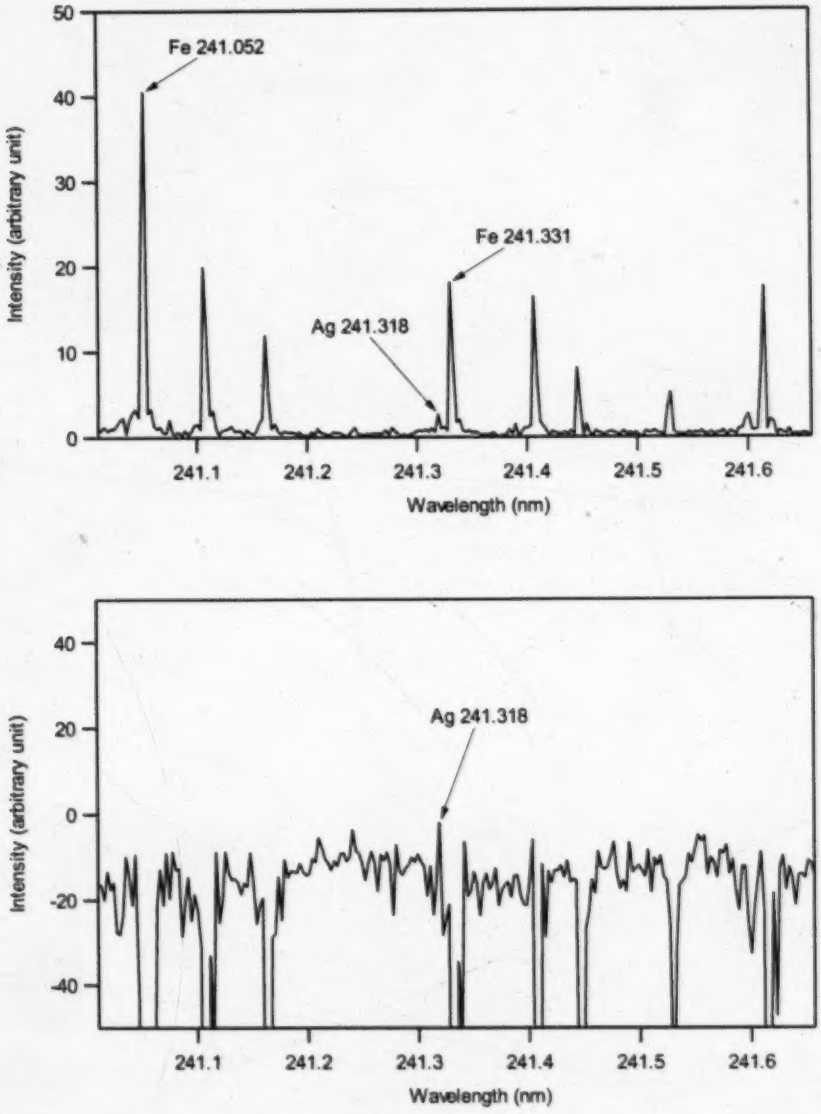

Figure 6-9. Ag 241.318 nm line was lost after spectrum over-subtraction.

From Table 6-3 it can be seen that all major spectral lines for all elements in SM-40 solution were observed in the UV spectrum. Os has the most intense lines, Au and Ru lines at about half intensity, and others are around 10 to 20%. Every element can be identified without doubt, primarily because of the high wavelength accuracy of the spectrum. In the visible spectrum (Table 6-4), spectral lines from four of the eight elements present with Pd lines showing the highest intensity. Os, Pd, Rh, and Ru have all five lines for each element identified, but for Au, Ir, Pt, and Re have no lines were unambiguously identified.

SM-50 shows similar results. Among a total of thirteen elements, eleven can be identified with at least three major lines in the UV spectrum (Table 6-5). In the visible spectrum, the top five lines of U can be found, Ga, Pb, and Sn have two lines each, while Ge, In, Th, and Tl have no line identified (Table 6-6). Tl has only one line found in the UV and no line in the visible region and thus its identification is questionable. No line was found for Se either in the UV or the visible spectra; therefore, it is not listed in any of these tables.

6.2. Powder Pump Sampling ICP-FTS Measurement

Direct sampling with solids for elemental analysis has been favorite research projects for many years (2). From the classic arc and spark (3), to the graphite furnace AA and glow discharge (4), and to the relatively recent success of laser ablation (5, 6) and direct sample insertion (DSI) for ICP-AES and ICP-MS (7), direct solid sampling has come a long way.

Table 6-3. Spectral lines in the UV spectrum of SM-40

	Lit Value			Spectral Library		SM-40 Spectrum		Difference
Ele.	Line	WL (nm)	Amp	WL (nm)	Amp	WL (nm)	Amp	(pm)
Au	I	242.795	76.5	242.7960	100.0	242.7957	60.2	0.7
Au	I	267.595	100.0	267.5952	76.9	267.5953	46.5	0.3
Au	I	274.826	32.4	274.8264	4.5	274.8250	2.9	-1.0
Au	I	208.209	44.1	208.2081	3.1	208.2078	2.0	-1.2
Au	II	211.068	17.7	211.0693	2.7	211.0688	1.6	0.8
Ir	II	224.268	31.6	224.2685	100.0	224.2690	17.9	1.0
Ir	II	236.804	4.5	236.8044	35.6	236.8045	6.0	0.5
Ir	I	254.397	100.0	254.3971	29.2	254.3972	6.0	0.2
Ir	II	212.681	57.9	212.6811	28.3	212.6815	5.4	0.5
Ir	I	263.971	44.7	263.9704	24.7	263.9709	5.7	-0.1
Os	II	225.585	44.7	225.5846	100.0	225.5849	100.0	-0.1
Os	II	228.226	31.6	228.2275	75.4	228.2281	76.4	2.1
Os	II	233.680	16.1	233.6802	44.3	233.6807	47.0	0.7
Os	II	236.735	11.1	236.7357	35.5	236.7359	34.3	0.9
Os	II	248.855	100.0	248.8542	20.4	248.8547	21.3	-0.3
Pd	II	248.892	5.0	248.8916	100.0	248.8916	9.4	-0.4
Pd	II	229.651	6.3	229.6519	80.1	229.6520	7.1	1.0
Pd	I	244.791	53.1	244.7911	51.5	244.7908	5.2	-0.2
Pd	II	244.618	5.0	244.6190	47.0	244.6190	4.4	1.0
Pd	II	248.653	1.9	248.6528	40.3	248.6547	2.6	1.7
Pt	I	265.945	100.0	265.9451	100.0	265.9454	15.5	0.4
Pt	II	224.552	3.6	224.5528	47.6	224.5528	5.6	0.8
Pt	I	270.240	71.4	270.2396	36.2	270.2399	6.0	-0.1
Pt	I	262.803	39.3	262.8027	35.1	262.8030	5.3	0.0
Pt	I, II	214.424	67.9	214.4252	35.0	214.4252	4.6	1.2
Re	II	227.525	100.0	227.5345	100.0	227.5275	12.4	2.5
Re	II	221.426	81.0	221.4345	62.0	221.4288	9.5	2.8
Re	II	260.850	14.3	260.8506	28.5	260.8501	5.2	0.1
Re	II	256.864	10.5	256.8642	11.4	256.8629	2.2	-1.1
Re	I	228.751	57.1	228.7521	11.0	228.7520	1.4	1.0
Rh	II	249.077	18.2	249.0764	100.0	249.0766	18.0	-0.4
Rh	II	233.477	27.3	233.4773	86.2	233.4778	13.2	0.8
Rh	II	252.053	22.7	252.0532	75.7	252.0530	12.7	0.0
Rh	II	246.104	15.9	246.1041	57.1	246.1040	9.1	0.0
Rh	II	251.066	9.1	251.0656	49.9	251.0658	8.3	-0.2
Ru	II	267.876	0.9	267.8747	100.0	267.8757	53.4	-0.3
Ru	II	240.272	1.0	240.2718	80.8	240.2723	39.4	0.3
Ru	II	245.657	0.5	245.6567	54.2	245.6568	28.1	-0.2
Ru	II	266.161	0.4	266.1604	35.3	266.1609	20.1	-0.1
Ru	II	245.644	0.2	245.6436	32.3	245.6441	16.4	0.1

Table 6-4. Spectral lines in the visible spectrum of SM-40

		Lit Value		Spectral Library		SM-40 Spectrum		Difference
Ele.	Line	WL (nm)	Amp	WL (nm)	Amp	WL (nm)	Amp	(pm)
Os	I	330.156	100.0	330.1566	100.0	330.1567	17.1	0.7
Os	I	442.047	55.0	442.0449	91.0	442.0464	22.4	-0.6
Os	I	426.085	55.0	426.0843	78.1	426.0846	9.8	-0.4
Os	I	375.252	45.0	375.2514	60.0	375.2524	11.5	0.4
Os	II	321.331	2.0	321.3310	59.4	321.3300	11.4	-1.0
Pd	I	363.470	84.6	363.4703	100.1	363.4685	96.0	-1.5
Pd	I	340.458	100.0	340.4592	94.3	340.4583	100.0	0.3
Pd	I	360.955	84.6	360.9547	80.2	360.9544	77.6	-0.6
Pd	I	342.124	53.8	342.1233	43.4	342.1223	43.0	-1.7
Pd	I	355.308	50.0	355.3082	38.6	355.3079	39.9	-0.1
Rh	I	369.236	80.0	369.2358	100.0	369.2356	74.4	-0.4
Rh	I	343.489	70.0	343.4881	89.8	343.4887	67.9	-0.3
Rh	I	365.799	75.0	365.7976	49.1	365.7983	38.0	-0.7
Rh	I	352.802	75.0	352.8024	43.6	352.8023	32.5	0.3
Rh	I	350.252	50.0	350.2520	34.8	350.2519	23.6	-0.1
Ru	I	372.803	100.0	372.8022	100.0	372.8019	51.8	-1.1
Ru	I	349.894	85.0	349.8939	63.7	349.8936	34.1	-0.4
Ru	I	372.693	80.0	372.6933	63.6	372.6922	32.4	-0.8
Ru	I	379.935	70.0	379.9347	58.0	379.9336	52.0	-1.4
Ru	I	379.890	10.0	379.8904	51.3	379.8883	29.0	-1.7

Considering the fact that a significant portion of practical samples are in a variety of solid forms, the reason for developing reliable and high efficiency sampling system for solids is quite understandable. In fact, for samples that occur naturally in solid forms, such as geological samples, there are many advantages for not converting the sample to liquid and for analyzing in their original form.

The first advantage of direct solid sampling is the simplified sample preparation process. This not only reduces the cost and labor of the analytical laboratory, but also eliminates possible contamination from reagents and the environment, and possible human errors during the digestion and dilution processes.

Table 6-5. Spectral lines in the UV spectrum of SM-50

	Lit Value			Spectral Library		SM-50 Spectrum		Difference
Ele.	Line	WL (nm)	Amp	WL (nm)	Amp	WL (nm)	Amp	(pm)
As	I	228.812	5.9	228.8116	100.0	228.8120	23.7	0
As	I	234.984	5.9	234.9841	81.7	234.9842	20.9	0.2
As	I	278.022	3.2	278.0210	13.9	278.0228	3.6	0.8
As	I	249.291	1.0	249.2937	7.0	249.2937	3.5	2.7
As	I	245.653	0.8	245.6532	6.8	245.6539	3.2	0.9
Bi	II	223.061	40.0	223.0628	100.0	223.0616	23.4	0.6
Bi	II	222.825	8.8	222.8228	34.2	222.8216	8.4	-3.4
Bi	II	227.658	9.0	227.6578	11.3	227.6555	3.0	-2.5
Bi	II	289.798	100.0	289.7986	4.0			
Ga	I	287.424	100.0	287.4235	100.0	287.4234	11.5	-0.6
Ga	I	294.364	100.0	294.3635	68.7	294.3634	7.5	-0.6
Ga	I	250.019	40.0	250.0177	43.9	250.0173	7.3	-1.7
Ga	I	245.008	100.0	245.0078	25.1	245.0067	5.5	-1.3
Ga	I	271.966	60.0	271.9664	22.2	271.9659	4.5	-0.1
Ge	I	265.118	100.0	265.1177	100.0	265.1175	100.0	-0.5
Ge	I	259.254	41.7	259.2540	37.7	259.2537	42.2	-0.3
Ge	I	270.963	70.8	270.9627	29.0	270.9629	33.0	-0.1
Ge	I	265.158	45.8	265.1576	25.7	265.1573	30.5	-0.7
Ge	I	275.459	54.2	275.4587	24.3	275.4593	26.5	0.3
In	II	230.599	--	230.5999	100.0	230.6014	19.0	2.4
In	II	230.609	100.0	230.6067	92.4	230.6078	16.5	-1.2
In	II	230.611	--	230.6124	72.7	230.6139	11.9	2.9
Pb	II	220.351	8.0	220.3533	100.0	220.3538	27.7	2.8
Pb	I	261.418	18.0	261.4168	59.6	261.4177	21.8	-0.3
Pb	I	280.200	24.0	280.1989	24.6	280.1998	8.9	-0.2
Pb	I	283.307	26.0	283.3048	16.9	283.3057	6.7	-1.3
Pb	I	266.317	23.0	266.3155	15.7	266.3160	6.2	-1
Sb	I, II	252.854	7.6	252.8510	100.0	252.8513	47.0	-2.7
Sb	I	231.147	6.0	231.1467	81.2	231.1466	23.8	-0.4
Sb	I	259.805	14.3	259.8053	77.6	259.8055	22.9	0.5
Sb	I	217.581	20.2	217.5823	47.5	217.5823	15.1	1.3
Sb	I	217.919	3.6	217.9195	13.3	217.9198	9.7	0.8
Sn	I	242.949	39.3	242.9484	100.0	242.9496	23.8	0.6
Sn	I	235.484	39.3	235.4840	81.8	235.4852	19.9	1.2
Sn	I	270.651	50.0	270.6495	67.5	270.6508	15.0	-0.2
Sn	I	283.999	100.0	283.9969	53.8	283.9988	11.8	-0.2
Sn	I	242.170	25.7	242.1689	53.2	242.1698	12.5	-0.2

Table 6-5. Spectral lines in the UV spectrum of SM-50 (continuing)

		Lit Value		Spectral Library		SM-50 Spectrum		Difference
Ele.	Line	WL (nm)	Amp	WL (nm)	Amp	WL (nm)	Amp	(pm)
Te	I	214.275	100.0	214.2805	100.0	214.2817	12.0	6.7
Te	I	238.576	10.7	238.5766	65.6	238.5784	12.0	2.4
Te	I	225.902	3.6	225.9013	35.4	225.9031	4.4	1.1
Te	I	238.325	7.9	238.3250	33.5	238.3269	6.4	1.9
Te	I	214.719	10.0	214.7242	12.5			
Th	II	269.242	42.0	269.2421	100.0	269.2373	5.6	-4.7
Th	II	274.716	46.0	274.7163	85.1	274.7153	4.8	-0.7
Th	II	283.730	100.0	283.7303	75.8	283.7302	3.7	0.2
Th	II	256.560	44.0	256.5599	70.2	256.5598	3.4	-0.2
Th	II	275.217	36.0	275.2167	60.9	275.2171	3.5	0.1
Tl	I	276.787	100.0	276.7905	100.0	276.7903	11.1	3.3
Tl	I	237.969	18.2	237.9607	12.6			
Tl	I	258.014	15.9	258.0197	12.3			
U		263.553	100.0	263.5526	100.0	263.5528	16.4	-0.2
U				256.5406	60.3	256.5408	9.7	0.2
U		264.547	77.8	264.5470	55.5	264.5472	9.2	0.2
U		275.416	77.8	275.4148	51.2	275.4149	9.2	-1.1
U		268.328	77.8	268.3274	45.8	268.3280	8.1	0

Table 6-6. Spectral lines in the visible spectrum of SM-50

		Lit Value		Spectral Library		SM-50 Spectrum		Difference
Ele.	Line	WL (nm)	Amp	WL (nm)	Amp	WL (nm)	Amp	(pm)
Ga	I	417.205	5.0	417.2040	100.0	417.2037	17.8	-1.3
Ga	I	403.298	5.0	403.2989	43.4	403.2976	8.2	-0.4
Ga				342.0548	3.4			
Pb	I	405.782	100.0	405.7820	100.0	405.7815	3.9	-0.5
Pb	I	368.347	100.0	368.3465	37.8	368.3461	1.7	-0.9
Pb	I	363.958	39.3	363.9577	18.4			
Sn	I	326.234	100.0	326.2343	100.0	326.2346	1.0	0.6
Sn	I	317.505	100.0	317.5038	79.6	317.5040	1.0	-1.0
Sn	I	380.102	50.9	380.1020	47.9			
U	II	385.958	100.0	385.9577	100.0	385.9565	6.1	-1.5
U	II	409.014	44.4	409.0142	82.0	409.0140	5.1	0.0
U	II	424.167	12.5	424.1674	71.5	424.1661	4.0	-0.9
U	II	393.203	4.2	393.2028	65.7	393.2016	3.9	-1.4
U	II	367.007	44.4	367.0084	53.4	367.0081	3.4	1.1

Another advantage is the enhanced analytical process. As the sample is not dissolved, its content is not diluted. This provides the potential of better method detection limits. As little or no sample preparation is required, sample loss in the digestion or transfer process is reduced or eliminated and thus a less amount of sample is required for analysis.

Currently the solid sampling devices commonly seen for ICP-AES or ICP-MS are DSI, laser ablation, and to some extent, electro-thermal vaporization (ETV). DSI, as the name suggests, insert the sample held in a graphite cup directly into the plasma with a mechanical arm. This type of device is simple, elegant, efficient, versatile, and inexpensive. Horlick's group has published many papers in this area, providing detailed information on the design and analytical performance of such a system.

Laser ablation is another "hot" area for solid sampling, and commercial systems are now available (8). The unique advantages for laser ablation are its ability to sample a wide range of diverse form of solids, and the ability to sampling a very small area, or provide non-destructive sampling (9, 10).

Although successful to some extent, laser ablation and DSI both have an inherent disadvantage: the transient analytical signal. This is the main reason why they are difficult to use with an FTS measurement, since the basic requirement for the signal source for an FTS is that it be stable, at least stable enough for the FTS to finish a complete signal average run.

Recently, a powder pump has been developed with which solid powder sample is filled in a glass or plastic capillary tube that is rotated and slowly raised by

a motor. As the tube rises, gas from a metal needle gradually blows the fine powder on the surface of the packing to form a fine aerosol stream. The carrier gas then carries the aerosol into the plasma. This device provides a continuous powder stream for the capacity of the capillary tube used. Depending on the nature of powder, the capillary can carry about 20 to 40 mg of solid and provides a stream that lasts about 3 to 4 minutes, which is reasonably long for an FTS measurement.

The first spectrum obtained with the powder pump is for Cu. The pump sampling gas flow was set to 0.40 L/min, and mixing gas 0.1 L/min at 8 psi. Plasma forward power was 1.5 kw, plasma gas flow 13 L/min, central gas flow 0.85 L/min, and the nebulizer gas off. The interferogram has 16384 data points and was sampled at four times of He-Ne laser frequency.

It can be seen from the interferogram (Figure 6-10 top) that the powder pump provides decent stability during the short FTS scan. Considering that the powder particles are never as homogenous as a solution, it is actually amazing to see that the interferogram showed fairly good symmetry. The spectrum shows the major Cu lines at an intensity ratio that is different from what one would be expected from a visible spectrum of a Cu solution. As the sample was Cu powder, more than likely the line intensities are affected by self-absorption.

In contrast to the spectra for solution mixtures in the previous sections, the resolution in the powder pump spectra is typically much lower. This results from the trade-off of spectrum quality and resolution. As discussed before, the sampling capacity of the capillary tube restricted the sampling time to about three minutes, and it is found that the quality of the spectrum would be better if the number of repetitive

scans was large enough to compensate for the instable nature of the powder pump. The typical conditions used throughout the Powder Pump-ICP-FTS experiments are listed in Table 6-7. The PMT voltage and amplifier gain varied from sample to sample.

Figures 6-11 and 6-12 show the interferograms and spectra for Cu and Ni powders, respectively. The line wavelength values are listed in Table 6-8. It can be seen that the wavelength errors increased compared to the solution spectra to 4 picometer. It is believed that this results mainly from the low resolution of the spectra.

Finally a visible spectrum was obtained for Cu coated Ni particles (Figure 6-13). Ni lines almost dominate the whole spectrum, but Cu lines can be identified. The wavelength errors are similar to those in the spectra of pure metals.

Table 6-7. Typical experiment conditions for the ICP-FTS measurement with powder pump sampling.

a. FTS Settings

Fringe Counted:	8192 (8k)	Clock Rate:	4
Interferogram Length:	32768 points	Signal Average:	16 scans

b. ICP Settings

Plasma Gas:	13 L/min	Nebulizer Gas:	off
Central Gas:	0.85 L/min	Forward Power:	1.5 kw

c. Signal Detection System

PMT type:	1P21 or P166	Amplifier Rising Time	4
PMT Voltage:	600 volt	Amplifier Gain:	10^5 V/A
Bandpass	10-21and 21-35 kHz	Amplifier Suppression:	10^{-5}

d. Powder Pump Settings

Sampling Gas:	0.40 L/min	Mixing Gas	0.1 L/min (8 psi)

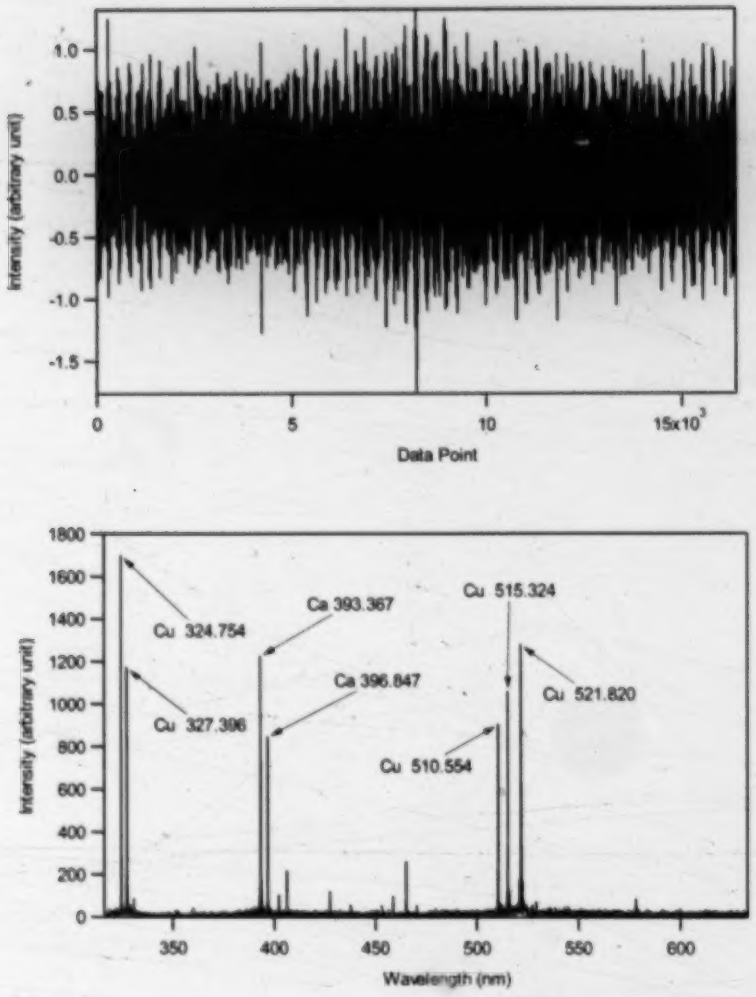

Figure 6-10. A single scan 16k interferogram and spectrum for Cu powder

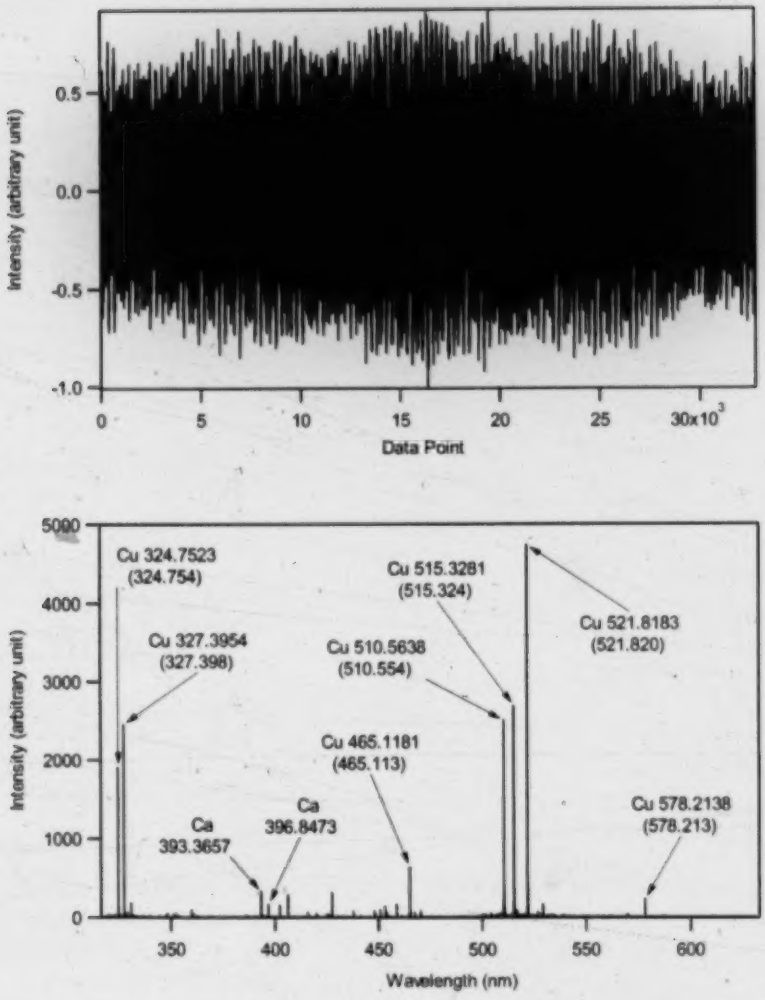

Figure 6-11. Cu visible interferogram and spectrum from powder pump-sampling ICP-FTS. Results of 16 repetitive scanning.

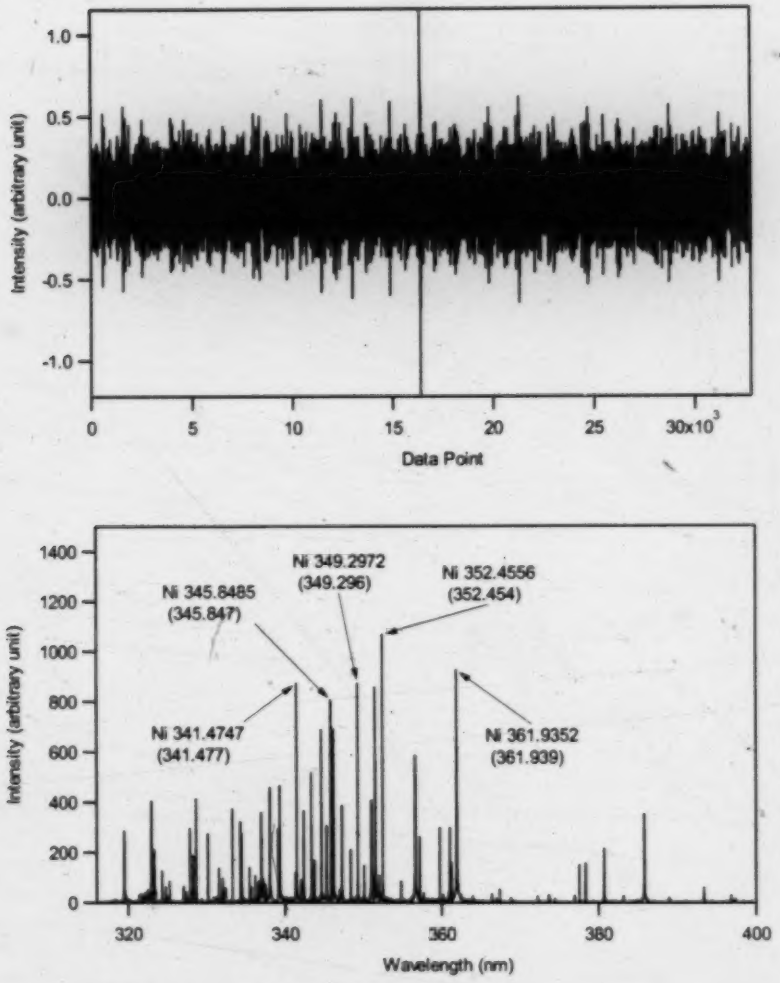

Figure 6-12. Ni visible interferogram and spectrum from powder pump-sampling ICP-FTS. Results of 16 repetitive scanning.

Table 6-8. Spectral line wavelength values for Cu and Ni powder visible spectra.

		Lit. value		Experimental value		WL error
Element	Line	WL (nm)	Amp (%)	WL (nm)	Amp (%)	(pm)
Cu	I	327.396	50.0	327.3922	100.0	-3.8
Cu	I	324.754	100.0	324.7517	94.3	-2.3
Cu	I	521.820	2.0	521.8174	77.1	-2.6
Cu	I	515.324	0.4	515.3272	46.5	3.2
Cu	I	510.554	0.8	510.5629	46.3	8.9
Ni	I	352.454	100.0	352.4556	100.0	1.6
Ni	I	361.939	80.0	361.9352	90.5	-3.8
Ni	I	341.477	100.0	341.4747	81.6	-2.3
Ni	I	349.296	66.7	349.2972	81.6	1.2
Ni	I	351.505	80.0	351.4997	80.1	-5.3
Ni	I	345.847	61.3	345.8485	75.3	1.5
Ni	I	346.165	61.3	346.1718	64.4	6.8
Ni	I	344.626	58.7	344.6300	64.3	4.0
Ni	I	356.637	53.3	356.6350	60.9	-2.0
Ni	I	338.057	40.0	338.0595	49.8	2.5
Ni	I	343.356	32.0	343.3518	48.5	-4.2
Ni	I	339.299	40.0	339.3013	45.1	2.3
Ni	I	351.034	32.0	351.0266	38.8	-7.4
Ni	I	347.255	20.0	347.2587	36.9	3.7
Ni	I	336.957	34.7	336.9526	35.5	-4.4
Ni	I	342.371	20.0	342.3767	34.3	5.7
Ni	I	385.830	17.3	385.8240	33.6	-6.0
Ni	I	345.289	16.0	345.2899	29.9	0.9
Ni	I	359.771	16.0	359.7688	28.0	-2.2
Ni	I	361.046	16.0	361.0466	27.9	0.6
Ni	I	339.105	16.0	339.1071	27.4	2.1
Ni	I	357.187	12.0	357.1909	24.4	3.9
Ni	I	380.714	9.3	380.7203	20.1	6.3
Ni	I	348.377	6.7	348.3817	19.9	4.7
Ni	I	343.728	12.0	343.7303	17.8	2.3
Ni	I	361.274	6.4	361.2699	15.0	-4.1
Ni	I	378.353	9.3	378.3585	14.7	5.5
Ni	I	377.557	8.0	377.5594	14.0	2.4
Ni	I, II	351.393	26.7	351.3984	13.2	5.4

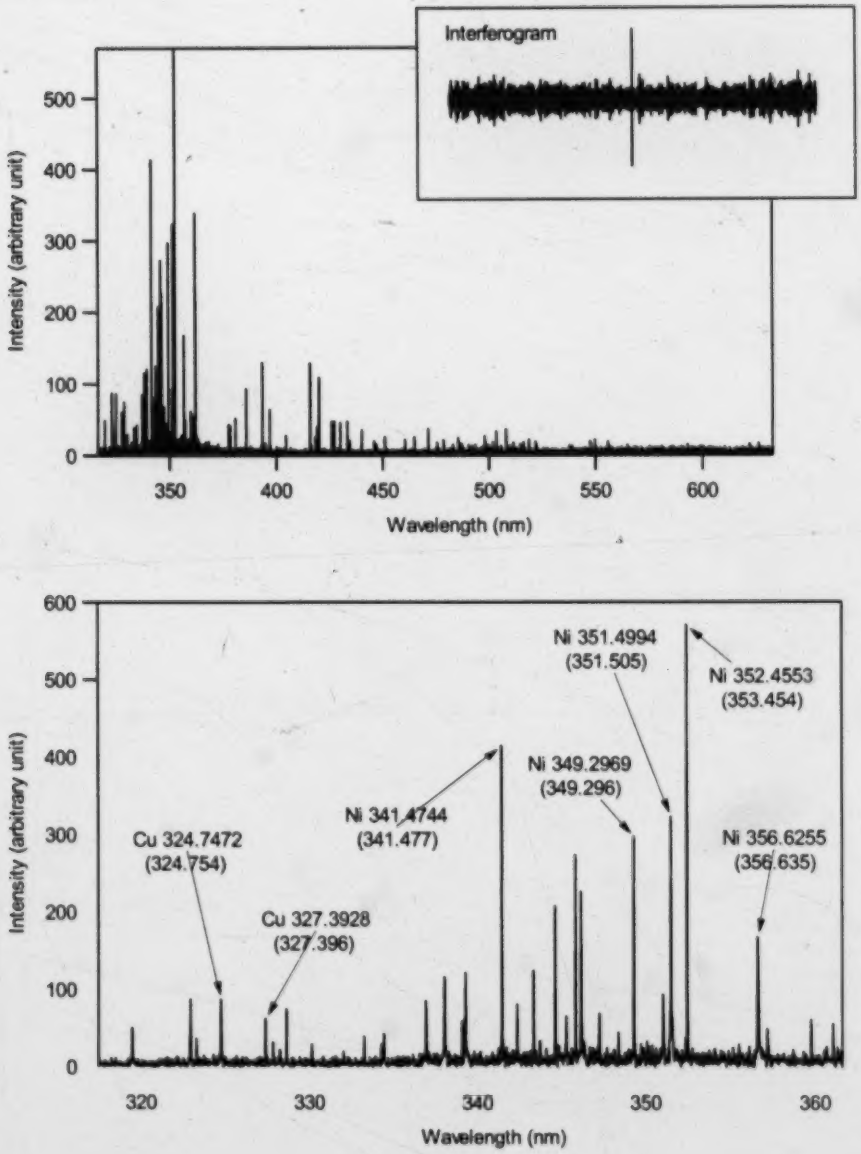

Figure 6-13. Visible interferogram and spectrum for Ni coated Cu particles from powder pump-sampling ICP-FTS. Results of 16 repetitive scanning (top). Wavelength expanded view of the spectrum (bottom).

6.3. Qualitative Measurement for Solid Standard Reference Materials.

Based on the measurements for the aqueous mixtures and Cu-Ni powders, qualitative measurements for some NIST SRMs and one Japanese standard have been conducted directly on the solid form. The elements and their concentration values are listed in Table 6-9 for Buffalo River Sediment (SRM 2704), Coal (SRM 1632), Pine Needles (SRM 1575) and Pepper Bush (Japan).

Figure 6-14 shows the interferogram and spectrum for the UV region for Buffalo River Sediment (BRS), and Table 6-10 lists the elements and lines found in the spectrum. It can be seen that only six out of 43 elements are detected. Among the 19 major elements that have concentrations higher than 100 ppm, Si (29%), Al (6.1%), Fe (4.1%), Mg (1.2%), Mn (555 ppm), and Zn (438 ppm) can be identified with at lease two lines for each element, while K (2%), Ti (4570 ppm), S (3970 ppm), and Na (5470 ppm) lines can not be found although they also have very high concentration due to the fact that they only exhibit very weak lines in this region. Ca (2.6%) again has high concentration but shows no lines, it is well known Ca emits strongly at 393 and 396 nm so if visible spectrum were measured, then Ca should be able to be identified.

Again this is a good (or bad) example of the poor sensitivity of the ICP-FTS resulting from the narrow dynamic range. As Si emits quite strongly in the UV region, at a dominant concentration of 29%, the amplification of the instrument had to be reduced to accommodate the high intensity of the Si lines to avoid distortion of the spectrum. This unfortunately also reduced the sensitivity of the measurement and reduced the number of elements identified.

Figure 6-15 and Table 6-11 show the spectrum and spectral lines for SRM 1632 coal. It can be seen that the spectrum is also dominated by lines from a few major elements. Mg lines, instead of those of Si, have the highest intensity in the spectrum and is not too high as Si lines in the spectrum of BRS. Thus some lines from rather relatively low content elements like Cu and Ni can be identified. Taking into account of the at least 100 times dilution if the sample were digested and dissolved to make an aqueous sample. Direct measurement of Cu and Ni at 18 and 15 ppm in a solid sample, respectively, is actually quite impressive with the ICP-FTS.

Two SRM biological samples were also measured with the powder pump sampling ICP-FTS. Compared with the two inorganic SRMs, the content of Si and Fe in SRM 1575 Pine Needle and Pepper Bush are considerably lower (Figures 6-16 and 6-17) In fact, Mg, Mn, and C lines are the major ones in these two spectra. Al, Cu, and Ni can be found in Pine Needles but not in the Pepper Bush sample, while the Pepper Bush has much higher concentration on Ba (165 ppm) and Ca (1.38%) and their lines are identified. Zn is present as weak lines in both of those spectra.

Table 6-9. Constituent elements of the solid SRMs (conc. in ppm).

Element	Coal (1632)	BRS (2704)	Pine Needle (1575)	Pepper Bush
Ag	0.1			
Al		61100	545	
As	5.9	23.4	0.21	2.3
Ba		414		165
Be	1.5			
C		33480		
Ca		26000	4100	13800
Cd	0.19	3.45	0.5	6.7
Ce		72	0.4	
Co	6	14.0	0.1	23
Cr	20.2	135	2.6	1.3
Cs		6		1.2
Cu	18	98.6	3.0	12
Dy		6		
Eu		1.3	0.006	
Fe	8700	41100	200	205
Ga		15		
Hf		8		
Hg	0.12		0.15	0.056
K		20000	3700	15100
La		29	0.2	
Li		47.5		
Lu		0.6		
Mg		12000		2030
Mn	40	555	675	4080
Na		5470		106
Ni	15	44.1	3.5	8.7
P		998	1200	1100
Pb	30	161	10.8	
Rb		100	11.7	75
S		3970		
Sb		3.79	0.2	
Sc		12	0.03	
Se	2.9	1.12		
Si	32000	290800		
Sm		6.7		
Sn		9.5		
Sr		130	4.8	36
Te	0.1			
Th	3.3	9.2	0.037	
Ti	800	4570		
Tl	0.59	1.06	0.05	0.13
U	1.4	3.13	0.020	
V	35	95		
Y		2.8		
Zn	37	438		340
Zr		300		

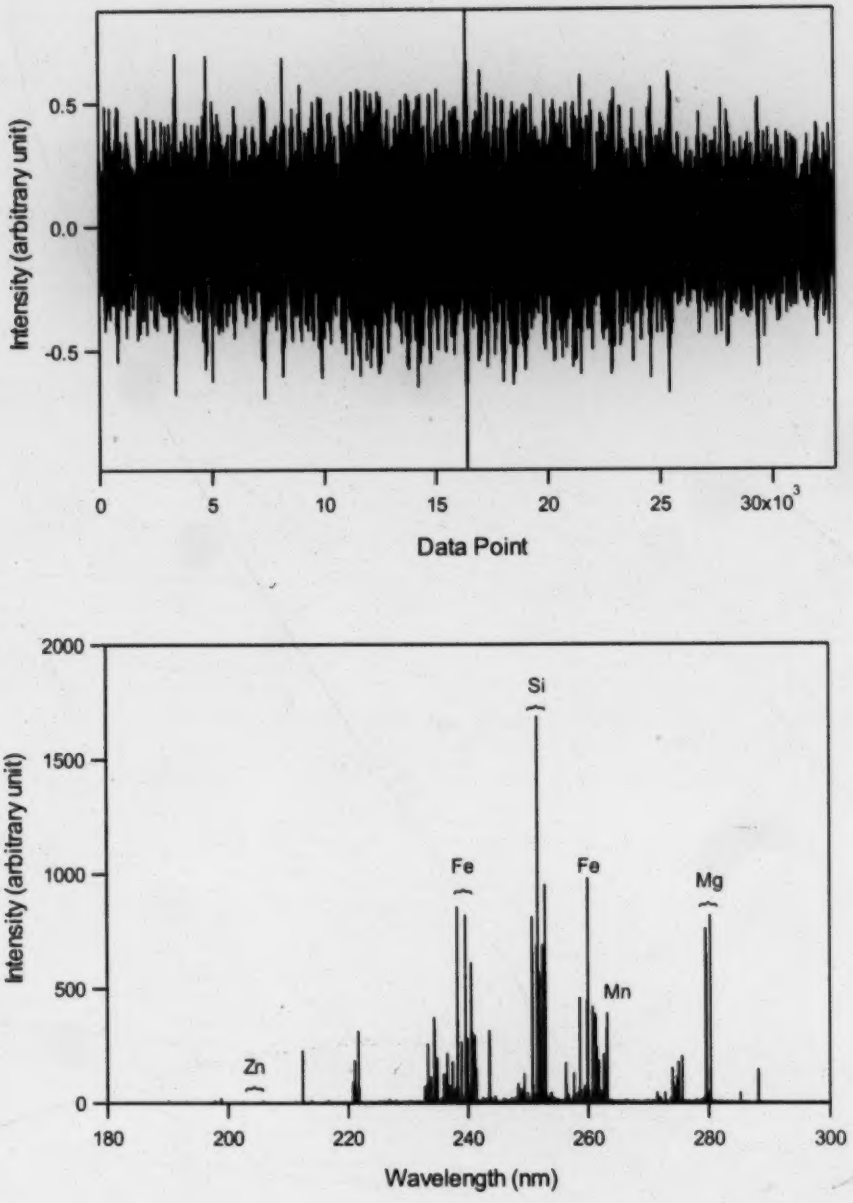

Figure 6-14. Elements in the NIST SRM 2704 Buffalo River Sediment

Table 6-10. Spectral lines found in NIST SRM 2704 Buffalo River Sediment

		Lit Values		Experimental		SRM Spectrum	WL error
Ele.		WL (nm)	Amp	WL (nm)	Amp	WL (nm)	(pm)
Al	I	237.312	100.0	237.3127	100.0	237.3204	8.4
Al	I	257.510	53.3	257.5094	73.2	257.5136	3.6
Al	I	236.705	50.0	236.7059	55.7	236.7136	8.6
Al	I	256.798	26.7	256.7983	42.4		
Al	I	266.039	22.2	266.0390	27.3		
Fe	II	259.940	100.0	259.9398	100.0	259.9411	1.1
Fe	II	238.207	75.0	238.2039	83.5	238.2037	-3.3
Fe	II	239.560	50.0	239.5627	61.9	239.5686	8.6
Fe	II	261.187	40.0	261.1876	41.6	261.1918	4.8
Fe	II	240.488	50.0	240.4885	35.8	240.4910	3.0
Mg	II	279.553	16.7	279.5530	100.0	279.5562	3.2
Mg	II	280.270	10.0	280.2704	51.7	280.2741	4.1
Mg	I	285.213	100.0	285.2127	5.5	285.2141	1.1
Mn	II	257.610	100.0	257.6106	100.0	257.6160	6.0
Mn	II	259.373	66.7	259.3723	80.7	259.3770	4.0
Mn	II	260.569	45.8	260.5684	54.2		
Mn	I	279.482	66.7	279.4821	2.3		
Mn	I	294.921	20.0	294.9206	1.8		
Si	I	251.611	100.0	251.6118	100.0	251.6145	3.5
Si	I	252.851	55.6	252.8512	34.2	252.8540	3.0
Si	I	250.690	47.2	250.6901	33.8	250.6898	-0.2
Si	I	252.412	66.7	252.4111	27.8	252.4108	-1.2
Si	I	251.432	44.4	251.4322	27.5	251.4314	-0.6
Si	I	251.921	33.3	251.9205	20.6	251.9201	-0.9
Zn	I	213.856	100.0	213.8580	100.0	213.8635	7.5
Zn	II	202.551	30.0	202.5491	28.4	202.5499	-1.1
Zn	II	206.191	100.0	206.2006	27.0	206.2065	15.5

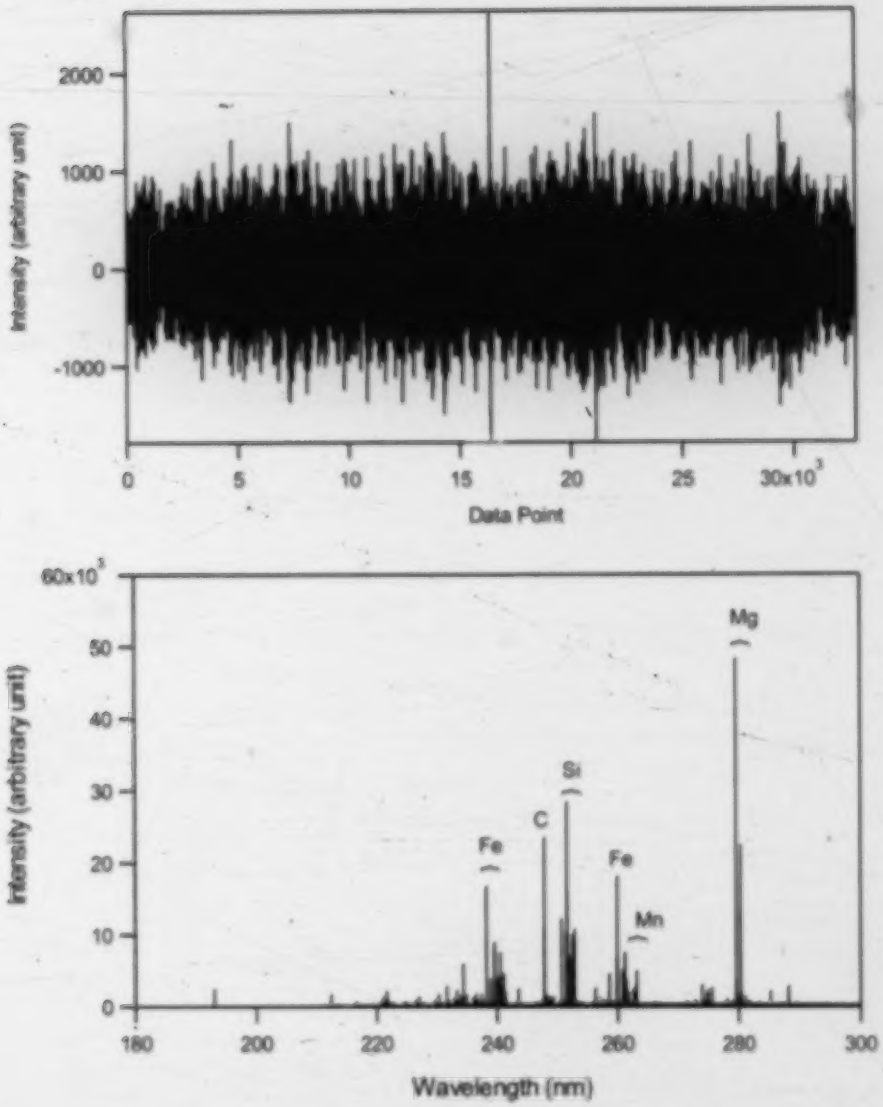

Figure 6-15. Elements in the NIST SRM 1632 Coal.

Table 6-11. Spectral lines found in NIST SRM 1632 Coal

	Lit Values		Experimental		SRM Spectrum	WL error
Ele.		WL (nm)	WL (nm)	Amp	WL (nm)	(pm)
Cu	II	224.700	224.7000	100.0	224.7006	-0.6
Cu	I, II	223.008	223.0109	58.3	223.0079	0.1
Cu	I	222.778	222.7785	41.2	222.7779	0.1
Cu	II	221.810	221.8111	39.5	221.8057	4.3
Cu	II	219.226	219.2271	34.7	219.2263	-0.3
Fe	II	259.940	259.9384	100.0	259.9411	-1.1
Fe	II	238.207	238.2022	48.3	238.2037	3.3
Fe	II	261.187	261.1857	39.9	261.1852	1.8
Fe	II	239.562	239.5615	38.8	239.5617	0.3
Fe	II	258.588	258.5868	30.0	258.5894	-1.4
Mn	II	257.610	257.6119	100.0	257.6144	-4.4
Mn	II	259.373	259.3743	77.3	--	
Mn	II	260.569	260.5703	58.7	260.5731	-4.1
Ni	II	231.603	231.6061	100.0	231.6058	-2.8
Ni	II	221.647	221.6499	63.3	221.6445	2.5
Ni	II	230.298	230.2995	54.9	230.2992	-1.2
Ni	I	232.003	232.0051	53.2	232.0023	0.7
Ni	I	239.452	239.4523	49.7	--	
Al	I	237.312	237.3150	100.0	237.3123	-0.3
Al	I	257.510	257.5095	89.7	257.5104	-0.4
Al	I	236.705	236.7082	53.7	236.7055	-0.5
Al	I	256.798	256.7984	52.3		
Al	I	266.039	266.0390	39.1		
Mg	II	279.553	279.5531	100.0	279.5505	2.5
Mg	II	280.270	280.2705	51.8	280.2741	-4.1
Si	I	251.611	251.6138	100.0	251.6114	-0.4
Si	I	252.851	252.8532	36.8	252.8509	0.1
Si	I	250.69	250.6922	35.1	250.6898	0.2
Si	I	252.412	252.4131	30.4	252.4108	1.2
Si	I	251.432	251.4338	30.3	251.4314	0.6
Si	I	251.921	251.9225	22.3	251.9201	0.9
Si	I	288.158	288.1600	17.7	288.1588	-0.8

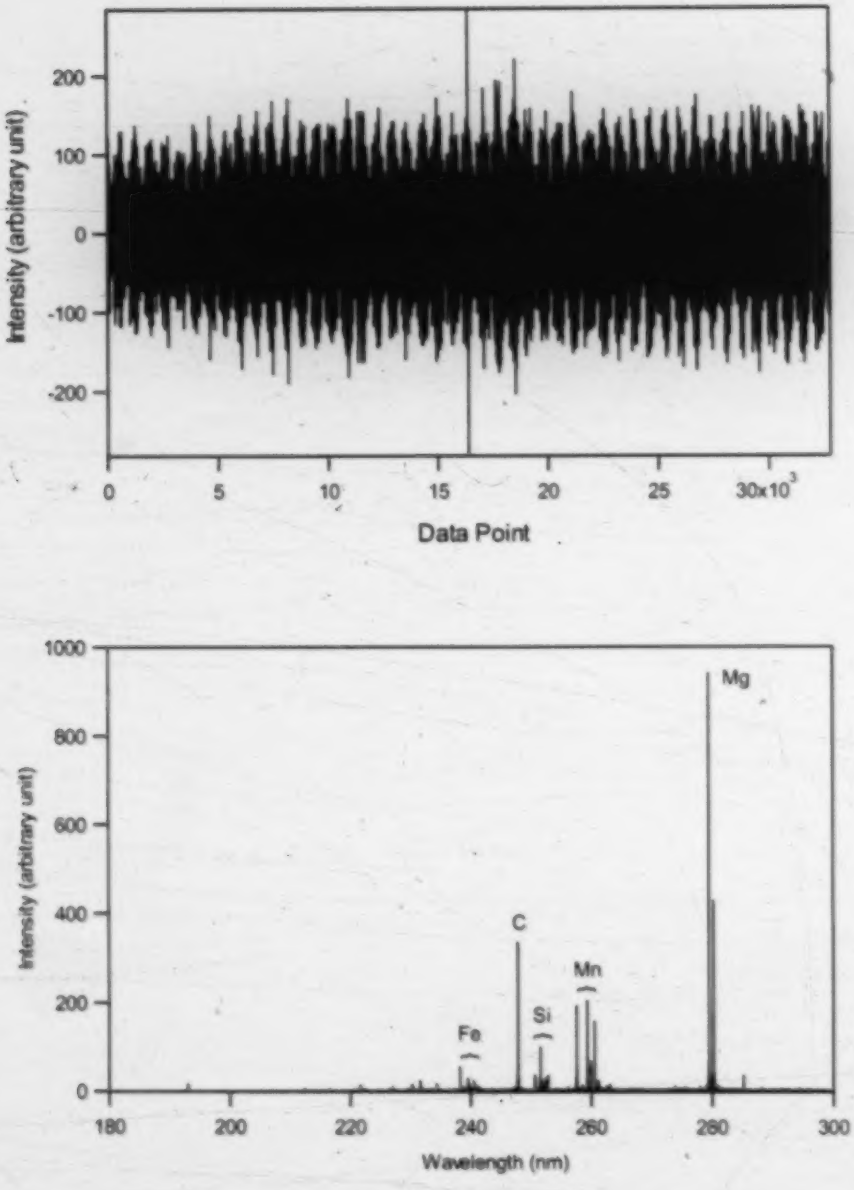

Figure 6-16. Elements in the NIST SRM 1575 Pine Needle.

Table 6-12. Spectral lines found in NIST SRM 1575 Pine Needle

		Lit Values		Experimental		SRM Spectrum	WL error
Ele.		WL (nm)	Amp	WL (nm)	Amp	WL (nm)	(pm)
Al	I	237.312	100.0	237.3127	100.0	237.3096	-2.4
Al	I	257.510	53.3	257.5094	73.2		
Al	I	236.705	50.0	236.7059	55.7	236.7028	-2.2
Al	I	256.798	26.7	256.7983	42.4		
Al	I	266.039	22.2	266.0390	27.3		
Cu	II	224.700	19.0	224.6992	100.0	224.6994	-0.6
Cu	I, II	223.008	47.6	223.0083	68.8	223.0079	-0.1
Cu	II	219.226	18.1	219.2261	49.8	219.2263	0.3
Cu	II	213.598	100.0	213.5972	44.0	213.5991	1.1
Cu	II	221.810	11.9	221.8099	40.4	221.8057	-4.3
Fe	II	259.940	100.0	259.9398	100.0	259.9411	1.1
Fe	II	238.207	75.0	238.2039	83.5	238.2037	-3.3
Fe	II	239.560	50.0	239.5627	61.9	239.5576	-2.4
Fe	II	261.187	40.0	261.1876	41.6	261.1852	-1.8
Fe	II	240.488	50.0	240.4885	35.8	240.4910	3.0
Mg	II	279.553	16.7	279.5530	100.0	279.5524	-0.6
Mg	II	280.270	10.0	280.2704	51.7	280.2722	2.2
Mg	I	285.213	100.0	285.2127	5.5	285.2101	-2.9
Mn	II	257.610	100.0	257.6106	100.0	257.6160	6.0
Mn	II	259.373	66.7	259.3723	80.7	259.3689	-4.1
Mn	II	260.569	45.8	260.5684	54.2	260.5682	-0.8
Ni	II	231.603	16.8	231.6041	100.0	231.6058	2.8
Ni	II	221.647	13.2	221.6479	80.5	221.6445	-2.5
Ni	II	230.298	7.9	230.2994	55.2	230.2992	1.2
Ni	II	239.452	12.1	239.4516	46.4	239.4469	-5.1
Ni	II	227.021	5.3	227.0214	41.5	227.0216	0.6
Si	I	251.611	100.0	251.6118	100.0	251.6129	1.9
Si	I	252.851	55.6	252.8512	34.2	252.8524	1.4
Si	I	250.690	47.2	250.6901	33.8	250.6898	-0.2
Si	I	252.412	66.7	252.4111	27.8	252.4108	-1.2
Si	I	251.432	44.4	251.4322	27.5	251.4314	-0.6
Si	I	251.921	33.3	251.9205	20.6	251.9201	-0.9

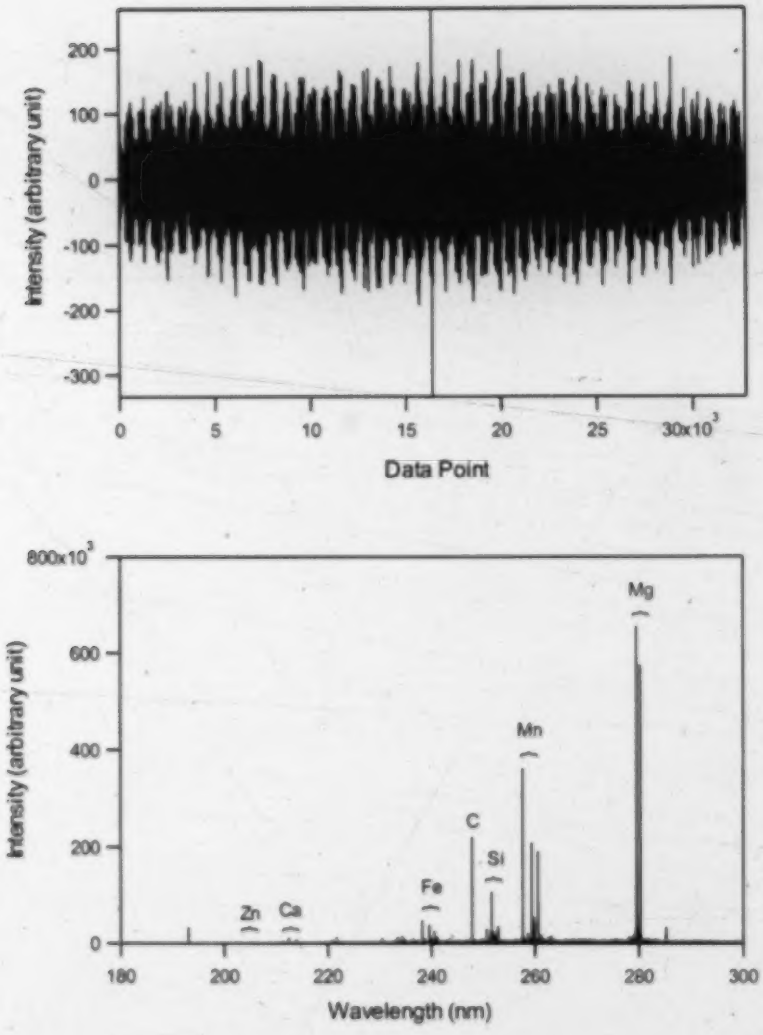

Figure 6-17. Elements in the Pepper Bush (Japan).

Table 6-13. Spectral lines found in Pepper Bush

		Lit Values		Experimental		SRM Spectrum	WL error
Ele.		WL (nm)	Amp	WL (nm)	Amp	WL (nm)	(pm)
Ba	II	233.527	100.0	233.5261	100.0	233.5321	5.1
Ba	II	230.424	70.0	230.4239	62.0	230.4328	8.8
Ba	II	234.758	9.5	234.7584	6.0		
Ca	II	211.276	100.0	211.2761	100.0	211.2836	7.6
Ca	II	220.861	50.0	220.8612	85.7	220.8608	-0.2
Ca	II	210.324	40.0	210.3236	50.5	210.3235	-0.5
Ca	II	219.779	50.0	219.7788	40.0		
Ca	I	239.856	40.0	239.8563	39.9		
Fe	II	259.940	100.0	259.9398	100.0	259.9411	1.1
Fe	II	238.207	75.0	238.2039	83.5	238.2037	-3.3
Fe	II	239.560	50.0	239.5627	61.9	239.5686	8.6
Fe	II	261.187	40.0	261.1876	41.6	261.1852	-1.8
Fe	II	240.488	50.0	240.4885	35.8	240.4910	3.0
Mg	II	279.553	16.7	279.5530	100.0	279.5562	3.2
Mg	II	280.270	10.0	280.2704	51.7	280.2760	6.0
Mg	I	285.213	100.0	285.2127	5.5	285.2101	-2.9
Mn	II	257.610	100.0	257.6106	100.0	257.6160	6.0
Mn	II	259.373	66.7	259.3723	80.7	259.3770	4.0
Mn	II	260.569	45.8	260.5684	54.2	260.5682	-0.8
Si	I	251.611	100.0	251.6118	100.0	251.6145	3.5
Si	I	252.851	55.6	252.8512	34.2	252.8540	3.0
Si	I	250.690	47.2	250.6901	33.8	250.6898	-0.2
Si	I	252.412	66.7	252.4111	27.8	252.4108	-1.2
Si	I	251.432	44.4	251.4322	27.5	251.4314	-0.6
Si	I	251.921	33.3	251.9205	20.6	251.9201	-0.9
Zn	I	213.856	100.0	213.8580	100.0	213.8635	7.5
Zn	II	202.551	30.0	202.5491	28.4	202.5499	-1.1
Zn	II	206.191	100.0	206.2006	27.0	206.2045	13.5

6.4. Calibration of ICP-FTS with Solid Samples.

To further characterize the powder pump sampling ICP-FTS system, two sets of solid powder calibration samples from SPEX industries, Inc, (3880 Park Ave, Edison, NJ 08820) were used for the calibration.

The two calibration sets have similar components composed of 49 elements. The matrix for TS-6 is SiO_2, and for G-7 is graphite. Each set has four different concentrations from 33 to 1000 ppm. Determined by the size of the capillary and the density of the standards, the amount of solid packed into the capillary was about 30-40 mg and powder steams last for approximately 200 seconds under experiment conditions (Table 6-14).

Considering the heavy matrix introduced with the solid standards (Si for the TS-6 and carbon for the G-7) and the simultaneous measurement nature of the FTS, it is not surprising to see that only a few very strong emission lines can be accurately measured. The intensities of these spectral lines for each run were plotted against standard concentration to obtain calibration curves (Figures 6-18 and 6-19).

From these calibration lines it can be seen that powder pump shows fairly high precision from run to run, and relatively good linearity in the calibration range for almost all detected lines. The correlation coefficients ranged from 0.95 to 0.99.

Table 6-14. Sample uptake for the Powder Pump-ICP-FTS calibration.

Conc.	Mass (mg)		Runs		Run Time (sec)		Mass (mg/run)	
(ppm)	Vis	UV	Vis	UV	Vis	UV	Vis	UV
33	38.2	30.7	3	3	174	174	10.16	9.57
100	41.2	43.1	4	4	232	232	9.64	10.08
330	31.9	41.7	3	4	174	232	9.69	9.75
1000	29.4	43.0	3	4	174	232	9.17	10.06

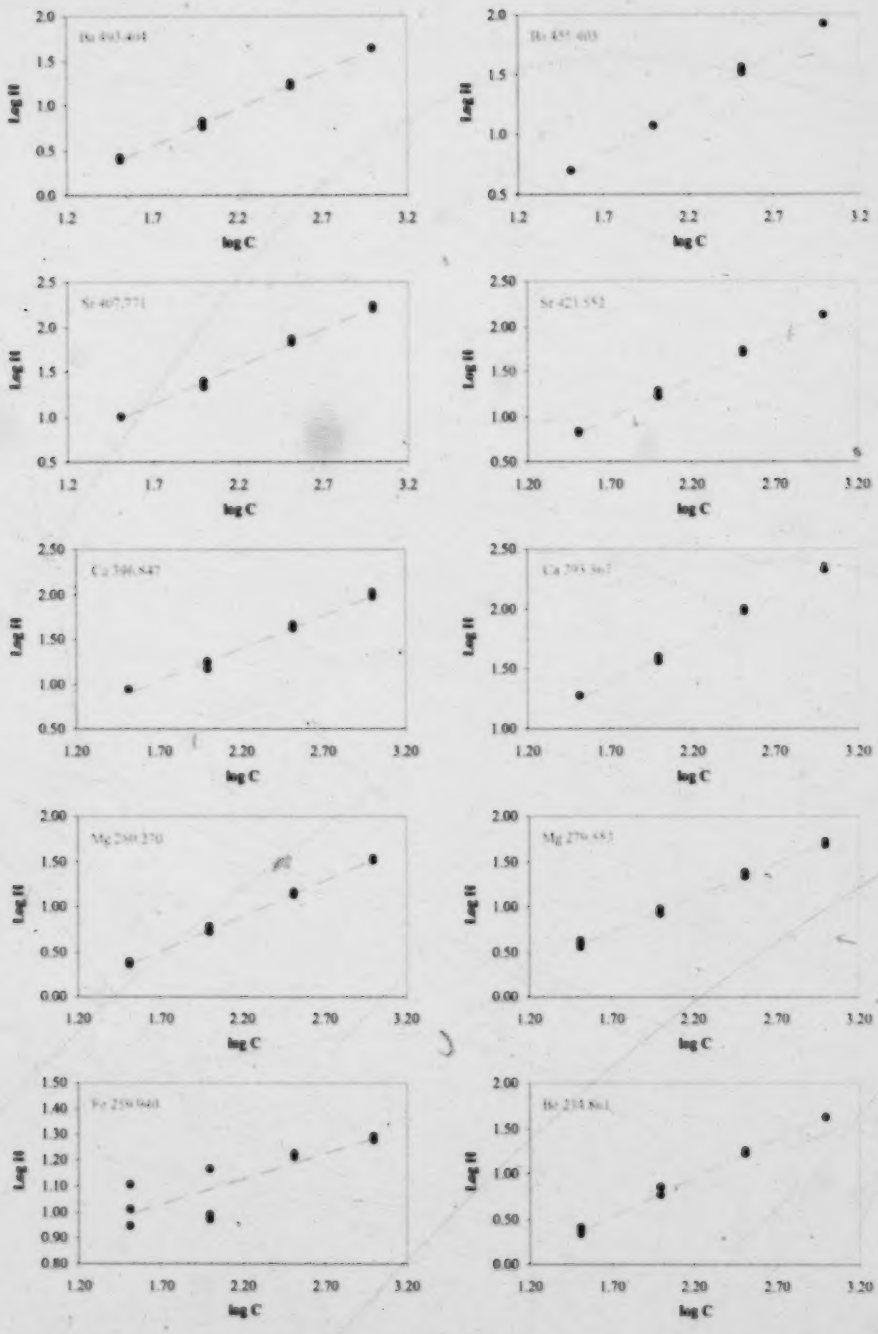

Figure 6-18. Calibration lines for ICP-FTS for solid mixture TS-6 (matrix SiO_2) sampled with powder pump.

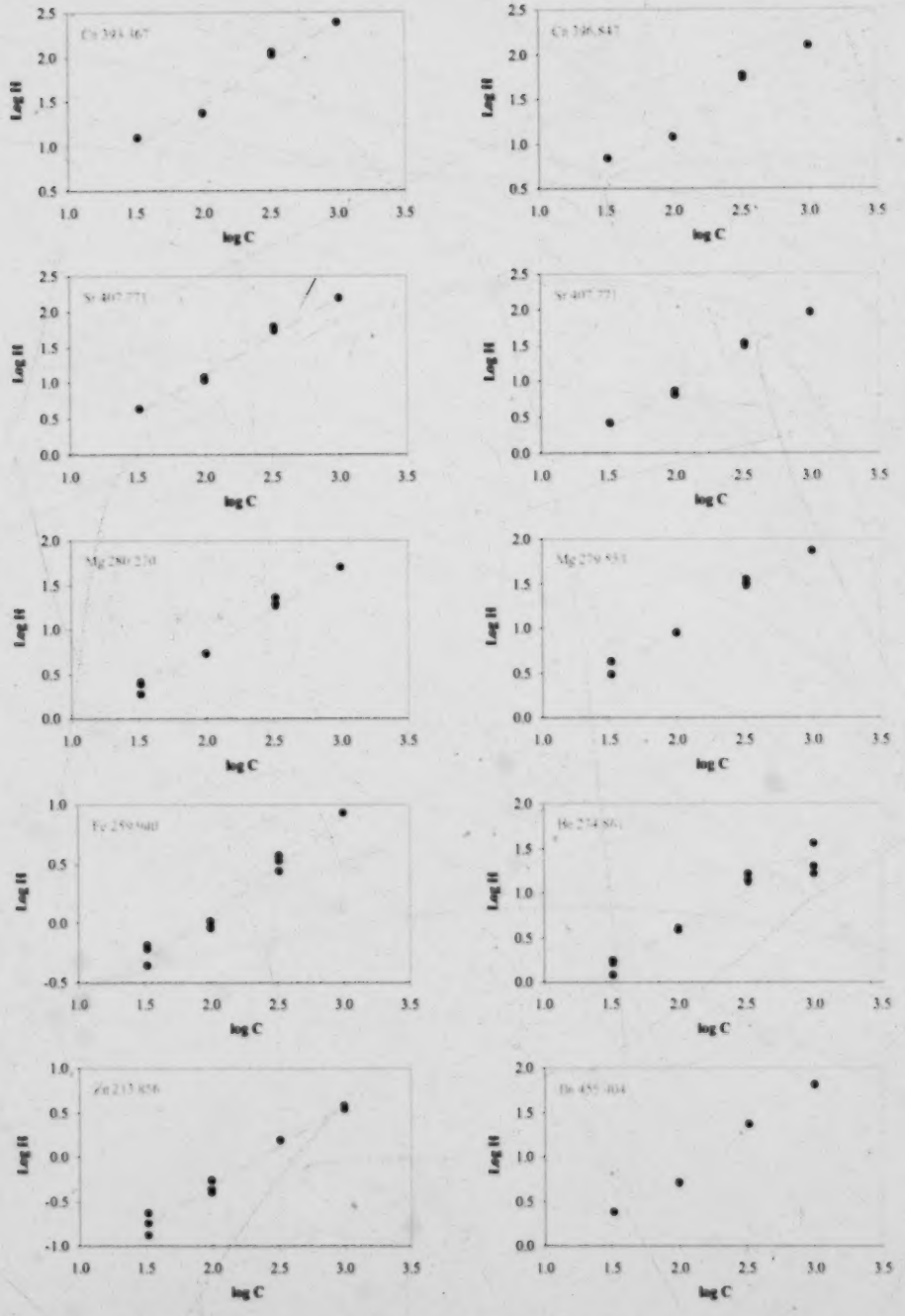

Figure 6-19. Calibration lines for ICP-FTS for solid mixture G-7 (matrix Graphite) sampled with powder pump.

Reference

(1) NIST Cetificate of Analysis for NIST SRM 1643.

(2) McLEOD, C. W.; Routh, M. W.; Tikkanen, M. W.: Introduction of Solids into Plasmas In Inductively Coupled Plasmas in Analytical Atomic Spectrometry; Montaser, A., Golightly, D. W., Eds.; VCH Publishers, Inc.: New York, NY, 1992.

(3) Bangia, T. R.; Dhawale, B. A.; Adya, V. C.; Sastry, M. D.: Fresenius' Z. Anal. Chem. 1988 332, 802-4.

(4) Salin, E. D.; Horlick, G.: Anal. Chem. 1979 51, 2284.

(5) Russo, R. E.: Applied Spectroscopy 1995 49, 14A.

(6) Miller, J. C. Laser Ablation: Principles and Applications In Springer Series in Materials Science; Springer Science, 1994; Vol. Vol 28.

(7) Shao, Y.; Horlick, G.: Applied Spectroscopy 1986 40, 386.

(8) Howe, T.; Shkolnik, J.; Thomas, R.: Spectroscopy 2001.

(9) Moenke-Blankenburg, L. Laser Microanalysis; Wiley InterScience: New York NY, 1989.

(10) Piepmeier, E. H.: Laser ablation for Atomic Spectrometry In Analytical Applications of Lasers; Piepmeier, E. H., Ed.; Wiley InterScience: New York NY, 1985.

Chapter 7. Summary and Future Directions.

7.1. Summary of Current Research Work.

The objective of this research work was to develop a spectral database for ICP-AES. An ICP-AES Spectral Library has been built with spectra acquired with high purity standards using a UV-Visible Fourier transform spectrometer for 71 elements that can be determined with ICP-AES.

The Spectral Library has separate interferograms and spectra for the UV and visible regions for every element. Thus every element has at least four data files: two interferograms and two spectra, for UV and visible, respectively. The wavelength coverage is from 180 to 315 nm for the UV region and from 316 to 530 nm for the visible region. In its basic configuration the Spectral Library takes about 280Mb disk space and can be distributed on CD-ROM for use on personal computers.

Each interferogram in the Spectral Library has 131072 data points acquired over a ±1 cm interferometer mirror scan. The theoretical resolution of the spectra is 0.97 cm^{-1}. This provides moderate resolution in an absolute sense, but is comparable to or exceeds the resolution of most commercial ICP spectrometers. The Cd and As 228 nm lines, which are often used as a measure for spectrometers, can be separated with near baseline resolution.

The FTS Spectral Library provides superior wavelength accuracy for all the spectral lines. All spectra, UV and visible, were carefully calibrated with Zaidel's wavelength values. The imperfect alignment of the reference laser, and the day-to-day variation of the alignment of the FTS optical system were corrected using the

concept of a "Reference Laser Apparent Wavelength" (λ_{LAW}). For the UV region, the λ_{LAW} is 632.8432 ± 0.0023 nm; and for the visible region, 632.8445 ± 0.0027 nm.

With few exceptions, the absolute values of the spectral line wavelength errors were less than two picometers with an average of 1.05 pm. The wavelength errors were even less when compared with a recent FTS study for some elements. Some of the large wavelength errors could be attributed to the hyperfine structure of the spectral lines, while others could not be readily explained but perhaps are reflective of minor errors in primary collections such as Zaidel's.

Generally the wavelength errors were not element dependent. That is, the wavelength errors were distributed rather randomly among the elements, except for those elements with spectral line hyperfine structure, e.g., Ho visible spectrum. For the visible region, no wavelength dependency was observed for the wavelength errors, meaning the wavelength errors were distributed almost uniformly across the wavelength region from 316 nm to 630 nm. For the UV region, however, the wavelength errors on the low wavelength end (180-200 nm) were slightly larger than for the rest of the region.

In general, spurious lines were few but when present they were attributable to sources such as modulated line frequencies, impurities, background species, counter ions, and aliases. Modulated line frequencies and harmonics appear either at the far end of the spectra (158-160 nm in the UV or infinity (0 cm^{-1}) in the visible), or in the vicinity of very strong lines. Impurity lines are simply lines from elements other than the desired element. Si UV lines appear in Hf, Sb, Sn, and W spectra; and B UV lines in the Zn spectrum. For visible spectra, Ca lines were present in Ge, Rh, and W

spectra and the Na yellow doublet in the Zn spectrum. Ar lines are, of course, present in all visible region spectra. A few spectra (UV and visible) have aliased lines in the 290-316 or 316-330 nm regions.

The Spectral Library provides the spectroscopy community with a set of spectral data, with genuine ICP-AES spectral line relative intensities and superior wavelength accuracy. The Spectral Library is computer-accessible; thus spectrum presentation, wavelength table generation, and spectrum manipulation are all possible and easy to perform. The Spectral Library is an interactive reference source. Ar visible line removal with spectrum subtraction, scanning spectrum simulation and spectral line identification with both spectrum addition and subtraction, and control of spectrum resolution with the corresponding interferograms were all demonstrated as examples of interactive spectral data processing. The simulation of the optical windows of the Perkin-Elmer Optima spectrometers, and the interference study simulation for rare-earth element lines were also presented and discussed. These examples demonstrated the potential of the Spectral Library in real-world applications, although sometimes the simulations of complex situations were less than ideal due to the limited signal-to-background ratio of spectra measured with the FTS in the UV-Vis regions.

To provide access to the Spectral Library for Microsoft Windows-based computers, two commercial Windows-based software packages were evaluated and the instructions for viewing and basic manipulation of the interferograms and spectra were presented. Either OriginLab's *Origin* or WaveMetrics *Igor Pro* is capable of implementing the basic tasks associated with the application of the Spectral Library.

Origin's user interface is more intuitive and easier to learn, but *Igor Pro* is more powerful and faster. Thus it will be up to the availability and personal preference of the user to decide which one to use. As neither of the two programs met completely the requirements of the Spectral Library, a brief attempt was made, but not completed, to develop a program similar to the *SpectroPlot* to run under Microsoft Windows.

In addition to the work on the Spectral Library, some analyses were also performed with the ICP-FTS system. Aqueous elemental ion mixtures and a NIST water standard were analyzed. It was found that for the NIST water sample only a few major elements with strong emission lines could be identified, because the major elements Mg and Ca dominated the UV and visible spectra, respectively, and obviated the detection of trace elements by dominating the signal-to-background ratio. For aqueous elemental mixtures with uniform concentrations, all constituent elements could be identified with multiple spectral lines.

A novel solid sample introduction device, a powder pump, was coupled with the ICP-AES and qualitative measurement of some NIST standards was performed directly with solid samples. It was rather amazing that the FTS could work with such a relatively unstable sample introduction system even without multiple scan averaging. Unfortunately, these spectra generally suffered similar problems to those seen with the NIST water standard, namely strong spectral lines of major elements dominated the spectra and buried trace elements in the background noise. The quantitative calibration of the spectrometer with solid sample standards was linear

for over two orders of magnitude for nine spectral lines of five different elements in a silica matrix, and for thirteen lines of seven elements in a graphite matrix.

7.2. Future Directions for the Spectral Library.

7.2.1. Improvements to the spectra.

As for all research work the Spectral Library is by no means perfect. Improvement of the spectra in the library can be done in many ways. The important areas are absolute wavelength determination and improvement of the signal-to-background noise ratio.

As discussed before, the absolute wavelength accuracy of FTS is almost always compromised in practice by the imperfect alignment of the reference laser. The current method of calibration relies on calibration standards, i.e., previously published wavelength values. This introduces uncertainties and, sometimes, errors into the current data set, as no set of previous values is perfect in its own right, and no complete previous set exists for the ICP.

To measure the wavelength absolutely, a laser with a stable wavelength could be used in conjunction with the ICP as a light source. If the laser light could be introduced into the FTS in the same optical channel as the ICP image, it would be a more ideal reference. A simple calibration of the laser wavelength would give the correction factor for the optical system under exact condition, and then all other lines could be calibrated with certainty.

It has been seen from the discussion in this thesis that the Spectral Library leaves some room for improvement with regard to the signal-to-background noise

ratio of the spectra, particularly for the visible spectra. Increasing the concentration of the standard solution is a simple and sometimes effective way to improve the situation. At present the background noise level of some visible spectra is determined solely by the dominant Ar lines, which leads to relatively low signal-to-background noise ratio for the elemental lines. With high concentration standards or an improved nebulizing system, or both, one would expect a significant change in the relative intensity of the elemental lines compared to Ar lines. Thus the baseline noise would be determined by the dominant elemental lines and maximal advantage of the limited dynamic range of the FTS could be utilized. This method would be much simpler than modifying the FTS to improve its dynamic range and stability.

Of course improvement of any research work could come from other approaches such as one proposed by the research groups at Los Alamos National Lab and NIST. They are trying to collect spectra for all elements over a nine-order range of concentration with a high-resolution echelle spectrometer in order to get experimental intensity values for all spectral lines. Then they will measure the wavelength values of the spectral lines with a high-resolution FTS designed by Thorne, and finally combine the results to get an ICP spectral database. This work would be great if it can be done as proposed and in time, but it is certainly beyond the resources and ability of a single person or even a single research group within a reasonable time frame.

7.2.2. Improve the accessibility to the data.

One of the design goals of the Spectral Library was to provide an easy access to the spectral data with personal computers. This goal has been achieved with the current Spectral Library. An area still in need of improvement is human access.

A spectral library that provides computer access is great, but a spectral library that requires a computer has its shortcomings. To put it in a simple way, carrying even a laptop computer today is still not as easy as carrying a book. The computer access of the spectra is great if one needs detailed information about a spectral line, a spectrum, or many spectra; but a wavelength table excels when one needs a quick lookup for the wavelength value of a particular line. Currently the Spectral Library lists about two thousand lines, with at least two-thirds of the total lines accessible only with a computer. This might be fine for persons in an academic environment. However, those working in industry would certainly appreciate an exhaustive listing of all lines available in the Spectral Library.

Another improvement in the accessibility would be the user interface, both in software and hardware. With the rapid development of computing and networking technologies, viewing and manipulating full-sized spectra and interferograms at an acceptable speed over the Internet will soon become a reality. However, up until now there is no software available or announced development. Imagine how convenient and successful electronic journals are today, then the future of the web-shared spectral library could soon follow. On the other hand, the technologies now on personal computers would be modified for handheld devices and palm-sized PCs. A dedicated device for the Spectral Library, working in ways like an electronic

dictionary and graphics calculator could combine the completeness of the computer accessible spectra with the ease of use of the wavelength table, providing unmatched power and utility for spectroscopists.

7.2.3. Not the end.

For the Spectral Library, it is true that this research work is just a beginning. The potential applications based on the spectral data could be described as the "sky is the limit". Now that the state-of-the-art instruments are offering full wavelength coverage, automated spectral line identification based on pattern recognition should be significantly improved in accuracy. This is not only valuable in qualitative analysis, but also very important for the automated spectral line selection and spectral interference corrections. With the rich data of the Spectral Library, an expert system could be developed to perform these actions with little intervention and significantly simplify the analysis process.

Appendix

A-1. Table of Contents for the CD-ROM

Mac-OS Section

1. *SpectroPlot* program, manual, and related papers.
2. The Spectral Library data files for some elements (*SpectroPlot* binary format).
3. Wavelength Tables (Adobe Acrobat PDF format).

Windows Section

1. The Spectral Library data files for some elements (delimited text format).
2. The Spectral Library data files for some elements (*Igor Pro* binary format).
3. *Origin* project file for the Spectral Library.
4. *Igor Pro* project file for the Spectral Library.
5. Wavelength Tables (Adobe Acrobat PDF format).

A-2. Circuitry for Some FTS Control Units

Module for v_{emf} Generation

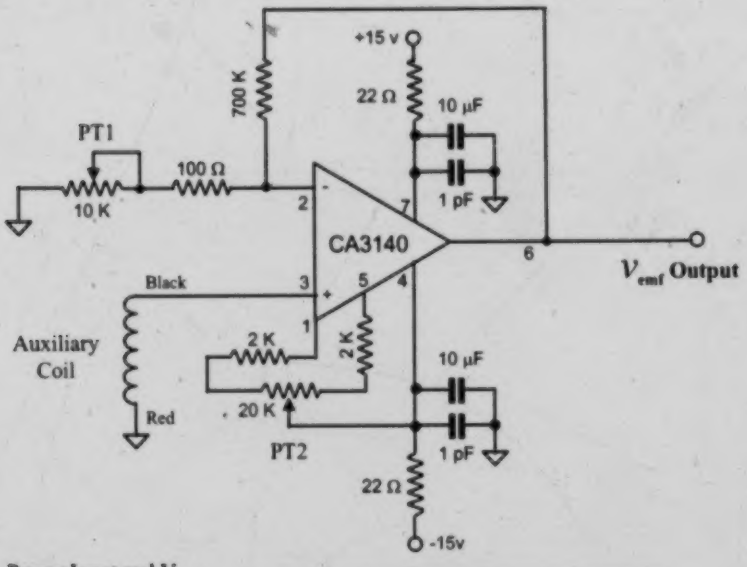

Power Input and V_{emf} Output to *Coarse Feed-back* Board

A. +15 v
B. -15 v
H. Ana. Com.
D. Chassis
E. V_{emf} Output

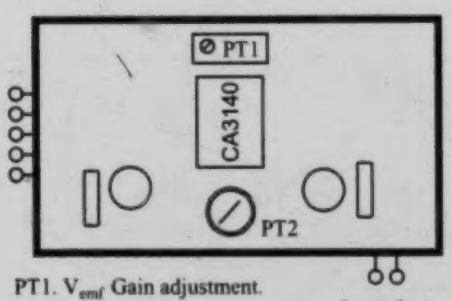

PT1. V_{emf} Gain adjustment.
PT2. Zero Offset adjustment.

Input from auxiliary coil

White Light Detection and Squaring Module

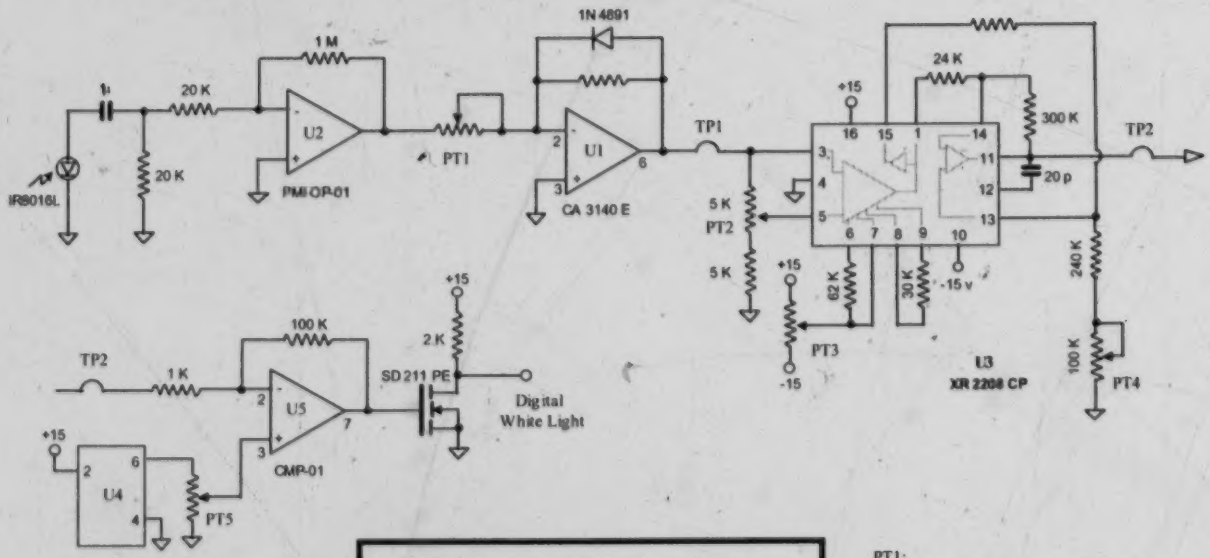

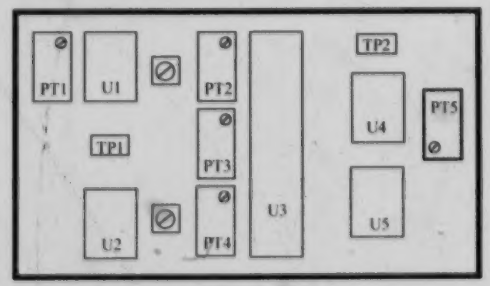

Connectors:

Power in:	Signal Out:
A. Com.	A. Ana. WL.
B. -15 v	B. Dig. WL.
D. +15 v	C. Case
E. Case	D. Com.

PT1:
PT2: Scale Factor adjustment.
PT3: Vs Offset adjustment.
PT4: Output Offset adjustment.
PT5: V_{ref} adjustment.
PT6: U1 Output Offset Voltage Adjustment.
PT7: U2 Output Offset Voltage Adjustment.

TP1: Clipped White Light
TP2: Squared Clipped White Light
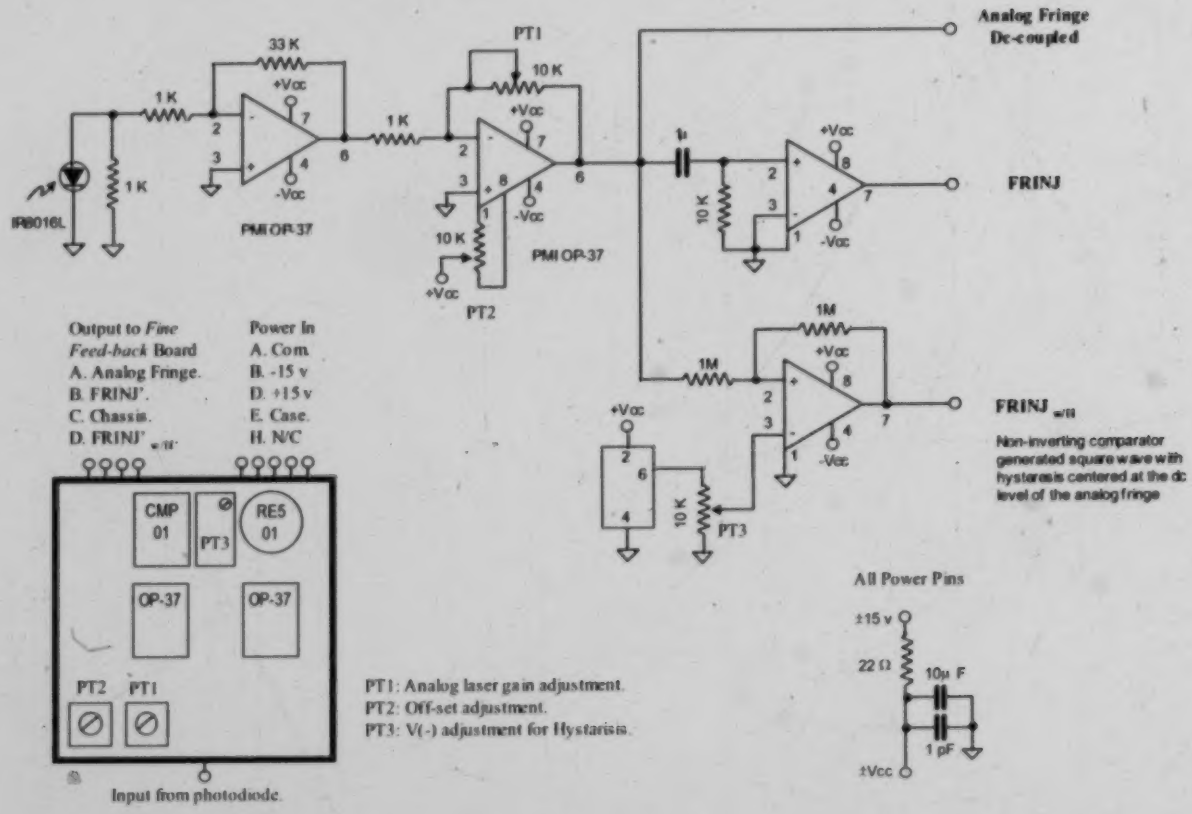
Reference Laser Detection and FRINJ Generation Module